The bone microenvironment as a therapeutic target in breast cancer bone metastasis

Veli Kaan AYDIN

A thesis submitted in partial fulfilment of the requirements for the degree of Doctor of Philosophy

Supervised by

Prof. Ingunn Holen and Prof. Nicola Brown

The University of Sheffield
Faculty of Medicine, Dentistry and Health
Department of Oncology and Metabolism

Submitted September 2022

Acknowledgements

Firstly, I would like to thank my supervisors Prof. Ingunn Holen and Prof. Nicola Brown for their truly extensive support, help, guidance and encouragement throughout my PhD. Thank you so much!

A special thank you goes to Dr Lubaid Saleh and Dr Lewis Quayle, who both helped with so many techniques, providing extensive support during my PhD. Thank you for answering my never-ending list of questions and becoming my lifelong friends, I could not have completed this work without you!

A big thank you goes to Dr Penelope Ottewell for her guidance with all my in vivo experiments and flow cytometry analysis. I also want to thank Alyson Evans and Dr Russell Hughes for teaching me many techniques and not giving up when I continuously asked for more information.

Dr Christopher George deserves special thanks for helping me with my lab work, specifically for answering all my questions about flow cytometry. Thank you so much, Victor Canuas, Jiabao Zhou, Jenny Down and Diane Lefley for being here to support me.

I also want to thank all people in the Bone Analysis Laboratory and the Flow Cytometry Core Facility for their assistance; Orla Gallagher for teaching me histology and how to use the microtome, Holly Evans for teaching and supporting me with the µCT analysis and the late Darren Lath for help with osteomeasure – thank you so much.

I would like to thank all the members of Biological Services Unit for their kind support with my in vivo experiments.

In addition, I would like to thank all the members of the Department of Oncology and Metabolism for their kind and welcoming attitude.

Last but not least the most important “THANK YOU“ goes to my amazing wife, Tugba Unsel Aydin. I could not achieve this degree without you in my life, thank you joining me on this journey in a country far beyond our home and for making any place home with you. Also, thank you for being an amazing mom to our son Ekin Mergen Aydin while I was away writing my thesis. I would like to thank my amazing family for their continuous and never-ending support and encouragement over the last years. Thanks for giving me the strength to follow my goals and for always believing in me – I hope I made you proud.

This project is funded by The Turkish Ministry of Education.

Declaration

I, the author, confirm that the Thesis is my own work under the guidance of my supervisors Prof. Ingunn Holen and Prof. Nicola Brown. I am aware of the University's Guidance on the Use of Unfair Means (www.sheffield.ac.uk/ssid/unfair-means).

This work has not previously been presented for an award at this, or any other, university.

Abstract

Bone marrow environment (BME) niches are shown to play a role in the development and progression of bone metastases, but the precise underlying mechanisms are unknown. This project aimed to investigate how altering bone marrow niches in vivo impacts the BME and tumour growth in bone, comparing different mouse models.

The BME was altered by induction of tumour growth, exposure to different doses of the chemotherapy agent doxorubicin and haematopoietic stem cell (HSC) mobilisation (with AMD3100 and G-CSF), comparing effects in BALB/c (immunocompetent) and BALB/c Nude (immunocompromised) female mice. Hind limb bones/bone marrow were analysed with □CT, flow cytometry and histology techniques.

I could detect differences in the BME between immunocompetent and immunocompromised mice, including in HSCs cells/progenitors, in immune cell populations such as B lymphocytes, monocytes, and granulocytes, in addition to T Lymphocytes being missing/defective.

In a triple negative bone metastasis model in immunocompromised mice, I found that different BM cell populations can be assessed with flow cytometry techniques in the presence of a solid tumour; however, a low tumour burden was insufficient to cause significant structural bone effects.

I confirmed doxorubicin-mediated bone loss (a known side effect), and bone structure and BME cell populations were affected, though these effects were dose-dependent and differed between the strains.

HSC mobilisation in both strains prior to metastatic model did not affect the bone or BME, yet there was a trend towards earlier tumour progression in bone compared to control.

Collectively, the work presented in this thesis supports the importance of the BME in tumour development and therapeutic response. My results highlight that different mouse strains responded differently to alterations in the BME; hence more than one model should be used in studies of bone metastasis. Finally, I showed that BME and its cell populations could be quantified with and without a tumour.

Table of contents

List of Figures

List of Tables

List of common abbreviations

ABBREVIATION	MEANING
ANXA 2	Annexin II
APCS	Antigen presenting cells
APPPL	Triphos- phoric acid 1-adenosin-50yl ester 3- (3-methylbut-3-enyl) ester
BC	Breast Cancer
BFGF	Basic fibroblast growth factor
BMDCS	Bone marrow derived cells
BME	Bone marrow environment
BMPS	Bone Morphogenetic Proteins
BMSPCS	Bone marrow stem/progenitor cells
BSP	Bone Sialoprotein
CTCS	Circulating Tumour Cells
CTGF	Connective Tissue Growth Factor
DCS	Dendritic Cells
DTCS	Disseminated Tumour Cells
EC	Endothelial cells
EGF	Epidermal growth factor
ER	Oestrogen Receptor
ERK	Extracellular Signal-Regulated Kinase
FGF	Fibroblast growth factor
GAS6	Growth Arrest-Specific 6
G-CSF	Granulocyte Colony Stimulating Factor
GM-CSF	Granulocyte-Macrophage Colony Stimulating Factor
GP130	Glycoprotein 130
GY	Gray
H^+-ATPASE	H^+-adenosine triphosphates
HER2	Human Epidermal Growth Factor Receptor 2
HIF	Hypoxia Inducible Factor
HLA	Human leukocyte antigen
HSC	Haematopoietic Stem Cell
HSP27	Heat Shock 27 Protein

IGF	Insulin-like growth factor
IL	Interleukins
IPP	Isopentenyl pyrophosphate isomerase
LOX	Lysyl oxidase
MAPKS	Mitogen-Activated Kinases
MBC	Metastatic Breast Cancer
MCAM	Melanoma cell adhesion molecule
MCP-1	Monocyte chemoattractant protein-1
M-CSF	Macrophage Colony Stimulating Factor (M-CSF)
MDSCS	Myeloid derived suppressor cells
MIP-2	Macrophage-inflammatory protein 2
MM	Multiple Myeloma
MMP	Matrix Metalloproteinase
MPL	Myeloproliferative leukaemia
MSCS	Mesenchymal Stem Cells
MSK1	Mitogen-Stress Activated Kinase
NK-	Natural Killer
ODF	Osteoclast Differentiation Factor)
OPN	Osteopontin
PCP	WNT-planar cell polarity
PD-1/PDL-1	Programmed Death Ligand 1
PGE	Prostaglandin-E
PGF	Placental Growth Factor
PI3K	Phosphoinositide 3-kinase
POSTN	Periostin
PPI	Pyrophosphate
PTEN	Phosphatase and tensin homolog
PTH	Parathyroid Hormone
PTN	Pleiotrophin
RKT	Receptor Tyrosine Kinase
S100A8/A9	Calgranulin A
SCF	Stem cell factor
SDF-1/CXCL12	Stromal cell-derived factor-1
SERMS	Selective Oestrogen Receptor Modulators

TAMS	Tumour Associated Macrophages
TGF-B	Transforming growth factor beta
TNBC	Triple Negative Breast Cancer
TNF	Tumour Necrosis Factor
TPO	Thrombopoietin
TS	Thymidylate Synthase
TSP-1	Thrombospondin-1
UNTX	Urinary N-telopeptide
VEGF	Vascular Endothelial Growth Factor
XRT	Radiotherapy

CHAPTER 1. INTRODUCTION

1.1. Breast Cancer: Overview of The Disease

Breast cancer (BC) is the most common malignancy in women, making up 11.7% of all new cancer cases worldwide with 6.9% resulting in patient death (Bray *et al*, 2018; Sung *et al*, 2021). In the UK, there were 350,960 reported new cancer cases and 55,122 of these were BC (≈15 %). 78% of the BC patients survive for 10 or more years in England and Wales. Despite improvements in diagnosis and treatment, BC caused 11,564 deaths in 2016, the vast majority of these from metastatic disease. Each year, 24% of the new cases occur in patients aged 75 years +, the mean age is around 60 for women at diagnosis (CancerResearch, 2018). BC is divided into various stages that require specific treatment for each stage. Breast cancer mostly develops in milk-producing ducts (known as ductal carcinoma) or in the lobes of breast (glands, known as lobular carcinoma) which is a much less common type and it is called primary breast cancer at this stage (Ramani *et al*, 2017). Approximately 70-80% of primary breast cancer patients have a high chance of being cured of the disease. When BC spreads to the distant organs like the skeleton, lungs, brain etc., it is called advanced (metastatic) BC (MBC) (Hiraga, 2019). Although MBC cannot be cured, it is treatable in different ways, depending on the histological and molecular characteristics of the BC (Waks & Winer, 2019).

The most crucial factor for a good prognosis in BC is early diagnosis. A widely used method to detect the cancer is mammography, which is a low dose x-ray imaging of the breast. Studies have shown that population screening reduces BC mortality by 30% (National Statics, 2020), however there are concerns regarding the rate of false positives leading to overtreatment (Roder *et al*, 2008). In 2018, 2.23 million women aged 45+ were screened for breast cancer in the UK. Of these, only 6.7% were either referred by their GP or were self-referrals, meaning that 93.3% of the women were part of the population screening programme. The rate of cancer detection was 8.8 per 1,000 women, 78.9% of these were confirmed as invasive BC and the rest were non-invasive or micro-invasive (National Statics, 2020). However, 51% of the invasive breast cancer cases were detected by 'two-week wait' referral route (79% of them are early stage), thus makes screening cases 31% of all invasive cases. Only 9% of cases were detected by routine or emergency GP controls and 4% cases were diagnosed after an emergency (Cancer Research UK, 2016). This result emphasises the importance of population screening in the UK.

BC is a complex disease, especially at the molecular level. The main molecular classifications depend on expression of the human epidermal growth factor receptor 2 (HER2, encoded by ERBB2), activation of hormone receptors (oestrogen receptor (ER) and progesterone receptor (PR)) and/or BRCA mutations (Table 1-1). ER and PR are nuclear hormone receptor which are found in cytoplasm and cell membrane. When they activated with oestrogen and progesterone, they get significantly translocated into the nucleus and activate the specific DNA locations (Esr1, Esr2 etc.). In the breast cancer, these hormones induce proliferate, survival and metastatic invasion (Mohanty *et al*, 2022). HER2 does exists on the cell surface on the cells, it controls the cell cycle and survival. However, amplification or overexpression of HER2 gene, thus result uncontrolled growth and proliferation of cells(Iqbal & Iqbal, 2014). BC can be divided into 4 major subgroups; Luminal A, Luminal B, basal-like and human epidermal growth factor receptor 2 (HER2)- enriched and triple negative. Luminal A type BC defined as expressing ER and PR while does not have HER2 amplification. They have low levels of the proliferation marker Ki-67 and tend to grow slowly and have a better prognosis (Gao & Swain, 2018). Luminal B type BC also express ER and PR, but high proliferation marker (Ki67) is found in Luminal B type. Luminal B is divided to 2 sub-groups, Luminal B HER2- and Luminal B-like HER2+ (Norum *et al*, 2014; Harbeck *et al*, 2019).. Luminal B-like HER2- BC also is ER and PR positive, however not strong as the Luminal A-like BC. They do not express HER2 and has high Ki-67 marker, grow slightly faster and are harder to cure than Luminal A-like. On the other hand, Luminal B-like HER2+ BC express ER and PR, which allow them to respond targeted therapies (Cheang *et al*, 2009). Also overly expressed HER2 results shedding of HER2, that creates soluble truncated HER2 molecules which can increase growth and survival of cancer but this complex allow us to detect cancer via blood (Tsé *et al*, 2012). Basal-like and HER2- types of BCs do not express any hormone receptors and are therefore aggressive and generally harder to treat than the luminal subtypes. However, they express HER2, making them responsive to agents targeting this receptor (Rakha *et al*, 2008). The last main molecular subtype of BC is called triple negative (TNBC), due to their lack of expression of hormone receptors and HER2. TNBC have high Ki67 levels which are aggressive, proliferate fast, and do not respond to hormone or targeted therapy. TNBC is mainly treated with systemic therapies, including neoadjuvant chemotherapy given to shrink the tumour before surgery.

In addition to the main subtypes described above, molecular profiling studies have revealed that BC is a heterogeneous disease that can be divided into further subtypes, e. g. the triple-negative sub type claudin-low tumours (Perou *et al*, 2000). These are generally characterised by low expression of cell-cell adhesion genes. The more subtypes that are described, the more targeted therapy approaches may be developed, with the aim to tailor treatment to the molecular characteristics of each patients' tumour.

Table 1-1: Molecular classification of breast cancer subtypes.

Subtypes of breast cancer classified as immunohistochemical markers and 5 years overall patient survival rate. ER: oestrogen receptor, PR: progesterone receptor, HER2: human epidermal growth factor receptor 2 and Ki67: proliferation marker

SUBTYPE	ER	PR	HER2	Kİ67	SURVİVAL RATE
LUMİNAL A	+	+	-	-	94%
LUMİNAL B	+	+	+/-	+	90%
HER2/BASAL	-	-	+	+	84%
TNBC	-	-	-	+	77%

Around 10% of BCs are genetically predisposed and associated with a family member (Shiovitz & Korde, 2015), predominantly caused by mutations in the germline BRCA1 and BRCA2 genes. The normal function of these genes is to code tumour suppressive DNA repair proteins (Miki *et al*, 1994; Wooster *et al*, 1995). Women with BRCA gene mutations have 70-75% risk of developing BC by the age of 80. Women who have 2 or more first and second degree relatives with BC with BRCA mutations have an approximately 20% higher risk of disease when compared with none carriers (Kuchenbaecker *et al*, 2017). According to a recent study, this high risk for developing breast cancer due to BRCA mutations does not affect survival rates between patients with mutations and those without (Copson *et al*, 2018).

BRCA1 (17q21) and BRCA2 (13q13) genes produce proteins that are responsible for DNA repair. Mutations of these genes have strong inheritance rates that varies between ethnic groups, it is lowest in the Asian group (0.5%) and highest in the Ashkenazi group (10.2%) (Huen *et al*, 2010; Shiovitz & Korde, 2015). Other genes associated with increased risk of BC include Li Fraumeni syndrome (TP53 Mutation), PALP2, CHECK2, Ataxia telangiectasia (ATM gene mutation), Cowden syndrome (PTEN mutation), Hereditary diffuse gastric cancer syndrome (CDH1 mutation), Peutz-Jegher syndrome (STK11 mutation) and Neurofibromatosis (NF1 mutations) (Harbeck *et al*, 2019) (Table 1-2). Different mutations trigger different subtype development such as BCRA1 mutations (80%) which mainly result in basal-like and triple-negative type BC in both females and males.

Table 1-2: Breast cancer development risk for different mutations at different ages.

Known mutations are associated with breast cancer development; even though carriers may not develop the disease, they have an increased risk of developing breast cancer at different ages (Breastcancer.org).

Mutation	Risk Percentage	Age
BRCA1 or BRCA2	72% increased	Lifetime
TP53	85% increased	By 60
PALP2	14% increased	By 50
CHECK2	28-37% increased	Lifetime
ATM	33-38% increased	By 80
PTEN	25-50% increased	Lifetime
CDH1	39-52%	Lifetime
STK11	45% increased	By 70
NF1	60% increased	Lifetime

In addition to the BRCA1/2 mutations, other mutations linked to increased risk of developing BC are TP53 (41%), PIK3CA (30%), MYC (20%), PTEN (16%), CCDN1 (16%), ERBB2 (13%), FGFR1 (11%) and GATA3 (10%). These genes regulate cell cycle, proliferation and apoptosis in the cells (Koboldt *et al*, 2012).

Most BC cases are caused by accumulation of multiple mutations (Nik-Zainal *et al*, 2016). Epigenetic alterations such as global hypomethylation (upregulation of oncogene and instability on chromosome) or local hypomethylation (gene repression and instable genes due to the DNA repair gene silencing) also contribute to development of BC. DNA methylation on the DNA tail, chromatin structure changes that cause gene silencing and nucleosome remodelling are other epigenetic mechanisms that can be seen in BC development (Romagnolo *et al*, 2016; Harbeck *et al*, 2019). Despite multiple factors, these epigenetic changes can be identified and are potentially reversible, e.g. inhibition of histone deacetylase can be reversed with the specific histone deacetylase inhibitor vorinostat (Munster *et al*, 2011).

Hormones are the other important drivers of BC, in particular oestrogen is a well-known promotor for BC. As described above, most breast cancers express ER/PR and oestrogen binds to the ER in the cells that promotes BC. Also, oestrogen has effect on bone turnover by regulating bone cells hence lack of oestrogen may result in osteoporosis (Khosla *et al*, 2012). Therefore, ER/PR+ breast cancer is treated with endocrine agents that are described in Section 1.2.3 (Fontanges *et al*, 2004; Williams & Lin, 2013). BC develops in complex environments, both in the primary location and the metastatic site, where multiple contributing factors should be considered. Therefore, extracellular signals can drive the ER mechanism where oestrogen is not found in the environment. Although we do not know what

causes the majority of breast cancer cases, research has revealed that there is an increased risk associated with high alcohol intake, gaining weight after menopause, not doing enough physical activity, not breastfeeding, age, early menarche (before age 12), late menopause (over age 55), height and family history - all known general risks for developing breast cancer (Willett *et al*, 2014).

1.2. Treatment of Breast Cancer: Clinical Methods and Effects

Treatment of BC depends on the stage/grade, the type of cancer, the general health of the patient and menopausal status. All of these factors must be considered in order to choose whether the patient will have surgery, chemotherapy, radiotherapy etc. Treatment of the disease changes with the tumour histology and biomarkers but in most cases, patients undergo surgery within a few weeks of diagnosis to remove the tumour from the breast and in some cases the associated lymph nodes to prevent its metastasis. Surgery is most often followed by adjuvant therapy to remove any remaining tumour cells and may include chemotherapy, radiotherapy, endocrine treatment, targeted agents and some novel agents depending on tumour and patient characteristics (Ramani *et al*, 2017).

Table 1-3: Breast Cancer Clinical Stage Description

Breast cancer is clinically staged depending on the location, tumour size and lymph node cell number which informs subsequent treatment.

Stage	Definition
0	Non-invasive breast cancer such as ductal carcinoma in situ (DCIS) and lobular carcinoma in situ (LCIS).
IA	The tumour is smaller than 2 cm and not spread outside the breast tissue.
IB	The size of the tumour is greater than 2 cm inside the breast or between 0.2-2 mm in the lymph nodes.
IIA	The tumours are larger than 2 mm in the lymph nodes with no tumour in the breast.
IIB	Tumour is between 2-5 cm in breast and 0.2-2 mm in lymph nodes, or 2-5 cm in lymph node or larger than 5 cm in the breast.
IIIA	The tumour cell number in the lymph nodes is 4 to 9 or larger than 5 cm and 0.2 to 2 mm in the lymph nodes or larger than 5 cm and 1 to 3 cells in lymph nodes.
IIIB	Tumour has spread to the chest causing ulcer or swelling with tumour cells in the lymph nodules up to 9.
IIIC	Any sized tumour spread around the chest and more than 10 tumours cells in lymph nodes.
IV	Cancer has spread to the distant organs such as brain, bones lungs and liver.

Breast cancer is divided into 5 stages (0-IV) depending on the extent of the disease (see Table 1-3) (Aydiner *et al*, 2019; Cabioglu *et al*, 2019).

1.2.1. Chemotherapy

Chemotherapy is a systemic treatment and usually planned based on tumour size, number of nodes, stage, spread ratio and receptor status. Chemotherapy can be divided 3 categories:

Neoadjuvant Chemotherapy is used to reduce the tumour size before the surgery and may also kill any cancer cells in the circulation or distant sites (micro-metastases). Depending on the type, chemotherapeutic agents are generally given once every three weeks for three cycles and is standard of care for patients with triple negative BC (NICE, 2020). After tumour shrinkage, surgery is performed. Use of neo-adjuvant therapy can also help to determine the combination of treatment to which a particular tumour will respond. Commonly used combinations are FEC (5-fluorouracil + epirubicin + cyclophosphamide), AC (doxorubicin + cyclophosphamide), TAC (docetaxel + doxorubicin + cyclophosphamide), TCH (docetaxel, carboplatin + trastuzumab) or weekly paclitaxel. The exact therapeutic combination used depends on patient-related factors as described above (Ramani *et al*, 2017; Waks & Winer, 2019). Each chemotherapy agent aims to target different points in key cancer cell survival and proliferation pathways. 5-Fluorouracil inhibits thymidylate synthase (TS, syntheses of nucleotides) and its metabolites merges with RNA and DNA thus disrupting their function (Longley *et al*, 2003). Epirubicin and doxorubicin are anthracyclines that interrupt DNA duplication by inhibition of topoisomerase-II (Bachur, 2002). Cyclophosphamide is an alkylating agent and the active form binds to and cross-links DNA and RNA (Emadi *et al*, 2009). Docetaxel stabilises the microtubule assembly in the cell, reduces free tubulin resulting in inhibition of cell division between the meta- and anaphase (Suzuki & Tokuda, 2001). Carboplatin drug binds plasma proteins and activated inside the cells that forms platinum complexes. This reactive complex causes DNA intra- and inter-strand cross-linkage, thus inhibits DNA synthesis (de Sousa *et al*, 2014).

Adjuvant Chemotherapy is given after the primary surgery, starting when the wound is healed (usually after 2-3 weeks). Treatment depends on different condition such as tumour size and type, receptors and other medical conditions like diabetes and cardiac disease. Therapy is given for 6-8 cycles with 3 week intervals and is often followed by radiotherapy and targeted drugs like trastuzumab (Ramani *et al*, 2017).

Palliative Chemotherapy is used to treat MBC. This treatment can be weekly or once every three weeks is dependent on patient-related factors. Which agents are used depends on the previous treatments and may be combined with targeted drugs like trastuzumab for anti-HER therapy, or to the organ such as zoledronic acid for bone to reduce pain and the risk of fractures (Ottewell *et al*, 2009; Ramani *et al*, 2017). There is no certain treatment if anthracyclines fail, but Capcitabine has the

potential to cover the gap for anthracycline and taxane-pretreated patients (Jiang *et al*, 2018). Capcitabine is selective for tumours because of its cytotoxic moiety. It has 2 main mechanisms, one is reducing thymidine production thus inhibiting DNA synthesis and the other is replacing uracil in RNA and protein synthesis which inhibits the regular process (Hoffman-La Roche, 2000).

Chemotherapy does not only target cancer cells but also affects healthy, proliferative cells, most commonly those of the bone marrow, hair follicles and digestive system. That is why toxicity of the drugs must be considered. For example, anthracyclines can cause damage to the cardiac myocytes by calcium overload with calcium channel activation. In addition, they produce reactive oxygen species and those species can trigger DNA damage and mitochondria dysfunction (Bachur, 2002; Ozer & Aydiner, 2019). Common side effects that patients experience, are hair loss, fatigue, infections, nausea, appetite change, weight change, emotional change, diarrhoea, constipation, kidney problems, fertility, and libido problems. These physiological effects are reducing the quality of life for the patients (Chu & DeVita, 2018; Bayraktar & Aydiner, 2019; Ozer & Aydiner, 2019) .

1.2.2. Radiotherapy

Radiotherapy is used for multiple purposes in BC treatment, either as primary treatment to shrink tumours before surgery or to kill tumour cells that are left deeper in the tissue or the lymph nodes after surgery. The standard regimen is to give 40 to 45 Gy (Gray: Unit for radiation intensity) as a daily treatment which reduces the tissue damage by decreasing the dosage. Radiation can be given to avoid surgery/chemotherapy and as palliative therapy to treat patients with bone metastasis (for 10 to 12 days only) to reduce cancer-induced bone pain (Ramani *et al*, 2017; Waks & Winer, 2019). A recent study showed that 26 Gy given in five fractions over 1 week is similar to the standard 40 Gy treatment (15 fractions over 3 weeks) and indicated that this regime can be used for up to 5 years in patients prescribed adjuvant local radiotherapy (Murray Brunt *et al*, 2020). Due to the COVID-19 pandemic this technique has been quickly adapted by the NHS, thus resulted in reduced patient visits to hospital (Coles *et al*, 2020).

1.2.3. Endocrine Treatments

Endocrine treatment, also known as hormonal therapy, is used to treat hormone-dependent BC. Oestrogen stimulates BC growth, which can be inhibited by treatment with anti-oestrogen drugs such as tamoxifen, anastrozole, letrozole or exemestane. (Ramani *et al*, 2017). These drugs are classified as aromatase inhibitors (anastrozole, exemestane and letrozole), selective oestrogen receptor modulators (tamoxifen) and oestrogen receptor down-regulators (fulvestrant) (Jordan *et al*, 2001;

Piccart *et al*, 2003; Fabian, 2007). Aromatase inhibitors supress the aromatase enzyme activity therefore inhibiting the oestrogen production from androgens in peripheral tissues. Before the menopause, the ovaries produce elevated levels of aromatase that cannot be blocked with inhibitors. However, after the menopause aromatase is mainly present in fat and muscle, at levels that can be blocked by these agents, which is the reason why aromatase inhibitors are widely used in postmenopausal women (Campos, 2004; Fabian, 2007). Selective oestrogen receptor modulators (SERMs) bind to the oestrogen receptors thus prevent the binding of oestrogen. They can also mimic the oestrogen in bone and the uterus (Jordan *et al*, 2001). Oestrogen receptor downregulatory drugs bind oestrogen receptors like SERMs, however they also block the protein kinase pathway which remains active with SERMs. Thus, downregulatory drugs inhibit dimerization and downregulates oestrogen receptor (Carlson, 2005; Johnston & Cheung, 2010).

Menopausal status, which alters the reproductive hormone levels, is one of the determining factors when deciding which endocrine treatment to use. Tamoxifen is generally used for 5 years in premenopausal patients. It has been shown that 10 year treatment with tamoxifen reduces recurrence by more than 20 % and it can be used in postmenopausal women if they cannot tolerate aromatase inhibitors (Davies *et al*, 2013). Since the side effects (including joint and muscle pain, stroke, bone loss (for premenopausal women only)) of tamoxifen is increased after 2-3 years of usage, anastrozole or letrozole can be given for 2-3 years if patients are postmenopausal. Aromatase inhibitors like anastrozole, letrozole and exemestane are usually given to post-menopausal women for 5 years. In general, it is safe to use however, patients can develop exhaustion, joint pain, and osteoporosis (which can lead to fractures) (Johnston & Cheung, 2010; Mehta *et al*, 2012).

1.2.4. Targeted agents

As described earlier, identification of breast cancer subtypes characterised by expression of specific molecules has led to the development of targeted agents. For example, patients with HER2 (20% of BC) expressing tumours can be treated with trastuzumab (also known as Herceptin). Trastuzumab has several mechanism of actions, including downregulation of HER2 when bound (Gajria & Chandarlapaty, 2011), attraction of immune cells to the site of HER2 overexpression (Vu & Claret, 2012), blocking of the shedding of the extracellular HER2 domain with metalloproteinase activity inhibition and pathways in phosphoinositide 3-kinase (PI3K) which plays a role in cell survival. Another known mechanism is angiogenesis inhibition by reducing VEGF (Valabrega *et al*, 2007). Drug is administered intravenously once every 3-4 weeks (12-17 doses) for 1 year at either the neoadjuvant or palliative stage to HER2+ cancers (Vu & Claret, 2012; Ramani *et al*, 2017). However, there are several mechanisms for trastuzumab resistance, including epitope masking with Mucin 4,

upregulation of HER2 with PTEN or PI3K mutations, alternative signalling via insulin-like growth factor-1 and failed immune-mediated response trigger (Pohlmann *et al*, 2009). However, 70 % of the HER2+ BC patients develop resistance to the trastuzumab during the treatment, therefore, alternative drugs have been developing to treat trastuzumab resistance breast cancer; Lapatinib (binds the cytoplasmic ATP-binding site of HER2) and Pertuzumab (binds another domain of HER2)(Wong & Lee, 2012).

1.2.5. Novel Agents

Despite of the high success rates of treatment in breast cancer, known treatment methods are not effective for all BC subtypes, as illustrated by the 11,400 BC deaths/year in the UK. Extremely aggressive types like TNBC have the highest mortality rate and poorest response to the classical treatments. Therefore, it is important to develop new therapeutic approaches to treat patients with this form of BC. CDK4/6 inhibitors such as abemaciclib, palbociclib, ribociclib are used for inhibition of cell cycle progression for hormone receptor positive and epidermal growth factor 2 negative BC types (Shah *et al*, 2018). Precilinal studies of palbociclib (combined with letrozol) (Slamon *et al*, 2015) and phase 1 trials for abemaciclib (Shapiro *et al*, 2013) and ribociclib (Infante *et al*, 2016) demonstrated their safety alongside positive effects on the tumour. In the PALOMA-1 trial, combination therapy (palbociclib and letrozol) showed higher median survival (20.2 months) when compared to the monotherapy with letrezol (10.2 month) in 165 ER+ MBC patients (Finn *et al*, 2015). The following PALOMA-2 trial with 666 patients also showed similar results with 24.8 month survival rate when compared with the letrozol only treated group (14.5 month) (Finn *et al*, 2016). The most recent PALOMA-3 study with 521 patients compared palbociclib combination therapy with fulvestrant (n=347) with placebo after fulvestrant therapy (n=174). Patients who received palbociclib before fulvestrant had significantly increased median survival rates (34.9 months) when compared to the placebo group (28 months) (Turner *et al*, 2018). Fulvestrant has also been combined with ribociclib as a second line treatment for postmenopausal patients in the MONALEESA-3 trial (n=484), showing that patients who received ribociclib had significantly increased median survival rate (20.5 months) when compared with the placebo group (12.8 months) (Slamon *et al*, 2018). These results from trials demonstrate that novel CDK4/6 inhibitors have promising results and can be used as combination therapy.

PARP inhibitors, like olaparib and talazoparib, are used for epidermal growth factor 2 negative BCs and interfere with normal cellular DNA damage repair (Vinayak & Ford, 2010). They have also showed positive results on BRCA mutation carrier breast cancers and especially with triple-negative BC. (Fong *et al*, 2009; Foulkes *et al*, 2010). There are multiple clinical trials of PARP treatments for both monotherapy and combination therapy (McCann & Hurvitz, 2018). In the EMBRACA phase 3 trial,

patients with HER2- advanced breast cancer either received talazoparib (n=287) or physician's choice of chemotherapy (n=144). Talazoparib-treated patients with HER2- advanced breast cancer showed tumour effects significantly later (24.3 median months) when compared to the classical treatment group (6.3 median months), indicating the positive effect of talazoparib in advanced breast cancer patients (Ettl *et al*, 2018).

The microenvironment is one of the target areas to treat breast cancer. Bisphosphonates are used since they inhibit osteoclast-mediated bone resorption and thereby prevent skeletal morbidity and relieve pain (Mundy, 2002; Coleman *et al*, 2015). AZURE trial was designed to determine the response to bisphosphonate (Zoledronic Acid) treatment in patients with stage II/III breast cancer. AZURE trial with 18766 women showed that bisphosphonates significantly reduced bone recurrence alongside reducing primary and distant recurrence, irrespective of bisphosphonate type, menopausal status, oestrogen receptor type or chemotherapy treatment. Results indicated that bisphosphonates significantly reduced recurrence but had no effect on mortality, hence it is used to prevent disease after treatment (Early Breast Cancer Trialists' Collaborative Group (EBCTCG), 2015). The subsequent AZURE trial with 3360 stage II/III breast cancer patients, scheduled for 10 years zoledronic acid treatment determined disease free survival, invasive free survival and overall survival rate. Zoledronic acid improved disease free survival and invasive free survival in postmenopausal woman alongside fewer skeletal fractures and reduced skeletal events after disease recurrence (Coleman *et al*, 2018). Despite identifying the benefits of adjuvant bisphosphonates in postmenopausal woman, the mechanism underlying this response is still unknown.

Breast cancer has been seen as an immunologically "cold" tumour, yet recent studies suggest that immunotherapy improves the outcomes of the disease. Breast cancer and immune cell relationships are described in detail in section 1.5.4. Briefly the immune system uses the neoantigens (antigen that is produced by cancer cells due to high mutations) to detect and eliminate cancer cells, however breast cancers have lower frequency of mutations thus a lower neoantigen burden and few tumour killer lymphocyte subtypes, therefore they are classified as immunologically silent (cold) (García-Aranda & Redondo, 2019). PD-1/PDL-1 (programmed death ligand 1) binding regulates T-cell activation and increases cancer survival thus this is a potential target for immunotherapy in BC. In order to block binding, antibodies such as pembrolizumab (PD-1 blocking antibody), atezolizumab (PD-L1 Blocking antibody) and avelumab (PD-L1 Blocking antibody) have been developed (Planes-Laine *et al*, 2019). Another developed small molecule is tucanitib which is a tyrosine kinase inhibitor of HER2 that inhibits phosphorylation of ErbB-2 thus resulting in growth inhibition and death of ErbB-2-expressing tumour cells (Murthy *et al*, 2019; Oh & Bang, 2020). Current approaches to improve immune sensitivity of

cold cancers are enhancing the expression of cancer cell surface HLA, increasing cancer exosomes and heat shock proteins (Toraya-Brown & Fiering, 2014). However, the immune response or escape is not the only factor in breast cancer progression, but other factors such as oestrogen, have an impact on tumour escape. Oestrogen in the microenvironment not only increases the tumour survival and growth factors like VEGF, EGF, IGF and FGF, it increases the immune tolerance, hence recent adjuvant hormonal therapies are used with HER2-targeted agents (García-Aranda & Redondo, 2019). This information indicates that immunotherapy has the potential as an adjuvant therapy with conventional or novel treatments.

1.3. Metastatic Breast Cancer

When BC spreads to other organs it is called MBC (Stage IV) and becomes a life-threatening disease that is incurable, but treatable. Patients are either initially diagnosed as stage IV BC or can develop metastasis later in the course of the disease. In the UK, 6-7% of patients are diagnosed as stage IV BC at presentation (CancerResearch, 2018) and up to 30% of the primary cancer patients eventually develop metastasis (Redig & McAllister, 2013). At this incurable stage, 25% of UK breast cancer patients can survive more than 5 years (CancerResearch, 2018), however the median survival is 2-3 years (Harbeck *et al*, 2019). Common sites for MBC are the skeleton (≈67%), liver (≈40%), lungs (37%) and brain (≈13%) (Harbeck *et al*, 2019; Hiraga, 2019). The metastasis rate to the different sites varies with subtypes such as triple-negative BC has a higher tropism rate to lung while luminal A tends to metastasise to the liver (Gerratana *et al*, 2015). MBC patients receive treatment mainly to relieve symptoms and decelerate disease progression. At this stage, the disease is complicated, and multiple are factors from distant organs are involved, making systemic treatment necessary.

1.3.1. The Metastatic Cascade

The multistep process of breast cancer metastasis starts when cancer cells invade surrounding tissues and enter the lymph or blood system. It has been shown in clinical trials that dissemination starts with development of the primary tumour (Bednarz-Knoll *et al*, 2011). In this process, the primary tumour microenvironment affects tumour development. Tumour cells that enter the blood stream are called circulating tumour cells (CTCs) and when they invade the distant organ or tissue, they are termed disseminated tumour cells (DTCs) (Figure 1-1). The primary tumour cells and their microenvironment continuously modify the distant tissue's microenvironment and creates a premetastatic niche through secretion of exosomes (Quail & Joyce, 2013). Different effects are created by various cell types with secretion of different exosomes. Fibroblasts secrete exosomes that contains Cd81 which drives breast cancer invasion by triggering WNT-planar cell polarity (PCP) (Luga

et al, 2012) and exosomes released by NK cells contain some NK markers alongside Fas ligand and perforin molecules which contribute to the tumour's immune escape (Lugini *et al*, 2012). The microenvironment of the distant tissue supports the premetastatic niche with chemo attractants such as CXCL12, Connective Tissue Growth Factor (CTGF) and Fibroblast Growth Factor (FGF) (Teicher & Fricker, 2010; Peinado *et al*, 2017). DTCs have 4 different fates; many of them die either in tissue or in the circulation due to stress and immune cells within 2-3 hours. However, if they survive they can either enter dormancy, divide a few times to generate micro-metastases or proceed to the outgrowth stage, with the microenvironment playing a crucial role in all stages (Scully *et al*, 2012; Pradhan *et al*, 2018). Proliferation of the cancer cells is balanced with apoptosis, cellular dormancy, or immune dormancy. The molecular mechanisms that regulate tumour cell dormancy remain to be identified, however it is known that the microenvironment, inflammation or tissue remodelling may trigger activation of the dormant tumour cells (Clements & Johnson, 2019). Our understanding of the mechanisms regulating tumour dormancy by different components of the bone microenvironment is described in section 1.4.2.1.

Tumours depend on formation of blood vessels (angiogenesis), in order to secure access to nutrients and oxygen required to grow beyond a certain size (Park & Nam, 2020). Tumour outgrowth promotes further angiogenesis and the microenvironment starts to support tumour growth by producing growth factors, tumour cells evade recognition and this results in elimination by the immune system (Al-Mahmood *et al*, 2018).

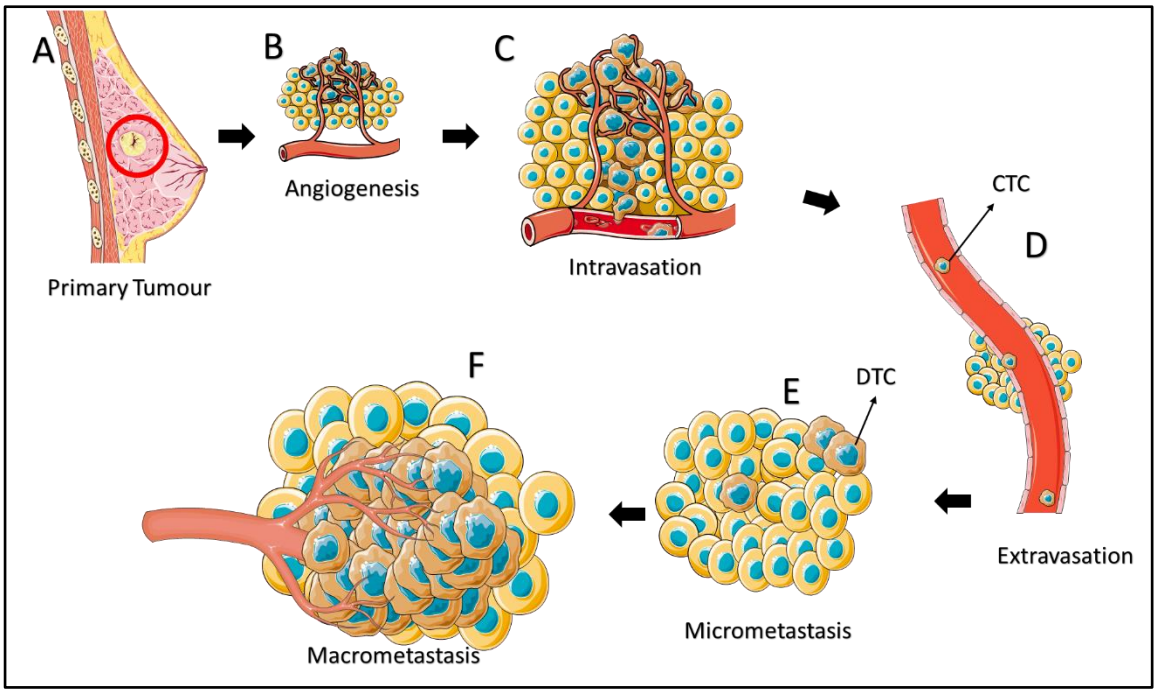

Figure 1-1: Simplified scheme of breast cancer metastasis stages to the distant tissue.

Primary tumour metastasis involves complex factors, but it can be divided into 5 simple stages. ***A)*** *When primary breast tumour reaches a certain size,* ***B)*** *it initiates angiogenesis which allows access to growth factors and energy supplies. After tumour outgrowth from the primary tissue* ***C)*** *some cancer cells intravasate to the blood or lymph system. When they find the suitable niche,* ***D)*** *circulating tumour cells (CTCs) extravasate through the blood/lymph system. Disseminated tumour cells (DTCs) may stay dormant or divide a few times to generate* ***E)*** *undetectable micrometastases. After locating to a supportive environment (the metastatic niche), microenvironmental signals trigger DTC proliferation and initiate tumour angiogenesis resulting in* ***F)*** *clinically detectable macro-metastasis. (Figure created with images from Servier Medical Art)*

1.4. Cancer in the Bone: Stages and Effects

Bone is the most common metastatic site, present in around 70% of the MBC cases (Hiraga, 2019). Patients with skeletal metastases may experience severe bone pain, fractures, hypercalcemia and spinal cord compression, reducing their quality of life (Zhu *et al*, 2019). Metastasis to the bone is a multistep process that includes intravasation to the blood/lymph system, extravasation in the bone marrow, survival with dormancy, reactivation and outgrow as illustrated in Figure 1-1. Bone metastasis involves immune resistance, location to a supportive niche and the self-renewal ability of the cancer cells. However, metastasis to skeletal tissue cannot be explained by tumour cell characteristics alone, there are more complex systems involved. Therefore, the “seed and soil” hypothesis (cancer cells interact with components of the bone microenvironment in order to successful metastasise) is used to explain bone metastasis (Fidler, 2003; Massagué & Obenauf, 2016; Zhang *et al*, 2019).

1.4.1. Pre-Metastasis; Enrichment of the soil

Before metastasis is established, the primary tumour secretes factors which induces the formation of a microenvironment that attracts tumour cells to a pre-metastatic niche "soil" in distant organs (Mundy, 2002). The pre-metastatic niche consists of tumour-derived components, tumour-mobilized bone-marrow-derived cells (BMDCs) and the local stromal microenvironment which secretes niche-promoting molecular components (Table 1-1, Table 1-2 and Table 1-3).

Table 1-4: Niche-Promoting Tumour Derived Factors

Factors produced by tumour that promote pre-metastatic niche for breast cancer cell homing.

Factor	Mechanism	Reference
VEGF (Vascular Endothelial Growth Factor)	Recruits BMDCs to promote niches in the lung.	(Kaplan *et al*, 2005)
PGF (Placental Growth Factor)	Recruits BMDCs and DTC to promote niches in the lung.	(Kaplan *et al*, 2005)
S100A8/A9 (Calgranulin A)	Recruits myeloid cells and DTC to promote niches in the lung.	(Hiratsuka *et al*, 2006)
CD44/CD44v6	Not for metastasis but it allows exosomes to organize receptive niches.	(Jung *et al*, 2009; Williams *et al*, 2013)
E, N- heterotypic adherens junctions	Mediates interactions between the osteogenic niche and cancer cells which promotes bone metastases.	(Wang *et al*, 2015a)
Versican	Overexpression of G3 versican promotes breast cancer metastasis to bone and soft tissues.	(Ricciardelli *et al*, 2009)
Tumour microvesical Osteopontin	Mobilizes BMDCs for niche formation, promotes metastatic growth.	(Fremder *et al*, 2014)
Tumour exosomal miR-112	Reprogrammes glucose metabolism in the niche and increases the nutrients.	(Fong *et al*, 2015)
$P2Y_2R$	Recruits BMDCs to the pre-metastatic lung niches.	(Joo *et al*, 2014)

Table 1-5: Niche-Promoting Stroma Derived Factors

Factors produced by the microenvironment that promote pre-metastatic niche for breast cancer cell homing.

Stroma Derived Factors		
Factor	**Mechanism**	**Reference**
Angiopoietin-2	Recruits macrophages and endothelial cells for niche formation.	(Srivastava *et al*, 2014)
Prostaglandin E2	Recruits BMDCs to lung niches.	(Liu *et al*, 2014)
Periostin	Creates an immunosuppressive niche.	(Ghajar *et al*, 2013)
Heat Shock Factor 1	Promotes tumour cell recruitment into the niche.	(Scherz-Shouval *et al*, 2014)
Exosomal miR-19a	Recruits myeloid cells into the niche.	(Zhang *et al*, 2015)
Exosomal miR-23b	Induces breast cancer cell dormancy in the niche.	(Ono *et al*, 2014)

Table 1-6: Niche-Promoting Tumour and Stromal Derived Factors

Factors produced by both tumour and the microenvironment that promote pre-metastatic niche for breast cancer cell homing.

Tumour and Stromal Derived Factors		
Factor	**Mechanism**	**Reference**
Stromal derived factor-1/Chemokine Receptor-4	Regulates angiogenesis in niche and recruits BMDCs to the niche.	(Seubert *et al*, 2015)
Lysyl Oxidase	Promotes extracellular matrix remodelling for niche formation.	(Erler *et al*, 2009)

1.4.2. Metastasis; Homing and Development

CTCs that survive in the circulation then extravasate to a suitable environment and bone has multiple factors that attract these CTCs. In the healthy bone environment, CXCL-12/CXCR-4 interaction plays a crucial role on haematopoietic stem cell (HSC) regulation with development and migration. This interaction anchors the HSCs in the HSC niche (Shiozawa *et al*, 2011b). CTCs like MDA-MB-231 cells are proposed to use similar pathways to extravasate to the bone environment (Hiraga, 2019). Also, breast cancer DTCs may localise the HSCs' niche as supported by studies from model studies carried out in the Holen group, showing that mobilizing the HSCs resulted in an increased number of tumour cells locating in niches following mobilisation of HSCs (Allocca *et al*, 2019). The HSC niche is a source of many blood cells self-renewal, and it has multiple factors that affect cancer development in bone, (see section 1.5.2). Tumour cells express cell surface integrins that can bind osteopontin (OPN), bone sialoprotein (BSP) and vitronectin which are secreted by osteoblasts (Wang *et al*, 2015a) and osteoblasts also express cell surface N-cadherins to which tumour cells can bind with their E-cadherins for homing (Croucher *et al*, 2016). RANKL is another cytokine that helps migration of breast cancer

cells to the bone since it is highly secreted in the bone marrow by osteoblasts (Jones *et al*, 2006; Ono *et al*, 2020). RANKL induces breast cancer cell migration with ERK and Akt pathway induction (Jones *et al*, 2006) alongside Src kinase and WNT pathways (Tang *et al*, 2011). RANKL has other roles in tumour development which is described in section 1.5.1.4. Taken together, factors that regulate healthy bone remodelling and haematopoiesis facilitate bone homing of CTCs, yet the detailed interactions of BC with components of the bone microenvironment remain to be identified.

1.4.2.1. Dormancy

BC can recur many years after the primary tumour appeared to be successfully treated, mainly due to the ability of tumour cells to remain dormant in peripheral tissues, in particular the bone marrow. One of the clinical aims is to maintain the DTCs inside the bone in a dormant state, thereby preventing the development of MBC. To understand the mechanisms that regulate tumour cell dormancy, different models have been developed to study dormancy and two main mechanisms are described, cellular and tumour dormancy. Cellular dormancy where a single DTC enters a non-proliferative, quiescent state in response to a repressive microenvironment or self-signalling. Tumour dormancy is the state where there is balance between DTC proliferation and apoptosis, as a result tumour cells remain below a clinically detectable number. This balance is controlled by environmental factors such as immunosurveillance (immunologic dormancy), vascularization (angiogenic dormancy) or stromal cell interactions (Clements & Johnson, 2019). Our current understanding of the cellular and molecular mechanisms of tumour cell dormancy have recently been described in a comprehensive review by Phan and Croucher (Phan & Croucher, 2020).

During cellular dormancy, cells begin their entry into quiescence by decreasing the expression of proliferation marker Ki67 and thereby enter G0/G1 cell cycle arrest. During this phase cells also inhibit the PI3K-AKT pathway, increased p38 activation and p21 cell cycle inhibitor expression. BCs cells also lose their cell surface β1-integrin receptors that results in decreased FAK tyrosine residues (White *et al*, 2004), and this creates a resistance to apoptotic cell death leading to cells entering a growth-arrested quiescence state (Quayle *et al*, 2015). Autophagy is a catabolic process that helps recycle cytoplasmic organelles or constituents in cells under metabolic stress (Mizushima, 2007). This complex system initiates or supresses tumour proliferation and needs further investigation, but there are *in vitro* and *in vivo* studies that show the importance of autophagy for cancer cell survival. Despite of this, blocking autophagy does not initiate apoptosis in cancer cells, they might adapt to other survival pathways, yet blocking autophagy is an potential combination treatment approach to maintain DTC dormancy (Sosa *et al*, 2013; Quayle *et al*, 2015; Gomis & Gawrzak, 2017; Vera-Ramirez *et al*, 2018). Under the stress conditions, cancer cells promote the p38 MAPK stress-response pathway

that results in a high p38 ratio when compared to ERK. Factors such as BMPs and TGFβ2 induce $p38^{high}/ERK^{low}$ ratio, hence, tumour cells can maintenance dormancy state (Gawrzak *et al*, 2018; Clements & Johnson, 2019; Mayhew *et al*, 2020).

Maintaining tumour cell dormancy is one of the goals to prevent overt metastasis. Therefore, we need to understand how the DTCs are influenced by the surrounding microenvironment. As mentioned above, angiogenesis is important for BC progression and bone is a highly vascular tissue with an extensive microvascular network. The area immediately adjacent to the vessels is described as the perivascular niche, which is suggested to play a role in regulating cancer cell dormancy. Using murine models, it has been shown that DTCs localize near the microvascular structures that are high in thrombospondin-1 (TSP-1: Angiogenic inhibitor) that is secreted by mature endothelial cells and suppresses tumour growth. However, sprouting tips lose their TSP-1 and have increased POSTN and TGF-β1 stimulates the tumour growth. Also, it has been found that downregulation of heat shock 27 kDA protein (HSP27: Thermotolerance protein) induces long-term dormancy (Straume *et al*, 2012; Ghajar *et al*, 2013). In poorly vascularised areas of bone, there is high chance of DTCs encountering hypoxic conditions. Cancer cells respond to hypoxia, which is another pathway that regulates dormancy through supporting tumour cell survival. In this process, hypoxia inducible factor (HIF) is involved in regulation of dormancy as shown in animal models of metastasis. Dunn *et a*l. (2009), demonstrated that blocking the HIF-α and TGF-β pathways in MDA-MB-231 cells decreased bone metastasis in animal models. In contrast, Hiraga et al. (2007), showed sHIF-1's metastasis promoting effect on bone metastasis tumour burden, with transfected CA-HIF-1α cDNA MDA-MB-231 cells, injected *in vivo* when compared to controls. Fluegen et al. (2017), found that hypoxia genes (*NR2F1, DEC2, p27*) were co-expressed with dormancy genes (*GLUT1*, *HIF1α*) in the microenvironment in animal models (BALB/c Nu) injected with MDA-MD-231-5RE-ODD-mCherry-GFP cells. This data is supported by observing the upregulated dormancy marker (GLUT1) in naturally occurring hypoxic samples (NR2F1) from 20 human head and neck squamous cell carcinoma patients (Hiraga *et al*, 2007; Dunn *et al*, 2009; Fluegen *et al*, 2017).

In tumour dormancy (micrometastatic dormancy), cell cycle occurs at slow rates, or the rate of proliferation and apoptosis are similar, thus resulting in no net growth of the micrometastases. This stage is mainly regulated by the factors from the microenvironment such as immune surveillance, hypoxia, angiogenesis and stromal interactions (Mayhew *et al*, 2020). The immune system supports tumour dormancy by eliminating some of the tumour cells. NK cells, $CD4^+$ and $CD8^+$ T-cells play crucial roles in this mechanism, with depletion of $CD4^+$ and $CD8^+$ T cells resulting dormancy escape in mouse models (Gomis & Gawrzak, 2017). Cells from the surrounding normal microenvironment secrete

numerous cytokines and growth factors that support tumour dormancy, including BMPs, TGFβ2 and miR-222/223+ exosomes (Quayle *et al*, 2015; Gomis & Gawrzak, 2017; Clements & Johnson, 2019). There is some evidence from *in vivo* breast cancer model systems that DTCs compete with HSCs for space in the HSC niche (Allocca *et al*, 2019), hence the factors that regulate HSC dormancy can potentially also influence tumour cells located in this niche. Annexin II (ANXA2) and growth arrest-specific 6 (GAS6) by osteoblasts and endothelial cells found in the HSC and peri-vascular niche regulate HSC dormancy and also drive dormancy in prostate cancer in animal and cell culture models (Jung *et al*, 2007; Shiozawa *et al*, 2010; Decker *et al*, 2016). As previously mentioned, the tumour needs support of functional vascular structure to grow in size. Tumours at a micrometastatic size cannot grow larger than 1 mm in diameter and this can be caused due to the lack of vascular structures, active repulsion of microenvironment vessels, increased thrombospondin 1 (TSP1: an anti-angiogenic factor), and/or decreased angiogenic factors such as VEGF, bFGF (Mayhew *et al*, 2020). TSP-1 has been shown to mediate metastasis suppression in breast cancer and it is secreted by sprouting vessels in the bone marrow which supresses tumour growth adjacent to them, however this still remains to be demonstrated in bone (Weinstat-Saslow *et al*, 1994; Ghajar *et al*, 2013).

1.4.2.2. Reactivation of the Dormant cells

The mechanisms underlying tumour cell escape from dormancy may differ between metastatic tissues. In bone, changes in the factors that induce dormancy also triggers escape from dormancy. Multiple ways of reactivation of cancer cells have recently been described. Endothelial cells in perivascular niche activates Wnt signalling pathway by secreting periostin which recruits Wnt ligands to serve cancer cells (Gomis & Gawrzak, 2017; Park & Nam, 2020). Mesenchymal cells release CXCL12 that activates AKT signalling by binding to CXCR4 receptor and osteogenic cells form junctions with N- and E- cadherins between cancer cells to activate mTOR signalling. Since both are important intracellular pathways that responds to nutrients, hormones and growth factors, hence they regulate proliferation and cell growth (Paplomata & O'Regan, 2014; Gomis & Gawrzak, 2017; Clements & Johnson, 2019). According to Sosa et al., (2014) dormant cancer cells may be activated by two mitogen-activated kinases (MAPKs) and extracellular signal-regulated kinase (ERK) (Sosa *et al*, 2014). Other pathways that also regulate breast cancer dormancy, include mitogen-stress activated kinase (MSK1) and downstream effector of p38 (Bernard *et al*, 2019). Annexin II receptor and AXL, growth arrest- specific protein 6 (GAS6) and Interleukin-6 (IL-6) may also control dormancy (Croucher *et al*, 2016).

Despite the mechanisms described previously , the precise regulation of tumour cell escape from dormancy in bone is yet to be fully determined. (Ren *et al*, 2015). However, there are a number of studies that might explain the outgrowth of the tumour after dormancy. Osteoclasts induce the reactivation of dormant cells by RANKL and TGFβ at the micro metastasis stage. Tumours stimulate osteoclast activity by secreting factors, including prostaglandin-E (PGE), transforming growth factor (TGF) α and β, epidermal growth factor (EGF), vascular endothelial growth factor (VEGF), tumour necrosis factor (TNF) and interleukins (IL) -1, -6, -8, and -11. This mechanism stimulates osteoclast activity, resulting in increased tumour proliferation which in turn leads to outgrowth of the tumour (Mundy, 2002; Rose & Siegel, 2006; Coleman *et al*, 2010). Another study shows that osteoclasts can drive the outgrowth of dormant cancer cells in bone. Increased osteoclast activity caused by ovariectomy in mice, increased tumour growth in this modal. Zoledronic acid treatment inhibited tumour growth, implicating a role for osteoclast activity (Ottewell *et al*, 2014).

1.5. The Skeleton: Environment and Cells

As described in previous sections, bone is the most common metastatic organ in BC thus needs special attention. To maintain DTC dormancy or treat MBC in skeletal tissues, the complex interactions between the healthy bone environment and BC must be clearly understood. Bone is made up of several components and niches, including the endosteal niche, haematopoietic niche, perivascular niche, immune niche, and other cell types such as adipocytes. The following sections will discuss the detailed functions of these different bone niches in healthy bone and the interactions with cancer cells that are known so far.

1.5.1. The Endosteal Niche

The endosteal niche is located along the internal surface of the bone, covering the area of trabecular and endocortical surfaces. The main niche components are the bone remodelling cells; osteoclasts (bone resorbing), osteoblasts (bone forming) and osteocytes (trapped and transformed osteoblasts in bone matrix that create networks) but also include other cells like fibroblasts (regulate haematopoiesis), macrophages (immune response, tissue regeneration and homeostasis), endothelial cells (homeostasis, first barrier against infections) and adipocytes (store and secrete fatty acids, cytokines and adipokines) that are located near to the endosteal niche. Bone remodelling occurs through life, constantly repairing micro-damage and in response to mechanical loading of bone with osteocytes (Salhotra *et al*, 2020). Underlying mechanisms for each cell type are described in detail in Sections 1.5.1.1, 1.5.1.2 and 1.5.1.3. Remodelling of healthy bone occurs in 5 steps described as follows :-(Lowe & Anderson, 2015a; Tamma & Ribatti, 2017).

1) Activation: The first step involves the recruitment and activation of osteoclast precursor cells. Osteoclast precursor cells merge with each other to form multinuclear cells that form a sealing zone underneath each osteoclast and isolate this area from surrounding bone (Hauge *et al*, 2001). Osteocyte apoptosis initiates the first signal by release of paracrine factors that induce angiogenesis and increase osteoclast and osteoblast precursor recruitment (Chen *et al*, 2015).

2) Resorption: The second phase is the resorption phase. Osteoblast and stromal cells express RANKL and macrophage colony stimulating factor (M-CSF). These factors are upregulated by parathyroid hormone (PTH) and induce osteoclast differentiation and bone resorption. Osteoclasts make the microenvironment acidic and mobilize the mineral phase of bone and through secretion of proteolytic enzymes that dissolve bone (Teitelbaum, 2000; Tolar *et al*, 2004; Wu *et al*, 2018), a detailed explanation of bone resorption is described in Section 1.5.1.1 .

3) Reversal: The third step is called as reversal, where bone formation starts.

4) Formation: Formation of new bone is the fourth phase of bone remodelling. Osteoblasts secrete osteoid matrix which is rich in Collagen type 1. Hydroxyapatite crystals are then deposited in between the collagen fibrils to mineralize the bone matrix (Kenkre & Bassett, 2018).

5) Termination: The formation phase is followed by a termination stage, when osteoblasts either terminated by apoptosis, transform to bone-lining cells or are entrapped in the bone matrix and differentiate to become osteocytes (Bonewald, 2011). In normal adult bone these processes occur at the same rate maintaining the balance between bone resorption and formation to retain bone structure and integrity and repair micro damage (Hadjidakis & Androulakis, 2006).

As it shown in the Figure 1-2, multiple factors such as insulin-like growth factors (IGFs), transforming growth factor-β (TGF-β), fibroblast growth factors, platelet-derived growth factors etc continuously secreted by bone and bone marrow cells (Mesenchymal stem cells, osteocytes, T-cells, and HSCs), thus these factors play crucial role on bone remodelling (Hiraga, 2019).

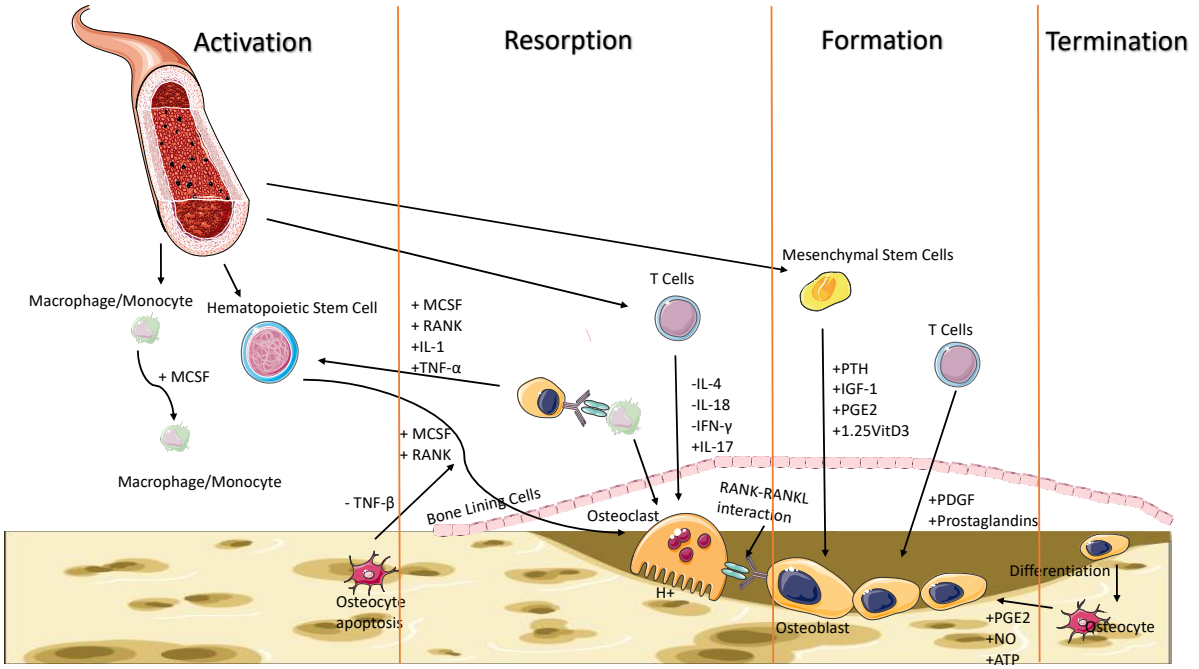

Figure 1-2: Scheme of bone remodelling stages.

Bone remodelling is a continuous process that mainly involves osteoblasts and osteoclasts. However, the key cells are insufficient to regulate entire process of bone maintenance Therefore, each stage requires factors from cells in different bone niches. The Figure represents some of the factors and cell types that play major roles in bone remodelling. (Modified from Wu et al., 2018)

1.5.1.1. Osteoclasts

Osteoclasts are multinucleated cells derived from HSC and originate from promyeloid precursors (with RANKL, OPG (Osteoprotegerin), ODF (osteoclast differentiation factor) which can be also differentiate to macrophages (by M-CFS (macrophage colony stimulating factor) or GM-CSF (granulocyte-macrophage colony stimulating factor)) or dendritic cells (with RANKL, GM-CSF, OPG (Osteoprotegerin)) (Vaananen *et al*, 2000). Osteoclasts attach to the bone surface by integrins to generate a sealing zone (Nesbitt *et al*, 1993) and creates a new membrane that has acidic vesicles that secrete H^+ (Blair *et al*, 1989; Ono & Nakashima, 2018). In these vesicles, bone mineralisation occurs (acidification phase, a process controlled by a vacuolar H^+ -adenosine triphosphates (H^+-ATPase, a proton pump). H^+-ATPase is responsible for ion transfer, releases HCl into the environment that reduces pH to ~4.5 (Teitelbaum, 2000). This acidification activates cysteine proteinase which degrades type I collagen as well as MMP-9 that degrades ECM proteins and activates tissue remodelling cytokines (IL-1β, TNF-α) (Yabluchanskiy *et al*, 2013; Ono & Nakashima, 2018).

1.5.1.2. Osteoblasts

Osteoblast are the bone forming cells that play a role in constant bone remodelling from MSCs; RUNX2, ALP and type I collagen play crucial roles in MSCs differentiation to osteoblasts (Dieudonne *et al*, 2013). When in the presence of bone inducing factors such as TGF- β and PTH, osteoblasts become active and create tight junctions in between thus creating matrix mineral deposition (Mackie, 2003; Caetano-Lopes *et al*, 2007). In the first step, they synthesise osteoids which are mostly made up of collagen type 1. After osteoid formation, calcium salts are deposited and alkaline phosphatase is secreted by osteoblasts for mineralisation (Parvizi & Kim, 2010; Lowe & Anderson, 2015a). Osteoblasts contribute to osteoclast differentiation through RANKL which is presented at their surface and binds to RANK on osteoclasts progenitors and this alongside with M-CFU secretion initiates osteoclast differentiation. They also secrete OPG which is a RANK decoy that inhibits osteoclast differentiation (Mackie, 2003).

1.5.1.3. Osteocytes

Osteocytes are differentiated osteoblasts that have become entrapped into their matrix and are produced by neighbouring osteoblasts. Continuous bone deposition covers the active osteoblasts that eventually stop secretion of osteoids (Caetano-Lopes *et al*, 2007). Osteocyte differentiation occurs in different phases, when osteoblasts start to trap into the osteoid they are in the pre-osteocyte phase, then the young and are finally mature when in the mineral phase (Dallas & Bonewald, 2010). Pre-osteocytes secrete factors like osteocalcin that inhibits mineralization and mature osteoclasts provide linking between osteocytes and bone surfaces by creating gap junctions (Bonewald, 2010). Previously, osteocytes were considered to have a role only in communication and maintaining the environment in bone by mechanical load sensing, however it is found that they are the main producer of RANKL, resulting in stimulating bone remodelling, cancer and most bone disease (Nakashima *et al*, 2011; Xiong *et al*, 2011; Bonewald, 2013). They also regulate bone remodelling by stimulation of WNT signalling with β-catenin activation (increased WNT increases osteoblast numbers), RANK and OPG pathways (increased RANK increases osteoclast and increased OPG decreases osteoclasts) (Bellido, 2014; Bellido *et al*, 2018). Osteocytes also can sense mechanical loading with cell surface integrins, hence trigger intercellular FAK that results in activation of ERK-1/2 and Akt. This stimuli is transferred by GAP junctions, ionic channels and factors like OPN thus affecting bone turnover (Takano-Yamamoto, 2014; Gusmão & Belangero, 2015). As 90% of the bone cells are osteocytes, their role in tumour cell-bone interactions requires special attention. Osteocytes can modify the endosteal niche through HSC mobilization via the CXCL12 pathway, thus might have similar

effect on bone metastasis (Asada *et al*, 2013; Atkinson & Delgado-Calle, 2019) with an *in vitro* study supporting the positive effect on breast cancer migration and proliferation (Cui *et al*, 2016).

1.5.1.4. Tumour cells and the endosteal niche

The endosteal niche is one of the components that creates the metastatic niche. As mentioned before, BC prepares the bone niche for subsequent seeding, for example by secreting lysyl oxidase (LOX) that alter homeostasis in the endosteal niche in bone that increases migration (Cox *et al*, 2015). Osteoblasts also secrete the chemokine CXCL12 that interacts with the CXCR4 receptor on osteoclast precursors thus might be playing a main role for homing of CXCR4 expressing cancer cells to bone (Ottewell, 2016). Moreover, osteoblasts produce matrix proteins TGFβ and IGF, known growth factors that attract the cancer cells that in turn produce proliferation factors that increase the number of osteoblasts (Hiraga, 2019). After the initial homing, the endosteal niche is proposed to support cancer cell dormancy with thrombospondin-1 expression by endothelial cells (Ghajar *et al*, 2013). In model systems, breast cancer cells colonising bone are found in close proximity to osteoblasts; 80% of the surrounding cells expressed ALP and 50% express Cox1 which both are osteoblastic cell markers (Haider *et al*, 2014; Wang *et al*, 2015a). *In-vitro* it is reported that tumour cells induce inflammatory cytokine production by the osteoblasts, such as IL-6, IL-8, monocyte chemoattractant protein-1 (MCP-1), macrophage-inflammatory protein 2 (MIP-2) with VEGF which suggest that these osteoblast derived cytokines might support cancer cell survival and colonization (Bussard *et al*, 2010). Junctions in between osteoblasts and tumour cells created by E- and N-cadherins, thus increasing mTOR activity in cancer cells. This interaction might be one of the routes for osteoblast regulation of breast cancer development in bone (Wang *et al*, 2015a). There are two main types of bone metastases; osteoblastic (bone forming or osteosclerotic, mainly in prostate cancer) and osteolytic (bone resorbing, mainly in breast cancer) metastasis, but mixed lytic and blastic lesions can also be found. In the osteolytic cycle, tumour cells produce activin A (a TGF-β family member), noggin, dickkopf-1 and sclerostin to suppressing osteoblast differentiation (Bernard *et al*, 2019). Osteoclasts resorb the bone matrix, resulting in release of the growth factors and calcium ions that increase homing of the cancer cells. At the end both activate RANKL system which is part of the vicious cycle supporting tumour growth in bone (Zhang *et al*, 2019) (Figure 1-3). Osteocytes are the main source of RANKL in bone (Xiong & O'Brien, 2012) and can also directly increase proliferation of cancer cells in the bone through notch signalling (Atkinson & Delgado-Calle, 2019).

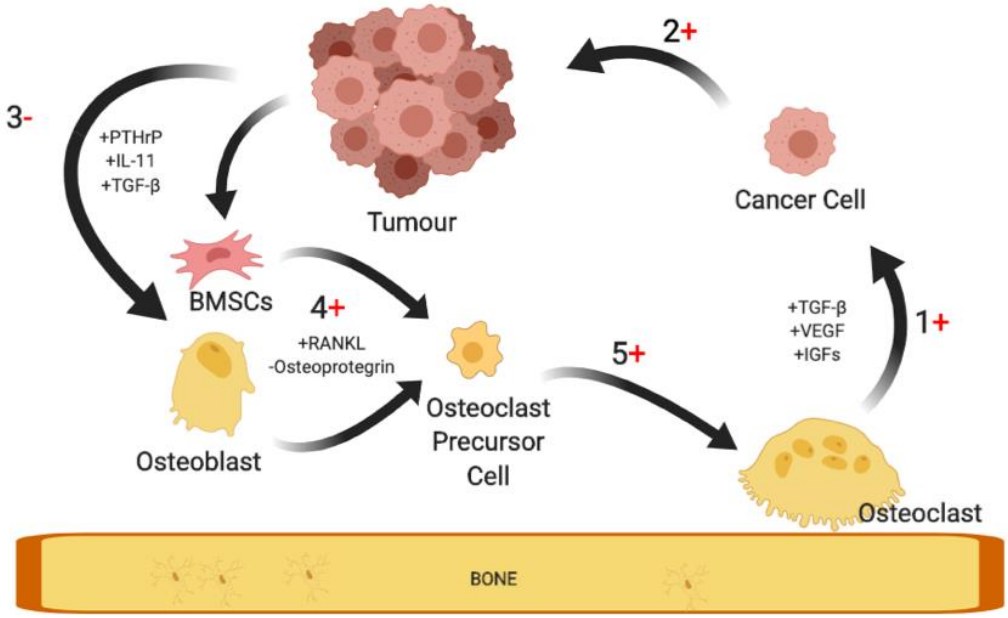

Figure 1-3: Schematic representation of the vicious cycle and associated factors.

The Vicious cycle describes a continuous process where cancer and bone cells influence each other. In the figure stimulation is indicated by + and inhibition by -. 1) Osteoclasts release growth factors that activate cancer cells 2) growth factors increase cancer cell proliferation 3) Tumour cells produce osteoclastic-stimulating factors which inhibits osteoblasts 4) that upregulates RANKL 5) RANKL promotes the osteoclastic precursor cells to form osteoclasts increasing bone resorption (modified from (Chen et al, 2010; Hiraga, 2019)).

1.5.2. The Haematopoietic Niche

The haematopoietic niche includes part of both the endosteal and perivascular niche where HSCs reside (Ugarte & Forsberg, 2013). HSCs are reside in bone marrow which is formed by mesoderm at embryonic phase and they are the source of the blood cells which is known as haematopoiesis (Wilson & Trumpp, 2006). Haematopoietic niche was described for the first time in 1978 by Schofield, as a specialised niche in bone marrow where HSC development and proliferation is regulated (Schofield, 1978). HSCs give rise to a number of different linages which can make it challenging to identify rare subpopulations, therefore, scientists have characterized HSCs in the quiescent state since they are slow-cycling, retain their DNA label with DNA damage resistance (Cheng *et al*, 2000). Quiescent populations are often found close to the interface region in between bone marrow and bone (endosteum), indicating interactions with osteoblasts. This link was demonstrated in 2003 with an *in vivo* study that showed increased HSCs by growth of trabecular bone and associated osteoblastic cell number (Calvi *et al*, 2003). Endothelial cells and pericytes are suggested to be involved in regulating HSC niches producing cell factors such as stem cell factor (SCF), which is a crucial growth factor for HSC that is required for survival, proliferation and cellular functions (Broudy, 1997). HSCs were only reduced when SCF was deleted from endothelial and pericyte cells, whereas deletion of SFC from

osteoblast or HSCs did not alter HSCs in bone marrow (Ding *et al*, 2012). HSCs and their interactions with other cell types in the niche are detailed in the following section.

1.5.2.1. Haematopoietic Stem Cells

The formation of new blood cells is called haematopoiesis, a continuous process where pluripotent stem cells multiply to produce new pluripotent stem cells and precursor cells which become mature blood cells (Figure 1-4). All the precursors of blood cells are produced by hematopoietic stem cells (HSCs) are the progenitor of blood cells and capable of self-renewal, differentiation, and proliferation. Despite the rare percentage (around 0.01%) in bone marrow, they are related to multiple cell types (Challen *et al*, 2009; Forest *et al*, 2013; Lowe & Anderson, 2015a).

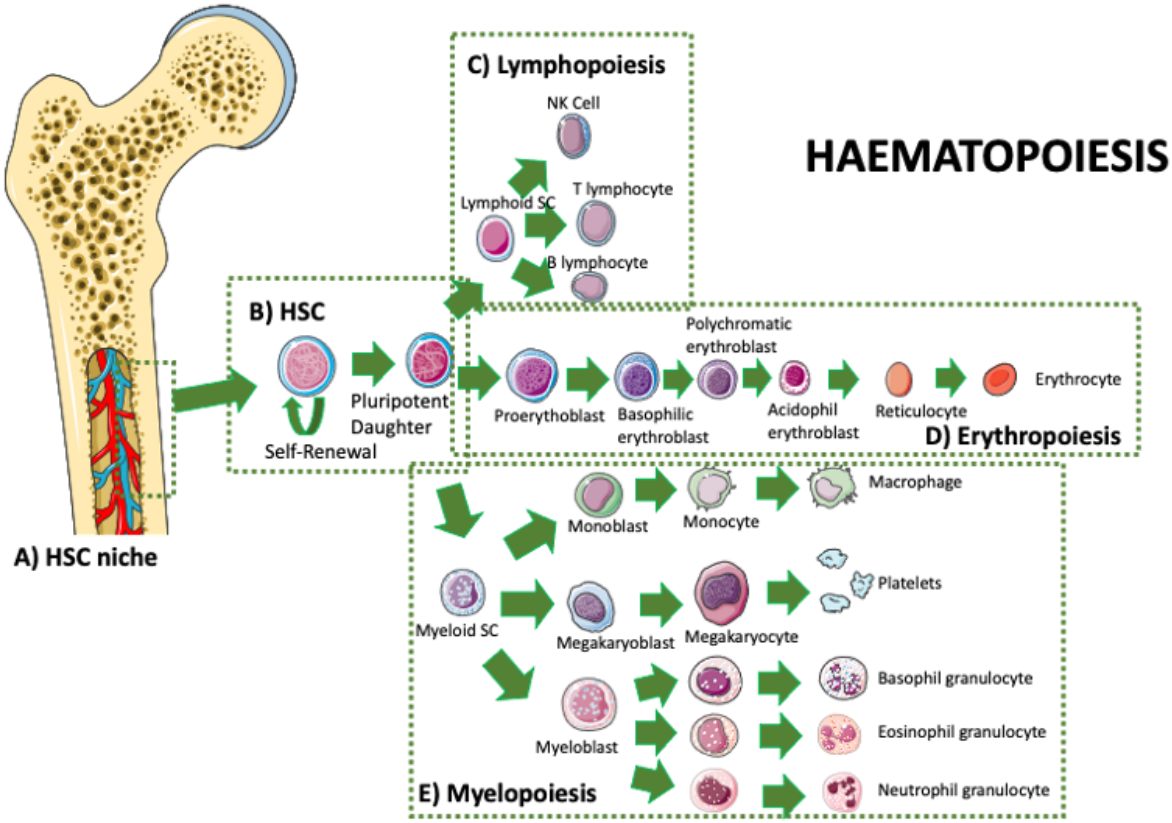

Figure 1-4: Haematopoiesis; formation of new blood cells from HSC progenitors.

Haematopoiesis is the process of new blood cell formation from HSCs. ***A)*** *HSCs are located in between endosteal and perivascular niche which is known as HSC niche,* ***B)*** *while they are keeping their DNA undamaged and telomerase length with self-renewal, they also divide into pluripotent daughter cells that can follow either* ***C)*** *lymphopoiesis which is production of adaptive immune cells (NK, T and B Cells.),* ***D)*** *Erythropoiesis; production of O_2 and CO_2 carrier erythrocyte or* ***E)*** *Myelopoiesis which is production of innate immune cells such as macrophages, platelets and granulocytes (Figure created with images from Servier Medical Art).*

HSCs maintenance requires growth factors such as SFC and CXCL12. SCF binds to the Kit receptor on HSCs thus increases survival and self-renewal. HSCs are depleted in steel mutant mice bone marrow which is missing its membrane-bound SCF, demonstrating that SCF/Kit binding is important for haematopoiesis (Barker, 1997). SCF is mainly produced by perivascular cells (pericytes and smooth muscle cells) and endothelial cells and expression is not detected in osteoblast or HSCs (Ding *et al*, 2012). CXCL12 (produced by endothelial cells and osteoblasts (Broxmeyer, 2008)) regulates HSC maintenance alongside with anchoring HSCs from blood in to the bone marrow, therefore, deletion of CXCL12 results in HSCs depletion (Sugiyama *et al*, 2006). Other important factors required for HSCs maintenance is thrombopoietin (TPO, produced by bone marrow stromal cells (Nagahisa *et al*, 1996)) which activates myeloproliferative leukaemia (MPL) protein on HSC cells. Both molecules are important for HSCs maintenance because, when either MPL (Kimura *et al*, 1998) or TPO is deleted from hepatocytes (since hepatocytes secrete TPO to the circulation) this effects bone marrow HSCs (Decker *et al*, 2018) therefore, HSCs in the bone marrow are depleted. Additional growth factors have been shown to modify HSCs in response to bone injury. Angiogenin, angiopoietin-like 3, FGF1, FGF2, IL-6, Notch 2 and pleiotrophin increased and suggested to promote HSCs regeneration during bone injury. However, it is unclear whether these are produced by HSCs niche cells or other bone marrow cells, therefore understanding the response to injury might help for future research (Crane *et al*, 2017).

1.5.2.2. Tumour cells and the HSC niche

Breast cancer metastasis to bone begins with the homing of cancer cells that have escaped the primary tumour site exiting into the circulation, followed by potential competition with HSCs for space in the bone niches. Previous studies have shown that the breast cancer metastatic niche overlaps with HSC niche in model systems (Allocca *et al*, 2019). HSCs migration from blood to bone marrow is achieved by CXCR4/CXCL12 and Annexin 2 (cell attachment factor) which is a chemoattractant in the HSC microenvironment, hence, breast cancer might use the same pathway for bone migration (Jung *et al*, 2007; Forest *et al*, 2013). The ability to enter a state of quiescence (or dormancy) is important for both HSCs and cancer cells in order for their survival and maintenance, therefore factors that control quiescence of HSCs, such as low oxygen or supports its growth such as FGF and angiogenin may also regulate tumour cell dormancy (Schuettpelz & Link, 2011; Decker *et al*, 2016). Several studies have been carried out to determine the effects of modifying the HSC niche on disseminated tumour cells. Administration of AMD3100 (a CXCR4 antagonist) in a breast cancer model system resulted in mobilisation of HSC progenitors from bone marrow to the circulation, but whether

this would result in increased number of and/or earlier development of overt bone metastases remains to be established (Allocca *et al*, 2019).

CXCR4/CXCL12 (Stromal cell-derived factor-1, SDF-1) interaction have effects on multiple pathways related to chemotaxis, cell proliferation, cell survival, cancer survival, angiogenesis etc. CXCR4 is expressed on many cell types, including HSCs, lymphocytes, epithelial cells, and cancer cells. Despite many other chemokines, CXCR4 is only activated by CXCL12 which allows modification of this interaction by binding AMD3100 to CXCR4 (Rosenkilde *et al*, 2004; Teicher & Fricker, 2010). Granulocyte colony-stimulating factor (G-CSF) is used for promoting HSCs in bone marrow and despite a of lack of understanding of the precise mechanisms, it is found that G-CSF reduce CXCL12 which results in increased HSCs mobilisation from bone marrow in murine models (Petit *et al*, 2002). Lee et al. (2014), investigated the effectiveness of AMD3100 and G-CSF on C57BL/6J and BALB/c mice (both aged 8-12 weeks). Both of these studies show a significant increase in the number HSCs colonies from PB which indicates AMD3100 mobilise HSCs from bone marrow. Lee et al. (2014), also showed that G-CSF is better mobilizer for both murine strains but AMD3100 works better on C57BL/6J. They conclude AMD3100 mediated mobilization depends on bone marrow stem/progenitor cells (BMSPCs) since they found C57BL/6J have significantly increased BMSPCs when compared to BALB/c strain (Lee *et al*, 2014a) . These studies indicate that the murine model system, as well as the pharmacological agent used to mobilise HSCs, may result in differential effects on the HSC niche and potentially also on the DTCs located there.

1.5.3. The Perivascular Niche

Bone is a highly vascularized tissue and endothelial cells (ECs) are the central component of bone marrow vascular microenvironment, having major roles in osteogenesis and haematopoiesis (Ding *et al*, 2012; Galán-Díez & Kousteni, 2018). Bone vessels are structured by molecularly and structurally distinct arteries and sinusoidal capillaries. Arteries covers the central diaphysis and branches to the endothelium with type L sinusoidal capillaries and type H vessels to the metaphysis region (Ramasamy, 2017). H vessels and L sinusoids are made up of several types of endothelial cells, H type endothelial cells are strongly positive for CD31 (PECAM1) and Endomucin compared to sinusoidal vessels named as L type. Type H endothelial cells have a strong relationship with osteoprogenitor cells. H vessels produce factors such as RANKL, HIF, VEGF thus they stimulate proliferation and differentiation of osteoprogenitors. Therefore, osteoprogenitors are found in abundance around H vessels and loss of type H endothelium can be observed during ageing alongside a reduction in the number of osteoprogenitor cells (Kusumbe *et al*, 2014; Ramasamy, 2017). H type endothelial cells are important for cancer development in bone since they mediate neo-angiogenesis (Kusumbe *et al*,

2014). The perivascular niche includes the area that is around the vascular structure and consists of ECs and pericytes. ECs have various roles, from initiating homing of cancer cells to the development of a mature fully growth tumour (Zhang *et al*, 2019). Endothelium and pericytes produce angiocrine factors, including stromal cell-derived factor 1/C-X-C motif chemokine 12 (SDF1/CXCL 12) and stem cell factor (SCF), that support hematopoietic stem cells (Ramasamy *et al*, 2015). However, a recent study with triple negative and ER+ MBC murine models showed that DTC fate does not depend on vessel structures. It was found that BC cells showed bias to H type vessels in an outgrowth model (ovariectomized mice) but bias to L type vessels in an indolence model (sham operated mice) (Hughes *et al*, 2021). It is important to note that the H/L vessel structures defined in murine models have not been shown in humans yet, and it is possible that different vessel subtypes have different effects on tumour cells located in the bone microenvironment.

1.5.3.1. Endothelial Cells

As mentioned above, bone marrow endothelial cells (EC) form a major part of the vascular structures, secreting growth factors or inhibitory factors that play crucial roles in haematopoiesis. Sinusoidal ECs express E-selectin that supports HSC differentiation and mobilization (He *et al*, 2014). While the osteoblastic niche provides HSCs with a quiescent microenvironment, sinusoidal ECs provide proliferative cues. Bone marrow ECs secrete factors like CXCL12 (which activates adhesion molecules therefore increases stromal migration of HSCs) (Sugiyama *et al*, 2006), whereas endothelial cells promote HSC expansion through Akt and p42/44 MAPK cell regulation pathways. Akt activation promotes self-renewal factors such as FGF2, IGFBP2 and downregulates inhibition factors such as Ang2 and dickkopf-1 (a WNT signalling pathway inhibitor) (Kobayashi *et al*, 2010). Despite the low effect of only MAPK activation on HSC differentiation, activation of both in ECs increases activation of Notch ligands, hence accelerates HSC differentiation (Mangialardi *et al*, 2016). Vascular ECs mainly secrete factors that regulate self-renewal and regeneration such as stem cell factor (SCF), E-Selectin, Glycoprotein 130 (gp130) and pleiotrophin (PTN) (He *et al*, 2014).

1.5.3.2. Pericytes

Pericytes were originally believed to only function as endothelial cell support to maintain the structural integrity of the vasculature, however recent discoveries have revealed other important pericyte functions. Pericytes share a common basement membrane with endothelial cells, and they are connected to each other through cell-cell junctions. Both cell types secrete factors that support adhesion of ECs and pericytes to the basement membrane (Kloc *et al*, 2015). Pericytes in bone marrow can be divided into two categories according to their anatomical position; perisinusoidal pericytes

(expressing CD146 [Melanoma cell adhesion molecule: MCAM]) secrete factors such as SCF, CXCL-12, Notch ligands, TGF-β and Angiopoietin and active HSCs can be found this area (Mangialardi *et al*, 2016). In contrast, periarteriolar pericytes express CD146 and β-adrenergic receptor; suggesting that they might be involved in HSC trafficking since downregulation of the β-adrenergic receptor gene resulted in significant HSCs reduction (Méndez-Ferrer *et al*, 2010). Deletion of SCF and CXCL-12 from mice resulted in HSC depletion and periarteriolar pericytes secrete SCF and CXCL-12 which might play a critical role for quiescence HSC maintenance (Sugiyama *et al*, 2006; Ding *et al*, 2012). Taken together, these data support interactions between pericytes and HSC through the CXCL12 pathway but whether DTC interact directly with pericytes remains to be established.

1.5.3.3. Tumour cell interactions with the bone microvasculature

The cell populations of the vascular niche and the molecules they produce have several different effects on cancer cells, creating a supportive microenvironment and the homing of disseminated tumour cells. The sinusoids (type L capillaries) have a large diameter and spread through the bone. This vessel has a specialized two-way permeability for hematopoietic cells, these characteristics are supporting tumour dissemination (Kusumbe, 2016). HSCs are located in close proximity to the vascular structures (Kunisaki & Frenette, 2014) that express E-selectin to maintain HSC dormancy, self-renewal and proliferation cell (Winkler *et al*, 2012). These dormancy-inducing effects on hematopoietic stem cells are proposed to have similar effects on DTCs in bone, yet this still needs to be confirmed in humans (Kusumbe, 2016). As described previously, peri-vascular niche cells have an impact on HSC migration with factors such as SCF, CXCL-12, thus they might also attract disseminated BC cells to bone (Kusumbe, 2016). Cancer cells can also use the mechanisms that maintain HSC quiescence , as described in the dormancy section 1.4.2.1. Ghajar et al. (2013), found increased expression of dormancy-supporting TSP-1 around the neovascular tips secreted from endothelial cells. Also, sprouting vessels produce factors such as periostin and TGFβ-1 which reactivate the dormant cancer cells (Ghajar *et al*, 2013), hence these factors support the vascularisation of the growing tumour after activation (Kusumbe, 2016). Collectively, data from model systems suggest that bone marrow vascular cells may have separate roles through progression of tumour growth in bone, with the capacity to affect dissemination, survival, dormancy, and progression.

1.5.4. The Immune Niche – role in bone metastasis

The relationship between the immune system and cancer has been studied for many years, immune cells either eliminate cancer cells, keep them in the equilibrium phase or cancer cells can escape from the immune cells in various ways and in some cases they can use immune cells to grow (Pandya *et al*, 2016). Since one of the main source for immune cells is bone marrow, this makes the relationship between immune cells and cancer cells more complicated as tumours can interfere with immune cell production and maintenance (Xiang & Gilkes, 2019). The immune system can be divided into 2 different categories: one responsible for innate immunity and the other for the adaptive immune response (Figure 1-5). The innate immune system works as a general defence mechanism, whereas the adaptive immune system works as a specialized defence. Both systems serve the same purpose but in different ways, with innate immunity protecting against foreign bodies, injuries and pathogens whereas adaptive immunity protects against specific pathogens or changed cells, which will be covered in detail in the next sections 1.5.4.1 and 1.5.4.2 (Janeway *et al*, 2001). Breast cancer cells can develop immune suppression through cross-talk with mesenchymal stem cells (MSCs), secreting chemokines, cytokines and growth factors such TNF-α, CXCL5 and CXCL12 that stimulate production of CSF1 which in turn recruit TAMs and myeloid derived suppressor cells (MDSCs) (Hill *et al*, 2017). *In-vitro* proliferation and transmigration assays of MSC and BCs showed that MSCs recruit regulatory T-cells, which have immunosuppressive activities in the tumour microenvironment, indicating this phenomena might be true in bone tumours (Patel *et al*, 2010). BCCs recruit mesenchymal stem cells to the primary tumour site where MSCs release cytokines that support the survival of cancer cells, which in turn attracts the immune suppressor cells. During metastasis, tumour stroma cells secrete MCP-1 that increase macrophage proliferation (Walker *et al*, 2016). At the early stages of tumour development, the innate and adaptive immune systems eliminate single tumour cells and small colonies (micrometastases). Surviving cancer cells begin to proliferate, with clones starting to manage the tumour antigens and MHC class I molecules by changing their surface proteins. Once established, the tumour starts to suppress T-cell activity (Calì *et al*, 2017). This requires multiple interacting processes, including production of granulocytes, lymphocyte precursors and initial B-cell maturation that all occur in the bone marrow, hence, it makes the immune niche an important regulatory component of the metastatic process (Lowe & Anderson, 2015b). After early development, T cells migrate to the thymus and B cells remain in bone marrow for maturation; many B cells migrate from the bone marrow but some remain associated with sinusoidal endothelial cells and contribute to immunoglobulin diversity (Pereira *et al*, 2009). Returning B cells mature and serve as antibody-secreting plasma cells (Benner *et al*, 1974). Dendritic cells in the bone marrow supports the naive B cells with survival factors such as macrophage migration inhibitory factor (Sapoznikov *et al*, 2008).

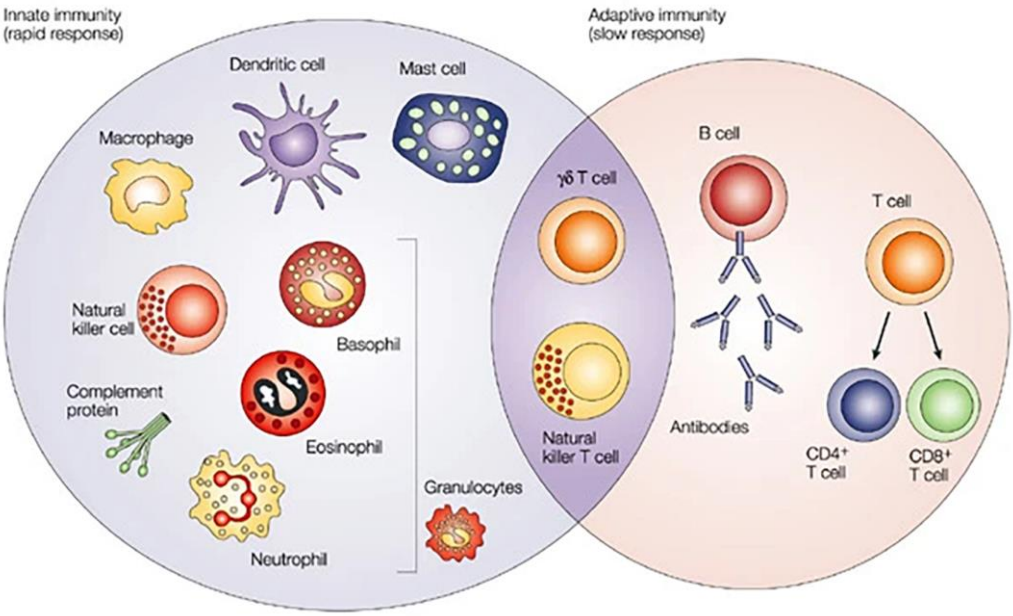

Figure 1-5: Innate and Adaptive Immune Cells.

Components of innate and adaptive response; innate immunity is the first line defence system where cells quickly detect foreign materials and eliminates it and includes NK cells, granulocytes, macrophages, dendritic cells. Adaptive immunity is a slower process providing specific defence and memory against foreign materials and includes B and T cells alongside antibodies. NK/T and γδT sub-lymphocyte cells are the bridge between both systems. Reprinted and reused by permission from Springer Nature: (Dranoff, 2004)

1.5.4.1. The innate immune system

Innate immunity is a non-specific process to target foreign pathogens, destroyed or neutralized by complement, interferon, cytokines, natural killer cells, neutrophils, and macrophages which can recognize the cancer cells through their surface molecules. The major cell types of the innate system that directly target cancer are natural killer cells, macrophages, neutrophils and dendritic cells (Liu & Zeng, 2012). Innate immunity has two key stages: recognition and elimination. Pattern recognition receptors on macrophages detect the 'foreign' molecules which are not part of the host (Delves *et al*, 2017). This detection can lead to direct lysis of pathogen or production of cytokines, chemokines and antimicrobial proteins that attract monocytes and neutrophils from the blood system to eliminate pathogens. After this stage, innate immunity triggers adaptive immunity, as dendritic cells mature to antigen-presenting cells (APCs) that capture and process the foreign molecules and present to the adaptive immune cells (T lymphocytes) (Shortman & Liu, 2002). There are 2 main subsets of T lymphocytes, $CD4^+$ T cells (Helper T and Regulatory T cells) and $CD8^+$ cells (Cytotoxic T cells). APCs bind to helper T cells through CD4 and the MHC II/Epitope-T cell receptor; this activates both cells to release cytokines which clone T cells to $CD4^+$ and $CD8^+$ T cells. B cells recognise foreign antigens and produce fragments that present antibodies that are recognised and

activate T cells. When a cell is infected, it presents some fragments of a foreign body with its MHC I; when $CD8^+$ T cells recognise that MHC I/Epitope structure it produces perforins (produce pores on cell membrane) and granzymes (break down proteins inside the cell) that lyse the infected cell (Charles *et al*, 2001; Janeway *et al*, 2001).

Natural killer cells generally recognize cancer cells through their NKG2D, CD16 and DNAM1 receptors that detect cancer cell surface ligands, resulting in their elimination (Janssen *et al*, 2017). MHC cell surface protein is another recognition pathway for NK cells; when this surface protein is missing, they destroy the cells with granule mediated exocytosis and Fas-Fas ligand interactions (Wu & Lanier, 2003). The role of NK cells in the BME is still not fully understood; current approaches are focused on the known cancer effecting factors. Mayol et al. (2011) studied NK trafficking from the bone marrow and found that maturation of NK cells was associated with downregulation of CXCR4 and upregulation of S1P5, which can increase mobilisation from BM (Mayol *et al*, 2011). NK cells can inhibit osteoclastogenesis with the MHC proteins since OCs have a lower surface MHC and secrete factors (IL12, IL15 and IL18) that induce cytotoxic NK cells (Tseng *et al*, 2015). In addition, NK cells express both RANKL and MCSF and are found to stimulate osteoclastogenesis in models of inflammatory arthritis (Söderström *et al*, 2010).

Macrophages have both pro- and anti-inflammatory effects in the bone marrow. The pro-inflammatory effects are mediated through secretion of cytokines IL-1, IL-6, IL-23, IL-12 and INF-γ that activate NK and T cells to destroy the cancer cells (Mantovani & Sica, 2010). The anti-inflammatory effects are mediated by tumour associated macrophages (TAMs), that have an important role in tumour progression (Lee *et al*, 2013). They secrete high levels of IL-10 and TGF-β that decrease the activation of cytotoxic T cells and using the chemokine CCL2 they induce breast cell colonisation to the bone and lung (Xiang & Gilkes, 2019). A recent murine model study showed that monocyte/macrophages expressing CD137 induce breast cancer metastasis with differentiation to osteoclasts, thus might contribute to the vicious cycle (Jiang *et al*, 2019). Also, decreasing the monocytes/macrophages in murine models by treating with clodronate encapsulated in liposomes resulted in inhibition of bone and muscle metastasis of lung cancer, suggesting that macrophages play an important role in metastasis (Hiraoka *et al*, 2008). Another mechanism in which TAMs might be involved in bone metastasis is through the CXCL10/CXCR3 pathway. Silencing CXCR3 in melanoma cancer cells or neutralising CXCL10 suppressed bone metastasis and *in-vitro* cocultures of BC cells with bone marrow macrophages revealed that cancer cells promote macrophage production of CXCL10, suggesting cancer cells might stimulate this pathway to induce tumour progression (Lee *et al*, 2012).

Neutrophils are granulocytes that are attracted to the cytokines produced by macrophages and are proposed to have multiple roles in cancer progression, including in regulating steps of the metastatic cascade, comprehensively reviewed by Coffelt (Coffelt *et al*, 2016).Neutrophils are abundant in the bone marrow, and the CXCRL4/CXCL12 signalling pathway is used to control neutrophils. They release CXCR4, VEGF and MMP-9, factors shown to have effect on cancer metastasis in bone (Xiang & Gilkes, 2019). Progression of prostate cancer and breast cancer to bone may involve similar pathways and *in-vivo* elimination of neutrophils resulted in increased prostate tumour growth in bone and expression of STAT5 by tumour cells, a prostate cancer promotor transcription factor, found to be suppressed by neutrophils (Costanzo-Garvey *et al*, 2020). Despite our limited knowledge of neutrophils in breast cancer bone metastasis, we know they can affect several mechanisms related with growth and initiation of different tumour types as demonstrated in murine and/or clinical studies. Neutrophils can interact with cancer cells in a number of ways; through production of ROS, RNS and proteases (Antonio *et al*, 2015); promote growth by crosstalk when activated by IL-17 secreting $CD4^+$ T cells (Charles *et al*, 2009) and activating senescent cancer cells to promote by IL1RA (Di Mitri *et al*, 2014); stimulate tumour progression by activating PI3K signalling (Houghton *et al*, 2010) and immunosuppression (Bodogai *et al*, 2015); modify the extracellular matrix via BV8 production and induce angiogenesis by activating VEGFA with MMP9 (Shojaei *et al*, 2007; Deryugina *et al*, 2014). All these findings indicate the importance of neutrophils in cancer development and tumour progression, hence, understanding their behaviour in BC bone metastasis might help us to develop better treatments.

1.5.4.2. The adaptive immune system

In contrast to the innate immune system that detects an unfamiliar molecule without the need for antigen recognition, the adaptive system requires the recognition of a specific antigen. Lymphocytes are the main components of the adaptive immune system with the help of dendritic cells and can be divided into 2 sub-groups; T- and B- cells (Lowe & Anderson, 2015c).

T cells make up 80 % of the lymphocytes in the bone marrow; cytotoxic T cells, Regulatory T cells and T helper cells are the main T cell types (Xiang & Gilkes, 2019). ***Cytotoxic T cells*** recognize MHC proteins on the host cell surface and sometimes cancer mutations result in the loss of these proteins. When cytotoxic T cells can not recognize the host MHC proteins, they induce cell apoptosis with fas-fas ligand or destruct the tumour cells by perforin-granzyme B (Janssen *et al*, 2017).

Regulatory T cells regulate cell trafficking to the bone marrow through CXCR4/CXCL2 signalling and they are also one of the major sources for RANKL, a molecule that is central to regulating

bone turnover. Since RANKL is an important cytokine for metastasis, Tregs might have an effect on disseminated tumour cell metastasis to bone marrow (Xiang & Gilkes, 2019). Another T cell subgroup is ***T helper cells***. T helper cells secrete RANK and IL-17, where IL-17 has been shown as a key regulator of OPG and RANKL balance by increasing RANKL and decreasing OPG production in several studies (Nakashima *et al*, 2000; Lubberts *et al*, 2003; Liu *et al*, 2015). Monteiro et al. (2013), created a primary mouse mammary cancer model by injecting 10^4 4T1 or 67NR cells into the mammary fat pads and achieved spontaneous metastasis in BALB/c mice. After 11 days, $CD3^+$ T cells were harvested from animals with bone metastasis and transferred to BALB/c nude mice with 4T1 cells to determine if T cells are responsible for early bone loss. Results indicated that T cells derived from 4T1-bearing mice induced bone loss in the presence of tumour antigens but without the tumour present. Also, they knocked down RANKL expression in T cells from 4T1 bearing mice and metastasis to lymph nodes was reduced by 5% and metastasis to bone was prevented. These findings highlight the importance of $RANKL^+$ T cells in bone metastasis (Monteiro *et al*, 2013).

B Cells turn into plasma cells which are responsible for humoral immunity where they secrete antibodies or immunoglobulins. In the adaptive immune system, B cells recognise foreign antigens with IgM on their surface and start to secrete antibodies that tag foreign bodies (Lowe & Anderson, 2015c). $CD4^+$ T cells recognise the B cells with fragments and produce cytokines that induce B cells proliferation to plasma cells (that produce antibody) and memory-B cells which can survive and rapidly proliferate in case of re-encounter with the same pathogen. However, the role of B cells in cancer progression is not clear. B cells were found increased in the blood of the breast cancer patients which indicates the importance of this population (Tsuda *et al*, 2018). In the murine models for cancer cell and B cell interaction, tumour growth is promoted by B cell-derived lymphotoxin; an angiogenesis inducing factor (Ammirante *et al*, 2010). Breast cancer cells can also induce a B-cell precursor population in blood by secreting thymic stromal lymphopoietin; a cytokine that also plays an important role in T cell maturation, B cell expansion and differentiation (He & Geha, 2010; Ragonnaud *et al*, 2019). Multiple myeloma (MM), a plasma cell malignancy that occurs in the bone marrow, is characterised by proliferation of B cells, and is associated with extensive lytic bone lesions, renal impairment and anaemia in patients. Plasma cells secrete factors such as RANKL, IL-1, IL-3 etc. and are found adjacent to osteoclasts which indicates direct cell-cell contact. This explains the increased osteoclastic activation, osteolytic bone lesions and the resulting hypercalcaemia in patients. Since MM-induced bone disease can cause skeletal related events, bone-targeted agents like denosumab and bisphosphonates are used to reduce such events (Edwards *et al*, 2008; van de Donk *et al*, 2021).

Dendritic cells are known as the antigen presenting cells (ACPs) in the adaptive immune system, as they induce cytotoxic T cell activation by presenting foreign antigens. Since they induce both T cell activation and proliferation, DCs have important roles in anti-tumour responses (Xiang & Gilkes, 2019). Dendritic cells secrete TGF-β, nitric oxide, IL-10, VEGF and arginase that supress the cytotoxic T cells and this mechanism might increase the tumour survival in bone marrow (Capietto & Faccio, 2014).

One of the challenges for increased understanding of the role of immune cells in bone metastasis is that the *in vivo* models developed to study metastasis often use human cancer cells injected into immunodeficient (mainly T cell deficient) mice and some models are lacking B cells. This situation makes it harder to understand the role of the adaptive immune system on bone metastasis (Buenrostro *et al*, 2014).

1.5.5. Osteoimmunology: immune and bone cell interactions

The term 'Osteoimmunology' was first used by Arron and Choi (2000) to describe the regulation of osteoclastogenesis by T cells in autoimmune arthritis (Arron & Choi, 2000). It was known that bone and the immune system shared the same environment, but studies now focused on immune cells during bone damage and found that immune and bone systems share a variety of molecules, including RANK, RANKL, OPG, M-CSF (Lorenzo *et al*, 2008). Studies show that depletion of CXCL12 in osteoblasts reduce B lymphoid progenitor numbers in the bone marrow (Greenbaum *et al*, 2013) and osteoblasts express Notch ligand delta-like 4 which supports T cell progenitors development (Yu *et al*, 2015). These findings indicate that osteoblasts support immune cell differentiation. A study investigated osteoblasts in sepsis using a caecal ligation and puncture model and showed that osteoblasts were ablated thus bone volume rapidly reduced. IL-7 expression by osteoblasts was decreased and additional IL-7 administration reduced the bone loss reduction (Terashima *et al*, 2016). Previous studies pointed out the importance of IL-7 in lymphocyte activation to survival from sepsis (Unsinger *et al*, 2010; Venet *et al*, 2012), thus these findings confirm the importance of osteoblast derived IL-7 on lymphoid progenitors. On the other hand, several cytokines which are also found in the immune system have known effects on osteoblast regulation, such as TNFα (inhibits osteoblast differentiation and collagen synthesis), IL-1, IFN-γ (inhibits collagen synthesis) (Lorenzo *et al*, 2008). In addition, activated T cells produce factors that induce alkaline phosphatase activity in bone marrow stromal cells, thus triggers rapid differentiation to mature osteoblasts such as upregulation of osteocalcin and Runx2 (Rifas *et al*, 2003). Numerous other cytokines are known to affect both bone turnover and the immune system as reviewed by Lorenzo et al.(Lorenzo *et al*, 2008) and Tsukasaki et al. (Tsukasaki & Takayanagi, 2019).

1.5.6. *In vivo* models of breast cancer bone metastasis

Around 70% of advanced breast cancer patients develop bone metastasis; however, bone metastasis progresses slowly in humans, often developing many years after initial treatment and is only detected when patients have advanced, symptomatic bone lesions (Bussard *et al*, 2008). Understanding the possible mechanisms that underpin bone metastasis might reveal new targets to improve the disease outcome and patients' quality of life. It is impossible to obtain sufficient quality and quantity of bone metastasis samples from patients, therefore well-characterised *in vivo* models required for studies of breast cancer bone metastasis.

Most bone metastasis models have used mice, as they are widely available and have short lifespans. However, spontaneous bone metastasis rarely occur in mice and studies using *in vivo* models may miss some essential molecules that drive development of human bone metastasis (Mundy, 2002). Complex interactions between the tumour and the BME, the involvement of various signalling pathways, and multiple different sub-types of breast cancers are some reasons for developing multiple different *in vivo* models (Ottewell & Lawson, 2021).

Table 1-7: Murine models of breast cancer bone metastasis.

Commonly used murine models that have been used to study breast cancer bone metastasis. Each model is given with the specific cell type, injection route, lesion type and required time to achieve that lesion, ratio of successful skeletal metastasis and metastatic site if occurs. IC: Intracardiac, IV: Intravenous, IT: Intratibial, O: Orthotopic, PDX: Patient-Derived Xenografts

Cell Type	Route	Lesion Type	Metastatic Site/Frequency
Xenograft Models			
MDA-MB-231	IC	Osteolytic (3-5 Weeks)	Long bones, spine, and jaw/ 60-90%
MDA-MB-231IV	IV	Osteolytic (2-3 Weeks)	Long bones and spine/ 80-90%
B02	IV	Osteolytic (2-3 Weeks)	Long bones, spine, and jaw/ 90%
MDA-MB-231	IT	Osteolytic (2-4 Weeks)	Long Bones/ 100%
PDX (BB2RC08)	IC,O	Osteolytic (14+ Weeks)	Long bones, lungs, human bone explants/ IC:80% to human explant, 20% to mice long bone O:100% to human explant, 80% to mice long bone
PDX (BB3RC32)	IC,O	Osteolytic (15+ Weeks)	Long bones, lungs, human bone explants/ IC:80% to human explant, 75% to mice long bone O:100% to human explant, 80% to mice long bone
PDX (BB6RC37)	IC,O	Osteolytic (12+ Weeks)	Long bones, lungs, human bone explants/ IC:30% to human explant, 20% to mice long bone O:20% to human explant, 30% to mice long bone
Syngenetic Models			
4T1	O	Osteolytic (3-4 Weeks)	Long bones, spine, jaw, lungs, and spleen/ 20%
4T1-2	IC	Osteolytic (2-3 Weeks)	Long bones, spine, jaw, and spleen/ 40-60%

No perfect model represents the entire bone metastasis process; therefore, several different models has been developed to address specific hypotheses (Table 1-7). Models can be categorised into two main groups, xenograft and syngenetic. Since human breast cancer cells' genetic and phenotypic properties are different from mouse mammary carcinoma, human breast cancer cells injected in immunodeficient mice (xenografts) were developed (Reviewed by Tulotta *et al*, 2019a). These mice have suppressed immune systems due to various mechanisms; lacking thymus due to the

Foxn1 gene mutation resulted in unmatured T lymphocytes. This mutation also resulted in fur loss, and this BALB/c strain was named "Nude" mice (Flanagan, 1966; Nehls *et al*, 1994). A limitation is that the immune system is also involved in different stages of disease development and progression; however, it is impossible to study human disease in mice with an intact immune system due to rejection of the human cancer cells. Therefore, syngenetic models of mouse mammary cancer have been used to investigate the role of the immune system in bone metastasis (Ottewell & Lawson, 2021).

The majority of published studies use xenograft models, where human breast cancer cells are modified to express green fluorescence (GFP), luciferase (Luc) or other markers to allow *in vivo* monitoring of tumour growth (Tulotta *et al*, 2019a). Generally, Nude mice are used with human breast cancer cells introduced via different injection routes (intracardiac, intravenous, intratibial) to generate skeletal metastasis, sometimes using bone-seeking tumour cell variants (Tulotta *et al*, 2019b, 2019a). Patient-derived xenografts are also used, and severe immunodeficient NOD SCID mice are used in those cases. These mice have defective T and B lymphocytes and reduced NK and myeloid cells (Ottewell & Lawson, 2021).

Disease progression differs between models, depending on the injection route and breast cancer cell type. Intracardiac injection of cancer cells into the left ventricle creates an early bone metastatic model, without complications caused by a primary tumour or visceral metastasis development (Wright *et al*, 2016). Alternatively, the isolation of bone-seeking tumour cell clones allows for intravenous injection, resulting in bone metastasis (Peyruchaud *et al*, 2001). Finally, another method that can be used is directly injecting the cancer cells into the long bone, bypassing homing and colonisation and allowing investigation of the late stage of the disease (Rose *et al*, 2007).

There are multiple types of breast cancer that may have different interactions with the BME. The most common method to study bone metastasis is injecting triple negative human breast cancer cell lines via i.c. route to young (4-8 weeks old) immunocompromised mice (Ottewell & Lawson, 2021). Injecting human triple-negative breast cancer cell lines (e.g. MDA-MB-231) (via i.c.) to immunodeficient mice results in osteolytic bone metastasis (long bones, spine and jaws) within 3-5 weeks (Brown *et al*, 2012; Wright *et al*, 2016; Allocca *et al*, 2019). It is a reproducible model, with 60-90% of the animals developing tumour growth in the long bones without extra-skeletal involvement, hence was the main model chosen for my studies of the impact of tumour growth on bone (Chapter 3). On the other hand, there are several disadvantages; most patients have ER+ skeletal tumours, whereas triple-negative breast cancer lacks hormone receptors. Skeletal metastasis has a long dormancy phase but outgrown is short in this model, therefore lacking the dormancy phase. I.c.

injections require technical expertise, and around 10% of the mice can die due to stroke or hind limb paralysis (caused by tumour cells getting stuck in the circulation; thus, careful preparation including pre-filtration of the cells is required before injection to reduce this risk). Finally, the immunocompromised models lack representation of the immune populations; therefore, this must be considered when interpreting the results (Wright *et al*, 2016; Tulotta *et al*, 2019a; Ottewell & Lawson, 2021). Another model using triple negative MDA-MB-231 cells is an intratibial injection (1-2x10^5 cells) to Nude mice, resulting in extensive osteolytic disease. This model is suitable for studies of the late stage of the disease, but one significant major disadvantage with it damages the bone during the injection and tumour cells frequently spill out of the bone and grow in the surrounding muscle (Zheng *et al*, 2007; Ottewell & Lawson, 2021). Peyruchaud *et al* have developed bone-seeking MDA-MB-231, called B02, and intra-arterial injection of these cells (1x10^5) results in osteolytic bone disease after around 18 days (Peyruchaud *et al*, 2001). Another bone-seeking MDA-MB-231IV is also used (1x10^5) via an intravenous route which results in osteolytic bone disease around 28 days, thus, eliminating the risks of intracardiac injection (Nutter *et al*, 2014). Immortalised cell lines have been used in the laboratory for more than 40 years; thus, it was suggested that they could not represent their original tumour due to losing their heterogeneity. Therefore, freshly isolated tumours (patient-derived xenografts) were suggested to be used with immunocompromised animals to generate a better, more representative breast cancer model (Lv *et al*, 2020). Lefley *et al* carried out *in vivo* experiments with PDX (BB3RC32, BB2RC08, and BB6RC37), MDA-MB-231, MCF-7 and T47D with immunocompromised mice (NOD/SCID, 8-10 Weeks female). They explanted human bone discs to the mice obtained from the femoral heads of postmenopausal women undergoing hip replacement surgery. They injected 1x10^5 tumour cells via intracardiac or fourth nipple (orthotopic). Their findings showed that with oestrogen supplementation (12 mg/L), ER+ PDX successfully metastasised to the human bone disc in 100% of the animals as well as to mouse bone (20-75% of the animals). In contrast, MDA-MB-231 cells only metastasised to the human bone (70% of the animals). Since oestrogen alters the bone microenvironment, their choice was the lowest amount that could cause overt metastasis in the bone. However, this dose failed to support bone metastasis from MCF-7 and T47D; thus, their findings provided a more precise genetically representative ER+ model breast cancer model (Lefley *et al*, 2019).

Orthotopic implantation of 4T1 mouse triple-negative mammary carcinoma cells is commonly used in immunocompetent BALB/c mice; however, spontaneous metastasis varies between subtypes, and the frequency of bone metastasis is low (20% from 4T1, 40% from 4T1-2 etc.). Introducing intracardiac injection with bone tropic 4T1-2 cell lines (1x10^4-1x10^5) resulted in osteolytic lesions in 2-3 weeks (Ottewell & Lawson, 2021) therefore this bone tropic 4T1 model was chosen to observe

effects of HSCs mobilisation on the tumour proregression in the immunocompetent strain (Chapter 5). Despite the presence of immune cell populations, this model is much more aggressive than the MDA-MB-231/immunodeficient i.c. model, resulting in a high frequency of lung metastasis, limiting the experiment time frame (Canuas-Landero *et al*, 2021).

1.6. Treatment of The Bone Metastasis; Clinical Drugs and Effects

As described previously, understanding the bone metastatic niche is important to develop treatments to eliminate disseminated cancer cells. Other factors, including tumour cell homing, dormancy and bone destruction must be considered therapeutic targets for better treatment to improve the patients' quality of life, disease-free survival, and overall survival. Therefore, therapeutic approaches targeting cancer cells which have overlapping effects on cells in the microenvironment such as inducing immune cells, supressing osteoclast-mediated bone resorption, reducing angiogenic factors, thus resulting in increased anti-tumour effect (Figure 1-6) (Weilbaecher *et al*, 2011).

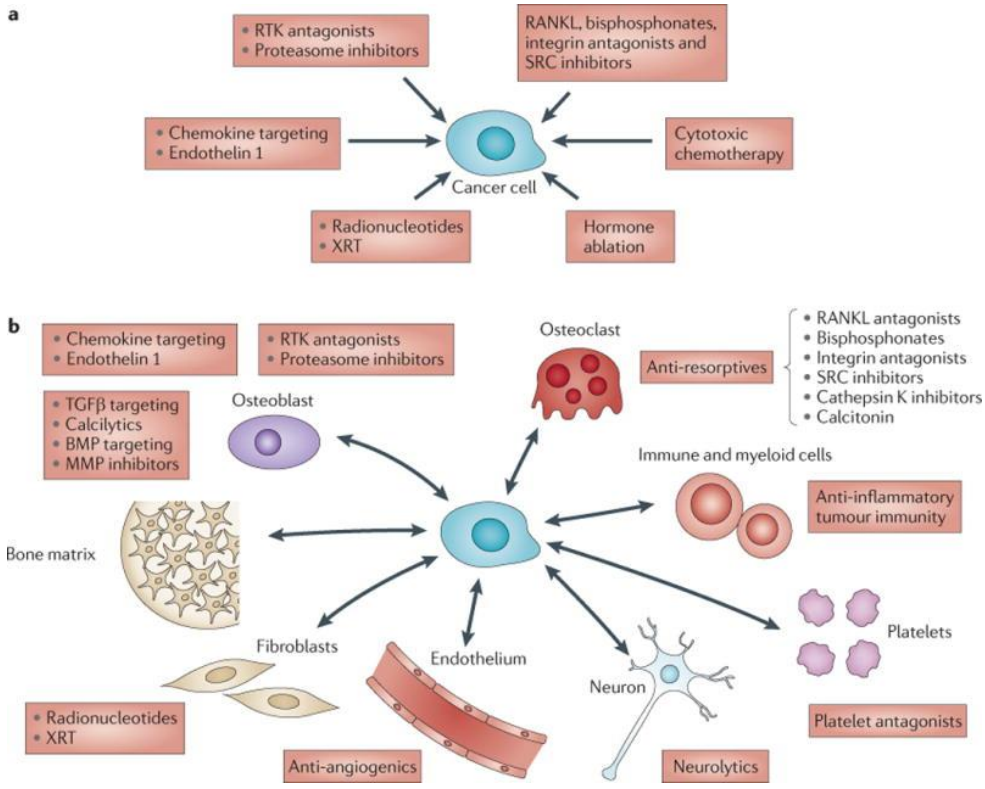

Figure 1-6: Therapeutic approaches to target the microenvironment.

*Cancer cells interact with stromal cells in the bone microenvironment to survive and promote their own growth, thus, cancer cell targeted therapies (**a**) have effects on the cells in the microenvironment (**b**) which result in increased anti-tumour effects. MMP= Matrix Metalloproteinase; XRT= Radiotherapy; RKT=Receptor Tyrosine Kinase; TGFβ=Transforming Growth Factor-β; BPMs=Bone Morphogenetic Proteins. Reprinted and reused with permission from Springer Nature: (Weilbaecher et al, 2011).*

When breast cancer cells are seeded in bone, their subsequent growth promotes osteoclast activation and differentiation which increases bone resorption. This releases embedded growth factors that promote tumour growth thus results in the vicious cycle (Zhang *et al*, 2019), which causes continuous bone destruction. Current approaches to limit development and progression of these bone lesions are aimed at supressing osteoclasts through different mechanisms with agents like bisphosphonates, anti-RANKL antibody (Denosumab), mTOR, c-SCR inhibitors (Sousa & Clézardin, 2018) or cathepsin K inhibitors (Dai *et al*, 2020).

1.6.1. Bisphosphonates

Bisphosphonates are the most common therapeutic agents for osteoclast-mediated diseases such as osteoporosis, cancer-induced osteolysis, Paget's disease of bone and multiple myeloma. Their activity against the bone resorption reduces bone pain and expansion of bone lesions (Drake *et al*, 2008). Bisphosphonates have two main actions against bone resorption; they attach to hydroxyapatite binding sites on the bone surface (especially to the active resorption area), thus inhibit enzymes with revealed phosphate (Rodan & Fleisch, 1996). They also decrease development of osteoclast progenitors and their recruitment along with inducing osteoclast apoptosis (Hughes *et al*, 1995). These two actions depend on the chemical structure of bisphosphonates: simple bisphosphonates and nitrogen containing bisphosphonates. Zoledronic acid, the most commonly used BP used in patients with bone metastases, is one of the nitrogen containing bisphosphonates with 10,000 fold higher anti-resorptive activity than the simple bisphosphonates (Widler *et al*, 2002).

1.6.1.1. Mechanism of Action

Bisphosphonates are chemically stable derivatives of inorganic pyrophosphate (PPi) and their molecular structure are similar but more stable due to their nonhydrolyzable central carbon (Figure 1-7, A). Because of the affinity to hydroxyapatite (like PPis) bisphosphates have high affinity to bone (Drake *et al*, 2008). Bisphosphonates' hydroxyl (R^1) and structural moiety (R^2) groups allows phosphonates to flank thus increase the affinity and determines bone potency (Figure 1-7,B). (Drake *et al*, 2008) Second or third generation bisphosphonates have amino or N groups which increases antiresorptive potency relative to the early bisphosphonates (Figure 1-7,C) (Drake *et al*, 2008).

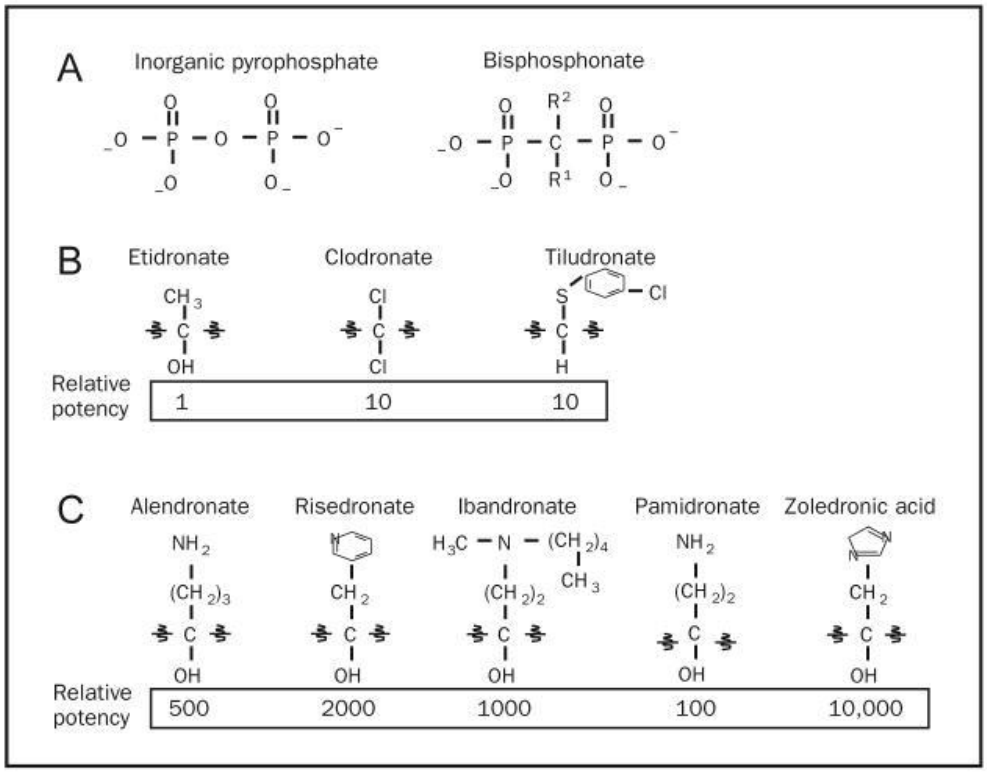

Figure 1-7: Molecular structures of bisphosphonates

*Molecular structure and relative potency of bisphosphonates. (**A**) Molecular similarity of a bisphosphonate to inorganic pyrophosphate. (**B**) Simple bisphosphates' molecular structures and their relative potency. (**C**) Second or third generation (nitrogen containing) bisphosphonates' molecular structures and their relative potency. Reprinted and reused with permission from Elsevier: (Drake et al, 2008).*

Both simple and nitrogen containing bisphosphonates induce osteoclast apoptosis, but their mechanisms of action are different. Simple bisphosphonates do not contain a nitrogen R chain thus allowing them to incorporate into newly formed adenosine triphosphate. However, because of their nonhydrolyzable property, they started to inhibit multiple ATP dependent process thus leading to the osteoclast apoptosis (Russell, 2006). Nitrogen containing bisphosphonates have two mechanisms to induce apoptosis; they inhibit farnesyl pyrophosphate (FPP), which is a key enzyme of the mevalonate pathway, thus reducing prenylation of small GTPase enzymes (Ras, Rab, Rho, and Rac) that play role in osteoclast proliferation, differentiation, and survival downstream pathways. Therefore, FPP inhibition results as osteoclast apoptosis (Rogers, 2003). Also, they can induce formation of Apppl (triphos- phoric acid 1-adenosin-50yl ester 3- (3-methylbut-3-enyl) ester), which is an endogenous ATP analogue. Isopentenyl pyrophosphate isomerase (IPP) accumulates because of the FPP inhibition, thus IPP is converted to Apppl that induces osteoclast apoptosis by inhibiting adenine nucleotide translocator (Mönkkönen *et al*, 2006).

Alongside bisphosphonate preservation of bone reduction, there are several *in vitro* (Boissier *et al*, 2000; Clézardin *et al*, 2000; Neville-Webbe *et al*, 2005) and *in vivo* (Neudert *et al*, 2003; Daubiné *et al*, 2007; Hirbe *et al*, 2009; Fournier *et al*, 2010) studies that focus on anti-tumour effects, reporting increased levels of apoptosis and reduced proliferation in many cancer types, including breast cancer. However, *in vivo* studies did not show similar anti-tumour effects of BPs when used as single agents. In contrast , there are several *in vivo* studies that indicate a reduction of tumour burden (Mönkkönen *et al*, 2006). A key point to remember is the administration of drug, which is directly on tumour cells in *in vitro* studies with high drug concentrations for prolonged periods of time. *In vivo* administration of BPs result in rapid binding to bone and a short half-life in the circulation, with tumours exposed to low doses for a limited period (Weiss *et al*, 2008).

Some potential effects of bisphosphonates from preclinical studies are inhibition of tumour proliferation and angiogenesis, apoptosis induction, promotion of cytotoxic agents, reducing the tumour cell adhesion to the bone, immune cell activation and reducing tumour cell migration. The majority of anti-tumour effects of bisphosphonates *in-vivo* are shown to be indirect through its bone resorption inhibition and thereby 'breaking' the vicious cycle (Zekri *et al*, 2014).

1.6.1.2. Clinical use

Bisphosphonates are used to prevent bone loss in patients with confirmed bone metastases, to reduce cancer treatment-induced bone loss and as an adjuvant therapy to prevent development of metastases in post-menopausal breast cancer patients. Breast and prostate bone metastasis and advanced multiple myeloma can cause hypercalcemia, spinal cord compressions, bone pain and fractures, therefore, bisphosphonates are well established in these diseases to reduce skeletal related events (SREs) (Coleman *et al*, 2012). In one of the early phase II clinical study for bisphosphonates, patients with skeletal metastasis (n=173) received clodronate as a two 400 mg capsule twice a day for two years and clodronate prevented SREs significantly when compared to placebo group (Kristensen *et al*, 1999). Patients with metastatic breast cancer patients (n=287) reported increased quality of life and decreased bone pain when receiving daily 50 mg ibandronate for up to 96 weeks (Body *et al*, 2004). Many studies carried with bisphosphonates, and everyone indicated reduced SREs, thus led to major analysis of 17 studies of bisphosphonates to compare the effects on many tumour types, including breast cancer. This major analysis showed zoledronic acid's SRE rate as 1.6 per 100 person-month which was the best outcome when compared with other bisphosphonates (Palmieri *et al*,

2013). As a result, zoledronic acid is now standard of care for patients with confirmed bone metastases in solid tumours and multiple myeloma.

The ability of BPs to prevent the development of bone metastases lead to an investigation of zoledronic acid's effect as adjuvant therapy, where it is combined with endocrine therapy, aromatase inhibitors and chemotherapy for post-menopausal women. This was investigated in the ABSCSG-12, AZURE and ZO-FAST clinical trials (Gnant & Eidtmann, 2010; Coleman *et al*, 2011, 2013, 2014; Coleman, 2019). In the ABSCG-12 trial (1998-2006), ER+ breast cancer patients (n=1,803) who received ovarian function suppression (therefore, patients considered as postmenopausal) were treated with either single anastrozole (an aromatase inhibitor) or anastrozole and zoledronic acid. Zoledronic addition to the treatment increased disease-free survival, reduced the bone metastasis and regional recurrence, and eliminated cancer treatment induced bone loses (Gnant & Eidtmann, 2010). ZO-FAST trial (2005-2011) carried out a similar treatment with letrozole (an aromatase inhibitor). Postmenopausal ER+ and/or PR+ breast cancer patients (n=1,065) were treated with immediate or delayed zoledronic acid alongside with letrozole. Results indicated that immediate zoledronic acid increased disease-free survival, with reduced bone metastasis (Gnant & Eidtmann, 2010; Coleman *et al*, 2013). In the AZURE trial (2003-2013), patients (n=3,360) with invasive breast cancer (regardless of their subtypes) were treated with standard adjuvant systemic treatment with or without zoledronic acid (Coleman *et al*, 2011). The AZURE trial did not show any difference in disease-free survival, however, further analyses showed that postmenopausal patients had delayed or prevented recurrence or bone metastasis (Coleman *et al*, 2011, 2014). All of these studies indicate that zoledronic acid has different effects on pre- and post- menopausal patients. An *in vivo* study that mimicked menopausal status in mice reflected the clinical findings from the AZURE trial, showing that zoledronic acid treatment prevented tumour growth in ovariectomized but not in sham operated animals (Ottewell *et al*, 2014), however, the underlying mechanisms for these effects are still unknown. One possibility is that zoledronic acid affects bone cells other than osteoclasts, including myeloid populations. Previous study carried out in our group, demonstrated transient changes in haematopoietic progenitors in the bone when treated with zoledronic acid (Ubellacker *et al*, 2017).

1.6.2. Denosumab: Monoclonal Antibody to RANKL

The importance of the RANK/RANKL pathway in bone remodelling, described in detail in previous sections, lead to the development of new therapeutic agents. Denosumab is a fully humanised immunoglobulin G2 monoclonal antibody with 2 heavy (448 a.a./chain with 4 intramolecular disulphides) and 2 light chains (215/chain) that targets RANKL expressed on both osteoclast precursors, osteoclasts, and cancer cells. Preventing RANK/RANKL interaction inhibits tumour

survival, tumour formation and osteoclast formation/activity thus, bone resorption is decreased (Hanley *et al*, 2012). Also, administration of denosumab is subcutaneous with a 60mg dose every 6 months (Stopeck *et al*, 2010) whereas zoledronic acid is an intravenous injection that requires 15 minute infusion every 3-4 weeks in hospital (Berenson, 2005). Therefore, denosumab administration is less stressful for patients.

Like bisphosphonates, denosumab is used to reduce skeletal-related events and is significantly more effective than zoledronic acid, as described below. A randomised phase II trial (Body *et al*, 2010) investigated the effects of different denosumab doses (n=42,30-180mg) on patients with/without previous bisphosphonate treatment. Patients were male or females with solid tumours or MM with at least 1 bone lesion history. The main outcome measure from this study at the 25th week, was the bone turnover marker urinary N-telopeptide (uNTx) by creatine, which is evidence for bone turnover. Results indicated that denosumab supressed bone turnover, thus reduced the risk of skeletal events for both breast and prostate tumours. Another randomised phase II trial (Fizazi *et al*, 2009) investigated denosumab's effects on the patients with metastatic breast or prostate cancer and multiple myeloma (n=46) with at least 50 nmol/L uNTx. Patients were treated with either 180 mg denosumab or a bisphosphonate every 4 weeks for 25 weeks. After 25 weeks, patients who still had at least 50 nmol/L uNTx, received treatment for an additional 32 weeks. At the end of the study, denosumab reduced bone resorption thus resulting in less skeletal related events such as fractures. A phase III trial of denosumab (Stopeck *et al*, 2010) compared its effects with bisphosphonates in breast cancer patients with at least one bone metastasis. Patients received either 120 mg denosumab or 4 mg zoledronic acid every 4 weeks for 34 months. Similar results were observed as in the previous trial; denosumab is better at slowing and reducing skeletal related events when compared to zoledronic acid. Allen et al. (2012), analysed the skeletal related events in patients with BC, prostate cancer, MM or other solid bone tumours in phase 3 clinical studies of doxorubicin and zoledronic acid, and found that denosumab was significantly better than zoledronic acid reducing skeletal related events by 17%. Disease progression and survival was similar for both zoledronic acid and denosumab treatments (Lipton *et al*, 2012).

Denosumab has also been investigated as an adjuvant treatment, in the phase III clinical trial (D-CARE) with early breast cancer patients (n=2253) receiving 120 mg denosumab every 3 months for 5 years or a matching placebo. Despite preclinical evidence suggesting RANKL inhibition might delay bone metastasis or disease recurrence in patients with early-stage breast cancer, denosumab did not improve disease-related outcomes for women with high-risk early breast cancer (Coleman *et al*, 2020a). All these clinical studies indicate denosumab's inhibitory effect on osteoclasts is better than

zoledronic acid, however, it still does not have the same effect in post-menopausal women in the adjuvant setting. This indicates that the benefits of zoledronic acid in this setting involves other mechanisms in addition to osteoclast inhibition.

1.7. Summary, conclusion, and outstanding question

In summary, the BME provides ideal niches for cancer cells, including the vascular and hematopoietic niches that support breast cancer cell homing, survival, and growth. Different cell types of the bone marrow such as hematopoietic, immune, and adipose cells contribute to the different stages of breast cancer metastasis, from tumour cell homing to overt tumour growth, both through direct cell contact and through release of soluble factors. However, more needs to be known about these complex interactions between the bone marrow and tumour cells in the early stages of metastatic breast cancer.

It is well established that chemotherapy has negative effects on the bone microenvironment, but the precise cellular, molecular, and structural consequences of cytotoxic agents remain an unstudied area. Alteration of the microenvironment can cause metastatic growth in bone; however, to what extent modification of any one component in the niche affects the other niche components as well as the disseminated cancer cells requires elucidation. Many therapeutics target the bone remodelling cells (primarily osteoclasts), but the main aim is generally on slowing disease progression and the associated bone degradation. Therefore, this project investigates the effects of current anti-cancer therapies on different cellular components of the bone marrow microenvironment, revealing possible additional therapeutic effects as well as indicating potential off-target effects in bone.

1.7.1. Hypothesis and aims of the thesis

The hypotheses underpinning this project are:

- **Therapeutic agents used in treatment of cancer modifies multiple cell types in bone**
- **The presence of tumours in bone modifies multiple cell types and bone marrow niches, including immune cell populations**
- **Therapeutic targeting of the bone marrow modifies progression of bone metastasis**.

To investigate the hypotheses, the following aims have been set:

- Characterise and quantify the bone marrow populations comparing different mouse strains (immunocompetent and immunocompromised).
- Determine how the bone marrow cell populations are affected by the presence of tumour cells.
- Determine how the bone marrow cell populations are affected by anti-cancer therapies.
- Investigate how modulation of the hematopoietic bone marrow niche affects tumour growth in bone.

CHAPTER 2. MATERIALS AND METHODS

2.1. MATERIALS

Table 2-1: Commonly Used Laboratory Agents

Reagent	Supplier	CaT. No.
Acetic Acid	AnalaR VWR	20104.298
AMD3100	Sigma-Aldrich	155148-31-5
Amphotericin B	HyClone	SV30078.01
DAB	Vector	SK-4100
DMSO	Sigma-Aldrich	472301
DMEM	Gibco	10569010
Doxorubicin	QC Release ITH Pharma LTD	N/A
DPX	VWR	360294H
EDTA	Sigma-Aldrich	0360
Eosin	Atom Scientific LTD	RRSP35-A
EtOH	Fisher	E/0665DF/17
Filgrastim (G-CSF or ZARXIO™)	Sandoz Inc.	NDC 61314-312
Foetal Calf Serum	Sigma-Aldrich	F7524-500ML
Gill's Haematoxylin	Merck	HXX2494994
H_2O_2	VWR	23622.298
Histo-Wax	Leica	S26.0280
IMDM	ThermoFisher	31980030
ISOFLURANE	Zoetis	NDC 0044-5260-03
Luciferin	Perkin Elmer	122796
MethoCult GF M3434	Stemcell Technologies	03434
MTT	Sigma-Aldrich	M5655
Naphthol AS-BI phosphonate	Sigma-Aldrich	N-2125
NGS	Vector	S-1000
Paraformaldehyde	Sigma-Aldrich	P6148
PBS	ThermoFisher	10010023
PenStrep	Gibco	15140-22
RPMI 1640(1X)+GlutaMAX™	ThermoFisher	61870036
Sodium Nitrite	Sigma-Aldrich	S-2252
Sodium Tartrate	Sigma-Aldrich	S-4797
Tri-Sodium Citrate	Merk	1.06448
Triton-X 100	Sigma-Aldrich	X100-500ML
Trypsin	Sigma-Aldrich	T3924-500ML
Tween-80	Sigma-Aldrich	P1754-500ML
Xylene	Fisher	X/0250/17

Table 2-2: Software used for analysis

Software	Supplier
CTAnalyser software	SkyScan, Burker microCT, CT-Analyser
GraphPad Prism 8	GraphPad Software Prism version 8
Image J	Image J Version 1.52s
LAS AF	Leica
NRecon	Osteometrics
Osteomeasure Software	Osteometrics
SkyScan	Bruker microCT

Table 2-3: Machines used

Machine	Supplier
Multi-Well Plate Reader	SpectraMax M5e, Molecular Devices
Leica EG1150H Wax Dispenser	Leica
Leica RM2135 Microtome	Leica
X-Ray Computed Microtomography	Bruker, aartselaar, Belgium
Leica AF6000LX	Leica
IVIS Lumina II	Perkin Elmer
SCIL vet Abc PLUS	SCIL Animal Care Company, Altorf, France

Table 2-4: List of the Antibodies used

Antibody	Supplier	Cat.No.	Clone	Fluorophore
CD11b	Biolegend	101225	M1/70	APC/Cy7
CD11c	Biolegend	117363	N418	KIRAVIA Blue 520
CD11c	Thermo-Fisher	61-0114-82	N418	PE-eFluor610
CD19	Biolegend	115507	6D5	PE
CD3	Biolegend	100353	145-2C11	BV510
CD4	Biolegend	100423	GK1.5	PerCP/Cy5.5
CD45	Biolegend	103134	30-F11	BV421
CD8	Biolegend	100724	53-6.7	AF647
F4/80	Biolegend	123113	BM8	PE/Cy7
Ly-6C	Biolegend	128007	HK1.4	PE
Ly-6G	Biolegend	127616	1A8	PerCP/Cy5.5
MHCII	Biolegend	107635	M5/114.15.2	BV510
NK 1.1	Biolegend	108713	PK136	PE/Cy7
Zombie UV	Biolegend	423107	N/A	UV450
Lineage Cocktail	Biolegend	558074	M1/70|145-2C11|RB6-8C5|TER-119|RA3-6B2	APC
CD117(c-Kit)	Biolegend	560185	288	APC-H7
Ly-6A/E (Sca-1)	Biolegend	561076	E13-161.7	PE
Fc Block (CD16/CD32)	Biolegend	553141	2.4G2	-

2.2. METHODS

2.2.1. In Vitro Experiments

2.2.1.1. Cell Lines

MDA-MB-231-IV PX462

MDA-MB-231 is an immortalised epithelial human breast cancer cell line. It is highly aggressive, invasive, and triple-negative breast cancer. It lacks oestrogen receptor (ER), progesterone receptor (PR) and human epidermal growth factor receptor 2 (HER2) amplification. The MDA-MB-231 cell line used in these studies are a GFP+ clone derived by Dr Vicky Cookson (named MDA-MB-231-IV PX462) of the highly bone-seeking MDA-MB-231 IV cells, previously transfected with a luciferase vector by Nutter et al. (Nutter *et al*, 2014). When mice are administered luciferin, tumours are traceable with the In Vivo Imaging System (IVIS). Bone metastasis models were created with an intra-cardiac injection of 1 x 10^5 cells per animal in 100 µl PBS. MDA-MB-231 cells were cultured in RPMI 1640 (1X) + GlutaMAX™ medium (ThermoFisher Scientific, UK) with 10% Foetal Calf Serum (FCS) (Sigma-Aldrich, UK) in air-filtered T75 flasks. Cells were incubated at 37 ˚C, %5 CO2 and 95% relative humidity. Their doubling time was 48 hours.

4T1 LUC BONE

4T1 LUC BONE cells are triple-negative mouse mammary carcinoma cell line specifically targets bones (transfected with a luciferase vector) and kindly provided by Dr Penelope Ottewell. These cells do not express GFP and were generated by the Ottewell team as follows: 4T1-Luc2 cells were injected (i.c.) into 12-week-old female BALB/c mice and tumour growth in bone was monitored using the IVIS Lumina II system (Calliper Life Sciences, UK). Animals were culled 2 weeks after tumour cell injection and tumour-bearing bones were isolated in a sterile environment and dissociated aseptically to collect the 4T1LUC BONE cells (Canuas-Landero *et al*, 2021).In my project, bone metastasis models were created with an intra-cardiac injection of 3x10^4cells per animal in 100 µl PBS. 4T1 LUC BONE cells were cultured in DMEM -pyruvate (Gibco, UK) with 10% Foetal Calf Serum (FCS) (Sigma-Aldrich, UK) in air-filtered T75 flasks. Cells were incubated at 37 ˚C, %5 CO2 and 95% relative humidity.

Cell lines underwent regular mycoplasma testing and have been authenticated, in house (by the Ottewell group), using short tandem repeat analysis of 10 loci.

2.2.1.2. Cell Passaging

Cells were passaged after two days (~80% confluent cells in T75 flasks). The old medium was discarded, and cells were washed three times with 6 ml sterile PBS (ThermoFisher, UK). 2 ml of 0.25% Trypsin EthyleneDiamineTetraacetic Acid (EDTA) (ThermoFisher Scientific, UK) was added to the flasks and incubated at 37 ˚C for 5 minutes. 8 ml cell culture medium with 10% FCS was used to deactivate the Trypsin-EDTA. The cell suspension was transferred to tubes and centrifuged at 1000 rpm for 5 minutes to form a pellet. The supernatant was discarded, and cells were re-suspended in 6 ml medium+10% FCS. 2 ml of the suspension was added to a T75 flask containing 10 ml media+10%FCS.

2.2.1.3. Cell Freezing and Thawing

For freezing cells, cells were suspended as described for cell passaging above. After removal of the supernatant, the cells were re-suspended in cold freeze medium (90% FCS + 10% DMSO), aliquoted to 1 ml per cryovial and frozen overnight at -80˚C. The vials were transferred to the liquid N_2 tank/biorepository for long-term storage.

For the thawing of cells, the vial containing the frozen cells was warmed in the 37 ˚C water bath until the sides were thawed, but the centre was kept frozen. The cells were collected by adding 3 ml medium +10% FCS, then transferred to the 15 ml falcon tube and centrifuged at 1000 rpm for 5 minutes. The supernatant was removed, and cells were re-suspended in 15 ml medium + 10% FCS and transferred to a T75 flask.

2.2.1.4. Cell Counting

Cells were counted with a haemocytometer under the light microscope. Cells were trypsinised and suspended as described for cell passaging above. 10 µl of the cell suspension was added to the sides of the haemocytometer. Four 4x4 corners were counted (4×10^{-5} ml volume); a total number divided by the number of counted squares and multiplied by the volume factor (1×10^{4}) gives the total number of cells per ml (Figure 2-1).

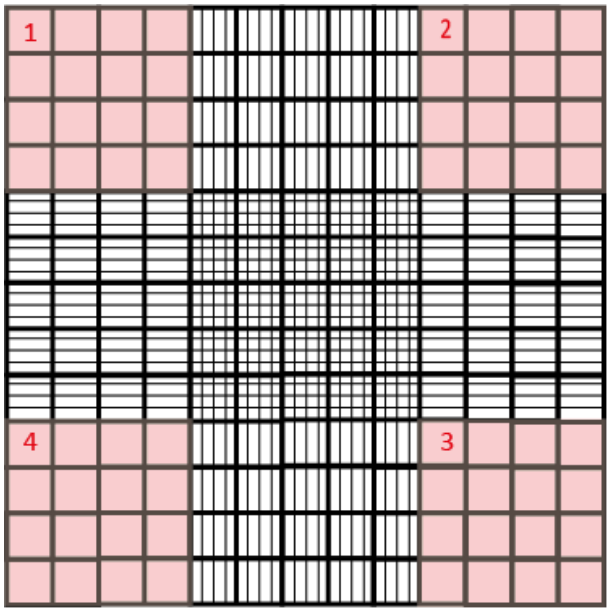

Figure 2-1: Representation of 1 haemocytometer grid.

Cells inside the squares that highlighted in red counted and cells are at the borders of those squares are not counted.

2.2.1.5. Half Maximal Inhibitory (IC_{50}) dose with MTT Assay

3-(4,5-dimethylthiazol-2-yl)-2,5-diphenyltetrazolium bromide (MTT) dye is used for assessing cell metabolic activity. The reduction of MTT dye inside the cells produces soluble formazan crystals, which gives a purple colour (Plumb, 2004). This specific reaction correlates with cell numbers. The effect of doxorubicin on MDA-MB-231 was analysed using the MTT assay. Cells (n=8) were seeded 10000 cells/cm^2 on to 96 well plates with 200 µl RPMI + 10% FCS. Cells were treated with media +10%FCS, media + PBS, 10^{-9} M, 10^{-8} M, $5x10^{-8}$ M, 10^{-7} M, 10^{-6} M, 10^{-5} M, $5x10^{-5}$ M, and 10^{-4} M doxorubicin for 72 hours in an incubator at 37 ˚C. Doxorubicin binds topoisomerase-II and blocks the DNA proliferation and MDA-MD-231 cell doubling time is around 38h (after I have seeded 1 x 10^4 cells/cm^2, 38 hours required to double their density). The cells were incubated for 72 hours to allow enough time to observe a significant difference between cell numbers. After 72 hours, all media was removed, and 100 µl MTT solution (1mg/ml media+10%FCS) was added to all wells. The plate was covered with aluminium foil, and cells were incubated for 4 hours in an incubator at 37˚C. After four hours, the MTT solution was removed by carefully inverting the plate onto the sterilised tissue paper. For the last step, 100 µl DMSO was added to the wells, and the plate was re-covered with aluminium foil. The plate was placed on the plate shaker for 15 minutes at 170 rpm to dissolve all formazan crystals. Multi-well plate reader reads absorbance at 570nm wavelength. GraphPad version 8 was used to calculate IC_{50}. First, concentrations were calculated as Log[X], and absorbance values were converted to cell viability based on the highest value from the concentration group set as 100%. These

X (concentrations) and Y (Cell viability) were fitted into the inhibition graph, and the X value is calculated where it intersects with 50% viability (Figure 2-2).

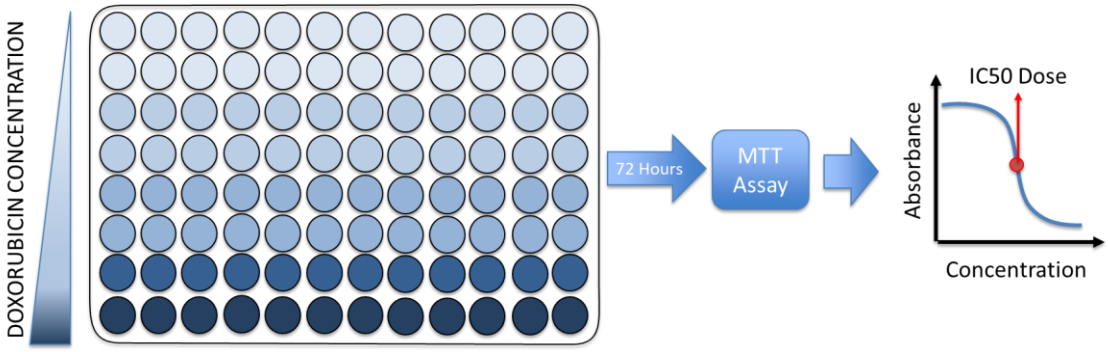

Figure 2-2: Schematic of dose response to identify IC_{50}.

Diagram of dose response experiment to determine IC_{50} dose of doxorubicin. 10000 cell/cm^2 cells were plated and serially treated at 10-fold dilutions ranging from 1x 10^{-4} M – 1x 10^{-8} M DOX doses and control media (media +10%FBS and media +PBS) for 72 hours. Absorbance values calculated with MTT assay and Log[M]-Absorbance graph plotted.

2.2.2. *In Vivo* Experiments

2.2.2.1. Home Office Approval

The Research Ethics Committee of the University of Sheffield (Sheffield, UK) reviewed and approved all the *in-vivo* experiments which were granted UK Home Office approval and performed in accordance with the UK Animals (Scientific Procedures) Act 1986 and Home Office Regulation under the Programme Project Licence PPL 70/8964 (Professor Nicola J Brown), P99922A2E (Dr Penelope D Ottewell) and Personal licence ID5F9D530 (Veli Aydin).

2.2.2.2. Animals

8-10 Weeks old female BALB/c, BALB/c nude, and C57BL/6J mice were ordered from Charles River (UK) and were housed in individually ventilated cages in a controlled environment with a 12-hour light/dark cycle at 22 ˚C. Water was available *ad libitum*. For all studies, animals were randomised to control, or treatment based on weight. All animals were weighed before the distribution to the cages, and the mean weight value of each cage was similar (4 or 5 animals per cage, depending on the size of the experiment). The treatment part of the studies was not blinded; however, sample analyses for histology were done in a random fashion to avoid bias. Flow cytometry and µCT analyses were not dependent on the observer; thus, samples were not blinded.

2.2.2.3. Tumour Cell Injection

Breast cancer bone metastasis was mimicked by intra-cardiac injection of Luc2+ve MDA-MD-231 cells. Mice were anaesthetised with 2-3% isoflurane (Zoetis, UK) inhalation. All mice were injected with 100 µl PBS containing $1x10^5$ MDA231 cells (xenograft models) or $3x10^4$ 4T1 cells (syngenetic models) into the left ventricle. Then, mice were kept in an incubator at 32˚C for 1-3 hours post-injection and observed closely for any adverse effects for at least 24 hours.

2.2.2.4. Administration of Drugs and Other Solutions

Doxorubicin Treatment of Mice

16-20 Mice were used for either BALB/c or BALB/c nude experiments, and randomly divided into 8-10 mice for each group (PBS control and Doxorubicin (DOX) treated). 4 or 8 mg Doxorubicin/kg concentration was used. Concentration calculation was made by assuming 20 g animal would be injected with 100 µl DOX diluted in PBS. Mice that have lower body weight received a lower volume but the same concentration. All mice were treated once a week with 100 µl PBS (control) or DOX for four weeks via tail vein injection (performed by Mr Matt Fisher). Animals were monitored every two days by checking their physical appearance and weights. Animals were culled two days after the last treatment with blood withdrawal by cardiac puncture, and dislocation of the neck was used to ensure death.

Modification of the HSC niche

10-16 Mice were used for all strains, randomly divided into 5-8 mice for each group (PBS control, AMD3100 treated, and filgrastim (G-CSF) treated). Animals were treated with PBS (100 µl i.p.) daily, the CXCR4 antagonist AMD3100 (5 mg/kg, i.p.) or G-CSF (123 µg /kg i.p.) for five days. Concentration calculation made by assuming 20 g animal would be injected with 100 µl of any drug. Animals were monitored every two days by checking their physical appearance and weights. Animals were either culled 2-6 hours after the last treatment with blood withdrawal by cardiac puncture and dislocation of the neck to confirm death, or tumour cells were injected via the intracardiac route to observe tumour development.

2.2.2.5. *In-Vivo* Imaging of Tumour Growth

As mice were injected with tumour cells that expressed firefly luciferase, tumour growth was monitored using the *in-vivo* imaging system (IVIS) LUMINA II (Calliper Life Sciences). Five minutes before the imaging, animals were injected with 100 µl D-Luciferin (30 mg/kg) via the sub-cutaneous

route. All procedures were done under anaesthesia with 2-3% inhalation of isoflurane (Zoetis, UK). Images were analysed with living image software version 4.1. Tumour size, presence time and counts were measured.

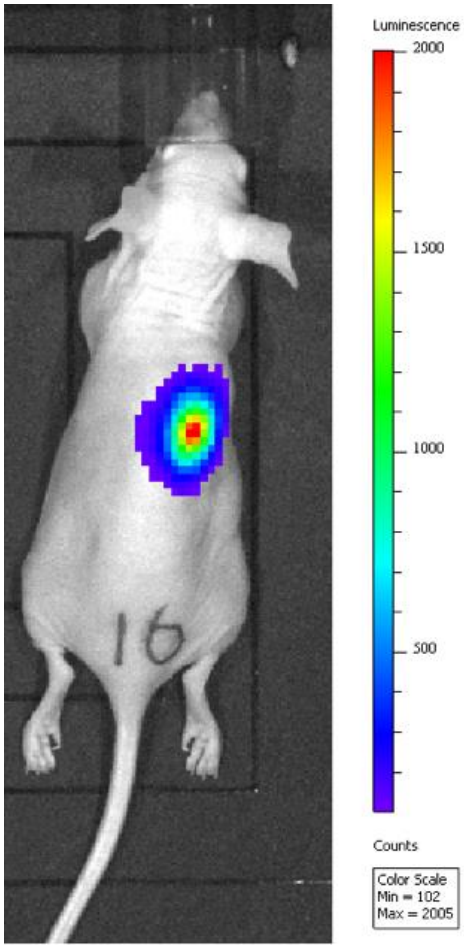

Figure 2-3: Example IVIS image.

IVIS example, the Scale on the right represents the level of intensity. The blue hue represents approximately 300 units, and the red hue represents 2000 units.

2.2.3. Ex Vivo Experiments

2.2.3.1. Collection of Bone Samples

Femurs and tibias of animals were collected at the end of the experiment. First, skin and most muscles were removed from the hind limbs. Then, the hind limbs were removed from the pelvis by cutting perpendicular to the limb bones to protect the integrity of the femoral heads of the bones. After removing the hind limbs, the tibia and femur were separated by cutting with scissors to obtain individual bones. Lastly, any remaining muscle and connective tissues were removed with forceps. The right tibias were fixed in 4% paraformaldehyde solution. Then, bones were decalcified with 0.5M EDTA solution and processed for histology following standard procedures (see Sections 2.2.3.2 and 2.2.3.3).

The left tibias were used for bone marrow isolation. Left and right femurs were snap frozen in liquid N_2.

2.2.3.2. Tissue Fixation and Decalcification

Fixative solution: The 4% Paraformaldehyde solution was used to fix the bones. The solution was prepared by adding 40 mg paraformaldehyde powder (Sigma-Aldrich, UK) to 1L PBS under the hood. The solution was heated to 55 ˚C while stirring until the solution became clear, followed by cooling on ice. 3 ml of 4% PFA solution was used for fixing mouse bones at 4˚C overnight—any excess 4% PFA solution was stored at -20˚C.

Decalcification solution: Bones were decalcified with 0.5M EDTA solution. 186.6 g EDTA powder was added to 700 ml PBS. Then, a 20 g NaOH pellet was added to help EDTA dissolve on the stirrer. After the solution became transparent, the pH was adjusted to 8 and the volume adjusted to 1 L with PBS. The solution was divided into aliquots and stored at 20 ˚C for up to 4 weeks. Bones were decalcified inside bijou containers that contained 5 ml 0.5 EDTA solution for two weeks at 4˚C. The solution was changed every one to two days for 14 days. After decalcification, bones were processed for histology by the University of Sheffield Bone Biology Lab.

2.2.3.3. Wax Embedding and Sectioning

After the bones were processed, tissues were embedded into histo-wax (Leica, UK) blocks using Leica EG1150. Bones were placed in a 58 ˚C paraffin bath for 30 minutes. The best-corresponded mould was chosen for the bone shape. A small amount of paraffin was put into the mould then, using warm forceps, bone was placed into the middle of the mould as diagonal to get the best result from the microtome. While pressing firmly, mould was placed on the cold surface to hold the bone. After that, the labelled tissue cassette was placed over it and filled until the cassette was full. For the last stage, the mould was placed under the cold plate for at least 30 minutes to cool down, the mould was then removed, and excess was cleaned near the cassette.

A Leica RM2135 microtome was used to section the paraffin-embedded bones. A new knife was used for each sectioning section, and all blocks were placed on the ice block inside the 4˚C fridge for at least 1 hour to achieve maximum hardness for the best cutting result. During the sectioning, blocks were softened due to the increased heat of the cutting process. To make them harder, they were placed on the ice block. 3 µm thickness was used for each section, and bones were trimmed until the first triangle that could be scored was achieved (Figure 2-4).

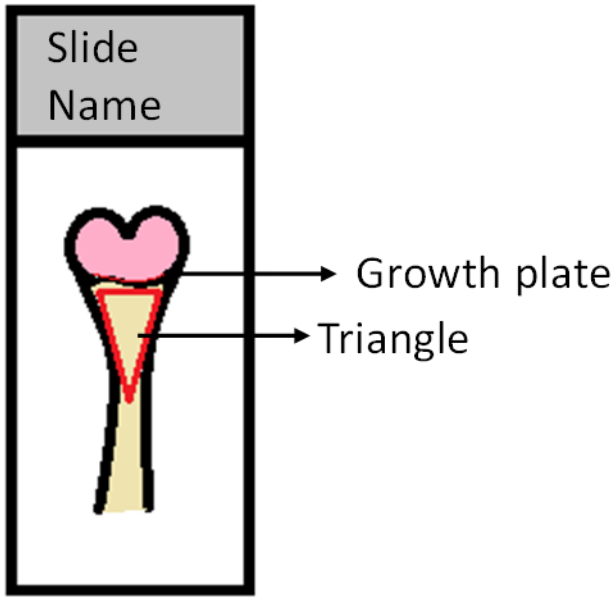

Figure 2-4: Schematic explanation of triangle.

Explanation of triangle when collecting slides on microtome cutting.

2.2.3.4. Blood Sampling

Mice were anaesthetised with 2-3% isoflurane (Zoetis, UK), and blood samples were collected with a cardiac puncture (terminal procedure) and placed into 50 µl EDTA to prevent clotting. Samples were analysed either with scil Vet abc Plus (SCIL Animal Care Company, Altorf, France) or used in FU analysis.

2.2.3.5. Bone Marrow Isolation

After dissection, bones were placed into ice-cold PBS. Under the sterile hood, bones were quickly dipped into 100% EtOH five times, and excess alcohol was immediately removed with tissue paper. Then, a similar approach was repeated with 70% alcohol. The top end (head) of the bone was carefully removed with scissors and placed into sterilised 0.2 ml PCR tubes where the bottom had been removed. Tubes containing bones were then placed into 1,5 ml Eppendorf tubes that contained 200 µl sterile PBS with 1% penicillin and streptomycin. Tubes were centrifuged at 6000-7000 rpm for 3-5 minutes to flush the bone marrow into the PBS. After removing the supernatant, bone marrow was suspended in PBS and centrifuged at 1000 rpm 5 minutes 3 times. All bone marrow cells were frozen in FCS with 10% DMSO, the same freezing media used for *in vitro* cell culture or the CFU Assay was performed.

2.2.3.6. Micro Computed Tomography (µCT)

Micro-computed tomography (microCT or µCT) is a non-destructive imaging tool to produce high-resolution three-dimensional (3D) images composed of two-dimensional (2D) trans-axial projections of a target specimen.

µCT has four major components: an x-ray tube, a collimator (which focuses the beam geometry to either a fan or cone beam projection), a specimen stand and a phosphor-detector/ charge-coupled device camera. Reconstruction of a 3D image is performed by NRecon software which constructs a 3D image from the 2D image that is gathered. SkyScan software wass used to obtain 2D images. Scanning was performed using a Skyscan 1172 X-ray computed microtomography scanner (Bruker, Aartselaar, Belgium). The 2016x1344 camera resolution with a 0.5 Al filter and 4.3 µm pixel size settings were used for all the bones. All bones were scanned 180˚with a default 0.7 rotation step.

Analysis of µCT data

Data were analysed with CTan software. Data was first selected from the software. The reference point was selected where the spongy bridge on the trabecular bone had broken. 0.2 mm from the reference point is the offset for trabecular bone (1 mm for cortical bone). After the offset value, 1 mm of the bone was set as the height to analyse (Figure 2-5).

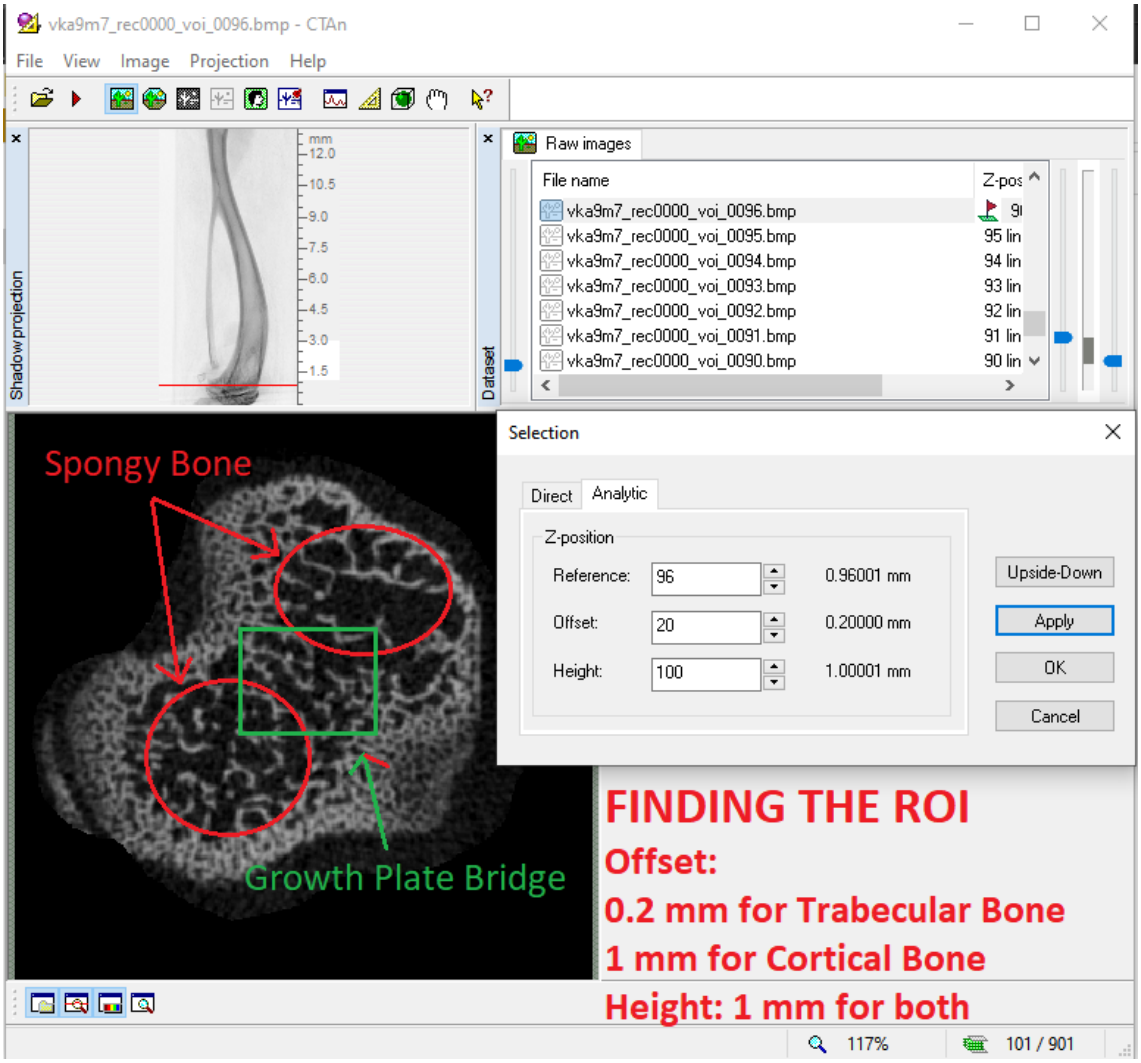

Figure 2-5: Setting the reference point.

Growth plate bridge used as reference point in the spongy bone, where spongy bone started to merge. After this point an offset was taken 0.2 mm for trabecular bone and 1 mm for cortical bone and measurement carred for 1 mm height on Osteomeasure.

After selecting the correct bone region, we selected the region of interest (ROI), either the trabecular or cortical area was selected (Figure 2-6).

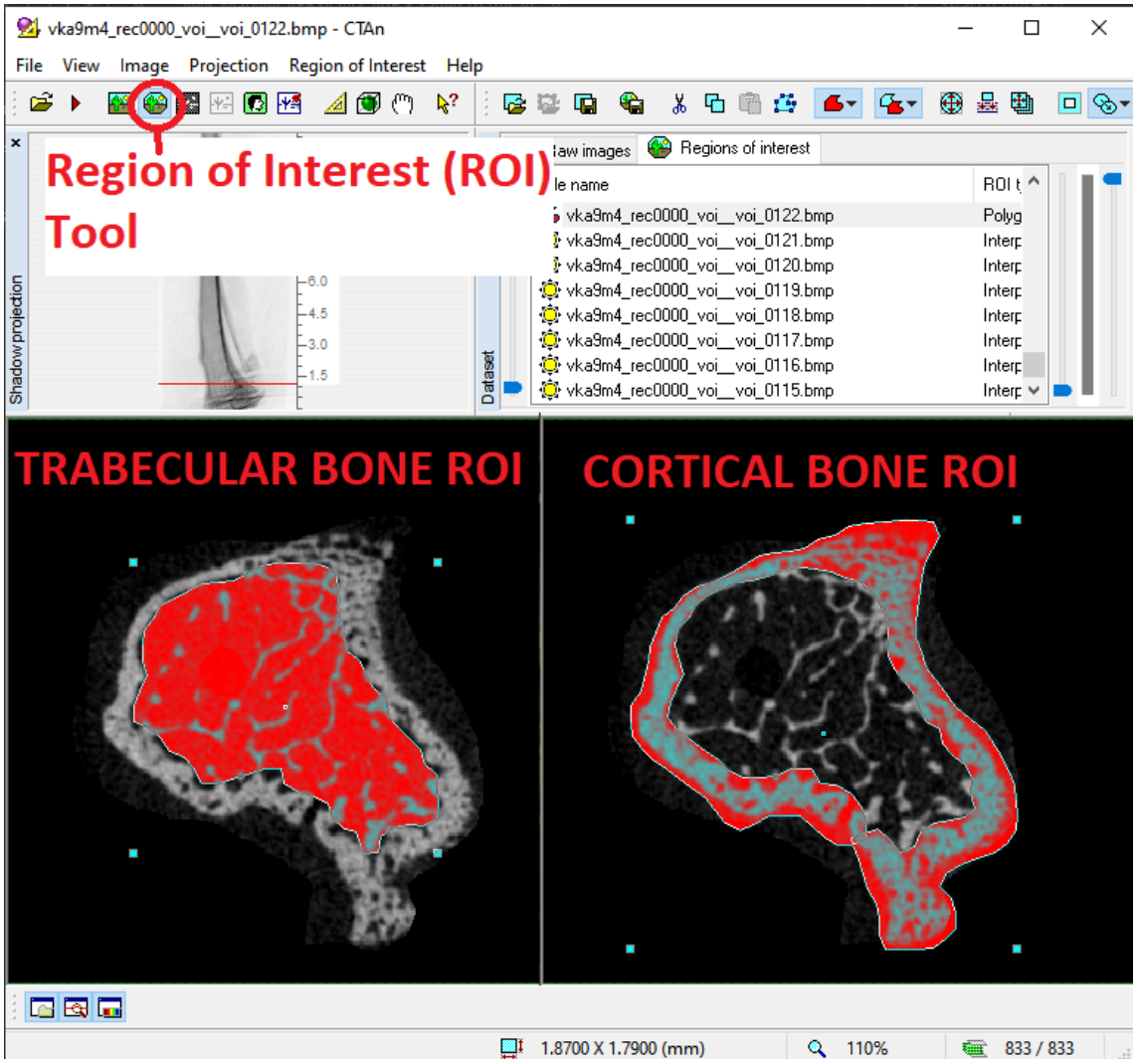

Figure 2-6: Selection of region of interest for trabecular and cortical bones.

Example drawing of trabecular and cortical bones ROI on Osteomeasure.

Bone ROIs were extracted for all the samples, then were analysed with the batch manager. In the analyses, all samples were run through "Thresholding", "Despeckle", and "3D Analysis" in sequence. The thresholding value was set to a minimum of 80-85 and a maximum of 255. Despeckle was set to remove white speckles of less than 10 voxels. Default settings were used for 3D analysis of trabecular bone thickness, number, and separation measurements.

2.2.3.7. Histochemistry

Haematoxylin and Eosin (H&E) Staining

H&E stain is used to visualise various tissue structures; the nucleus of the cells stains blue; cytoplasm and connective tissue are stained pink. Histological sections from paraffin-embedded bones were stained with a standard protocol. Briefly, sections were dewaxed in xylene (2 times, 5

minutes each) and rehydrated with decreasing concentrations of alcohol (99%, 99%, 95% and 70%, 1 minute each) to distilled water. Sections were placed in Gill's Haematoxylin solution (Merck, UK) for 2 minutes. After that, sections were rinsed under the tap water for 5 minutes. After clearing the water, sections were placed in 1% eosin solution (Atom Scientific LTD, UK) for 5 minutes. Before the dehydration, samples were rinsed again with tap water. Slides were dehydrated with increasing alcohol concentrations (70%, 95%, 99%, 99%, 30 seconds each), cleared in xylene and mounted on a cover slip with DPX [(distyrene), plasticizer (tricresyl phosphate) and xylene] (VWR, UK).

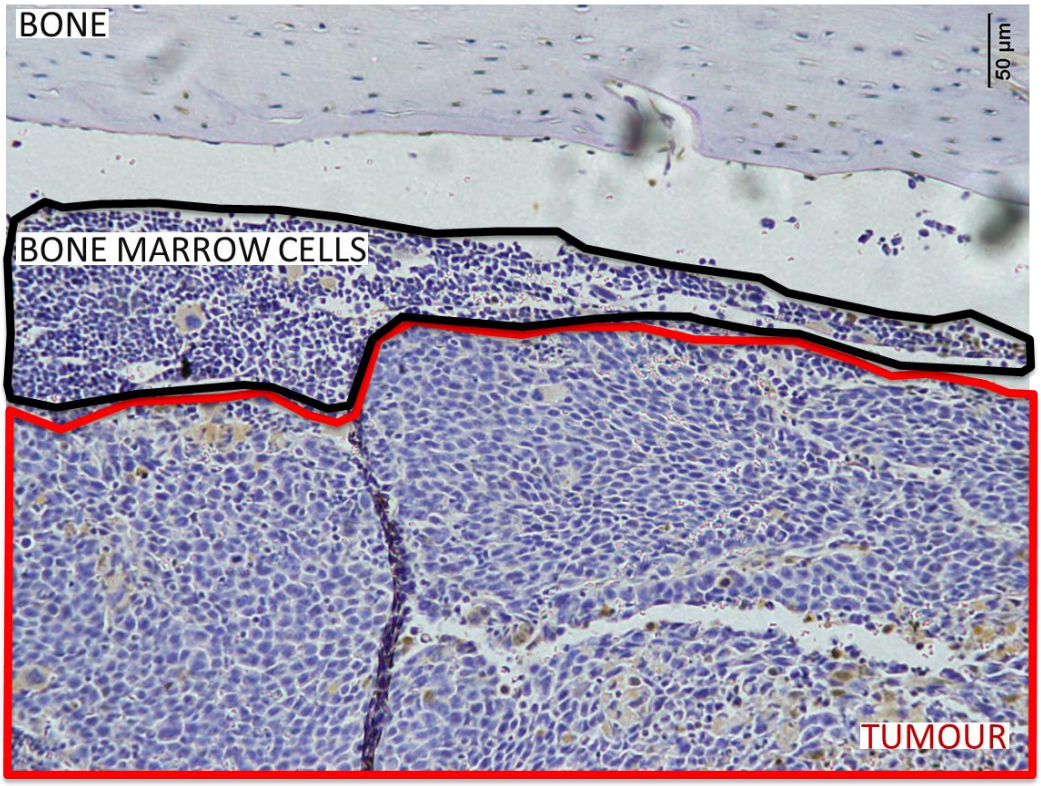

Figure 2-7: Haematoxylin and Eosin Stain.

10x image of bone with breast cancer that shows the H&E staining results on bone marrow cells. Tumour were marked with red border while black border was used to mark the bone marrow cells and the pink-purple coloured area where the widely purple nucleus cells (osteocytes) buried is the bone.

Staining for Tartrate-Resistant Acid Phosphate (TRAP)

Tartrate-Resistant Acid Phosphatase (TRAP) staining is a histological stain that shows osteoclast activity. TRAP is the catalysis of a naphthol-AS-BI phosphate substrate, a key enzyme in bone resorption. Red areas indicate high TRAP activity, which shows osteoclast presence and correlates with the number of osteoclasts. Gill's haematoxylin is used as a counterstain to show cell perimeters and nuclei.

Paraffin-embedded samples were cut at 3 µm thickness and placed on slides left to dry in an incubator at 37 ˚C overnight. Slides were dewaxed and immersed for 5 minutes in a pre-warmed acetate-tartrate buffer prepared by mixing sodium tartrate (Sigma-Aldrich, UK) (2.18% (w/v)) into an acetate buffer of diluted acetic acid (1.2% acetic acid (v/v) (AnalaR, UK) in dH2O) in H2O (20% diluted acetic acid (v/v) in H2O). After the immersion, slides were incubated in naphthol/dimethylformamide solution (2% w/v naphthol AS-BI phosphonate (Sigma-Aldrich, UK)) for 30 min at 37 ˚C. Next, slides were incubated in 4% (w/v) sodium nitrite (Sigma-Aldrich, UK) solution in H2O for 15 min at 37 ˚C. Slides counterstained for 20 seconds in Gill's haematoxylin and dehydrated with increasing alcohol concentrations (70%, 95%, 99%, 99%, 30 seconds each), cleared in xylene and mounted on a cover slip with DPX [(distyrene), plasticiser (tricresyl phosphate) and xylene] (VWR, UK).

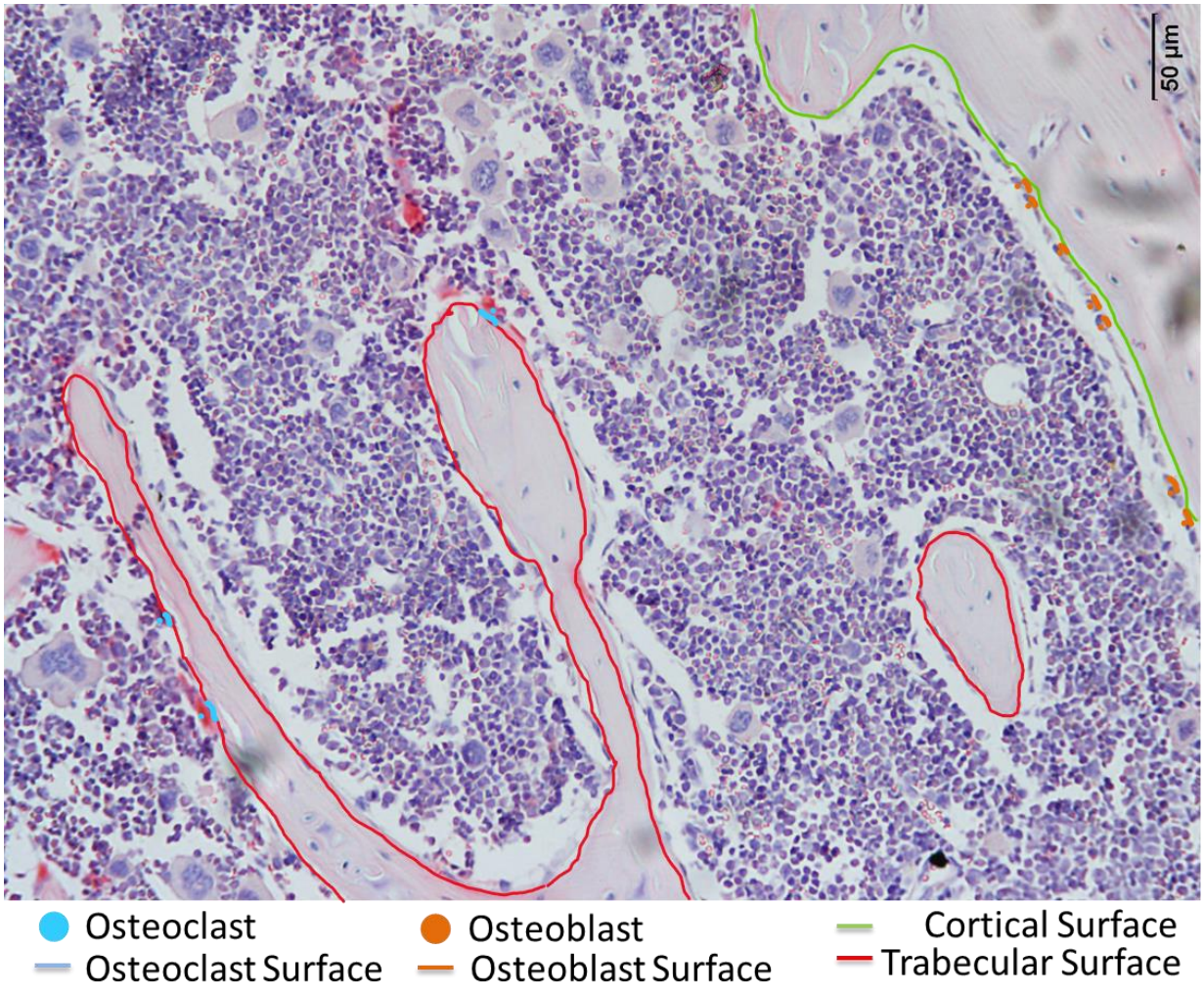

Figure 2-8:Bone section stained for TRAP.

10x image of the bone that shows the stain for TRAP and measured parameters on bone marrow cells. Cortical bone surface (marked with green) and trabecular bone surface (marked with red) measured. Active osteoclasts which are multinuclear and positive for red TRAP stain (marked with cyan dots) and active osteoblasts which are big rectangular cells (marked with orange dots) were counted for both bones. Also, their bone adjacent cell surfaces were measured (cyan line marker for osteoclast and orange line marker for osteoblast)

2.2.3.8. Scoring of Histological Slides

Bone histomorphometry was performed on stained histological sections using Osteomeasure software (Figure 2-9). Osteoblasts were identified by their characteristic cuboidal shape; osteoclasts were identified by bright pink staining under the microscope. This software allows quantification and measurement of the specific bone parameters such as the endocortical and trabecular zone. For the endocortical zone, the chondrocyte zone was taken as a reference point (Figure 2-10), and 250-300 µm was taken as an offset at the end of the chondrocyte zone. After that point, 1.8 mm of the cortical bone was analysed (Figure 2-11).

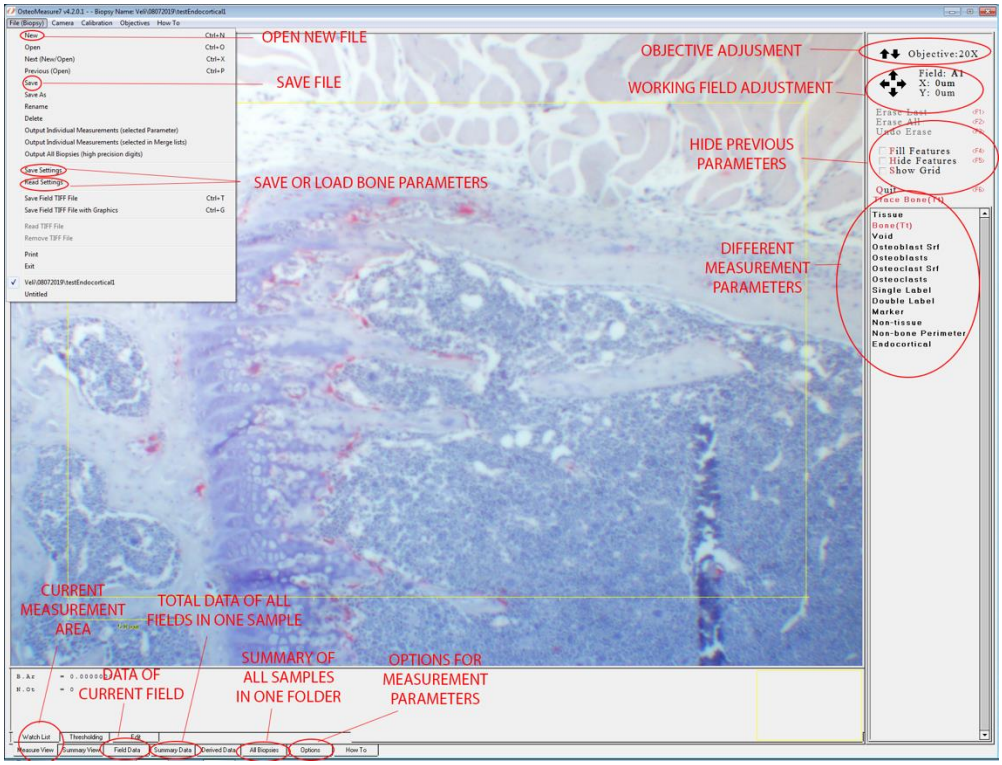

Figure 2-9: Overview of Osteomeasure software.

New: *Opens a new file,* ***Save:*** *Saves current file,* ***Save Settings:*** *Saves settings for Osteomeasure software,* ***Read Settings:*** *Opens saved settings,* ***Objective:*** *Adjusts pixel/distance ratio to the objective,* ***Field:*** *Adjust working field,* ***Features:*** *Adjusts visible analyse features,* ***Measurements:*** *Current settings that are set for different analyse features and list,* ***Measure View:*** *Measurement area,* ***Field Data:*** *current analyse results,* ***Summary Data:*** *Current file's results with all areas,* ***All Biopsies:*** *Summary results of all files that are scored,* ***Options:*** *Options for analysing features settings.*

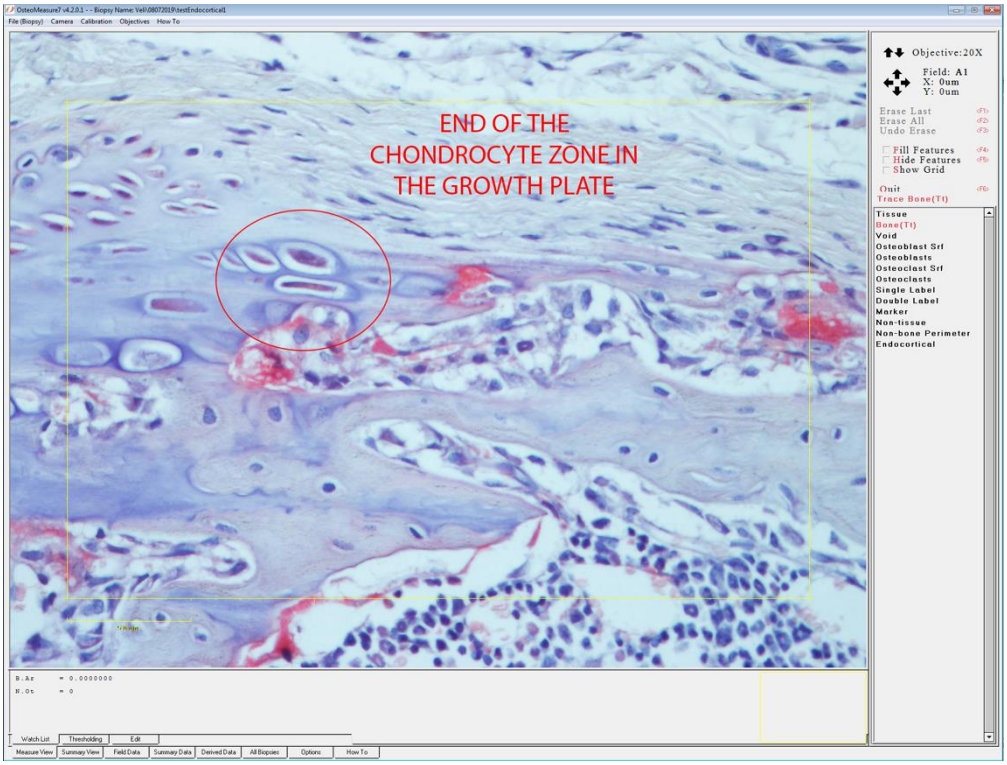

Figure 2-10: Chondrocyte zone for reference point.

Finding the chondrocyte zone in the growth plate as a reference point.

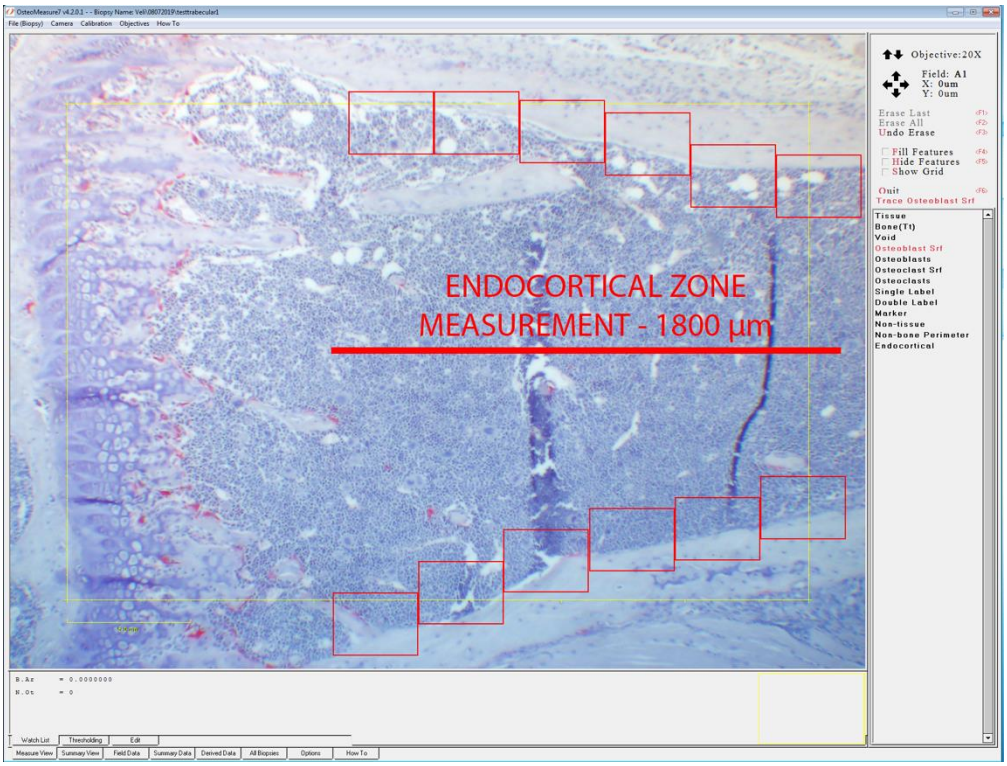

Figure 2-11: Endocortical zone measurement.

Example TRAP scoring for endocortical zone.

The number of osteoclasts (N.Oc), number of osteoblasts (N.Ob), osteoclast surface area(Oc.Pm) on bone, osteoblast surface (Ob.Pm) on bone and bone surface were measured. 0.6 mm of the area was analysed after the offset. For the trabecular zone, the offset value was taken from the ending of the growth plate (Figure 2-12).

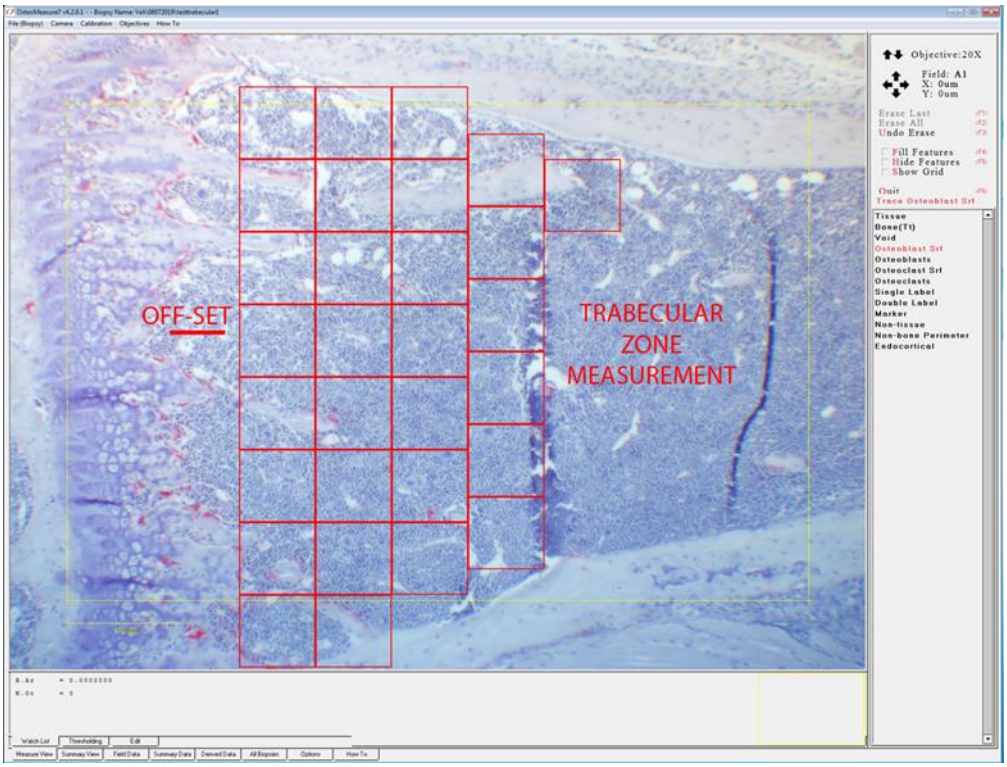

Figure 2-12: Trabecular zone measurement.

Example TRAP scoring for the trabecular zone.

2.2.3.9. Colony Forming Unit (CFU) Assay

Haematopoietic stem cells have different progenitor cells which differentiate into many different types. When these progenitor cells are cultured in suitable semi-solid media, they form colony-like structures, which divide and can be identified. Each colony is derived from a single cell when optimal dilutions and plating conditions are applied. MethoCult GF M3434 is a semi-solid media that can be used to grow different hematopoietic progenitor cells such as erythroid progenitor cells (CFU-E), burst-forming unit-erythroid (BFU-E), granulocyte and/or macrophage progenitor cells (CFU-GM), multi-potential progenitor cells (CFU-GEMM) and B lymphocyte progenitor cells (CFU-pre-B).

$1x10^4$ cells/well were seeded on 6-well plates with 1.1 ml MethoCult GFM3434 (StemCell Technologies, UK) + 10% IMDM (2% FCS+%1 P/S/A), samples were seeded in triplicate. Samples were checked once every two days to detect colony formation for 14 days. Each well had 1.1 mL media

(Figure 2-13). At the end of the experiment, images were taken by an automated system using a Leica AF6000LX inverted microscope, and colonies counted using ImageJ software (Figure 2-14).

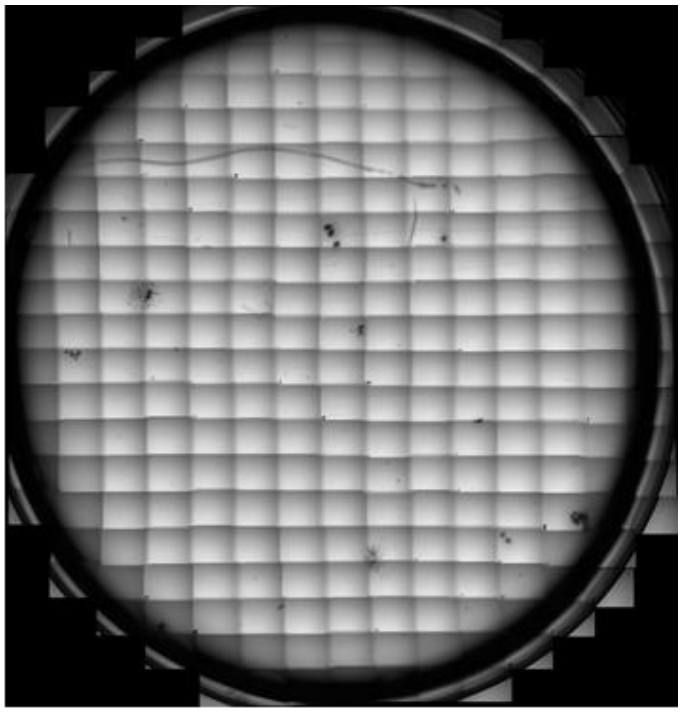

Figure 2-13: Merged image of one well.

Each square image was taken using the Leica AF6000LX inverted microscope with its automated plate reading software, LMX and merged.

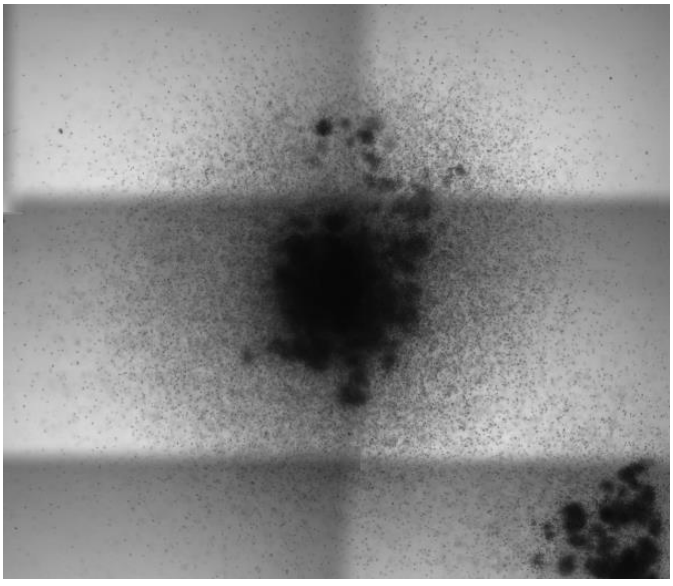

Figure 2-14: Example colony image.

Burst-Forming unit-erythroid (BFU-E) identified from its morphology

2.2.3.10. Flow Cytometry

Either fresh or defrosted cryopreserved bone marrow was used in flow cytometry. Bone marrow was washed in ice-cold PBS supplemented with 1% v/v FBS (FACS buffer). Samples were aliquoted and incubated with fluorochrome-conjugated antibodies and live/dead dyes (

Table 2-4) (diluted 1:100) for 45 min. In flow cytometry, samples were unstained, or labelled with every single stain and fluorescence minus one (FMO: staining the sample with all except one stain) to determine gate. First, samples were stained with live/dead dye (Zombie UV) at room temperature for 30 minutes. After that, samples were incubated with antibodies on ice for 45 min. After each staining process, samples were washed with ice-cold FACS buffer and centrifuged at 500g for 5 minutes to remove the supernatant. After the staining, samples were washed twice with FACS and ran with flow cytometry. Cell populations were compared using a statistical T-Test (Table 2-5).

Table 2-5: Cell populations and flow cytometry markers

Lymphocytes	
T Cells	$CD45^+$, $CD3^+$, $CD19^-$
CD4+ T Cells	$CD45^+$, $CD3^+$, $CD19^-$, $CD4^+$, $CD8^-$
CD8+ T Cells	$CD45^+$, $CD3^+$, $CD19^-$, $CD8^+$, $CD4^-$
B Cells	$CD45^+$, $CD3^-$, $CD19^+$
Natural Killer (NK) Cells	$CD45^+$, $CD3^-$, $CD19^-$, $NK1.1^+$
Myeloid Cells	
Dendritic Cells	$CD45^+$, $CD11b^+$, $CD11c^+$, $MHCII^+$
Neutrophils	$CD45^+$, $CD11b^+$, $Ly6G^+$
Macrophages	$CD45^+$, $CD11b^+$, $Ly6G^-$, $Ly6C^{lo}$, $F4/80^{hi}$
Monocytes	$CD45^+$, $CD11b^+$, $Ly6G^-$, $Ly6C^{hi}$, $F4/80^{lo}$
Granulocytes	$CD45^+$, $CD11b^+$, $Ly6G^-$
HCSs and progenitors	
LSK Cells	Lin^-, $Sca\text{-}1^+$, $cKit^+$
LK Cells	Lin^-, $Sca\text{-}1^-$, $cKit^+$

Analysed cell populations from bone marrow and their markers.

Gating Strategies for flow cytometric analyses

Gating around the cell populations with common characteristics, using forward/side scatters and marker expression level, allows quantification of populations of interest. The following figures show the gating strategies for haematopoietic populations (Figure 2-15), lymphocytes (Figure 2-16) and myeloid populations (Figure 2-17) using side scatter area (SSC-A), forward scatter area (FSC-A) and height (FSC-H) and the markers listed in Table 2-5. All positive or negative gating was determined using fluorescence minus one (FMO) and a single stain for the marker.

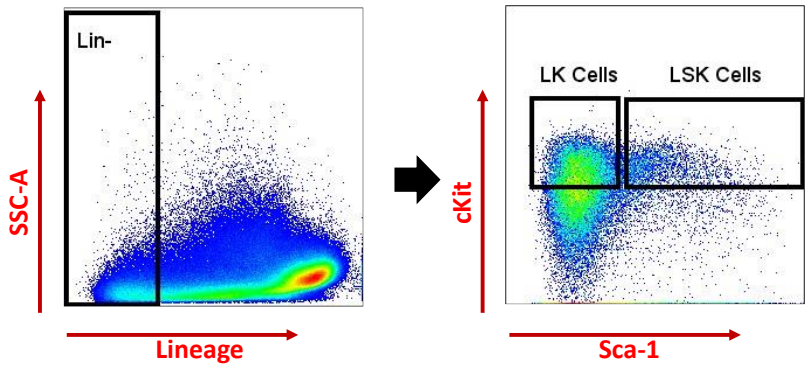

Figure 2-15: Gating strategy for haematopoietic populations.

Gating strategy of HSCs and progenitors: LK Cells (common progenitors) and LSK Cells (HSCs and their multipotent progenitors) were gated under the lineage negative live bone marrow cells.

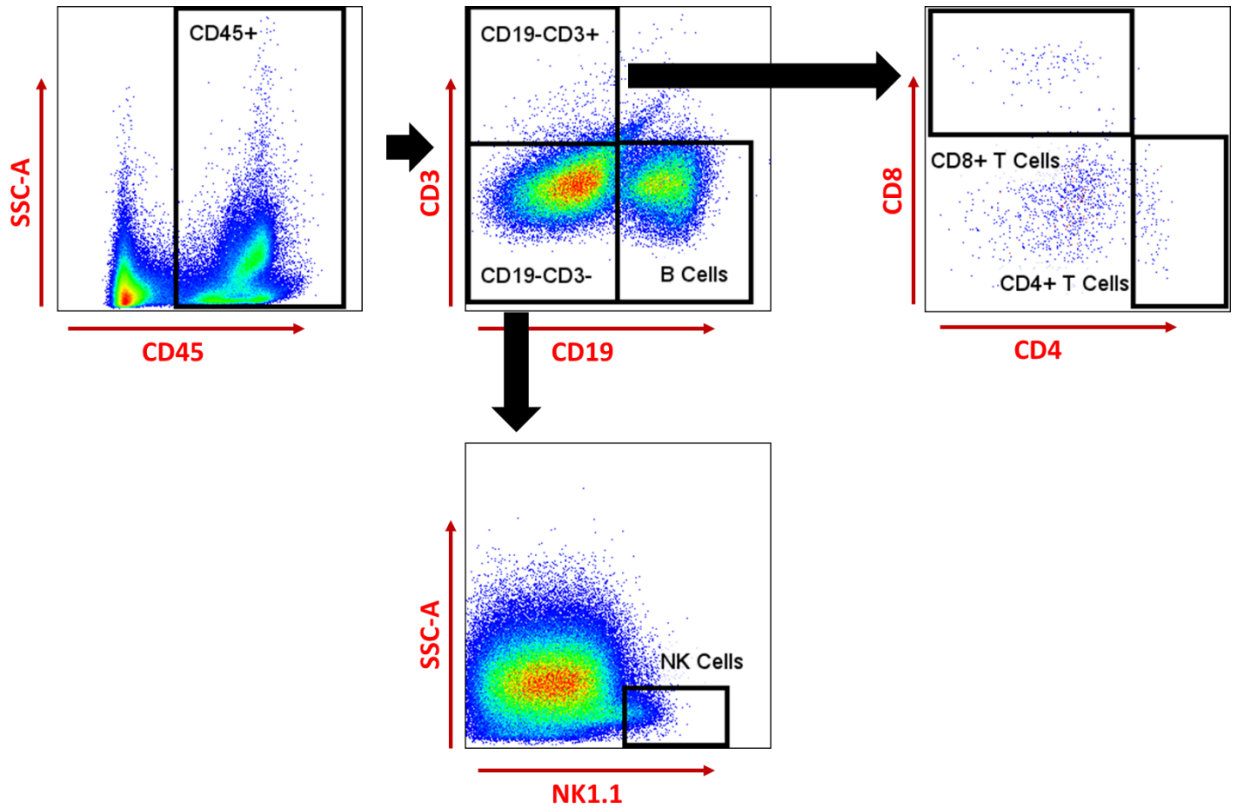

Figure 2-16: Gating strategy for lymphocyte populations.

Gating strategy of Lymphocyte cell populations: CD19/CD3 gating were carried under CD45 positive cells, CD19 positive and CD3 negative cells were gated as they are B lymphocytes, CD19 negative and CD3 positive cells were further gated with CD8 and CD4 antibodies for CD8 positive T cells and CD4 positive T Cells. CD19 and CD3 negative cells were further gated with NK1.1 for NK Cells.

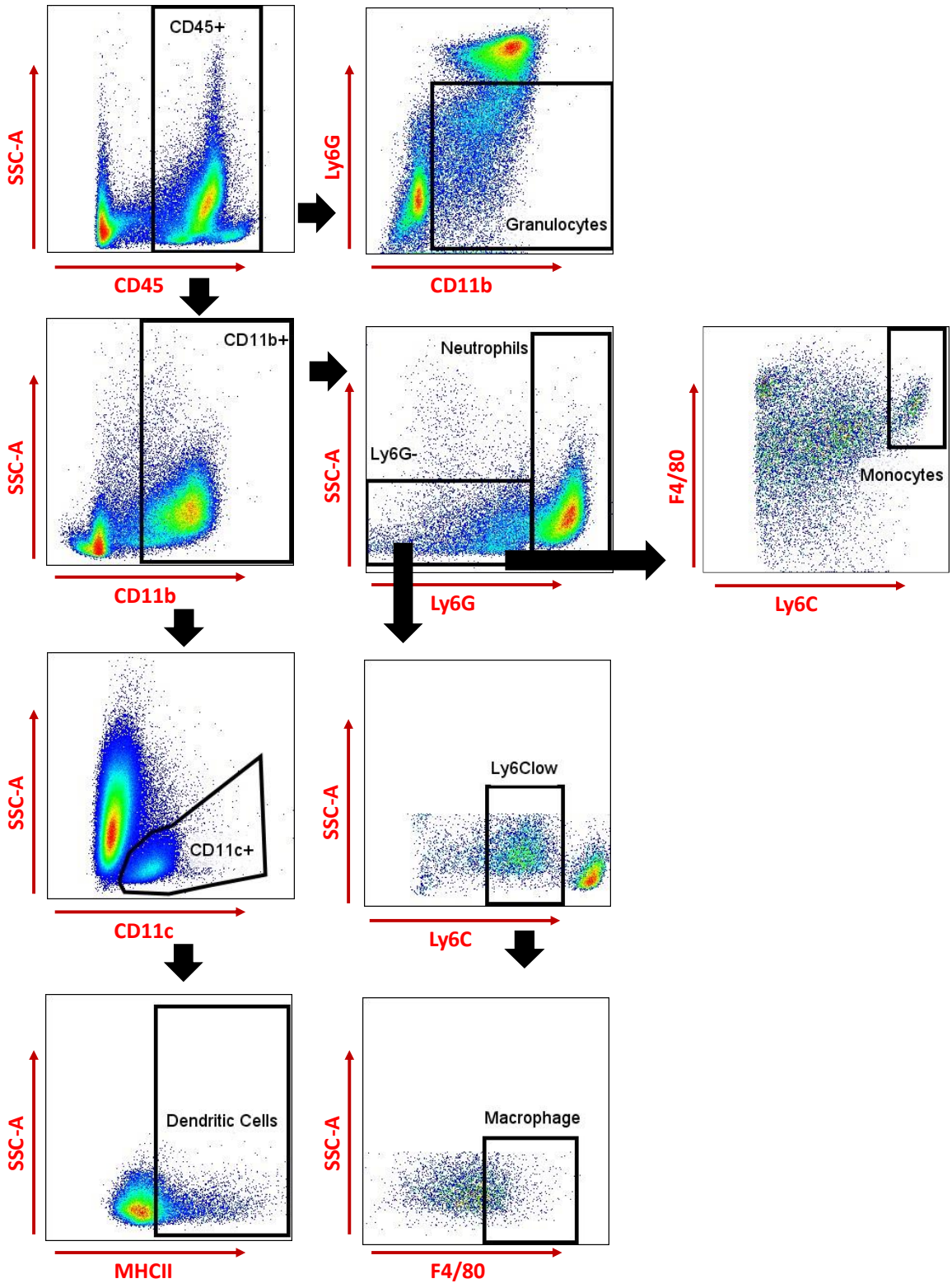

Figure 2-17: Gating strategy for myeloid populations.

Gating strategy for myeloid populations: Granulocytes arise from live CD45 positive bone marrow cells; Neutrophils were gated under the CD11b positive cell populations, and Ly6G negative population giving rise to monocytes and macrophages. Dendritic cells arise from the CD11c positive population from CD11b positive cells.

2.2.4. Statistical Analysis

Statistical analysis was performed using GraphPad Prism version 8.0. All the sample results were compared on GraphPad and used t-test, 2-way ANOVA or Mantel-Cox (Log-Rank) analysis to determine their significance. All experiments were carried out at least three times in triplicates. Data is considered statistically significant at $p<0.05$. $P\leq0.05$ is the first-degree significance (*), $P\leq0.01$ is the second-degree significance (**), $P\leq0.001$ is the third-degree significance (***) and $P\leq0.0001$ is the fourth-degree significance (****)

RESULTS

CHAPTER 3. THE BONE MARROW MICROENVIRONMENT IN DIFFERENT MOUSE STRAINS – IMPACT OF TUMOUR GROWTH

3.1. Summary

Bone metastatic breast cancer causes bone pain and fractures, with current treatments only slowing disease progression. Therefore, understanding the bone and bone marrow composition can help researchers develop better treatments to improve quality of life and survival rates. Murine models are often used to understand the mechanisms underlying breast cancer. However, there is not a single model that comprehensively allows replication of human bone metastasis. Many studies use xenograft models, requiring immunocompromised mice that do not allow investigation of the role of the immune system in this process. Modelling bone metastasis in immunocompetent models has been limited, mainly because of widespread concomitant soft tissue metastasis. It is unclear whether differences in the bone microenvironment between immunocompetent and compromised mice contribute to the different patterns of metastasis. Age and weight-matched immunocompetent syngeneic (BALB/c) and immunocompromised xenograft (BALB/c Nude) strains were used. Bone parameters such as bone structure, bone remodelling cells, haematopoietic stem cell populations, lymphocytes and myeloid cell populations and complete blood count were measured to evaluate whether these models have similarities or detectable statistical differences between them. It is known that the BALB/c Nude strain has defective immunity due to the lack of a thymus, which results in T-Lymphocyte deficiency.

Results obtained from the current study showed that haematopoietic stem cells (HSCs), B-Lymphocytes and myeloid cells from bone marrow were different in the BALB/c Nude strain compared to BALB/c strain. Flow cytometry obtained quantifiable differences from liquid bone marrow. Using μCT there were differences in trabecular bone thickness or numbers between the strains and trabecular separation was found longer in the BALB/c Nude mice. However, no significant differences were observed in bone remodelling cells between the strains, except osteoclast perimeter was found to be longer in the BALB/c Nude trabecular bone. These findings indicate that determination of exact differences is required to understand mechanisms under the disease progression or possible drug effects.

The second study described in this chapter was to explore and, if possible, quantify the early effects of tumours on the bone and bone marrow populations. The xenograft model was used to test this hypothesis. The earliest detectable tumours appeared nine days after injection of the breast cancer cells, and the experiment ended on day 21. Nine out of the ten mice had tumours with measurable hind limb signals, but no measurable difference was found between bone volumes despite the visual observation of the tumour causing bone destruction. However, GFP+ cells could be sorted from the all-signal-bearing bones (9/9). No difference was found in the bone marrow populations in the presence of tumours, which might be the reason for the low tumour burden. Overall, studies in this chapter identified possible differences between different mouse strains used in the studies and indicate these populations might be the reason behind the different results obtained. Also, it shows that the tumour's bone destruction effects, alongside its effects on the cell population, can be observed given sufficient time for tumour development.

3.2. Introduction

Bone metastases are incurable, causing pain, fractures, and hypercalcemia, especially in late-stage breast cancer patients (Hiraga, 2019). Understanding the mechanisms underlying these effects is required to reveal novel potential therapeutic targets, which can help to improve the patient's quality of life and increase the survival rates. As it is impossible to obtain sufficient quantity/quality of bone metastasis samples from patients, well-characterised *in vivo* models must be studied for breast cancer bone metastasis.

Multiple murine models are used to study breast cancer metastasis (Ottewell & Lawson, 2021), and each has different advantages and disadvantages. Achieving spontaneous bone metastasis from a primary tumour is rare; thus, it is hard to reproduce the same efficient model (Mundy, 2002). None of the models can represent all genetic and phenotypic properties of human breast cancer bone metastasis; therefore, a specific problem must be tackled using either the most suitable model or a combination of models. In xenograft models, the immune system is suppressed. Therefore, genetically modified strains or techniques that eliminate the immune system (such as radiation) are used (Wright *et al*, 2016). There are several types of immunodeficient mice; most are T cell deficient, and some lack B cells. Because of this, the role of the adaptive immune system in the development of bone metastasis cannot be explored in xenograft models (Buenrostro *et al*, 2014)

The first immunodeficient mice were defined by Flanagan (Flanagan, 1966); they did not have hair and a thymus and thus were named 'nude'. They lacked the *Foxn1* gene or the HNF-3/forkhead homolog 11 gene (Nehls *et al*, 1994). Lacking a functional thymus significantly reduced the T cells, and only a small number of CD3, CD4, CD8 and Thy-1 antibodies were detected on the remaining T cells. However, they had mature B, dendritic, and NK cells (Belizario, 2009). Therefore, the only difference was expected to be HSC cells.

On the other hand, understanding the immune cells and their interactions with tumour cells has led to new therapeutic strategies (Lal *et al*, 2021). Cancer cells can be eliminated, kept under equilibrium or outgrow, partly depending on the immune system (Pandya *et al*, 2016). The immune system has two sub-categories, innate and adaptive immune cells (Janeway *et al*, 2001). They both consist of different types of myeloid and lymphoid cells and different pathways, yet there is always crosstalk between them. Adaptive immunity is where the immune system remembers the foreign material in the body and produces antibodies, whereas innate immunity detects and eliminates 'non-self' (Delves et al., 2017).

Lacking T cells affects cancer studies, and immune cells interact with the bone and bone marrow cells. Regulatory T cells secrete RANKL (both critical for bone remodelling and cancer) (Xiang & Gilkes, 2019), helper T cells secrete RANK and IL-17 (an essential regulator for RANKL and osteoprotegerin) (Liu *et al*, 2015), and T Helper 17 cells supports bone resorption while regulatory T cells suppress bone resorption (Zhang *et al*, 2020). Therefore, transgenic and syngeneic (immunocompetent) models have been developed to study the immune system interactions with cancer and anti-cancer drugs. Some genes such as the P53 and TGFα are manipulated in transgenic models for spontaneous breast cancer development. However, bone metastasis is hard to achieve with this random manipulation, therefore, syngeneic models with mouse breast cancer cells injected has been used to study bone metastasis (Ottewell & Lawson, 2021).

Understanding the tumour effect on bone and determining if there is a detectable effect on the bone and bone marrow is also essential. Previous studies have shown that increasing tumour burden results in increased bone destruction by showing reduced trabecular bone number and density(Brown *et al*, 2012). Thus, understanding the differences between immunocompetent and immunocompromised models can help us to interpret the results and determine the pathways and cells involved.

3.3. Aims

The work presented in this chapter aims to investigate if there are any differences in the bone and bone marrow in different mouse strains, with and without tumours. The main objectives are:

- To compare the bone microenvironment in immunocompetent and immunocompromised mice.
- To establish protocols for isolation and analysis of bone marrow cell populations from tumour-bearing bones
- To establish if the metastatic bone tumour has quantifiable effects on the bone and bone marrow at the early stages of disease progression

3.4. Material and Methods

3.4.1. Breast Cancer Cell Lines

The triple negative human MDA-MB-231-IV PX462 cell line was cultured in RPMI 1640 with 10% FCS at 37°C 5%CO_2.

3.4.2. *In vivo* Studies

All *in vivo* studies were carried out according to local guidelines and with Home Office approval under project licence PPL 70/8964 held by Professor Nicola Brown or P99922A2E held by Dr Penelope D Ottewell, University of Sheffield, UK. Studies were completed using female BALB/c (immunocompetent) and BALB/c Nude (immunocompromised) mice.

3.4.2.1. Determinating the differences between immunocompetent and immunocompromised strains.

In the subsequent chapters, age-matched immunocompetent (BALB/c) and immunocompromised mice (BALB/c Nude) have been used as control groups for both drug and tumour studies. Data in this chapter are the combined data from the control groups, which were treated with saline once a week for four weeks. Animals were culled two days after the last saline treatment, and peripheral blood (PB) and bone marrow were collected for the colony formation assay. Hind limb bones were collected for µCT to determine bone structure and integrity, and histology (H&E, staining for TRAP) carried for bone remodelling cells. Bone marrow from hind limbs were used for flow cytometry to determine HSCs, lymphocytes, and myeloid populations. Data obtained from downstream analysis were compared using the statistical students' T-tests (Figure 3-1).

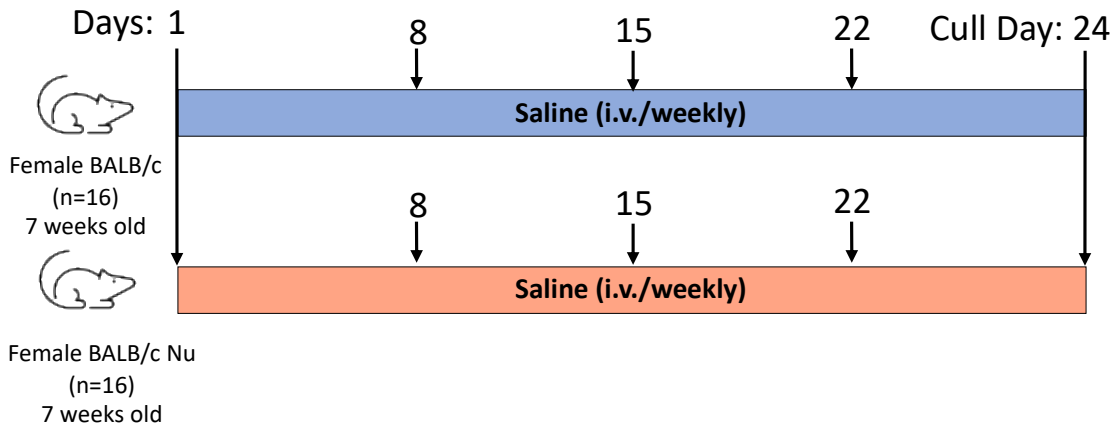

Figure 3-1: Comparison between immunocompetent and immunocompromised strains.

Experimental outline to compare the differences between immunocompetent and immunocompromised strains. Data from saline-treated 7-week-old female BALB/c and BALB/c Nude animals (n=16/group) were statistically analysed using a T-Test.

3.4.2.2. Effects of bone metastatic breast tumour on the bone and bone marrow.

6-week-old female BALB/c Nude animals were injected with either saline (n=5) or $1x10^5$ Luc2+ve MDA-MB-231 cells (n=10) via the intracardiac route to determine whether there is a quantifiable effect of bone metastatic breast tumours on the liquid bone marrow. Animals were observed with *in vivo* imaging and culled one week after the hind limb tumour development (day 21); peripheral blood was collected for blood counts, and hind limbs were collected for µCT and flow cytometry (Figure 3-2).

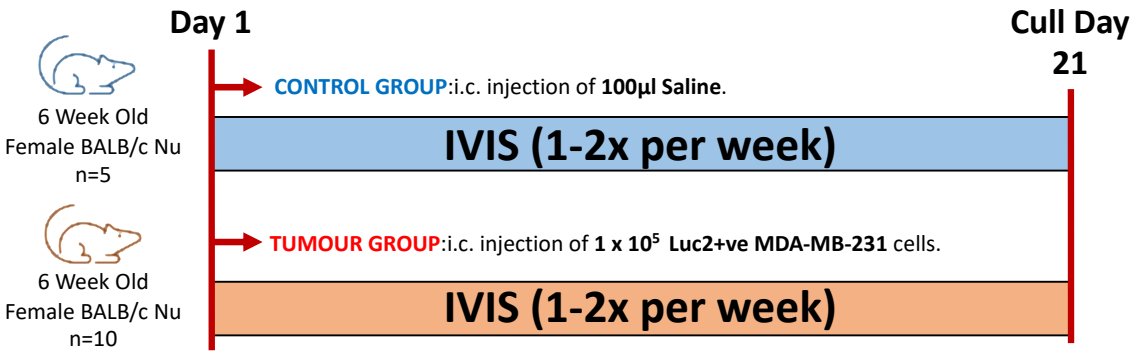

Figure 3-2: Determining the quantifiable effects of the tumour on the liquid bone marrow and bone.

The effects of bone metastatic breast tumours on the bone and bone marrow were tested with this experimental design. 6-Week-old female BALB/c Nude animals had an intracardiac injection of either saline (n=5) or 1x10^5 Luc2+ve MDA-MB-231 cells (n=10). In vivo imaging was used to monitor the tumour growth, and animals were culled one week after the hind limb tumour development. Hind limb bones and peripheral blood were collected for ex vivo analysis.

3.4.3. *In vivo* imaging of tumour development.

Mice were put under anaesthesia with 2.5% isoflurane, then injected with 100 µl 30 mg/mm Luciferin subcutaneously. After 5 minutes, animals were placed in the imaging chamber, and non-invasive *in-vivo* imaging was performed. The bioluminescent signal was visualised in animals at different time intervals to compare tumour development. First, images were normalised by setting thresholds that depend on the image that has the lowest detectable tumour (Figure 3-3, i), each specific spheroid was counted as a separate tumour, and images in Figure 3-3, ii represent different signals from tumours in the skull (A), spine (B), hind limbs (C) and jaw (D). Depending on the model, some animals had chest signals caused by tumour cells in the sternum or the lungs. After the collection of hind limb bones, *ex vivo* images were captured to detect the numbers/location of tumours inside the bones (Figure 3-3, iii). The total count of the signal was divided by 4 to calculate the overall tumour number/per mouse hind limb bone (example calculation for the image in Figure 3-3,iii: 4 bones had signals which are 4 / 4 = 1 tumour per bone).

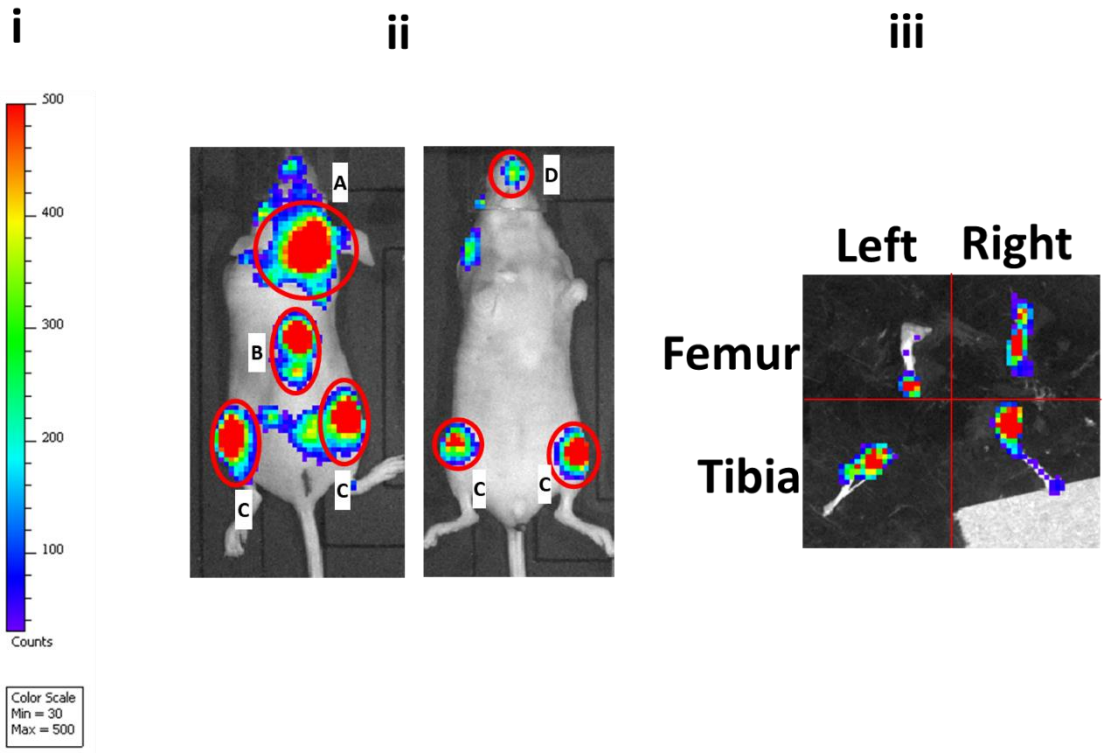

Figure 3-3: Calculating *in vivo* and *ex vivo* bone tumour numbers.

Example images to illustrate tumour number calculations. i) Example threshold to normalise the tumour signals for that specific experiment, given threshold was used in these example images. ii) In-Vivo imaging of a mouse that has a signal in the skull (A), spine (B), hind limbs (C) and jaw (D), whereas each spherical signal count as one tumour. iii) Ex-Vivo image of hind limb bones, where each signal counts as separate tumours.

3.4.4. *Ex Vivo* analyses of tumour growth in bone

3.4.4.1. Collection and preparation of the bones for microcomputed tomography (µCT) and histology.

Hind limbs were removed from the carcass, all soft tissue removed, and tibias separated from the femurs. Bones were placed in 4% PFA overnight and then washed and stored in PBS at 4°C. Random tumour-free tibias (n=3-4) were selected for µCT and then decalcified, processed, embedded in wax and sectioned to 3 µm slides. Slides were either stained with TRAP or H&E for bone remodelling cell analyses.

3.4.4.2. Collection of bone marrow.

After separation of the femurs from the carcass, they were dipped in 100% EtOH for surface disinfection. Under the sterile hood, the femoral head was removed, and the bone was placed into 0.2 ml PCR tubes with a hole pierced in the bottom. Tubes were placed into 1.5 ml Eppendorf containing 200 ml PBS and bone marrow spun out with 3000 g for 5 min. After collection of bone marrow, it was washed with PBS containing 10% FCS and processed by colony formation assays or stained for flow cytometry.

3.4.4.3. Collection and preparation of peripheral blood of colony forming unit and blood count.

Peripheral blood (PB) was collected via terminal cardiac puncture. 0.5-1 ml PB was taken from each animal to the syringe, and 100 µl of PB was transferred into 1.5 ml Eppendorf containing 50 µl EDTA (anticoagulant) for blood analyses and 0.5 ml of PB was transferred into 1.5 ml Eppendorf containing 50 µl EDTA (anticoagulant) for colony-forming assays.

3.4.4.5. Flow Cytometry

Flow cytometry analysis was conducted using the LSRII, and fluorescent activated cell sorting was conducted on the FACSMelody. Data analysis was conducted using FlowJo software. Lymphocyte, myeloid and haematopoietic stem cell populations were analysed (Table 3-1).

Table 3-1: Cell populations and flow cytometry markers

Lymphocytes	
T Cells	$CD45^+$, $CD3^+$, $CD19^-$
CD4+ T Cells	$CD45^+$, $CD3^+$, $CD19^-$, $CD4^+$, $CD8^-$
CD8+ T Cells	$CD45^+$, $CD3^+$, $CD19^-$, $CD8^+$, $CD4^-$
B Cells	$CD45^+$, $CD3^-$, $CD19^+$
Natural Killer (NK) Cells	$CD45^+$, $CD3^-$, $CD19^-$, $NK1.1^+$
Myeloid Cells	
Dendritic Cells	$CD45^+$, $CD11b^+$, $CD11c^+$, $MHCII^+$
Neutrophils	$CD45^+$, $CD11b^+$, $Ly6G^+$
Macrophages	$CD45^+$, $CD11b^+$, $Ly6G^-$, $Ly6C^{lo}$, $F4/80^{hi}$
Monocytes	$CD45^+$, $CD11b^+$, $Ly6G^-$, $Ly6C^{hi}$, $F4/80^{lo}$
Granulocytes	$CD45^+$, $CD11b^+$, $Ly6G^-$
HCSs and progenitors	
LSK Cells	Lin^-, $Sca\text{-}1^+$, $cKit^+$
LK Cells	Lin^-, $Sca\text{-}1^-$, $cKit^+$

Analysed cell populations from bone marrow and their markers.

Gating Strategies for flow cytometric analyses

Gating around the cell populations with common characteristics, using forward/side scatter and marker expression level, allows quantification of populations of interest. The following figures show the gating strategies for haematopoietic populations (Figure 3-4), lymphocytes (Figure 3-5) and myeloid populations (Figure 3-6) using side scatter area (SSC-A), forward scatter area (FSC-A) and height (FSC-H) and the markers listed in Table 3-1. All positive or negative gating was determined using fluorescence minus one (FMO) and a single stain for the marker.

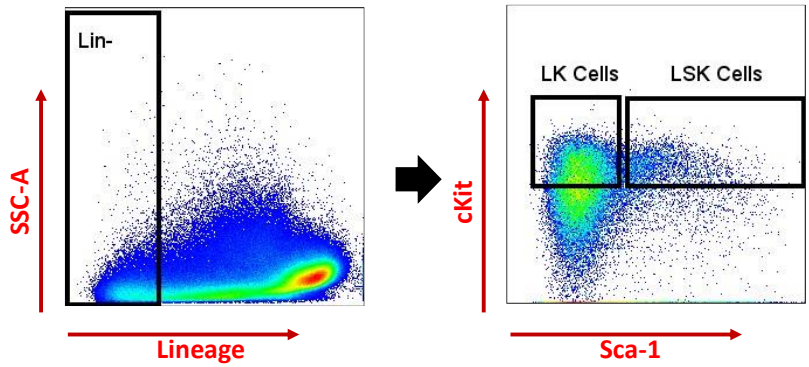

Figure 3-4: Gating strategy for haematopoietic populations.

Gating strategy of HSCs and progenitors: LK Cells (common progenitors) and LSK Cells (HSCs and their multipotent progenitors) were gated under the lineage negative live bone marrow cells.

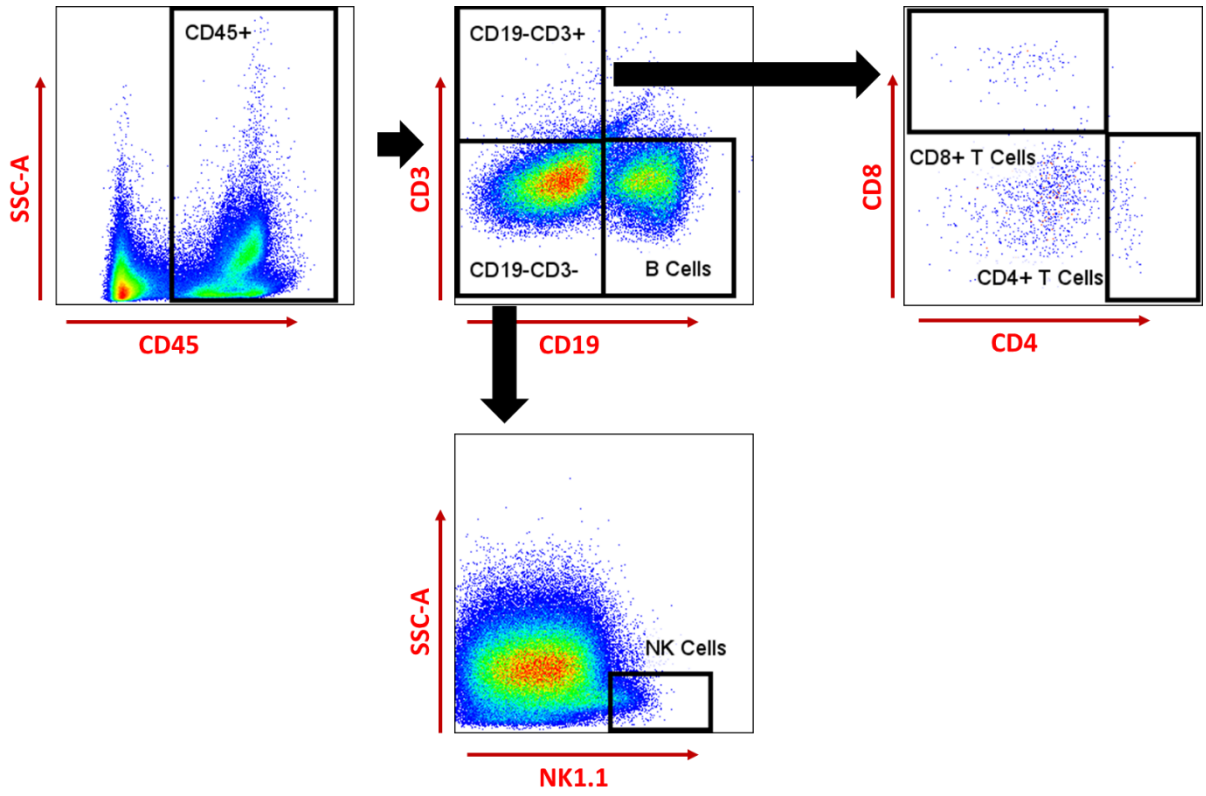

Figure 3-5: Gating strategy for lymphocyte populations.

Gating strategy of Lymphocyte cell populations: B Lymphocytes were gated under the live CD45 positive bone marrow cells, CD19 negative and CD3 positive compartment giving rise to the T Lymphocytes and both CD19, CD3 negative compartment giving rise to the NK Cells.

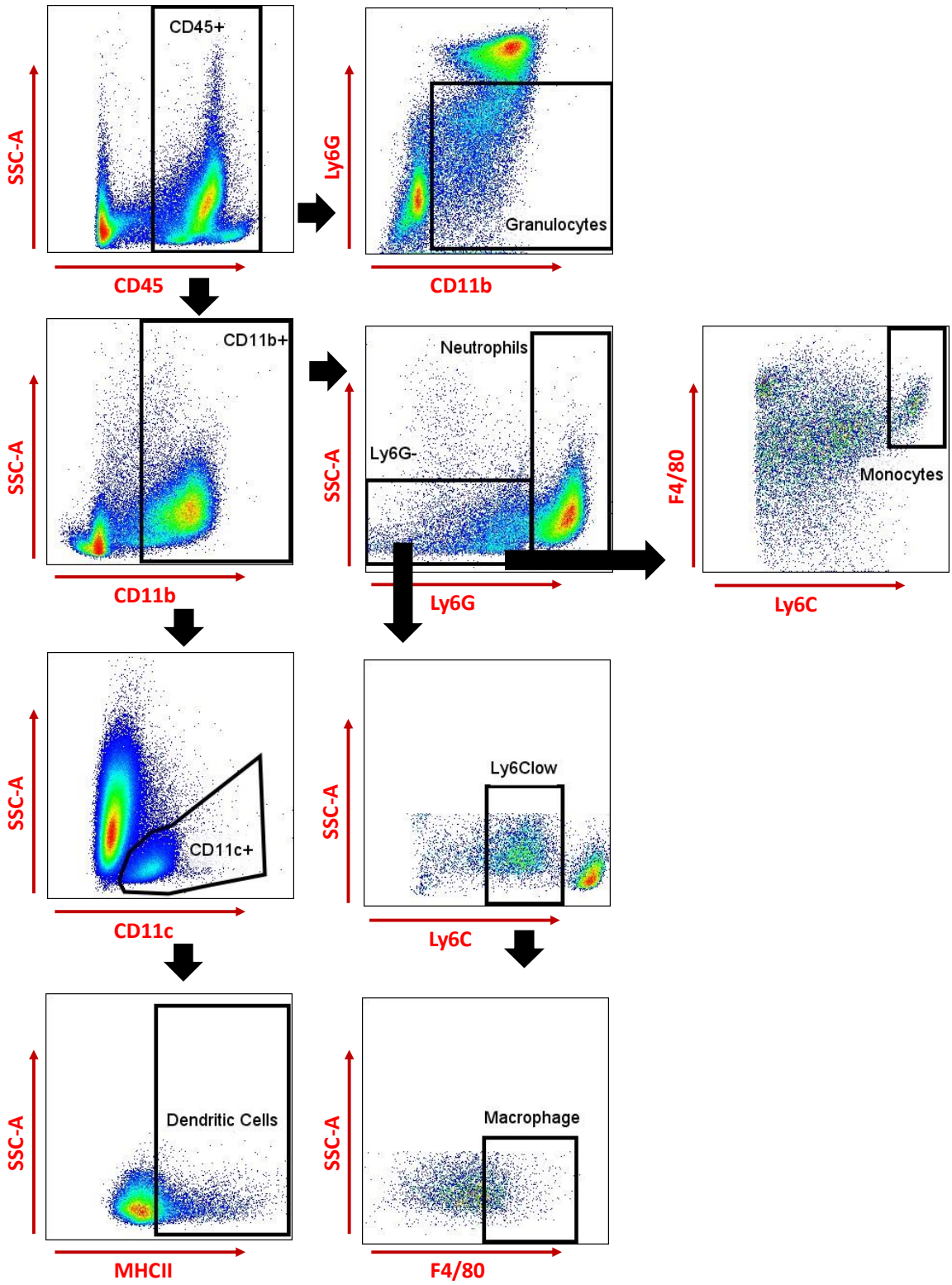

Figure 3-6: Gating strategy for myeloid populations.

Gating strategy for myeloid populations: Granulocytes were given arise from live CD45 positive bone marrow cells, Neutrophils were gated under the CD11b positive cell populations, and Ly6G negative population gave rise to monocytes and macrophages. Dendritic cells were given arise from the CD11c positive population from CD11b positive cells.

3.5. Results

3.5.1. Comparison of immunocompetent and immunocompromised mice bone marrow

To establish the structural and cellular differences of the BME between age-matched immunocompetent and immunocompromised mice, a detailed analysis of the data from the control groups of previous experiments described in subsequent chapters was conducted. Briefly, 6-week-old female BALB/c and BALB/c Nude mice were treated with saline (i.v.) for four weeks (Figure 3-1). After cull, samples of hind limbs were analysed with µCT, stained for TRAP, colony-forming unit analysis for HSCs and flow cytometry. Data from experiments were combined and compared using a statistical T-test.

The body weight of animals is an indicator of health, and it also represents the animal's size, which may create biological differences between groups. There were no significant differences in weight between the two groups over the 28 days of the experiment; therefore, there was no difference between groups except in their strains (Figure 3-7).

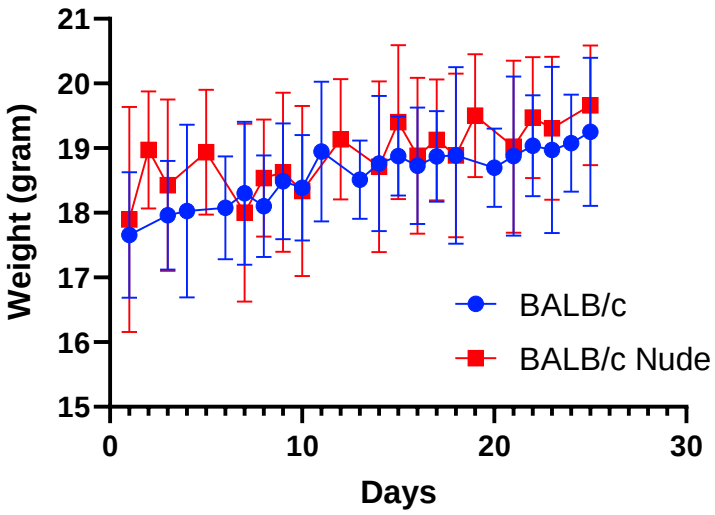

Figure 3-7: Body weight change for immunocompetent and immunocompromised strains.

Daily body weight comparison between BALB/c and Nude strains, 2-way ANOVA was used for statistical analysis, n=16/group, data in the graph given as Mean+/-SD

Bone structure and integrity

Impact on bone structure and integrity is crucial for all bone diseases; therefore, it is widely used to determine the damage caused by metastatic breast cancer. Establishing whether there is a structural difference in the bone between immunocompetent and immunocompromised mice could help interpret experiments and allow the comparison of results obtained in different strains. Since the experiments are designed to test one or multiple comparisons to the appropriate control, it is always shown as change (% etc).

Data comparison showed that (Table 3-2), there were no differences found in trabecular bone density (BALB/c: 11.36±1.39, NUDE: 9.86±2.25,p:ns)(Figure 3-8A), trabecular number (BALB/c: 2.62±0.28, NUDE: 2.34±0.5, p:ns)(Figure 3-8B) and trabecular thickness (BALB/c: 0.04±0.002, NUDE: 0.04±0.002, p:ns)(Figure 3-8C) between BALB/c and BALB/c Nude strains. Trabecular separation (main diameter of cavities in trabecular bones) was significantly higher in BALB/c Nude than BALB/c (BALB/c: 0.81±0.06, NUDE: 0.68±0.05, p:<0.0001) (Figure 3-8D). The cortical bone volume of the BALB/c Nude strain was significantly lower than the BALB/c strain. (BALB/c: 0.2±0.036, NUDE: 0.25±0.03, p:0.0003) (Figure 3-8E).

Table 3-2: Quantifying structural bone parameters of immunocompetent and immunocompromised strains.

	BALB/c	**NUDE**	**P**
Trabecular Bone Density (BV/TV, %)	11.36±1.39	9.86±2.25	ns:0.052
Trabecular Number (Tb.N., mm)	2.62±0.28	2.34±0.5	ns:0.09
Trabecular Thickness (Tb.Th., mm)	0.04±0.002	0.04±0.002	ns:0.1759
Trabecular Separation (Tb.Sp., mm)	0.2±0.036	0.25±0.03	***:0.0003
Cortical Bone Volume (BV, mm^3)	0.81±0.06	0.68±0.05	****:<0.0001

*Overall µCT quantification of trabecular bone density (BV/TV, %), Trabecular Number (Tb.N., mm), Trabecular Thickness (Tb.Th., mm) and Cortical Bone Volume (BV, mm3) was assessed at the end of the experiment. T-Test was used for statistical analysis, and ns is non-significant, ** is ≤0.01, *** is ≤0.001, **** is ≤0.0001, and data show Mean±SD, n=13 for BALB/c and BALB/c Nude.*

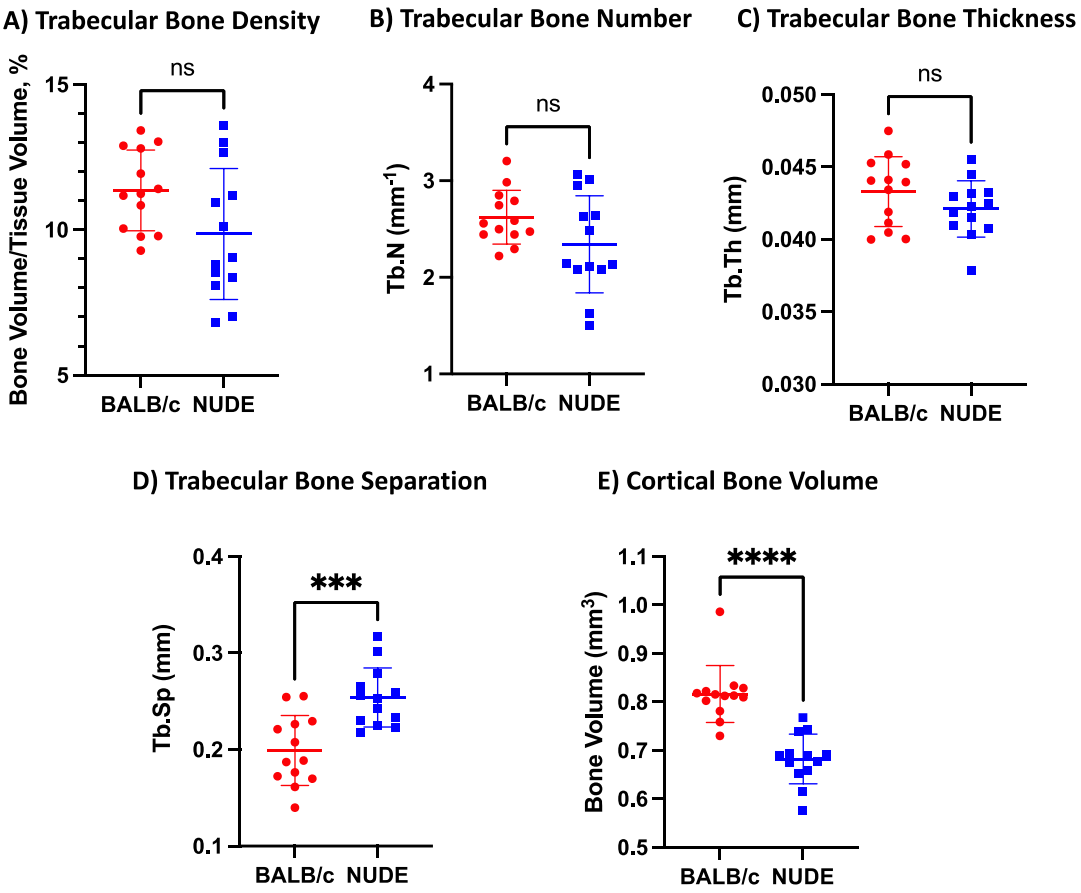

Figure 3-8: Comparison of structural bone parameters of immunocompetent and immunocompromised strains.

*Comparison of bone structure parameters between BALB/c and BALB/c Nude strains. A) Trabecular Bone Density (BV/TV, %), B) Trabecular Number (Tb.N., mm), C) Trabecular Thickness (Tb.Th., mm), D) Trabecular Bone Separation (Tb. Sp, mm) and E) Cortical Bone Volume (BV, mm3) was assessed at the end of the experiment. T-Test was used for statistical analysis, and ns is non-significant, ** is ≤0.01, *** is ≤0.001, **** is ≤0.0001, and data show Mean±SD, n=13 for BALB/c and BALB/c Nude groups.*

Although the trabecular bone thickness and density were similar between both strains, trabecular separation was larger in BALB/c Nude strain. The most significant difference was in the cortical bone, with BALB/c having a greater cortical bone volume than the BALB/c Nude (Figure 3-8).

Bone remodelling cells

Osteoblasts and osteoclasts are the main cell types responsible for bone remodelling, and despite the different bone lesion types (osteolytic or osteoblastic), they play crucial roles in tumour progression. Therefore, comparing the two mouse strains, the number of osteoblasts and osteoclasts in different bone regions (endocortical and trabecular) was determined.

Endocortical Bone

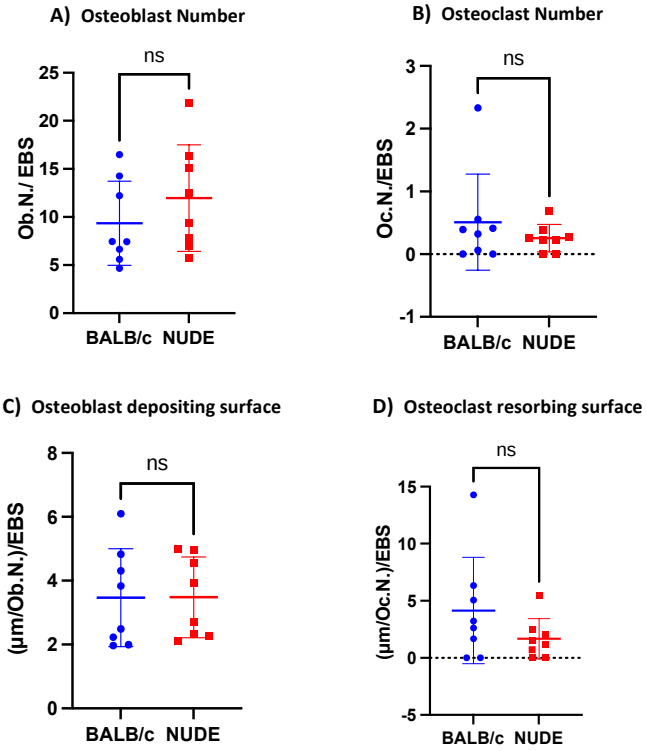

Figure 3-9: Bone remodelling cells comparison between immunocompetent and immunocompromised mice's endocortical bone region.

Comparison of the bone remodelling cell numbers and depositing/resorbing surface parameters of BALB/c and BALB/c Nude groups. Graphs show (A) osteoblast number(Ob.N.) per mm endocortical bone surface (EBS), (B) effects on osteoclast number (Oc.N.) per endocortical bone surface (EBS), (C) overall of per osteoblast bone depositing surface per mm EBS, (D) overall of per osteoclast bone resorbing surface per mm EBS (E) Osteoblast and Osteoclast ratio, T-Test was used for statistical analysis, ns is non-significant, data show Mean±SD n=8 for BALB/c and BALB/c Nude groups.

Endocortical bone is the bone marrow surface of the cortical bone where osteoblasts predominantly. The data showed no significant difference in either osteoblast or osteoclast numbers per mm endocortical bone surface (Figure 3-9) or their active depositing/resorbing surface between the two mice strains (Table 3-3).

Table 3-3: Bone remodelling cell numbers in the endocortical region of immunocompetent and immunocompromised strains.

	BALB/c	NUDE	P
Osteoblast Number (Ob.N./mm EBS)	9.34±4.37	11.97±5.54	ns:0.31
Osteoclast Number (Oc.N./mm EBS)	0.5±0.76	0.25±0.22	ns:0.38
Osteoblast depositing surface ((µm/Ob.N.)/ mm EBS)	3.47±1.54	3.48±1.26	ns:0.98
Osteoclast resorbing surface ((µm/Oc.N.)/ mm EBS)	4.15±4.65	1.67±1.77	ns:0.18

Bone remodelling cell numbers and their active depositing/resorbing surface parameters of BALB/c and BALB/c Nude mice's endocortical bone region. Data show Mean±SD n=8 for BALB/c and BALB/c Nude groups. T-Test was used for statistical analysis, and ns is non-significant.

Trabecular Bone

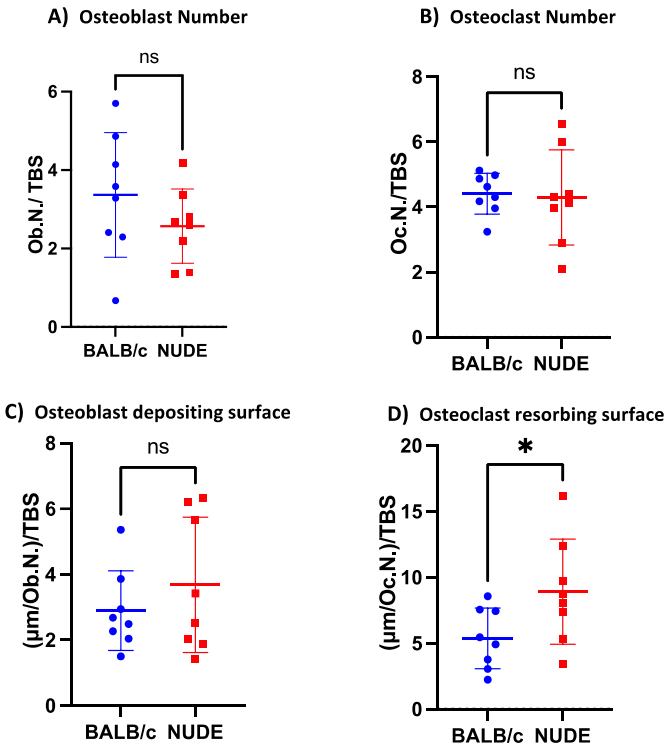

Figure 3-10: Bone remodelling cells comparison in the trabecular region in immunocompetent and immunocompromised mice.

*Comparison of the bone remodelling cell numbers and depositing/resorbing surface parameters of BALB/c and BALB/c Nude. Graphs show (A) osteoblast number(Ob.N.) per mm trabecular bone surface (TBS), (B) effects on osteoclast number (Oc.N.) per trabecular bone surface (TBS), (C) overall of per osteoblast bone depositing surface per mm TBS, (D) overall of per osteoclast bone resorbing surface per mm TBS (E) Osteoblast and Osteoclast ratio, T-Test was used for statistical analysis, ns is non-significant, * is p<0.05, data show Mean±SD n=8 for BALB/c and BALB/c Nude groups.*

Results obtained from analysing the data (Table 3-4) showed that, osteoblast (BALB/c: 3.36±1.59, NUDE: 2.57±0.95, p:ns) (Figure 3-10A) and osteoclast number (BALB/c: 2.89±1.21, NUDE: 3.68±2.06, p:ns)(Figure 3-10B) per mm trabecular bone is similar for both BALB/c and BALB/c Nude strains. The average active bone depositing surface per osteoblast in the mm trabecular bone was also similar (BALB/c: 4.41±0.62, NUDE: 4.3±1.46, p: ns) (Figure 3-10C). However, BALB/c Nude mice had a greater osteoclast surface for active bone-resorption than the BALB/c mice (BALB/c: 5.38±2.3, NUDE: 8.91±3.99, p: *:0.048) (Figure 3-10D).

Table 3-4: Bone remodelling cell numbers in the trabecular bone region of immunocompetent and immunocompromised strains.

	BALB/c	**NUDE**	**P**
Osteoblast Number (Ob.N./mm EBS)	3.36±1.59	2.57±0.95	ns:0.24
Osteoclast Number (Oc.N./mm EBS)	2.89±1.21	3.68±2.06	ns:0.37
Osteoblast depositing surface ((µm/Ob.N.)/ mm EBS)	4.41±0.62	4.3±1.46	ns:0.84
Osteoclast resorbing surface ((µm/Oc.N.)/ mm EBS)	5.38±2.3	8.91±3.99	*:0.048

*Bone remodelling cell numbers and their active depositing/resorbing surface parameters of BALB/c and BALB/c Nude mice's trabecular bone region. T-Test was used for statistical analysis, and ns is non-significant, * is p<0.05 data show Mean±SD n=8 for BALB/c and BALB/c Nude groups.*

Overall, the number of osteoblasts and osteoclasts were similar in both strains for both endocortical and trabecular bone regions; the only difference found was that the average osteoclast perimeter/mm trabecular bone was higher in the BALB/c nude strain compared to the BALB/c mice.

Haematopoietic Stem Cells

The haematopoietic stem cell niche has been suggested as a potential niche for breast cancer metastasis. ***LSK cells*** (Lineage(-), Sca-1(+), C-Kit(+)) (defined as HSCs and progenitors) and ***LK cells*** (Lineage(-), Sca-1(-), C-Kit(+)) (common myeloid populations, granulocyte-macrophage progenitors and megakaryocytes-erythrocyte progenitors), are the main components of the HSCs niche. Therefore, flow cytometry was used to quantify these cell populations in bone marrow samples from BALB/c and BALB/c nude mice.

Comparison of the flow cytometry results showed that the number of both LSK (BALB/c: 0.54±0.13, BALB/c Nude: 0.19±0.05, p:<0.0001)(Figure 3-11A) and LK cells (BALB/c: 2.97±0.62, BALB/c Nude: 1.86±0.35, p: 0.0006)(Figure 3-11B) expressed as % of live cells were significantly lower in the BALB/c Nude strain compared to the BALB/c strain.

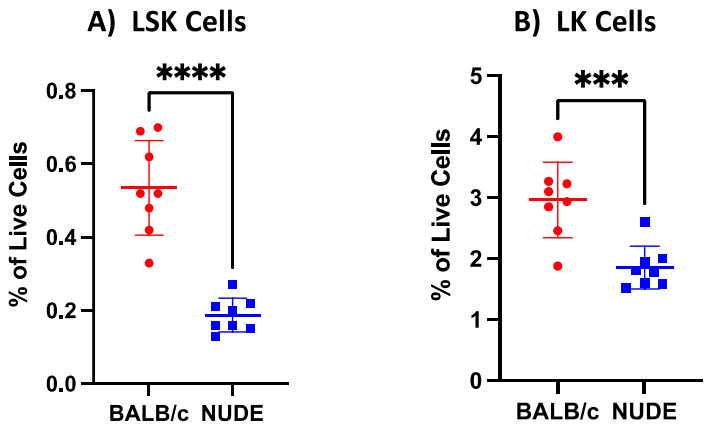

Figure 3-11: Bone marrow haematopoietic stem cells and progenitors in immunocompetent and immunocompromised strains.

*Comparison of A) LSK Cell and B) LK Cell data as % of live cells from BALB/c and BALB/c Nude bone marrow, T-Test was used for statistical analysis, ns is non-significant, *** is p<0.001, **** is p<0.0001 and data show Mean±SD, n=8 for BALB/c and BALB/c Nude groups.*

Table 3-5: Immune Cell Characteristics of strains used.

	BALB/c	**BALB/c NUDE**
Mature T Lymphocytes	Present	Absent
Mature B Lymphocytes	Present	Present
NK Cells	Present	Present
Genetics	Inbred	Inbred
Hair Coat	Yes	No

The supplier provided immune phenotypes of the strains used in this study (BALB/c Nude Mouse | Charles River).

Lymphocytes.

As described before, due to the lack of the *Foxn1* gene, Nude mouse strains have no functional T Lymphocytes, yet they do have antibody-bearing, non-mature T lymphocytes. Lymphocyte numbers were compared between BALB/c and BALB/c nude mice to determine if there are detectable differences or similarities between BALB/c and BALB/c Nude.

The difference between B Lymphocytes is shown in Figure 3-12A. The % of B cells of live CD45+ bone marrow cells in BALB/c was significantly higher than in BALB/c Nude mice (BALB/c: 40.99±7.16, BALB/c Nude: 17.42±6.58, p:****:<0.0001).However , both $CD8^+$ T (BALB/c: 0.1±0.06, BALB/c Nude:

0.1±0.07, p:ns) and CD4⁺ T lymphocytes (BALB/c: 0.13±0.07, BALB/c Nude: 0.16±0.06, p:ns) were similar in the two strains (Figure 3-12B,C).

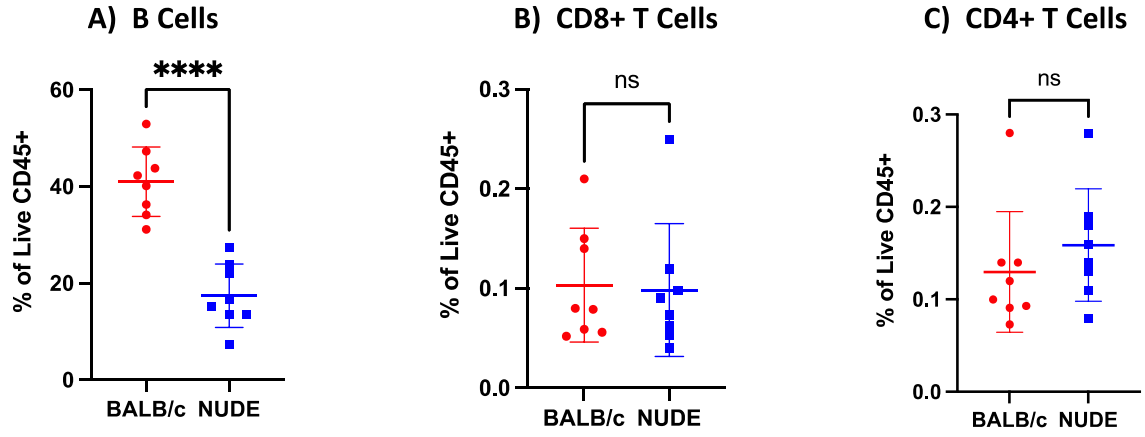

Figure 3-12: Comparison of bone marrow lymphocytes between immunocompetent and immunocompromised strains.

*Statistical analysis of flow cytometry data of bone marrow to determine the differences between A) B Lymphocytes, B) CD8⁺ T Lymphocytes, and C) CD4⁺ T Lymphocytes. T-Test was used for statistical analysis; ns is non-significant, **** is p<0.0001 and data show Mean±SD, n=8 for BALB/c and BALB/c Nude.*

Myeloid Cells

The BALB/c Nude strain has a functioning myeloid population, which has a significant role in cancer, some promoting or supporting cancer to escape immunity and some having anti-cancer functions (Liang *et al*, 2020). Therefore, it is essential to establish similarities and differences in these critical cell populations between BALB/c and BALB/c Nude strains, as this may have implications for tumour development and progression in bone.

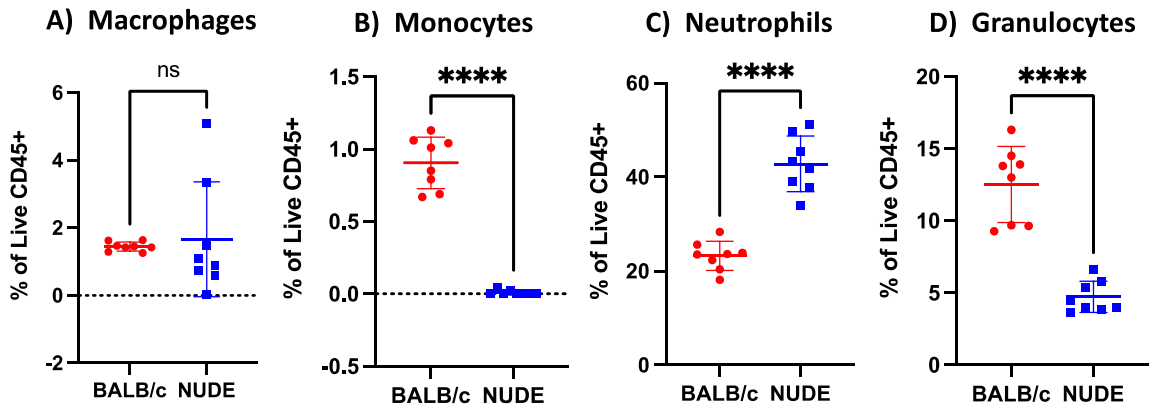

Figure 3-13: Bone marrow myeloid populations from immunocompetent and immunocompromised mice.

*Statistical analysis of bone marrow flow cytometry data to determine the differences between A) macrophages, B) monocytes, C) neutrophils, and D) granulocytes. T-Test was used for statistical analysis; ns is non-significant, **** is p<0.0001 and data show Mean±SD, n=8 for BALB/c and BALB/c Nude groups.*

The % of macrophages in the live CD45+ bone marrow cells were not significantly different between the strains (BALB/c: 1.45±0.14, BALB/c Nude: 1.66±1.7, p: ns:0.073) (Figure 3-13A). On the other hand, monocyte % was significantly lower in the BALB/c Nude mice compared to BALB/c (BALB/c: 0.91±0.18, BALB/c Nude: 0.01±0.02, p:<0.0001) (Figure 3-13B). Interestingly, neutrophils were significantly higher in the BALB/c Nude mice (BALB/c: 23.21±3.1, BALB/c Nude: 42.8±5.92, p:<0.0001)(Figure 3-13C), but granulocytes were significantly lower in the nude strain compared to the BALB/c strain (BALB/c: 12.51±2.64, BALB/c Nude: 4.72±1.08, p:****:<0.0001)(Figure 3-13D).

Haematology Analysis

Total blood counts were obtained in further experiments (mapping effects of treatment Chapter 4), allowing me to compare between control groups of BALB/c and BALB/c mice.

Table 3-6: White blood cell counts from peripheral blood between immunocompetent and immunocompromised strains.

	BALB/c	Nude	P
White Blood Cells ($10^3/mm^3$)	2.34±0.88	3.04±0.85	ns:0.16
Lymphocyte Cell Counts ($10^3/mm^3$)	1.86±0.71	1.54±0.46	ns:0.31
Monocyte Cell Counts ($10^3/mm^3$)	0.07±0.08	0.2±0.05	**:0.002
Granulocyte Cell Counts ($10^3/mm^3$)	0.41±0.15	0.81±0.2	***:0.0009
Eosinophil Cell counts ($10^3/mm^3$)	0.06±0.05	0.03±0.02	ns:0.051

Blood cell counts of BALB/c and BALB/c Nude strains from saline-treated control groups. Counts were obtained with Sci Vet ABC+ and received 10^3 cells per mm^3 peripheral blood. T-Test was used for statistical analysis; ns is non-significant, and data show Mean±SD n=7 for CON. and n=8 for DOX groups

There was no difference in total white cell blood count, lymphocyte or eosinophil numbers between the strains. Interestingly, both monocyte cell (BALB/c: 0.07±0.08, BALB/c Nude: 0.2±0.05, p: **:0.002)(Figure 3-14C) and granulocyte cell counts (BALB/c: 0.41±0.15, BALB/c Nude: 0.81±0.2, p: ***:0.0009)(Figure 3-14D) were significantly higher in the BALB/c Nude strain, compared to BALB/c strains (Figure 6.14 and Table 3-6).

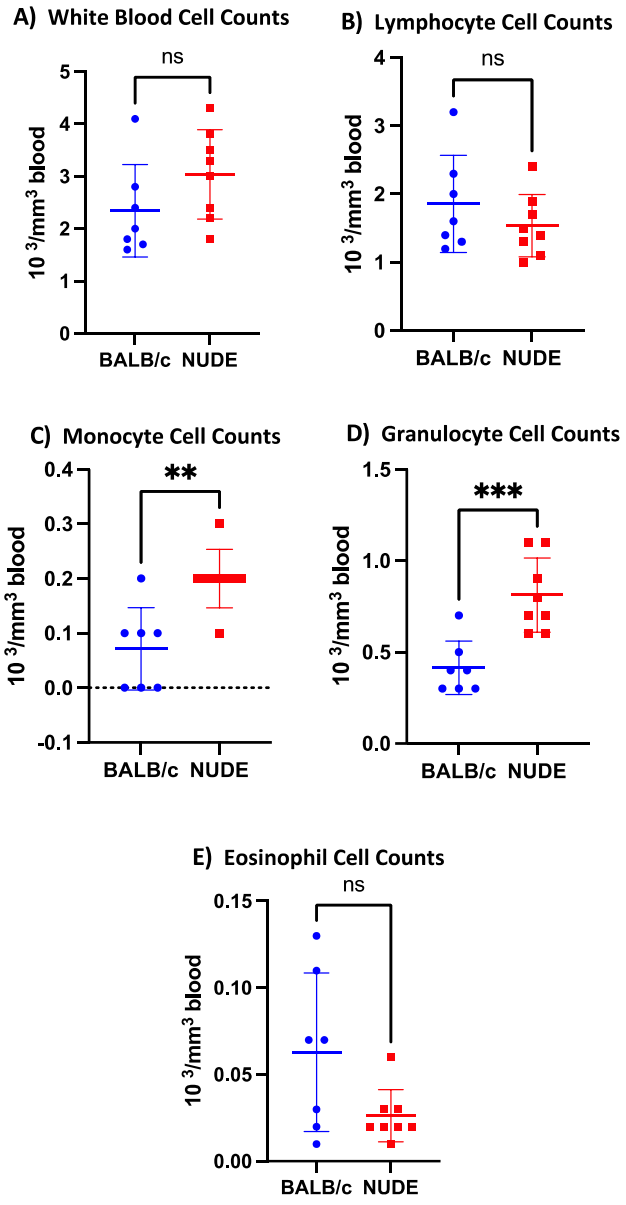

Figure 3-14: Total white blood cell counts in peripheral blood between immunocompetent and immunocompromised mice.

Comparison of A) total white blood cells, B) lymphocyte cell count, C) monocyte cell count, D) granulocyte cell count and E) eosinophil cell count of BALB/c and BALB/c Nude strains from saline-treated control groups. Counts were obtained with Sci Vet ABC+ and used 10^3 cells per mm^3 peripheral blood. T-Test was used for statistical analysis; ns is non-significant, and data show Mean±SD n=7 for CON and n=8 for DOX groups

Taken together, analyses of the myeloid populations in blood and bone marrow showed some significant differences between the two strains of mice. However, it is essential to note that these measurements represent a snapshot of the populations at a single time point of cells that have a short life and rapid turnover in the circulation (for example, granulocyte life span around six hours, and large numbers are produced every day) (DeLeo & Nauseef, 2015).

3.5.1 Effect of tumour on immunocompromised mice bone marrow.

The presence of a tumour alters bone and bone marrow in its favour. The xenograft model used throughout this study was made by injecting a human triple-negative breast cancer cell line (MDA-MB-231) via the intracardiac route, a model widely used to mimic bone metastasis (Allocca *et al*, 2019; Ottewell & Lawson, 2021). This model allows study of osteolytic lesions. Apart from structural (µCT) or histological analysis, it is hard to obtain data from tumour-bearing bone due to the variability of tumour burden between animals and the complexity of obtaining reproducible numbers of live cells or good quality RNA. In this part of the study, data from tumour-bearing hind limb bones (mainly tibias) and non-tumour-bearing control hind limb bones (from animals culled one week after bone tumour growth was confirmed by *in vivo* imaging) were compared. Data from µCT (bone integrity and structure) and cell populations in the liquid bone marrow (measured by flow cytometry) were compared.

Bone Structure and Integrity

Once established, osteolytic tumours create a vicious cycle that induces osteoclasts to cause excessive bone resorption in both trabecular and cortical areas. µCT was used to determine the overall effect of tumours on bone volume, and the results are presented in Figure 3-15.

Different regions of interest were chosen to determine the effects on the bone. The first approach (Figure 3-15A) measured the bone volume (mm^3) from the tibiofibular joint to the head of the bones. Surprisingly, despite tumour growth in these bones being confirmed by IVIS, there were no differences in bone volume between tumour-bearing and non-tumour-bearing bones (CON:5.06±0.21, TUM:4.96±0.54, p: ns). Next, a more standardised approach was used, setting two reference points, with bone volumes measured from the tibiofibular joint to the growth plate (Figure 3-15B). Again, there was no statistical difference between tumour-bearing and non-tumour-bearing bones (CON: 4.2±0.41, TUM: 4.32±0.37, p: ns). Regular bone structure and analysis for cortical bone includes the bone up to2 mm, and 1 mm for trabecular bone. Bone volumes were measured at 2 mm from the growth plate similar to the standardised methods, but no difference was found between bones (CON: 1.28±0.11, TUM: 1.25±0.14, p: ns:0.7) (Figure 3-15C). The final approach was to limit the region of interest to the trabecular bone, the area most commonly harbouring tumours and susceptible to tumour-induced bone loss, which was found to be similar to the tumour-free control (CON: 0.67±0.07, TUM:0.65±0.09, p: ns)

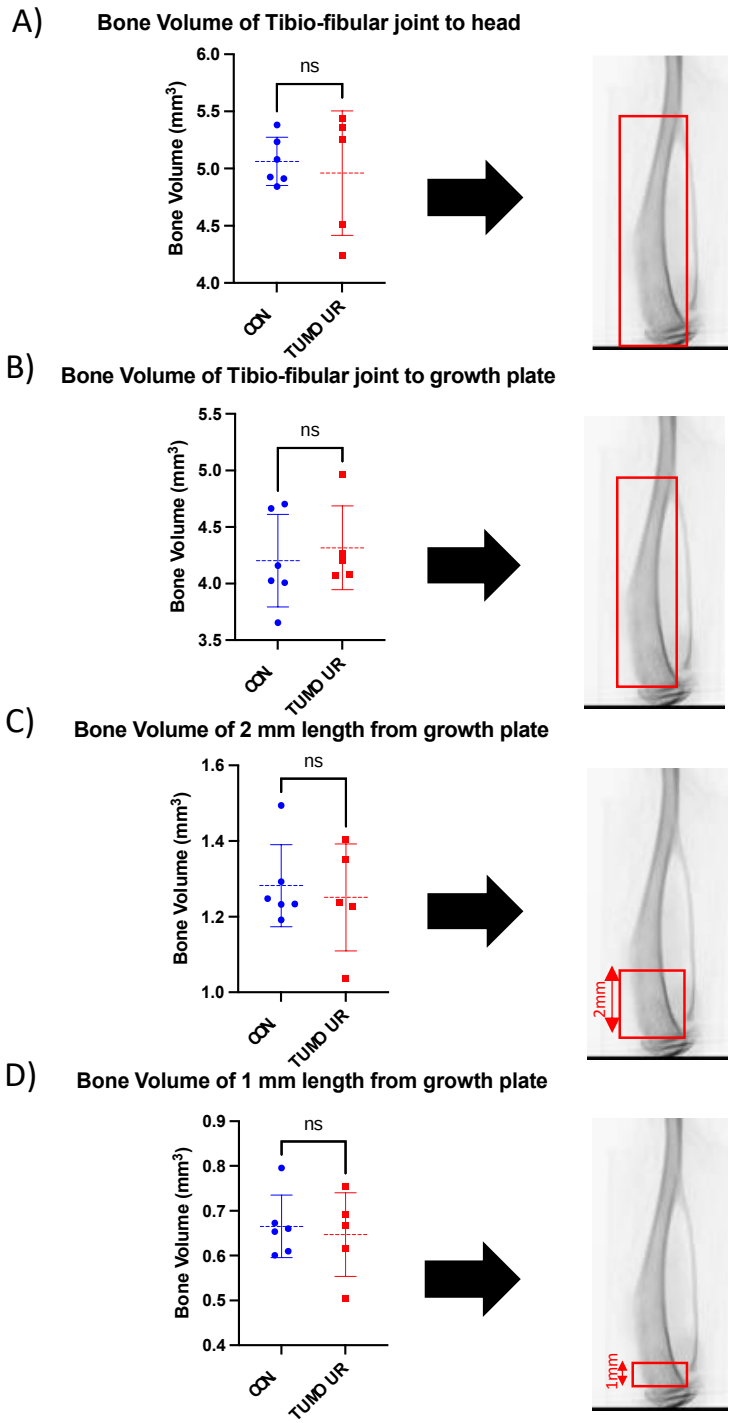

Figure 3-15: Tumour effects on overall bone volume in the xenograft model.

Comparison of the effect of the tumour on bone volume with control. Different heights were used to analyse bone volume: A) data from the tibiofibular joint to the head, B) data from the tibiofibular joint to the growth plate, C) data from the 2 mm region of interest from the growth plate and C) data from the 1 mm region of interest from the growth plate were obtained. T-Test was used for statistical analysis, n=6 for control and n=5 for tumour-bearing hind limbs, ns= non-significant.

Overall, there was no effect of the tumour on bone volume; however, lesions were found on the bones with tumours that can be seen by 3D reconstruction (Figure 3-16).

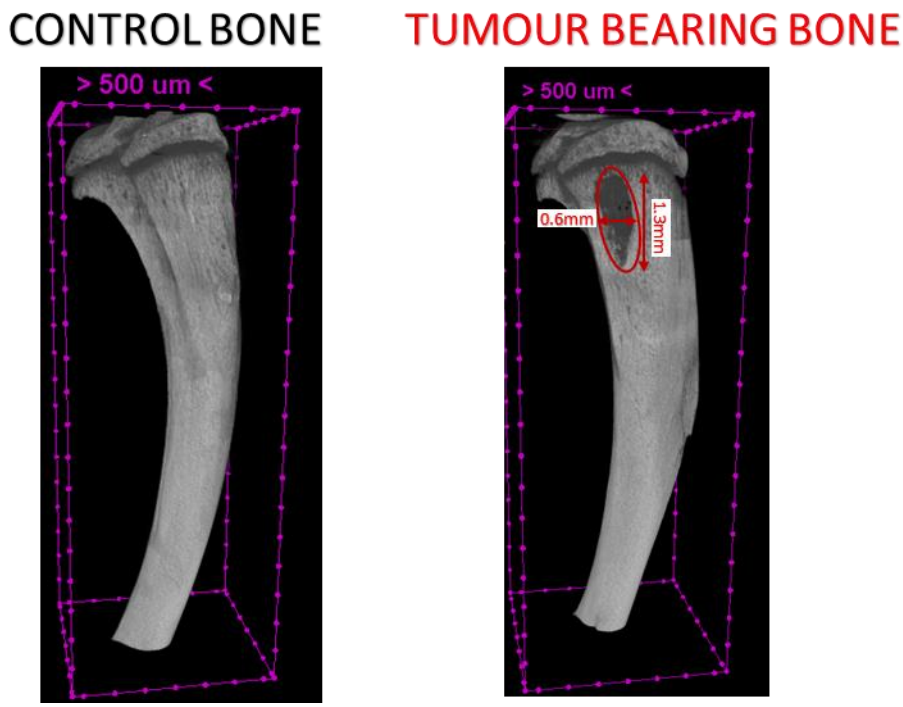

Figure 3-16: 3D reconstruction of bones from tumour-bearing and control mice.

3D reconstruction of the bones from control and tumour bearing immunocompromised mice. Bones with closest to the mean bone volume value of their group were selected to represent. Distance between each purple bead is 500 µm, dimensions of the tumour lesion was shown on the graph (longest diameter is 1.3 mm, shortest diameter is 0.6mm) and marked with red circle.'

After no difference was found in bone data despite lesions, trabecular bone analyses were carried out. A comparison of the trabecular bone density (%) showed no difference between tumour-bearing and tumour-free bones (CON: 4.73±1.79, TUM: 4.71±0.47, p: ns:0.98) (Figure 3-17A). Trabecular bone numbers (1/mm) were also similar between groups (CON: 1.14±0.41, TUM: 1.19±0.16, p: ns:0.81) (Figure 3-17B). There was no effect on trabecular thickness (mm) by tumour (CON: 0.0415±0.0021, TUM: 0.0399±0.0026, p: ns:0.29) (Figure 3-17C). Finally, there were no differences in trabecular separation (CON: 0.3792±0.0955, TUM: 0.339±0.051, p: ns:0.29) (Figure 3-17D).

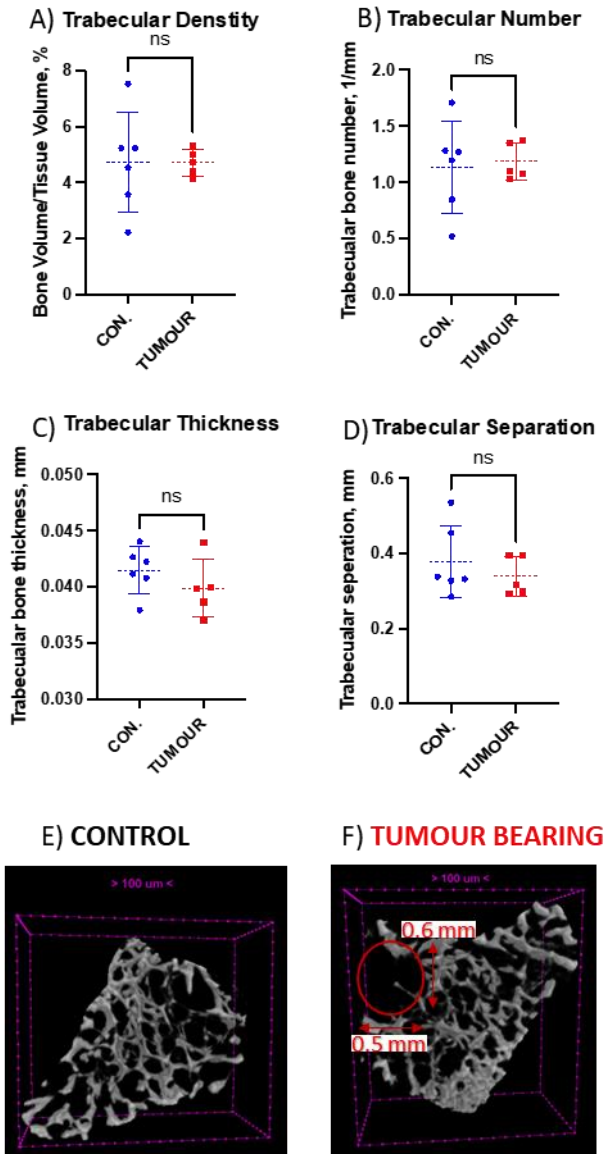

Figure 3-17: Trabecular bone structure and integrity between tumour-bearing and tumour-free bone.

Comparison of trabecular bone structure parameters between tumour-bearing hind limbs and tumour-free hind limbs of immunocompromised strain. A) Trabecular Done Density (BV/TV, %), B) Trabecular Number (Tb.N., mm), C) Trabecular Thickness (Tb.Th., mm) and D) Trabecular Bone Separation (Tb.Sp., mm) was assessed at the end of the experiment. Visual comparison of 3D reconstructed trabecular bone of E) control bone and F) tumour bearing bone was given from the bones which are closest to the mean trabecular density result for their groups. Distance between each purple bead is 100 µm and lesion caused by tumour marked with red circle, longest diameter (0.6 mm) and shortest diameter (0.5 mm) was marked on with red arrows. T-Test was used for statistical analysis; ns is non-significant, data shown as Mean±SD, n=6 for control and n=5 for tumour-bearing hind limbs.

Like the total bone volume analysis, no difference was found in trabecular bone structure between tumour-bearing and tumour-free hind limb bones (Figure 3-17). When the trabecular bones were 3D reconstructed with CTvox, osteolytic lesions were visible (Figure 3-17).

To summarise the results, overall, there was no difference in bone structure and integrity between tumour-bearing bones compared to their control, despite detected lesions from tumours.

Flow cytometry of tumour-bearing bone marrow.

Flow cytometry is a reliable and quick quantification method for cells compared to histology. However, limitations with flow cytometry begin with the extraction of the bone marrow since it is always hard to extract whole bone and bone marrow cell content. The presence of tumours in bone adds an extra challenge to cell isolation and subsequent analyses. Triple-negative breast cancer is a solid tumour; removing all the tumour cells is impossible as they adhere to each other and the bone surfaces. In this part of the study, liquid bone marrow was assessed with flow cytometry to determine any differences in the essential cell populations and to test whether GFP+ MDA-MB-231 cancer cells could be detected.

Since detecting cancer cells from bone marrow was one of the main aims, more GFP cells were gated. As can be seen from Figure 3-18, there is a clear significant difference between tumour percentage compared to the saline control (CON:0.002±0.006, TUM:0.065±0.06, p:**:0.004), confirming that using the method of flushing with centrifugal spinning, I was able to isolate sufficient tumour cells from the bone marrow to confirm their presence by flow cytometry.

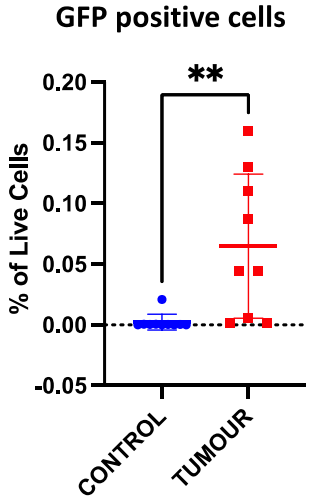

Figure 3-18: Flow cytometry of green-fluorescence-protein positive cells.

Comparison of GFP positive cells between tumour-bearing bone and tumour-free controls of immunocompromised strain. T-Test was used for statistical analyses; data given as Mean±SD, n=10 for control and n=9 for tumour groups.

As explained earlier, the HSC niche is a possible location for breast cancer dissemination. Flow cytometry was used to determine if there was a quantifiable difference in the number of LSK and LK cells in the presence of tumours in the bone. The analysis showed no detectable difference in the number of either LSK (CON:0.186±0.093, TUM:0.19±0.065, p: ns) (Figure 3-19A) or LK cell populations in the presence of tumour, compared to the tumour-free controls. (CON:1.27±0.65, TUM:1.92±0.33, p: ns) (Figure 3-19B).

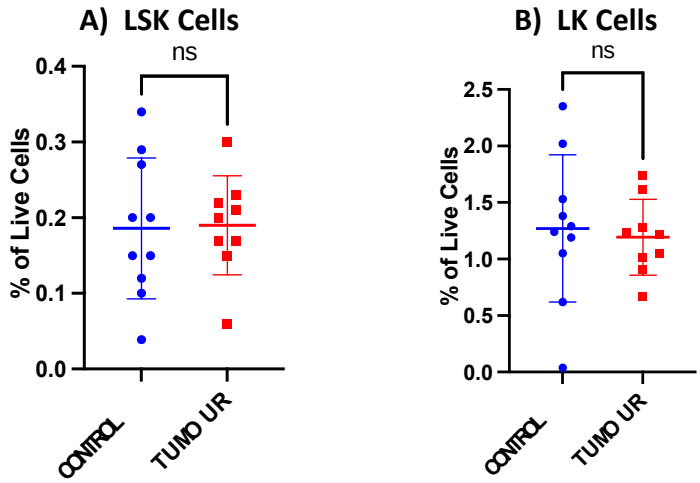

Figure 3-19: % of HSCs and progenitor' in the presence of tumour.

Comparison of A) LSK Cell and B) LK Cell data as % of live cells from tumour-free control bone marrow and tumour-bearing bone marrow of immunocompromised strain, T-Test was used for statistical analysis, ns is non-significance, data was given as Mean±SD, n=10 for control and n=9 for tumour.

The immunocompromised mouse strain I have used largely lacks T lymphocytes; however, some sub-populations are present. In this part of the study, functioning B cells and dysfunctional T cells were analysed to determine if the presence of a tumour in bone impacts these populations. Results showed that B cell percentages in the live CD45+ bone marrow cells were similar in the presence of tumours compared to tumour-free control (CON:24.95±10.44, TUM:19.7±10.77, p: ns) (Figure 3-20A). In addition there was no difference in both $CD8^+$ T lymphocyte percentages (CON:0.15±0.15, TUM:0.18±0.15, p: ns) (Figure 3-20B) and the percentage of $CD4^+$ T cells in the live CD45+ bone marrow cells (CON:0.485±0.066, TUM:0.532±0.187, p: ns) (Figure 3-20C) in the presence of tumour compared to control.

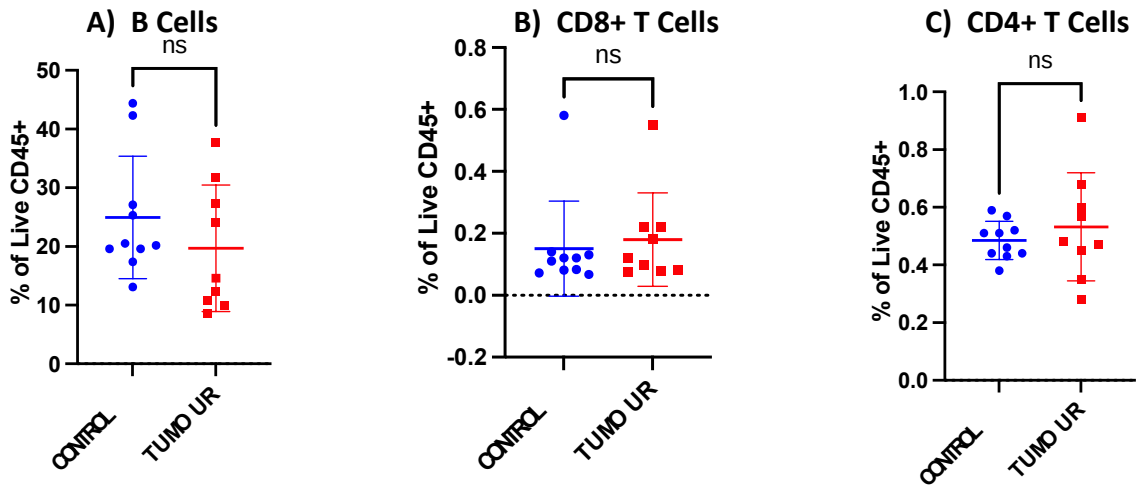

Figure 3-20: Alteration of the Lymphocyte numbers from the bone marrow in the presence of the tumour.

Comparison of A) B cells, B) CD8+ T cells, and C) CD4+ T cells numbers as % of live CD45+ cells from tumour-free control bones and tumour bearing bones' bone marrow in immunocompromised strain, T-Test was used for statistical analysis, ns is non-significance, data was given as Mean±SD, n=10 for control and n=9 for tumour.

The final bone marrow population analysed was myeloid cells, where some sub-populations play a crucial role in cancer progression. Results showed that the % macrophages in the live CD45+ cell population was not altered in the presence of a tumour (Figure 3-21A). There was also no effect of the tumour on monocyte cells, neutrophils, granulocyte cells and dendritic cells, as seen in Figure 3-21.

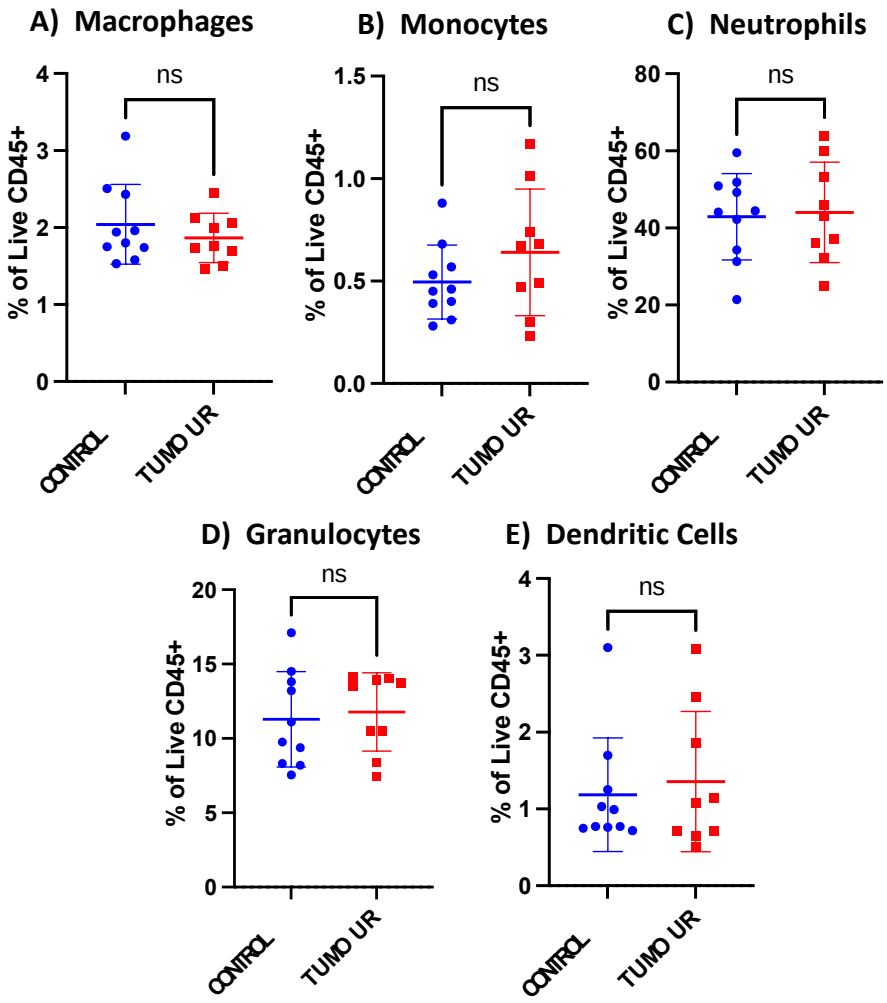

Figure 3-21: Alteration of the myeloid cell numbers from the bone marrow in the presence of the tumour.

Comparison of A) Macrophages, B) Monocytes, C) Neutrophils, D) Granulocytes, and E) Dendritic Cell numbers as % of live CD45+ cells from tumour-free control bones and tumour-bearing bones' bone marrow in immunocompromised strain, T-Test was used for statistical analysis, ns is non-significance, data is presented as Mean±SD, n=10 for control and n=9 for tumour groups.

To summarise the results, tumour cells could be detected significantly in the liquid bone marrow of the tumour-bearing hind limbs. However, no significant difference was found in either cell percentages or integrity of bone structure despite osteolytic lesions.

White Blood Cells

PB of the tumour-bearing mice was compared to tumour-free animals to determine any differences between some key cell populations. White blood cell counts were given in the table below (Figure 3-22). Results have shown that total white blood cell counts were not affected by the presence of the tumour (CON: 5.45±1.68, TUM: 5.13±1.76, p: ns) (Figure 3-22A). Also, there was no detectable difference in any of the cell types measured, as shown in Figure 3-22.

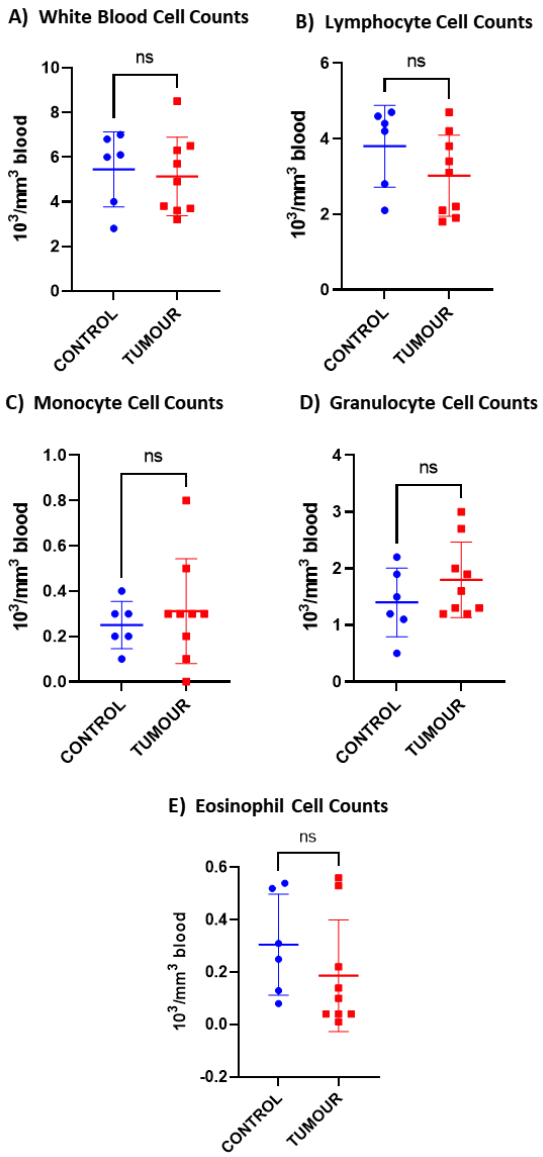

	CONTROL	TUMOUR	P
White Blood Cells (10^3/mm^3)	5.45±1.68	5.13±1.76	ns:0.73
Lymphocyte Cell Counts (10^3/mm^3)	3.8±1.08	3.02±1.07	ns:0.19
Monocyte Cell Counts (10^3/mm^3)	0.25±0.1	0.31±0.23	ns:0.56
Granulocyte Cell Counts (10^3/mm^3)	1.4±0.6	1.8±0.66	ns:0.26
Eosinophil Cell counts (10^3/mm^3)	0.3±0.19	0.187±0.21	ns:0.3

Figure 3-22: Total white blood cell counts in peripheral blood compared between tumour-free and tumour-bearing mice.

Comparison of A) total white blood cells, B) lymphocyte cell count, C) monocyte cell count, D) granulocyte cell count and E) eosinophil cell count of tumour-free and tumour-bearing immunocompromised mice. Counts were obtained with Sci Vet ABC+ and displayed as 10^3 cells per mm^3 peripheral blood. T-Test was used for statistical analysis, ns is non-significant, data show Mean±SD n=6 for control and n=9 for tumour groups.

3.6. Discussion

Bone metastases development occurs spontaneously from the primary tumour, and this complex, multistep process includes many steps such as dissemination, homing to bone, colonisation, survival and progression (Coleman *et al*, 2020b). Therefore, generating bone metastases from a primary tumour is complex in murine models, with syngeneic models that include a primary tumour often resulting in aggressive lung metastases and/or outgrowth of the primary tumour before bone metastasis can develop (Ottewell & Lawson, 2021). This is why intracardiac injection of the triple-negative human MDA-MB-231 cell line is commonly used to generate a bone metastatic xenograft model resulting in mainly hind limb tumours (Wright *et al*, 2016; Allocca *et al*, 2019; Ottewell & Lawson, 2021). A syngeneic equivalent of this model uses the bone homing variant of the triple-negative mouse breast carcinoma 4T1 cells, which allows studies of the role of immune populations (Ottewell & Lawson, 2021). To evaluate the effects of the tumour on the bone, generally *in vivo* imaging, *in vivo* and *ex vivo* μCT and histological sectioning are used. Since both models use osteolytic cancer cells and effects on bone destruction are important, osteoclast activity is shown to promote bone tumour growth in murine models (Hiraga, 2019; Riffel *et al*, 2022). However, tumour interactions with other cells in the bone microenvironment may also be meaningful (Wang *et al*, 2015b). The experiments in this chapter aimed to determine any differences in the bone microenvironment between the immunocompetent and immunocompromised mice that have been used in this PhD project. This analysis will help to understand the murine bone and bone environment, determine the main differences/similarities between strains and their possible effects on tumour development in bone. Also, I have tried to answer the question “can tumour effects on the other cell populations in bone marrow be determined using simple flow cytometry?”.

3.6.1. Differences in the BME between the immunocompetent and immunocompromised strains

Age and weight-matched animals allow additional bone and bone marrow analyses in murine models. Using the data from the saline-treated controls of the immunocompetent (BALB/c) and immunocompromised (BALB/c Nude) strains, differences/similarities between the strains were studied.

Since the models generated osteolytic bone lesions, bone structure and integrity in (tumour-free animals) were compared between the groups. Interestingly, the cortical bone volume of the BALB/c Nude strain was lower than the BALB/c strain, and trabecular bone separation was higher in the BALB/c Nude strain. I could not find any relevant published studies to allow comparison with the

bone values obtained in this study. However, Lee et al. carried out a study on wild-type and nude C57BL/6 animals to test the effects of T lymphocytes with ovariectomy (Lee *et al*, 2006). A significant difference was found in the cortical bone area with a larger area in the nude strain. However, they also saw a reduced bone density, whereas I found no difference between the strains. Immunocompromised mice lack a thymus that affects functioning T cells, and some studies have shown that T cells can play a role in bone remodelling (reviewed in Yuan et al., 2010). For example, some subpopulations of T cells (CD4+,CD25+,Foxp3+ T cells) were found to inhibit monocyte differentiation to osteoclasts *in vitro* and suppress M-CSF and RANKL osteoclast formation *in vivo* (Zaiss *et al*, 2007). Li *et al* showed that ovariectomy did not induce bone loss and resorption on the T cell depleted or CD40L lacking (primarily expressed on activated T cells) mice (Li *et al*, 2011). Effects of the T cells should be considered, especially since breast cancer bone metastasis triggers the vicious cycle of bone destruction that drives tumour progression (Hiraga, 2019). A better understanding of the underlying mechanisms might reveal the impact of the immune system on the BME (Terashima & Takayanagi, 2018).

Osteoblasts and osteoclasts are the primary cells responsible for bone remodelling. As there is a difference in cortical bone volume (lower in BALB/c Nude) and trabecular separation (larger in BALB/c Nude), osteoblast and osteoclast cells were compared to determine if the differences in bone structure/volume were reflected by a corresponding difference in bone cell numbers. Overall, there was no difference in bone remodelling cell numbers between BALB/c and BALB/c Nude, and only osteoclast perimeter was found to be larger in the BALB/c Nude trabecular region compared to BALB/c. This finding means osteoclasts covered a larger surface area on the trabecular bone in the BALB/c Nude strain. My data partially agree with the study by Lee et al., who found increased osteoclasts in the nude mice compared to wild type in *ex vivo* culture (Lee *et al*, 2006). If a similar *ex vivo* experiment were carried out, more osteoclastic cells could be isolated from the BALB/c Nude in this experiment compared to the BALB/c. One possible explanation for this increased osteoclast activity discussed by Gillespie (Gillespie, 2007), is that T cells secrete factors such as OPG that can inhibit osteoclastic activity, and the lack of T cells in the nude mice may result in increased activity of osteoclasts in the trabecular bone. Although the increase in the osteoclastic surface area is statistically significant, it might not be biologically meaningful, and this needs to be established in functional studies. Also, bone turnover markers from serum should be compared in future studies; since samples were collected at the end of the experiments it only shows the bone remodelling activity at that time. To be able to better understand the differences between the two strains, a similar experiment should be carried out using various time-points to collect serum to assess the bone turnover markers.

As discussed in previous chapters, the hematopoietic stem cell niche is suggested to be a homing niche for breast and prostate cancer cells in bone (Shiozawa *et al*, 2011b; Allocca *et al*, 2019). Therefore, LSK and LK cells were compared and were found to have significantly lower percentages in the BALB/c Nude mice. Similar HSCs reduction (with colony forming unit assay from C57BL/6 Nude strain) was observed by Pritchard and Micklem (1973) (Pritchard & Micklem, 1973). I could not find an updated study comparing LSK and LK populations, yet Geerman et al. have found that CD8+ T cells support the maintenance of HSCs in the bone marrow. These findings might be an explanation for the lower number in the LSK and LK populations in the nude mice due to a lack of HSC maintenance (Geerman *et al*, 2018)

Since we know that despite having non-functioning T cells, BALB/c Nude mice have T cells that express CD4, and CD8 surface antibodies (Belizario, 2009), therefore, it was not surprising that there were no significant differences in the numbers of $CD8^+$ T cells and $CD4^+$ T cells between BALB/c and BALB/c Nude mice (Belizario, 2009). However, as nude strains have functioning B cells, lowered maintenance of HSCs might explain the reduced number of B cells I observed in the BALB/c nude mice, yet this hypothesis must be tested.

Myeloid cells (including granulocytes and monocytes) are produced by common progenitors derived from HSCs in the bone marrow (Kawamoto & Minato, 2004). They have been linked to inducing tumour growth with multiple mechanisms, such as differentiation to tumour-associated macrophages or osteoclasts (Alsamraae & Cook, 2021), yet many studies have been carried out in the presence of the tumour. In this study, I aimed to determine the bone's myeloid populations without a tumour. Several myeloid populations were found to be significantly lower in BALB/c nude mice, except neutrophils which were found to be significantly elevated in BALB/c nude mice. Despite the controversial role of neutrophils in the presence of solid tumours, murine studies show they might have immunosuppressive effects in the tumour microenvironment (Li *et al*, 2020). In this study, I have found more neutrophils in the BALB/c Nude strain compared to the BALB/c strain. The mechanisms underlying these differences in myeloid populations are unknown and must be investigated. One reason might also be the lower HSC population, as CXCR4 plays an important role in the neutrophil mobilisation to the circulation (Eash *et al*, 2010). Future studies might include neutrophil counts from PB for both strains to see whether similar significant differences can be observed.

White blood cell count results were found to be in line with those indicated in the supplier's data sheet (Charles River); for example, they have found total white blood counts between 3-13 $x10^3$ /ml PB for 8-10 weeks old female BALB/c Nude mice, and I also found 3 $x10^3$ /ml PB too. As supplier also showed the difference between lowest and highest detected white blood cell counts as 100,000

cells per ml PB, biological variation plays major role in the analyses. According to the results from this study, there was no difference in total white blood cell counts between strains; however, monocyte and granulocyte numbers were increased in the BALB/c Nude strain. Since the monocyte and granulocyte counts from bone marrow were found to be lesser in nude strain, both results might indicate a higher trafficking rate of monocyte and granulocyte to the PB; however, future studies are needed to confirm this hypothesis.

Overall, my results show that almost all of the immune and HSCs populations are somewhat different in the BALB/c Nude and BALB/c strains, which may affect cancer development and progression. However, it is essential to note that these baseline measurements are insufficient to draw any conclusions about the potential involvement of the different populations in bone metastasis. Experiments to determine the underlying mechanisms must consider any alterations that might have been caused by the lack of non-functioning T cells; however, these two models should have differences in disease progression.

3.6.2. Detectable effects of hind limb tumours on the bone and bone marrow

MDA-MB-231 is a human triple-negative breast cancer cell line that, when injected through the intracardiac route, metastases to long bones, the spine and the jaw, resulting in the development of osteolytic lesions within 2-3 weeks (Ottewell & Lawson, 2021). Downstream analyses of this model usually involve *in vivo* imaging of the tumour and/or *ex vivo* scanning of the structural alteration of the bones, followed by histological sectioning and bone histomorphometry. Whilst this standard methodology allows quantification of bone remodelling cells on the bone surface in the presence or absence of a tumour (Ottewell *et al*, 2008b; Wang *et al*, 2014), no direct study has been published to find alterations in the bone marrow population by the bone tumour. I therefore, wanted to determine if the fast and reproducible analysis method of flow cytometry can be used to study tumour-bearing bones and to understand how a tumour's presence modifies the bone marrow's cellular composition.

Before investigating the flow results, the bone structure was compared in animals with a positive hind limb *ex vivo* signal (confirming tumour presence). I expected to see a reduction in bone volume due to the osteolytic lesions and measured total bone volume from different reference points (Figure 3-15). First, I have measured the bone volume from the tibio-fibular joint to the bone head and found no statistical difference. Then, to reduce the excess volume I have compared the bone volumes from tibio-fibular joint to growth plate. As this result also showed no statistical difference, thus I have narrowed down the region of interest to the area measured for both trabecular and cortical bone which is 2 mm from growth plate where no statistical difference was also not found. Finally, I

have decided to measure the only trabecular bone area (1 mm from the growth plate) where mainly tumour resides whether to determine statistical difference on the bone volume could be detected. Interestingly, despite the bones having visible lytic lesions, there were no differences in bone structure and integrity as quantified by μCT. It is possible that the tumour cells had a powerful luciferase signal despite being relatively small and that lesions were not big enough to be accurately detected. Future experiments should allow tumours to grow larger before culling, increasing the impact on the bone microenvironment and integrity.

Patients with bone metastases may experience haematological complications due to cancer-mediated impairment of the bone marrow (Pasquini *et al*, 1995). Therefore, I wanted to determine if it was possible to detect the impact of tumour cells on bone marrow cell populations such as HSCs and immune cells. Triple negative breast tumours in bone grow as solid tumour masses that adhere to bone, making isolation of tumours and the cells of the surrounding microenvironment from these sites difficult. The MDA-MB-231 breast cancer cell line expressing green fluorescence protein (GFP) allows easy flow cytometry detection. Despite not having high numbers in the collected bone marrow samples, there were enough GFP-positive cells to confirm that it is possible to detect cancer cells from the tumour-bearing hind limb bones using this method. Surprisingly, no differences were found in the numbers of HSCs, lymphocytes, and myeloid cells between the tumour-free and tumour-bearing hind limb bones. It is possible that the tumour foci were relatively small and hence had not grown to the size they would start to alter the cellular composition of the surrounding microenvironment significantly.

Cancer can trigger inflammatory responses; thus, there are clinical studies investigating whether total white blood cell counts can be used as an indicator of patients' response to the therapy and survival rate (Asano *et al*, 2016; Zhang *et al*, 2016; Xu *et al*, 2017b; Graziano *et al*, 2019). However, studies investigate the effects of the treatment rather than the effects of the tumours (Stopeck *et al*, 2010; Garcia *et al*, 2011; Fujiwara *et al*, 2013; Chang *et al*, 2018; Chen *et al*, 2020a; Maluf *et al*, 2021). Therefore, total white blood cells were compared between tumour-bearing and tumour-free animals. No difference was found between the groups.

Overall, many parameters were not altered despite visible osteolytic lesions. One possible explanation for this situation might be due to the metastasis being at an early stage. Animals were culled one week after the hind limb tumour detection, therefore, in future studies end of the experiment should be at a later time point. However, when combined with other methods such as histology and *in vivo* imaging, flow cytometry might be a fast and reliable method to analyse tumour-bearing bones. However, more studies must be carried out to optimise this methodology.

3.7. Conclusion

In summary, these data have shown that:

- HSCs, B Cells and myeloid cell populations quantify differently in the nude strain, compared to its wild type, in addition to the lack of T Lymphocytes.
- Due to these alterations, the bone structure was different in nude cortical bone volume.
- Flow cytometry can be used to determine the cell populations from the tumour-bearing bone marrow when it is optimised.
- Tumours have to reach a specific size before there is a significant impact on bone marrow populations

CHAPTER 4. ALTERATION OF BONE MARROW CELL POPULATIONS WITH COMMON CHEMOTHERAPEUTIC AGENT; DOXORUBICIN.

4.1. Summary

Surgery followed by chemotherapy, radiotherapy, and endocrine treatment is the general approach to treating breast cancer. Choosing the correct chemotherapy agents and schedule is a complex process mentioned in Chapter 1, Section 2. Treatment can be changed depending on the patient's disease, including factors such as hormone receptor status, stage, metastatic status and may include additional endocrine therapies, targeted agents, or supporting drugs such as bisphosphonates. Patients with a high risk of developing bone metastasis and osteolytic bone damage may receive doxorubicin, an anthracycline class chemotherapy agent. It is unclear whether doxorubicin may harm the bone, with some reports of bone damage caused by doxorubicin in murine models.

This part of the study established the impact of doxorubicin on bone structure, cells, and selected bone marrow cell populations. Effects of two different doses of doxorubicin were investigated in both immunocompetent and Immunocompromised mice, compared with a saline control. Results were obtained from µCT data from hind limb bones (bone structure and integrity), bone histomorphometry of the same bones (quantifying osteoblasts and osteoclasts) and flow cytometric analysis of bone marrow (lymphocytes, myeloid cells, HSCs and their progenitors), as well as haematological analysis.

Administration of 4 and 6 mg/kg of doxorubicin (DOX) once a week for four weeks did not alter body weight; hence both doses were well tolerated in both strains of mice. Initial experiments showed that the lower but effective dose of doxorubicin from the literature (4 mg/kg) did not affect bone remodelling cells and HSC progenitors. Despite reducing the trabecular bone number of the immunocompetent mice, there was no effect in immunocompromised mice. The experiment was repeated with the higher dose of 6 mg/kg DOX, significantly impacting the bone structure and integrity by reducing trabecular bone in both strains. The changes in bone structure were not reflected in altered numbers of osteoclasts/osteoblasts, suggesting that doxorubicin affects the activity of these bone remodelling cells to cause the observed trabecular bone loss. Effects on the immune populations were observed following doxorubicin treatment of immunocompetent mice.

Interestingly, B lymphocytes were significantly reduced in both strains. These results showed that the destructive effects of doxorubicin on bone structure and bone marrow cells could be observed in immunocompetent mice at the 4 mg dose, yet the dose must be increased to 6 mg for the immunocompromised strain to respond. Despite the differences in some cell types, damage caused by the 6 mg doxorubicin was observed in the bones of both murine strains.

4.2. Introduction

Doxorubicin (DOX) is an anthracycline-type chemotherapy agent used to treat various cancer types such as breast, lung, gastric, ovarian and thyroid (Thorn *et al*, 2011). The primary mechanism of action of DOX is targeting topoisomerase II, and alongside DNA helicases and DNA itself, DOX creates a cleavable complex, thus resulting in DNA double-strand breakage and cell death (Bachur, 2002). Also, it is found that anthracyclines increase reactive oxygen species that can also destroy DNA and macromolecules. These create toxicities that lead to damage to bone marrow regeneration, cardiac tissue damage, and extravasation necrosis (Bachur, 2002; Ozer & Aydiner, 2019). The inflammatory response is typical in many chemotherapy treatments alongside bone marrow damage since they mainly target highly proliferative cells. Multiple reactive oxygen species produced by doxorubicin (such as NADPH, NOXs and NOSs) trigger oxidative stress (such as Nrf2) damage to the subcellular structures alongside fewer antioxidants produced in cardiac tissue, resulting in apoptosis; these might be the reasons for cardiac failure (Kong *et al*, 2022). However, doxorubicin is still an effective treatment agent for cancer, and its side effects can be reduced with dexrazoxane (cardioprotective agent that inhibits toxic iron-anthracycline complex) (Ganatra *et al*, 2019).

Doxorubicin is not tumour cell-specific, and *in vivo* and *in vitro* studies showed that doxorubicin also affects bone and bone cells. Rana et al. treated 5-week-old female BALB/c mice with a 5 mg/kg DOX dose for three weeks once a week. A similar study was carried out with an orthotopic bone metastatic breast cancer model (with an injection of bone-tropic 4T1 cells), and results showed that non-tumour and tumour-bearing mice had significantly lower bone density than their controls. They also showed increased osteoclasts from *ex-vivo* spleen and bone marrow samples when treated with DOX (Rana *et al*, 2013). Fonseca et al. conducted another study on the Wistar rats that shows DOX deterioration effects on the bone. They treated 8-week-old male rats with 2 mg/kg DOX for seven weeks (once a week) with a running wheel in their cage. Their conclusion also showed that DOX reduces bone structure, and these effects were found to be increased when the activity of the rats increased (Fonseca *et al*, 2016). Overall, these studies indicate the damage of DOX on the bone.

Despite some pathways revealed in these studies (Friedlaender *et al*, 1984; Rana *et al*, 2013; Yang *et al*, 2013; Fonseca *et al*, 2016), there are still gaps in our knowledge . What are the main indicators on the bone and bone cells caused by doxorubicin? Are specific bone cell populations affected more, and what are the possible reasons for this? The following chapter describes the effects of doxorubicin on bone, bone cells, and some of the critical bone marrow cell populations to answer some of these questions. The data will help elucidate whether a commonly used chemotherapy agent may contribute to the weakening of bone associated with breast cancer bone metastases.

4.3. Aims

The purpose of this investigation has been to examine the effects of a commonly used chemotherapy agent (doxorubicin) on bone and bone marrow cells. The main goals of the work are to:

- Determine the half-maximal inhibitory concentration (IC50) of doxorubicin on triple-negative breast cancer cells (confirm drug activity).
- Establish effects of different doxorubicin doses on bone structure, integrity, and bone marrow cell populations *in vivo*
- Compare the effects of doxorubicin on bone in immunocompetent vs immunocompromised mice

4.4. Material and Methods

Detailed information can be found in the Material and Methods Chapter 2.

4.4.1. Breast Cancer Cell Lines

The triple negative human MDA-MB-231-IV PX462 cell line was cultured in RPMI 1640 with 10% FCS at 37°C 5%CO_2.

4.4.2. *In vivo* Studies

All *in vivo* studies were carried out according to local guidelines and with Home Office approval under project licence PPL 70/8964 held by Professor Nicola Brown or P99922A2E held by Dr Penelope D Ottewell, University of Sheffield, UK. Studies were carried out using BALB/c (immunocompetent) and BALB/c Nude (immunocompromised) mice.

4.4.2. Half Maximal Inhibitory (IC50) assay with MTT

IC50 dose of doxorubicin for MDA-MB-231-IV PX462 cells was calculated using an MTT assay. PBS was used as a vehicle *in vivo*. Concentrations for IC50 were set to media +10% FCS, media + PBS, 10^{-9} M, 10^{-8} M, $5x10^{-8}$ M, 10^{-7} M, 10^{-6} M, 10^{-5} M, $5x10^{-5}$ M, and 10^{-4} M doxorubicin. Graphpad version 8 was used for dose-respond analysis. 3-(4,5-dimethylthiazol-2-yl)-2,5-diphenyltetrazolium bromide (MTT) dye was used for assessing cell metabolic activity. Seeding density was 10000 cells/cm^2 in 96 well plate with 200 µl RPMI + 10% FCS (n=8/group). Cells were treated with the doxorubicin doses for 72 hours. After 72 hours, all media was removed, and 100 µl MTT solution (1mg/ml media+10%FCS) was added to all wells. The plate was covered with aluminium foil, and cells were incubated for 4 hours at 37˚C. After four hrs, the MTT solution was removed by carefully inverting the plate to the sterilised tissue paper. Then, 100 µl DMSO was added to the wells, and the plate was re-covered with aluminium foil. The plate was placed on the plate shaker for 15 minutes at 170 rpm to dissolve all formazan crystals. Multi-well plate reader read absorbance results at 570nm wavelength.

4.4.3. Effect of 4 and 6 mg/kg doxorubicin doses on bone and bone marrow in BALB/c and BALB/c nude mice strains.

To compare the effects of doxorubicin on bone and bone marrow, 7-week-old BALB/c and BALB/c Nude mice (n=8 per group) were treated weekly with saline control or doxorubicin (4 mg/kg) for four weeks. The dose of DOX was chosen based on previous studies carried out by Ottewell

(Ottewell *et al*, 2008b) who showed that 4 mg/kg DOX weekly for 6 weeks was required to inhibit subcutaneous breast tumour growth *in vivo*. Importantly this study also showed that a dose of 8 mg/kg DOX weekly for 6 weeks dis not induce toxicity.

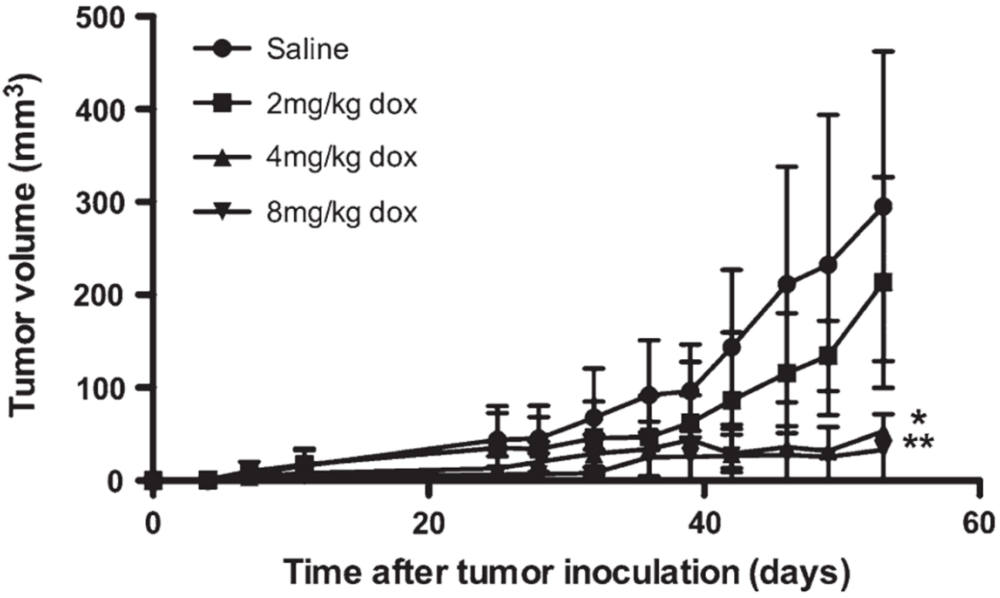

Figure 4-1: Dose-response curve for doxorubicin in a mouse model of breast cancer.

*Doxorubicin (2, 4, or 8 mg/kg body weight) and saline (control: 100 µl) were administered once per week for 6 weeks to female MF1 nu/nu mice bearing subcutaneous human MDA-G8 breast tumour cell-derived tumours by Ottewell et al. Tumour volumes were measured with calliper every 3-4 days. Data are shown as mean tumour volume (mm^3) (n=8 /group). *P= 0.054 for 8 mg/kg DOX vs control and **P=0.038 for 4mg/kg DOX vs control. One-way nonparametric Kruskal-Wallis test followed by Dunn's multiple comparisons tests was used for statistical analysis. Reused by the permission of* (Ottewell *et al*, 2008b).

Guided by these studies, the dose of 4mg/kg DOX administered weekly for 4 weeks was chosen as a starting point for my studies. The dose was subsequently increased to 6mg/kg to explore the impact of higher doses of DOX, as the Ottewell study had indicated that this was a safe dose to use. The group size (n=8) was based on these previous studies by Ottewell, showing that this was sufficient to detect the effects of DOX on tumour growth. In addition, studies from our group have demonstrated that group sizes of n=4-7 was sufficient to detect drug-induced changes on the BMEV in tumour free mice (Haider *et al*, 2014, 2015). Animals were culled two days after the last treatment, and peripheral blood (PB) and bone marrow were collected for colony formation assay. Hind limb bones were collected for *ex vivo* analysis (Figure 4-2, A). A similar experiment was carried out for 6 mg/kg doxorubicin, and PB was collected for haematopoietic cell analysis. Bone marrow was collected for flow cytometry, and hind limb bones were collected for *ex vivo* analysis (Figure 4-2, B).

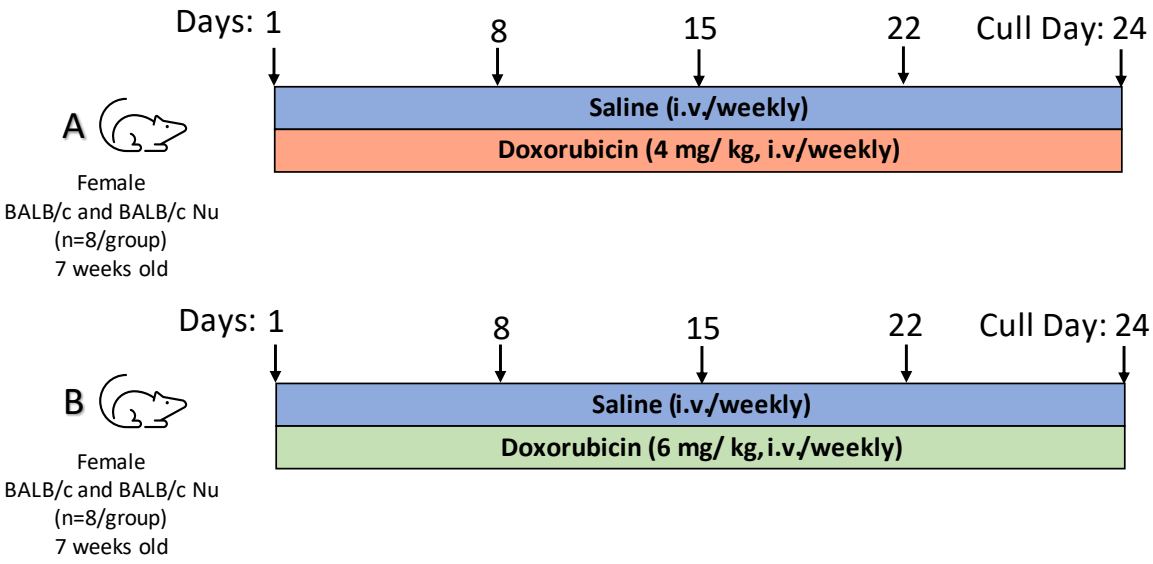

Figure 4-2: Experimental outline - effects of doxorubicin on bone and bone marrow cells.

Experimental design for 4 mg/kg doxorubicin dose (A) and 6 mg/kg doxorubicin dose (B) on both BALB/c (n=8/group) and BALB/c Nude (n=8/group) mice. Mice were treated with doxorubicin or saline once a week for four weeks and were culled two days after the last treatment. Peripheral blood, bone marrow and hind limb bones were collected for ex-vivo analyses.

4.4.3. *Ex Vivo* analyses

4.4.3.1. Collection and preparation of the bones for microcomputed tomography (µCT) and histology.

Hind limbs were removed from the carcass, all soft tissue removed, and tibias separated from the femurs. Bones were placed in 4% PFA overnight and then washed and stored in PBS at 4°C. Random tumour-free tibias were selected for µCT, and the same bone was decalcified after the scan for 14 days. Decalcified bones were processed and embedded with wax, then sectioned into 3µm slides. Slides were either stained with TRAP or H&E for bone remodelling cell analyses.

4.4.3.2. Collection of bone marrow.

After separation of the femurs from the carcass, they were dipped into 100% EtOH for surface disinfection. Under the sterile hood, the femoral head was removed and placed into 0.2 ml PCR tubes with a hole pierced in the bottom. Tubes were placed into 1.5 ml Eppendorf containing 200 ml PBS and bone marrow spun out at 3000 g for 5 min. After collection of bone marrow, it was washed with PBS containing 10% FCS and processed with colony formation assays or stained for flow cytometry.

4.4.3.3. Collection and preparation of peripheral blood for colony forming unit assays and blood count.

Before culling the animals, peripheral blood (PB) was collected via terminal cardiac puncture. 0.5-1 ml PB was taken from each animal into the syringe, and 100 µl of PB was transferred into 1.5 ml Eppendorf containing 50 µl EDTA (anticoagulant) for blood analyses and 0.5 ml of PB was transferred into 1.5 ml Eppendorf containing 50 µl EDTA (anticoagulant) for colony-forming assays.

4.4.3.4. Colony Forming Unit analyses.

As detailed in section 2.2.3.9, $1x10^4$ cells/well from both PB (after red blood cells were lysed) and BM were seeded in a 6-well plate with 1.1 ml MethoCult GFM3434 (StemCell Technologies, UK) + 10% IMDM (2% FCS+%1 P/S/A), samples were seeded in triplicate. Samples were checked once every two days to detect colony formation for 14 days.

4.4.3.5. Flow Cytometry

Flow cytometry analysis was conducted using the LSRII. Fluorescent activated cell sorting was conducted on the FACSMelody. Data analysis was conducted on FlowJo software. Lymphocyte, myeloid and haematopoietic stem cell populations were analysed (Table 4-1).

Table 4-1: Cell populations and flow cytometry markers

Lymphocytes	
T Cells	$CD45^+$, $CD3^+$, $CD19^-$
CD4+ T Cells	$CD45^+$, $CD3^+$, $CD19^-$, $CD4^+$, $CD8^-$
CD8+ T Cells	$CD45^+$, $CD3^+$, $CD19^-$, $CD8^+$, $CD4^-$
B Cells	$CD45^+$, $CD3^-$, $CD19^+$
Natural Killer (NK) Cells	$CD45^+$, $CD3^-$, $CD19^-$, $NK1.1^+$
Myeloid Cells	
Dendritic Cells	$CD45^+$, $CD11b^+$, $CD11c^+$, $MHCII^+$
Neutrophils	$CD45^+$, $CD11b^+$, $Ly6G^+$
Macrophages	$CD45^+$, $CD11b^+$, $Ly6G^-$, $Ly6C^{lo}$, $F4/80^{hi}$
Monocytes	$CD45^+$, $CD11b^+$, $Ly6G^-$, $Ly6C^{hi}$, $F4/80^{lo}$
Granulocytes	$CD45^+$, $CD11b^+$, $Ly6G^-$
HSCs and progenitors	
LSK Cells	Lin^-, $Sca\text{-}1^+$, $cKit^+$
LK Cells	Lin^-, $Sca\text{-}1^-$, $cKit^+$

Analysed cell populations from bone marrow and their markers.

Gating Strategies for flow cytometric analyses

Gating around the cell populations with common characteristics, using forward/side scatters and marker expression level, allows quantification of populations of interest. The following figures show the gating strategies for haematopoietic populations (Figure 4-3Figure 2-15), lymphocytes (Figure 4-4) and myeloid populations (Figure 4-5) using side scatter area (SSC-A), forward scatter area (FSC-A) and height (FSC-H) and the markers listed in Table 4-1. All positive or negative gating was determined using fluorescence minus one (FMO) and a single stain for the marker.

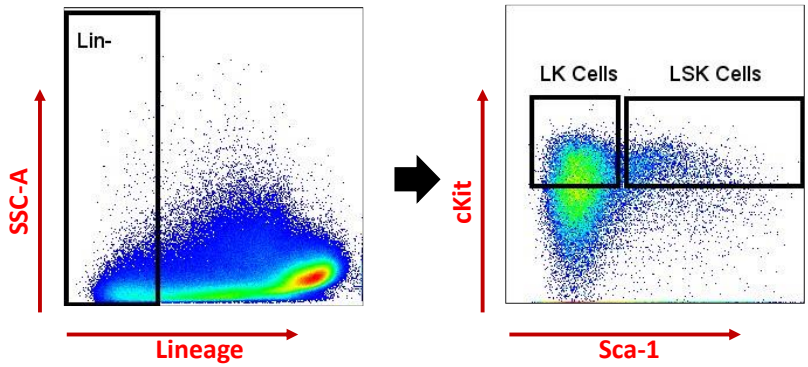

Figure 4-3: Gating strategy for haematopoietic populations.

Gating strategy of HSCs and progenitors: LK Cells (common progenitors) and LSK Cells (HSCs and their multipotent progenitors) were gated under the lineage negative live bone marrow cells.

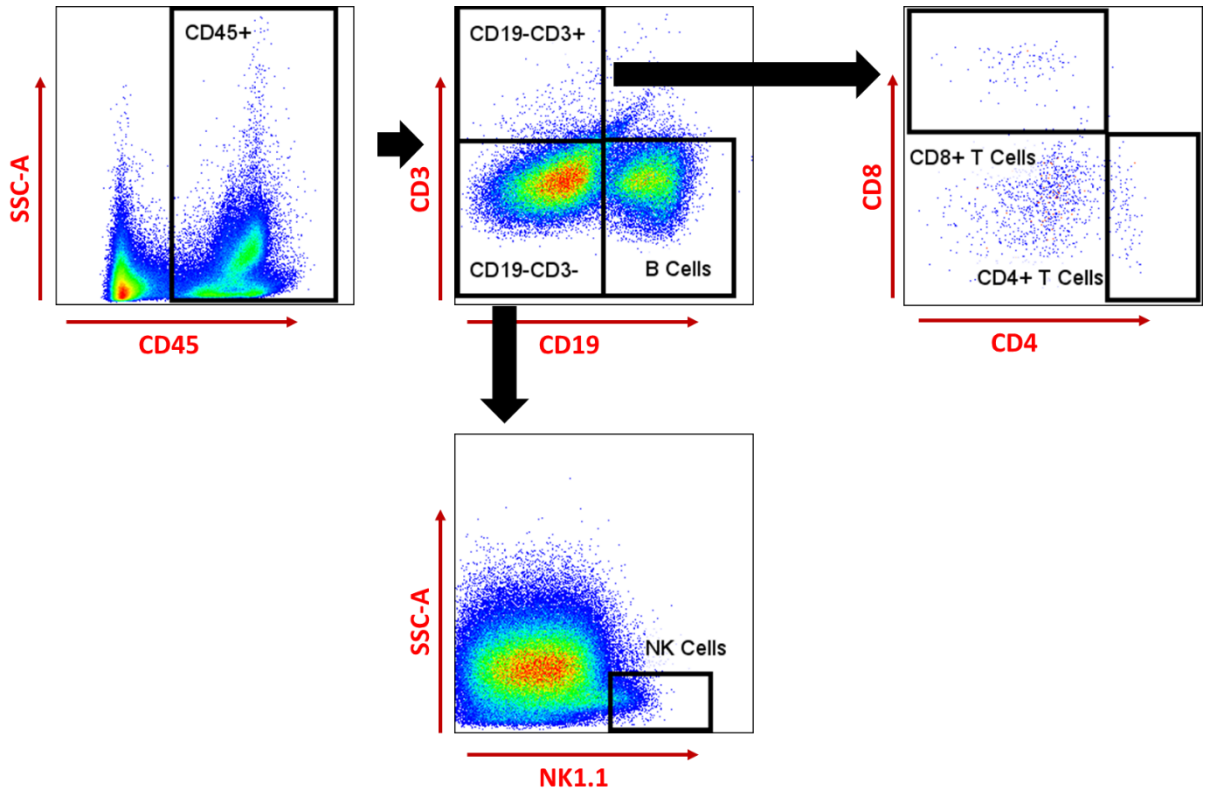

Figure 4-4: Gating strategy for lymphocyte populations.

Gating strategy of Lymphocyte cell populations: B Lymphocytes were gated under the live CD45 positive bone marrow cells, CD19 negative and CD3 positive compartment giving rise to the T Lymphocytes and both CD19, CD3 negative compartment giving rise to the NK Cells.

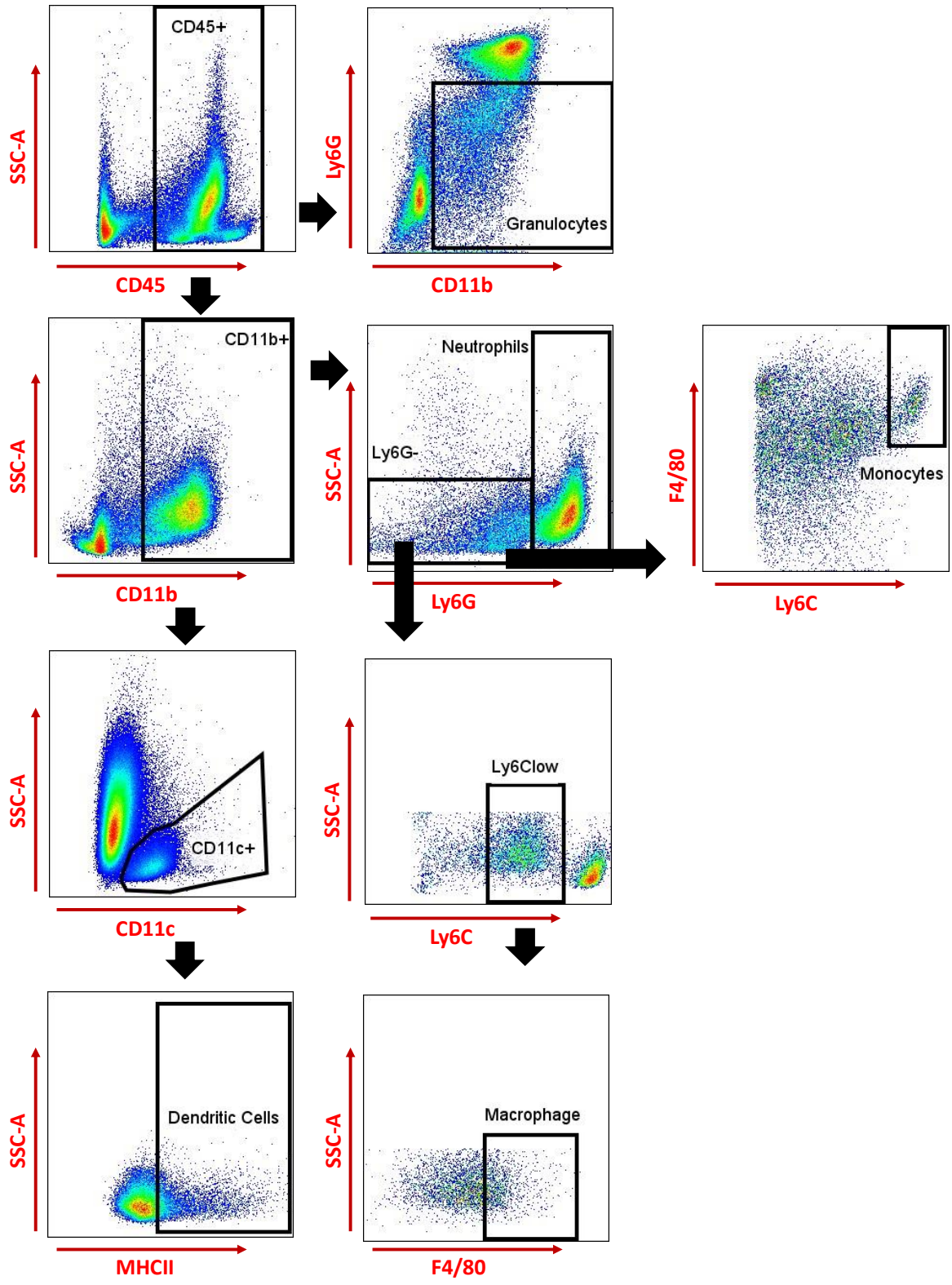

Figure 4-5: Gating strategy for myeloid populations.

Gating strategy for myeloid populations: Granulocytes arise from live CD45 positive bone marrow cells, Neutrophils were gated under the CD11b positive cell populations, and Ly6G hostile population gave rise to monocytes and macrophages. Dendritic cells were given arise from the CD11c positive population from CD11b positive cells.

4.5. Results

The bone microenvironment plays an essential part in tumour development and response to treatment ((Müller *et al*, 2001; Karnoub *et al*, 2007; Ghajar *et al*, 2013; Morris & Edwards, 2016; Maroni, 2019; Clézardin *et al*, 2020)). However, anti-cancer agent studies focus on the outcome of the tumour, not the impact on the bone cells. Chemotherapy agents can be used to modify the BME, which already targets metastatic disease. Previous studies show that 4 and 8 mg /kg doses of doxorubicin can successfully reduce the size of the metastatic breast cancer tumours in bone without the effects on the bone in model systems (Ottewell *et al*, 2008b); thus, I investigated the effects of DOX on the cells of bone marrow and bone integrity in both immunocompetent and compromised mice (Ottewell *et al*, 2008a).

4.5.1. Half Maximal Inhibitory (IC50) of doxorubicin on MDA-MB-231-IV PX462 cells.

The IC50 level (the half maximal inhibitory concentration) was determined by a dose-response curve generated with an MTT assay to establish that the drug effectively inhibited tumour cell growth. MDA-MB-321-IV PX462 human breast cancer cells were treated by a series of dilutions for 72 hours, resulting in a final DOX concentration of 1 nM- 100 µM. The effects of DOX were compared to the vehicle, which was the same volume as the PBS control. After the MTT assay, absorbances were measured using a plate reader at 570 nm.

Absorbance values of control (Media Only: 2.53±0.72) and vehicle control (PBS: 2.48±0.28) are not significantly different (p=ns:072). The lowest concentration of DOX (10^{-9} M: 2.240±0.31) is not significantly different from the control. 10^{-8} M DOX concentration (10^{-8} M: 1.86±50.4) is significantly different (p=0.0018) than control. When the concentrations were increased to $5x10^{-8}$ M (1.19±0.13), 10^{-7} M (1.13±0.08), 10^{-6} M (0.20±0.02), 10^{-5} M (0.18±0.01), $5x10^{-5}$ M (0.1±0.01) and 10^{-4} M (0.01±0.01), individual absorbance values were significantly different ($p \leq 0.0001$) when compared to the control.

The sum of absorbance values of blank wells was extracted from all values. Then, all values were normalised to the maximum absorbance values of the control group, which were set to 100% (Normalised Value: Absorbance/Maximum Absorbance x 100). Molarity values were turned to Log[X] values to fit the curve. Then, the IC50 was calculated with GraphPad version 8 using these values (Figure 4-6).

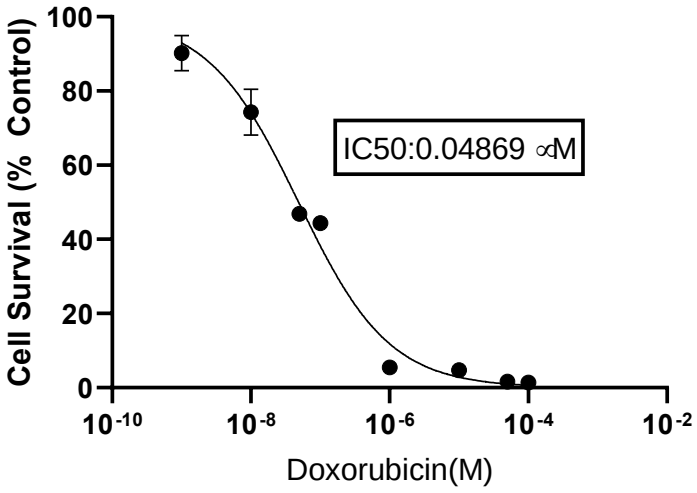

Figure 4-6: Effect of increasing DOX concentration on MDA-MB-231-IV PX462 cells survival

Seeded cells were treated with different concentrations of DOX for 72 hours, and a MTT assay was used to determine cell density. The cell survival rate was compared with increasing doxorubicin concentration. Data are shown as Mean+SEM. n=8.

These results demonstrate that DOX is active and causes a dose-dependent reduction in MDA-MB-231-IV PX462 cell viability with an IC50 of 0.049 µM.

4.5.2. Effects of 4 mg/kg doxorubicin on bone, bone cells and bone marrow cells.

As explained in the introduction, DOX is an anthracycline that targets the DNA, which is why it targets fast multiplying cancer cells more than the other cells. However, this is not the only mechanism; it also creates reactive oxygen species that trigger oxidative stress and apoptosis. This oxidative stress may explain the cardiotoxicity. Immunocompetent and immunocompromised mice were treated with a low but effective 4mg/kg dose used in a previous murine study to determine the deteriorated effects on bone structure, bone and bone marrow cells (Ottewell *et al*, 2008a).

General Toxicity Effect of 4 mg/kg doxorubicin on mice

Tracking body weight is an easy and practical analysis to determine mouse health, with weight loss being one of the indicators of toxicity. From the graphs in the figure below, no weight loss in animals treated with 4 mg/kg DOX indicated toxicity in either immunocompetent (Figure 4-7A) or immunocompromised mice (Figure 4-7B).

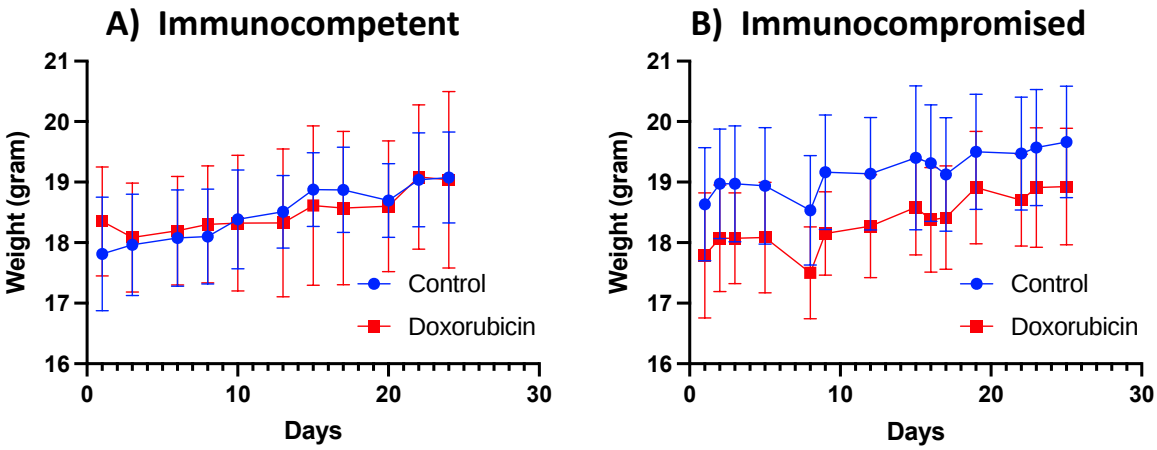

Figure 4-7: Effect of 4 mg/kg DOX on mouse body weight.

Body weight of A) immunocompetent and B) immunocompromised mice treated with either saline (control) or 4 mg/kg DOX weekly for four weeks. 2-Way ANOVA test was used for statistical analysis, and no significant difference was found in multiple comparisons, n=8/group for both graphs and data showed as mean +/- SEM.

4.5.2.1. Immunocompetent mice

The effect of DOX on bone in immunocompetent mice was established by treating 7-week-old female BALB/c mice (n=8/group) with a single dose of DOX (4mg/kg, i.v.) or sterile PBS control once a week for four weeks. Animals were culled 48h after the last drug injection, and bones were collected for downstream analysis.

Bone Structure and Integrity

Previous studies using murine models showed bone loss due to the cytotoxicity caused by DOX [6], and µCT was used to establish if bone structure and integrity were affected. As seen in Figure 4-8, this DOX regime significantly reduced trabecular bone density (CON: 11.35±1.42, DOX: 6.09±1.89) (Figure 4-8A) and trabecular number (CON: 2.68±0.31, DOX: 1.43±0.46)(Figure 4-8B), when compared to control. This reduction of the trabecular bone was also observed as an increase in trabecular separation (gap in between the trabecular bones) in the treated group (CON: 0.18±0.02, DOX: 0.23±0.03) (Figure 4-8D). There were no significant differences found in trabecular thickness (CON: 0.04±0.002, DOX: 0.04±0.002)(Figure 4-8C) and cortical bone volume (CON: 0.83±0.07, DOX: 0.83±0.05)(Figure 4-8E) in between control and treatment groups.

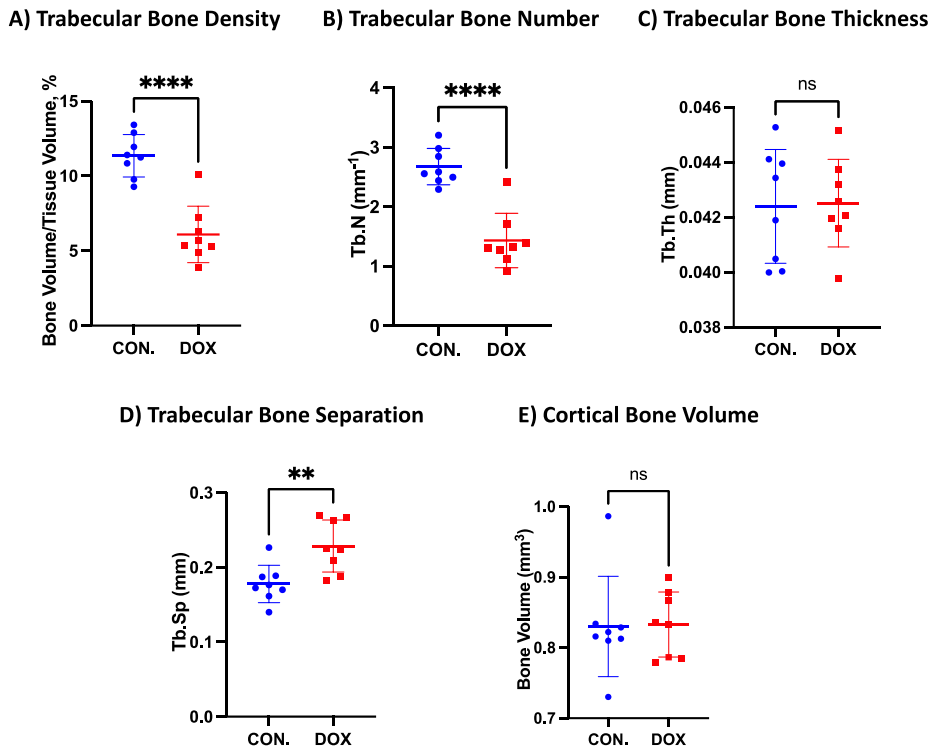

	Control	DOX	P
Trabecular Bone Density (BV/TV, %)	11.35±1.42	6.09±1.89	****: ≤0.0001
Trabecular Number (Tb.N., mm)	2.68±0.31	1.43±0.46	****: ≤0.0001
Trabecular Thickness (Tb.Th., mm)	0.04±0.002	0.04±0.002	ns:0.9
Trabecular Separation (Tb.Sp., mm)	0.18±0.02	0.23±0.03	**:0.0048
Cortical Bone Volume (BV, mm^3)	0.83±0.07	0.83±0.05	ns:0.92

Figure 4-8: 4 mg/kg DOX reduces trabecular bone features in immunocompetent mice.

*7-week-old female BALB/c mice received a dose of doxorubicin (DOX, 4mg/kg, i.p.) or sterile PBS control for four weeks once a week. (A) Effects on trabecular bone density (%), (B) Trabecular Thickness (mm-1), (C) Trabecular Bone Thickness (mm), (D)Trabecular Bone Separation (mm), (E) Cortical Bone Volume (mm3), T-Test was used for statistical analysis; ns is non-significant, ** is ≤0.01, *** is ≤0.001, **** is ≤0.0001 data show Mean±SD n=8 for CON. and DOX.*

Overall, weekly administration of 4 mg/kg DOX for four weeks significantly reduced trabecular bones in immunocompetent mice compared to control (Figure 4-8).

Bone Remodelling Cells

Bone histomorphometry was performed to determine if DOX altered osteoblasts or osteoclasts in both endocortical and trabecular bone regions. 3µm thick sections from hind limb bones were stained for TRAP to determine the doxorubicin effect on osteoblasts and osteoclasts. Stained sections were quantified by their numbers and active surface length under the light microscope. Results were obtained from endocortical (active osteoblast zone) and trabecular (osteoclast active zone) bone regions. In both regions, active osteoblasts and osteoclasts and their perimeter per mm bone were measured. Active osteoclasts are the osteoclasts on the bone surface with TRAP activity,

and active osteoblasts are the osteoblasts on the bone surface with a rectangular shape (Figure 4-9). Osteomeasure was used to quantify those parameters.

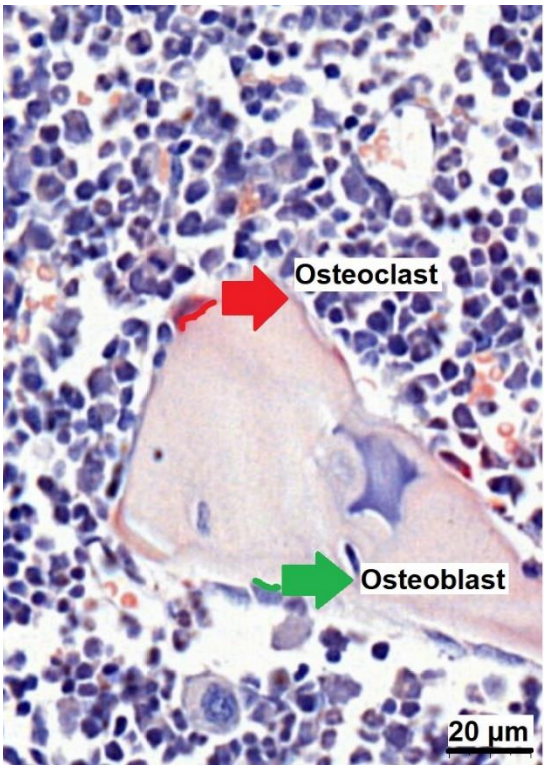

Figure 4-9: Representative image of the active osteoblasts, osteoclasts, and their depositing/resorbing surface.

Image from the region of trabecular bone that is stained for TRAP. An active osteoblast and active osteoclast were quantified and shown in the image. The bone depositing surface of osteoblasts is shown with a green marker, and the bone-resorbing surface of osteoclasts is shown with a red marker. Similar parameters were measured in both mm trabecular and endocortical bones.

Endocortical bone

Results from the endocortical bone region stained for TRAP indicated that there was no significant difference in osteoblast number per mm endocortical bone surface (EBS) (CON: 9.04±5.02, DOX: 8.32±4.21)(Figure 4-10A) and osteoclast number per mm EBS (CON: 0.84±1.02, DOX: 0.12±0.15)(Figure 4-10B). Also, the osteoblast depositing surface, which is the overall cell surface (µm) per osteoblast in mm EBS (CON: 2.17±0.24, DOX: 2.47±0.45) (Figure 4-10C) or osteoclast resorbing surface (overall cell surface (µm) per osteoclast mm EBS) (CON: 3.14±1.42, DOX: 0.96±1.22) (Figure 4-10D) were similar in both control and treatment group. In healthy bone, osteoblasts deposit bone when osteoclasts resorb it. Therefore, the ratio between these cell types reveals whether the bone remodelling favours bone production or reduction. The osteoblast/osteoclast ratio in the endocortical region was unchanged by DOX treatment (CON: 43.22±54.91, DOX: 56.93±38.57) (Figure 4-10E).

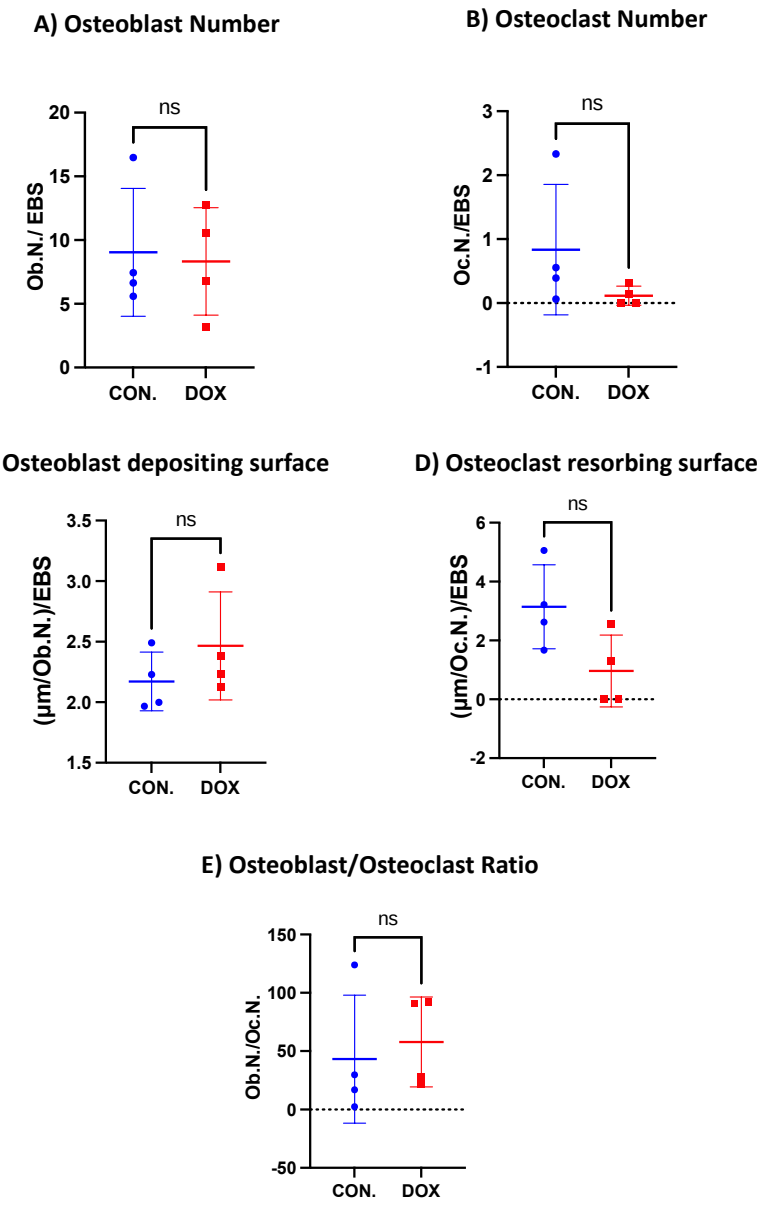

	Control	DOX	P
Osteoblast Number (Ob.N./mm EBS)	9.04±5.02	8.32±4.21	ns:0.83
Osteoclast Number (Oc.N./mm EBS)	0.84±1.02	0.12±0.15	ns:0.21
Osteoblast depositing surface ((µm/Ob.N.)/ mm EBS)	2.17±0.24	2.47±0.45	ns:0.29
Osteoclast resorbing surface ((µm/Oc.N.)/ mm EBS)	3.14±1.42	0.96±1.22	ns:0.06
Osteoblast/Osteoclast Ratio (Ob.N./Oc.N.)	43.22±54.91	56.93±38.57	ns:0.68

Figure 4-10: 4 mg/kg DOX does not alter endocortical bone remodelling cells in immunocompetent mice.

7-week-old female BALB/c mice received a dose of doxorubicin (DOX, 4mg/kg, i.p.) or sterile PBS control for four weeks once a week. (A) Effects on osteoblast number (Ob.N.) per mm endocortical bone surface (EBS), (B) effects on osteoclast number (Oc.N.) per endocortical bone surface (EBS), (C) overall of per osteoblast bone depositing surface per mm EBS, (D) overall of per osteoclast bone resorbing surface per mm EBS (E) Osteoblast and Osteoclast ratio, T-Test was used for statistical analysis; ns is non-significant, data show Mean±SD n=4 for CON. and DOX.

As shown in Figure 4-10, histology results from endocortical bone indicate that 4 mg/kg/week DOX treatment for four weeks does not alter bone remodelling cells in immunocompetent mice (

Figure 4-14, E).

Trabecular Bone

Osteoclasts are most active in trabecular bone areas, and changes in bone caused by drugs or tumours are therefore most prominent in these. As shown in Figure 4-11, B, osteoclast numbers (Oc.N./mm Trabecular Bone Surface (TBS)) were increased in the doxorubicin treated group compared to the control (CON: 4.09±0.71, DOX: 6.49±1.08, p: 0.0099). On the other hand, there was no difference in the osteoblast number (CON.: 4.57±0.92, DOX: 6.66±3.54) (Figure 4-11A), overall bone depositing surface (CON: 3.08±1.64, DOX: 5.86±2.07) (Figure 4-11C) or overall bone resorbing surface (CON: 5.5±2.99, DOX: 10.1±2.32) (Figure 4-11D). The osteoblast/osteoclast ratio was unchanged by DOX treatment compared to control (CON: 1.15±0.31, DOX: 1.03±0.56) (Figure 4-11E).

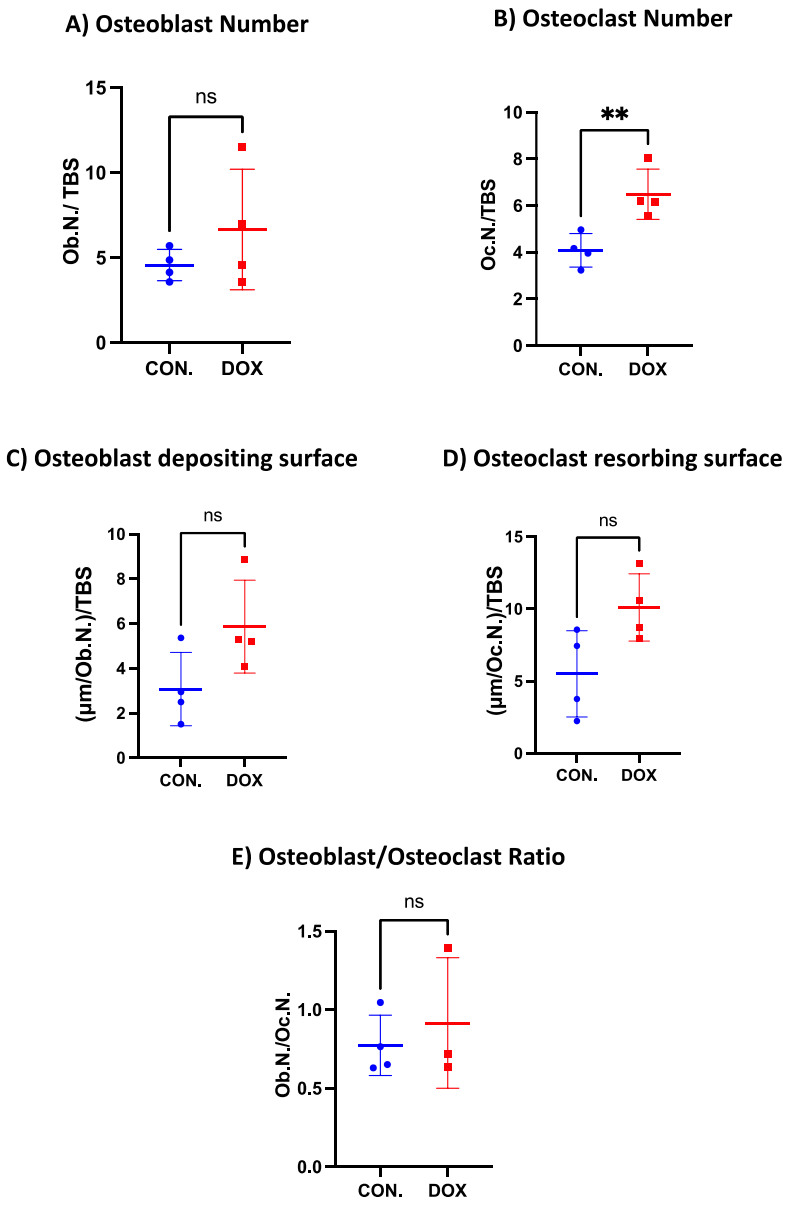

	Control	DOX	P
Osteoblast Number (Ob.N./mm TBS)	4.57±0.92	6.66±3.54	ns:0.3
Osteoclast Number (Oc.N./mm TBS)	4.09±0.71	6.49±1.08	**:0.0099
Osteoblast depositing surface ((µm/Ob.N.)/ mm TBS)	3.08±1.64	5.86±2.07	ns:0.08
Osteoclast resorbing surface ((µm/Oc.N.)/ mm TBS)	5.5±2.99	10.1±2.32	ns:0.051
Osteoblast/Osteoclast Ratio (Ob.N./Oc.N.)	1.15±0.31	1.03±0.56	ns:0.71

Figure 4-11: 4 mg/kg DOX only increases osteoclast number in trabecular bone in immunocompetent mice.

*7-week-old female BALB/c mice received a single dose of doxorubicin (DOX, 4mg/kg, i.p.) or sterile PBS control once a week for four weeks. (A) Effects on osteoblast number (Ob.N.) per mm trabecular bone surface (TBS), (B) effects on osteoclast number (Oc.N.) per mm TBS, (C) overall of per osteoblast bone depositing surface per mm TBS, (D) overall of per osteoclast bone resorbing surface per mm TBS (E) Osteoblast and Osteoclast ratio, T-Test was used for statistical analysis; ns is non-significant, ** is ≤0.01, data show Mean±SD n=4 for CON. and DOX.*

Overall, histology scores from the trabecular bone region showed that a regime of 4 mg/kg/week DOX treatment significantly increased osteoclast numbers with a trend toward increased osteoclast resorbing ratio (Figure 4-11).

HSCs

Establishing the effects of doxorubicin on HSCs is important since it was suggested that HSCs share their niche with breast cancer cells in bone (Allocca *et al*, 2019). To determine whether weekly 4 mg/kg DOX treatment altered the HSCs, liquid bone marrow was collected at the end of the experiment and cultured in semi-solid media specific for HSCs and HSC progenitors (as described in section 2.2.3.9). Counting of colony forming units showed that similar colony numbers were generated from HSCs in DOX-treated mice compared to the control group (DOX:30.33±9.62, CON: 25.78±4.44). This result concludes that weekly 4 mg/kg DOX treatment did not alter the HSCs and HSC progenitors from liquid bone marrow in the immunocompetent strain (Figure 4-12).

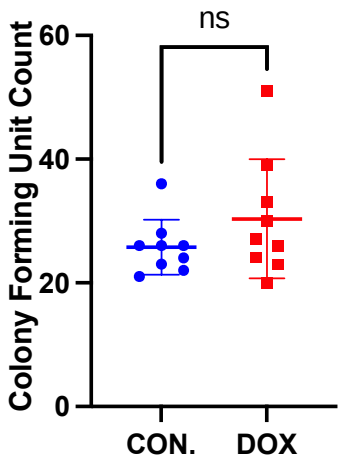

CON.	DOX	P
25.78±4.44	30.33±9.62	ns:0.22

Figure 4-12: Effect of 4mg/kg DOX on bone marrow HSCs and their progenitors in immunocompetent mice.

The dose of 4mg/kg mouse DOX treatment affects on HSCs and its progenitors' colony counts from immunocompetent mice's liquid bone marrow. T-Test was used for statistical analysis; ns is non-significant, and data show Mean±SD n=3 (3 replicates) for CON. and DOX.

4.5.2.1. Immunocompromised mice

The effect of DOX on bone in immunocompromised mice was established by treating 7-week-old female BALB/c nude mice (n=8/group) with a single weekly dose of DOX (4mg/kg, i.v.) or sterile PBS control once a week for four weeks. Animals were culled 48h after the last drug injection, and bones were collected for downstream analysis as described in the following sections.

Bone Structure and Integrity

µCT was used to assess the effects of DOX on bone structure and volume by comparing trabecular thickness, trabecular number and separation, and volume of trabecular and cortical bone from the region of interest (ROI) to control.

As shown in Figure 4-13, there was no difference in any of the bone parameters measured between the control and DOX treated group, indicating that treatment for four weeks, once a week, with 4mg/kg DOX had no adverse effects on bone volume or structure in immunocompromised mice.

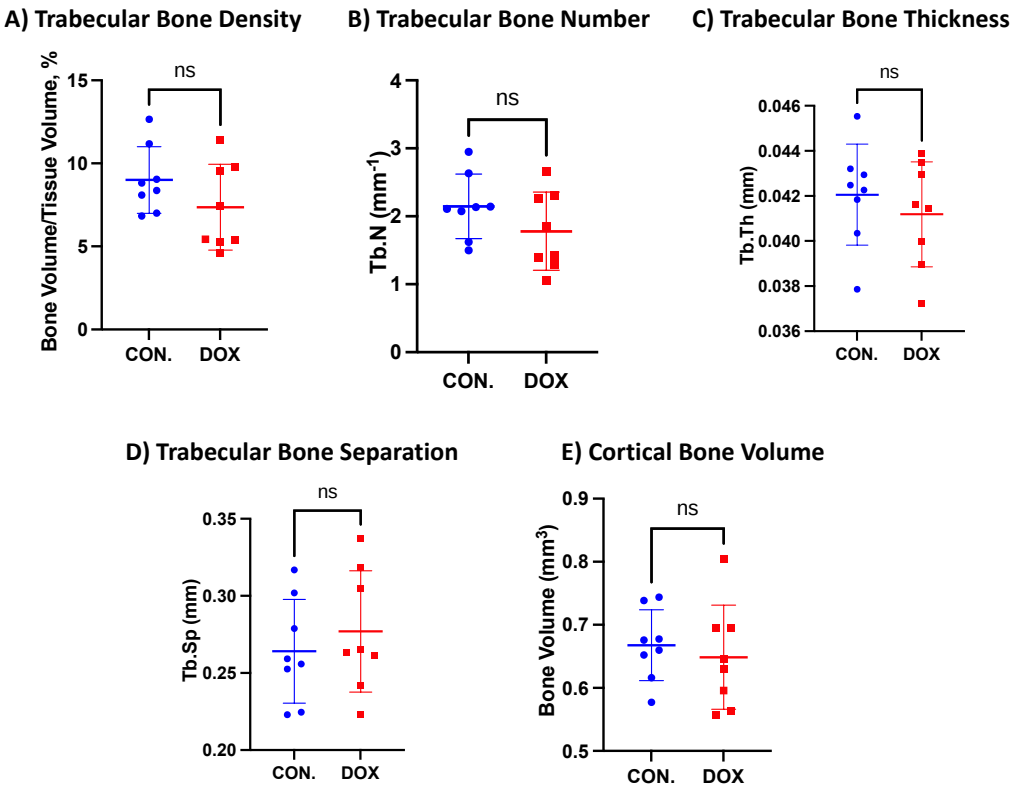

	Control	DOX	P
Trabecular Bone Density (BV/TV, %)	9±2	7.36±2.58	ns:0.18
Trabecular Number (Tb.N., mm)	2.15±0.47	1.78±0.58	ns:0.19
Trabecular Thickness (Tb.Th., mm)	0.04±0.002	0.04±0.002	ns:0.46
Trabecular Separation (Tb.Sp., mm)	0.26±0.03	0.28±0.04	ns:0.49
Cortical Bone Volume (BV, mm^3)	0.67±0.06	0.65±0.08	ns:0.6

Figure 4-13: 4 mg/kg DOX does not alter the bone structure and integrity in immunocompromised mice.

7-week-old female BALB/c nude mice received a single dose of doxorubicin (DOX, 4mg/kg, i.p.) or sterile PBS control once a week for four weeks. (A) Effects on trabecular bone density (%), (B) Trabecular Thickness (mm-1), (C) Trabecular Bone Thickness (mm), (D)Trabecular Bone Separation (mm), (E) Cortical Bone Volume (mm3), T-Test was used for statistical analysis, ns is non-significant, data show Mean±SD n=8 for CON. and DOX.

Bone Remodelling Cells

To compare the bone remodelling cells, osteoclast and osteoblast, bone was stained for TRAP (Tartrate-resistant Acid Phosphatase) to allow identification of osteoclast and osteoblast numbers under the light microscope.

Endocortical bone

As expected from the μCT results described above, the bone histomorphometry results showed that there was no significant difference between control and DOX treated groups in osteoblast number per mm endocortical bone surface (EBS) (CON: 7.49 ± 1.51, DOX: 11.8 ± 3.37, p= ns)(

Figure 4-14A) and osteoclast number per mm EBS (CON: 0.38 ± 0.22, DOX: 0.9 ± 0.8, p= ns)(

Figure 4-14B). In addition, there was no difference in either the osteoblast depositing surface which is overall cell surface (μm) per osteoblast in mm EBS (CON: 2.27 ± 0.25, DOX:2.1 ± 0.24, p=ns) (

Figure 4-14C) or the osteoclast resorbing surface (overall cell surface (μm) per osteoclast mm EBS) (CON:2.45 ± 2.02, DOX:2.28 ± 1.98, p=ns)(

Figure 4-14D) between the control and DOX treatment group. Bone remodelling is associated with osteoblast and osteoclast ratio. Therefore, I compared the osteoblast/osteoclast ratio of control (CON: 23.23 ± 26.92) and DOX treated (DOX:28.79 ± 26.22) groups and found no significant difference (p=ns) between the groups (

Figure 4-14E).

There was high variability in the measurements from individual animals in control, and DOX treated groups, with no osteoclasts detected in some samples in the DOX treated group. Also, the sample size was n=4 for the control and n=3 for the DOX-treated group; therefore, the standard deviation was higher in the group. These might be the reason for no difference between the groups. The sample size must be increased in future studies to obtain more accurate results.

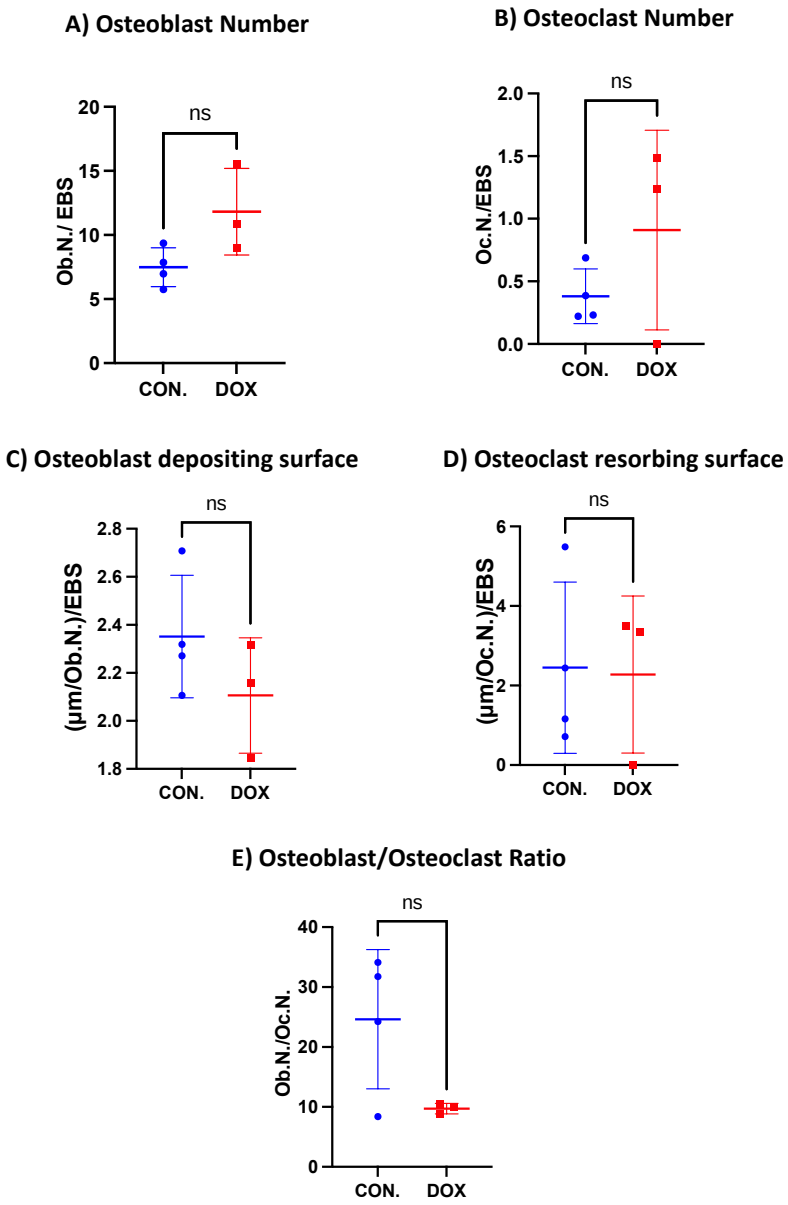

	Control	DOX	P
Osteoblast Number (Ob.N./mm EBS)	7.49±1.51	11.8±3.37	ns:0.07
Osteoclast Number (Oc.N./mm EBS)	0.381±0.218	0.9±0.8	ns:0.25
Osteoblast depositing surface ((µm/Ob.N.)/ mm EBS)	2.27±0.25	2.1±0.24	ns:0.25
Osteoclast resorbing surface ((µm/Oc.N.)/ mm EBS)	2.45±2.02	2.28±1.98	ns:0.92
Osteoblast/Osteoclast Ratio (Ob.N./Oc.N.)	24.63±11.62	9.71±0.86	ns:0.08

Figure 4-14: 4 mg/kg DOX does not alter the bone remodelling cells in the endocortical bone of immunocompromised mice.

7-week-old female BALB/c nude mice received a single dose of doxorubicin (DOX, 4mg/kg, i.p.) or sterile PBS control once a week for four weeks. (A) Effects on osteoblast number (Ob.N.) per mm endocortical bone surface (EBS), (B) effects on osteoclast number (Oc.N.) per endocortical bone surface (EBS), (C) overall of per osteoblast bone depositing surface per mm EBS, (D) overall of per osteoclast bone resorbing surface per mm EBS (E) Osteoblast and Osteoclast ratio, T-Test was used for statistical analysis, ns is non-significant, data show Mean±SD n=4 for CON. and n=3 for DOX.

As shown in

Figure 4-14, these results demonstrated that 4 mg/kg/week of DOX treatment for four weeks has no significant effect on bone remodelling cells in endocortical bone (

Figure 4-14E).

Trabecular Bone

As expected from the µCT results, bone histomorphometry analysis of the trabecular bone area showed that there was no significant difference in any of the measured parameters (osteoblast/osteoclast number, deposition/resorption surface, osteoblast: osteoclast ratio) between the control and the DOX treated group (Figure 4-15).

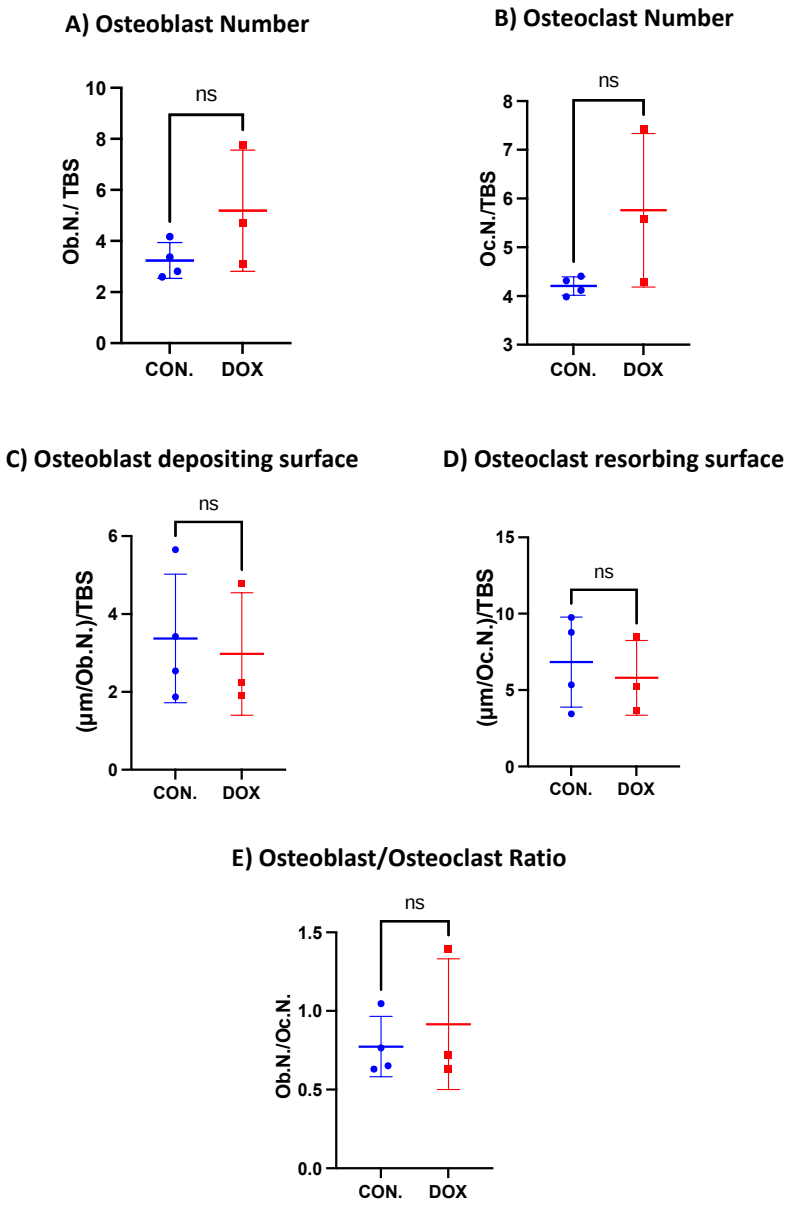

	Control	DOX	P
Osteoblast Number (Ob.N./mm TBS)	3.24±0.7	5.18±2.37	ns:0.17
Osteoclast Number (Oc.N./mm TBS)	4.21±0.19	5.76±1.58	ns:0.1
Osteoblast depositing surface ((µm/Ob.N.)/ mm TBS)	2.27±0.25	2.98±1.57	ns:0.76
Osteoclast resorbing surface ((µm/Oc.N.)/ mm TBS)	6.83±2.95	5.8±2.44	ns:0.65
Osteoblast/Osteoclast Ratio (Ob.N./Oc.N.)	0.77±0.19	0.91±0.41	ns:0.56

Figure 4-15: 4 mg/kg DOX does not alter the bone remodelling cells in immunocompromised mice's trabecular bone.

7-week-old female BALB/c nude mice received a single dose of doxorubicin (DOX, 4mg/kg, i.p.) or sterile PBS control once a week for four weeks. (A) Effects on osteoblast number (Ob.N.) per mm trabecular bone surface (TBS), (B) effects on osteoclast number (Oc.N.) per mm TBS, (C) overall of per osteoblast bone depositing surface per mm TBS, (D) overall of per osteoclast bone resorbing surface per mm TBS (E) Osteoblast and Osteoclast ratio, T-Test was used for statistical analysis; ns is non-significant, data show Mean±SD n=4 for CON. and n=3 for DOX.

HSCs

As previously mentioned, the HSC niche in bone overlaps with the bone metastasis niche (discussed in chapter 5), and both the HSC and the niche may be affected by DOX. Therefore, the effects of DOX on HSCs and progenitors in the liquid bone marrow were determined by the colony forming unit assay.

Bone marrow from 2 mice/group was seeded using three replicates. Results from the CFU assay showed that haematopoietic stem cell colony numbers in DOX-treated mice (DOX:84.5±49.5) were similar (p=ns:0.09) to that of the control group (CON: 123.8±14). However, there was considerable variability between the samples and a trend toward reduced HSCs can be seen when mice were treated with 4 mg/kg DOX (Figure 4-16).

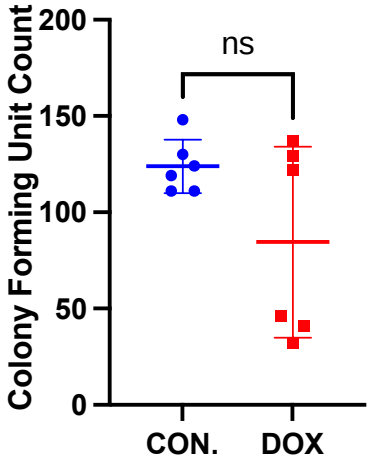

CON.	DOX	P
123.8±14	84.5±49.5	ns:0.09

Figure 4-16: 4mg/kg DOX treatment effect on HSCs and their progenitors from immunocompromised mice's bone marrow.

4mg/kg DOX effect on HSCs and their progenitors measured as colony counts from the liquid bone marrow of immunocompromised mice. T-Test was used for statistical analysis, and ns is non-significant. Data show Mean±SD n=2 (3 replicates) for CON and DOX.

4.5.3. Effect of 6 mg/kg doxorubicin on bone, bone cells and bone marrow cells.

It is possible that the initial dose of 4mg/kg of DOX was too low to cause significant changes to the bone microenvironment. I therefore decided to determine the effects of the increased dose of 6 mg/kg DOX on bone, bone cells and bone marrow cells in both immunocompetent and

immunocompromised mice. Bones were analysed with µCT to determine whether there was structural damage. Bones were embedded in wax for sectioning, bone histomorphometry was performed on TRAP-stained sections to quantify the bone cells and their active bone surface length. Liquid bone marrow was collected and analysed with flow cytometry to quantify a selection of the immune and HSC populations.

General Toxicity Effect of 6 mg/kg doxorubicin on mice

No indication of toxicity was identified by weekly administration of 6 mg/kg DOX for four weeks in either immunocompetent (Figure 4-17A) or immunocompromised mice (Figure 4-17B).

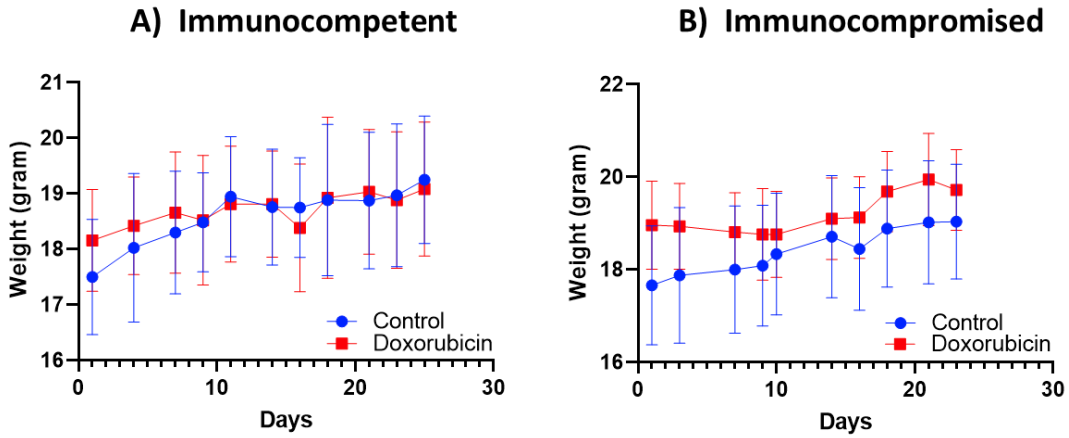

Figure 4-17: 6 mg/kg DOX effect on mouse weight.

Change of weight by day for A) immunocompetent and B) immunocompromised strains were treated with either saline (control) or 6 mg/kg DOX. 2-Way ANOVA test was used for statistical analysis, and no significant difference was found in multiple comparisons, n=8/group for both graphs and data showed as mean + error.

4.5.3.1. Effects of 6mg/kg DOX in immunocompetent mice

The effect of DOX on bone in immunocompetent mice was established by treating 7-week-old female BALB/c mice (n=8/group) with a single dose of DOX (6 mg/kg, i.v.) or sterile PBS control once a week for four weeks. Animals were culled 48h after the last drug injection, and bones were collected for downstream analysis.

Bone Structure and Integrity

The µCT results showed that overall trabecular bone density (BV/TV, %) was significantly reduced in the 6 mg/kg DOX treated group compared to the saline control (CON: 11.37±1.51, DOX: 4.39±0.48, p:****≤0.0001) (Figure 4-18A). In addition, the number of trabecular bones were significantly lowered in the DOX-treated group (CON: 2.54±0.24, DOX: 0.99±0.16, p:

****≤0.0001)(Figure 4-18B), but trabecular thickness was unaffected by DOX treatment (CON: 0.04±0.002, DOX: 0.04±0.003, p: 0.98)(Figure 4-18C). On the other hand, trabecular separation (the space between the trabecular bones) was significantly lower in the DOX-treated group compared to the saline control (CON: 0.8±0.025, DOX: 0.79±0.046, p: **≤0.0051) (Figure 4-18D). Endocortical bone volume of both DOX and saline-treated groups was similar in the two groups (CON: 0.234±0.02, DOX: 0.387±0.08, p:0.73) (Figure 4-18E). Taken together, four weeks of weekly 6 mg/ kg DOX treatment significantly reduced the trabecular bone content without affecting the cortical bone volume and density or trabecular bone thickness.

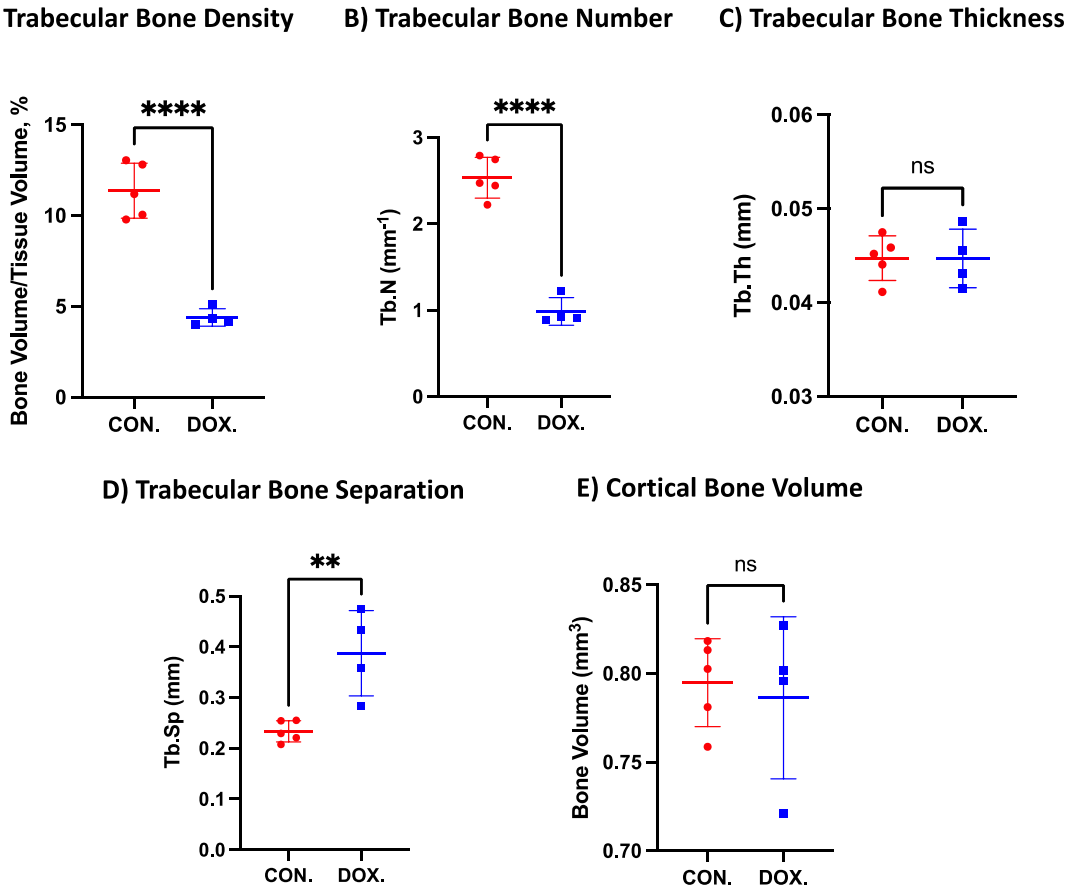

	Control	DOX	P
Trabecular Bone Density (BV/TV, %)	11.37±1.51	4.39±0.48	****≤0.0001
Trabecular Number (Tb.N., mm)	2.54±0.24	0.99±0.16	****≤0.0001
Trabecular Thickness (Tb.Th., mm)	0.04±0.002	0.04±0.003	ns:0.98
Trabecular Separation (Tb.Sp., mm)	0.234±0.02	0.387±0.08	**≤0.0051
Cortical Bone Volume (BV, mm^3)	0.8±0.025	0.79±0.046	ns:0.73

Figure 4-18: 6 mg/kg DOX reduces trabecular bone number in immunocompetent mice.

*7-week-old female BALB/c mice received a single dose of doxorubicin (DOX, 6 mg/kg, i.p.) or sterile PBS control once a week for four weeks. (A) Effects on trabecular bone density (%), (B) Trabecular Thickness (mm-1), (C) Trabecular Bone Thickness (mm), (D)Trabecular Bone Separation (mm), (E) Cortical Bone Volume (mm3) was compared using T-Test statistical analysis between DOX and saline-treated groups, and ns is non-significant, ** is ≤0.01, *** is ≤0.001, **** is ≤0.0001 data show Mean±SD n=5 for CON. And n= 4 for DOX.*

Bone Remodelling Cells

To determine the effects of 6 mg/kg DOX on osteoblasts and osteoclasts, bones (n=5 for saline-treated, n=4 for DOX treated) were cut and stained for TRAP (a marker for osteoclastic activity). In both endocortical and trabecular bone regions, osteoblast numbers per mm bone, osteoclast numbers per mm bone, osteoblast depositing surface (average µm of active osteoblast depositing surface in per mm bone) and osteoclast resorbing surface (average µm of active osteoclast resorbing surface in per mm bone) were scored. Student T-Test was used to statistically compare the groups to check if there was a meaningful difference.

Endocortical Bone

The endocortical bone region was the area of 1.8 mm bone from the reference point (300 µm from chondrocytes) on both sides of the sectioned bones where the majority of osteoblasts exist; therefore, the main effects on osteoblasts can be observed if they exist.

As seen from the results, osteoblast (CON: 9.45±3.82, DOX: 11.46±3.98, p: ns) and osteoclast numbers (CON: 0.17±0.19, DOX: 0.07±0.14, p: ns) per mm endocortical bone were similar between saline control and DOX treated groups (Figure 4-19A, B). In addition, there was no significant difference in the osteoblast depositing surface (CON: 4.77±0.84, DOX: 5.13±1.55, p: ns) and osteoclast resorbing surface (CON: 7.04±7.22, DOX: 10.07±20.13, p: ns) between the groups (Figure 4-19C, D).

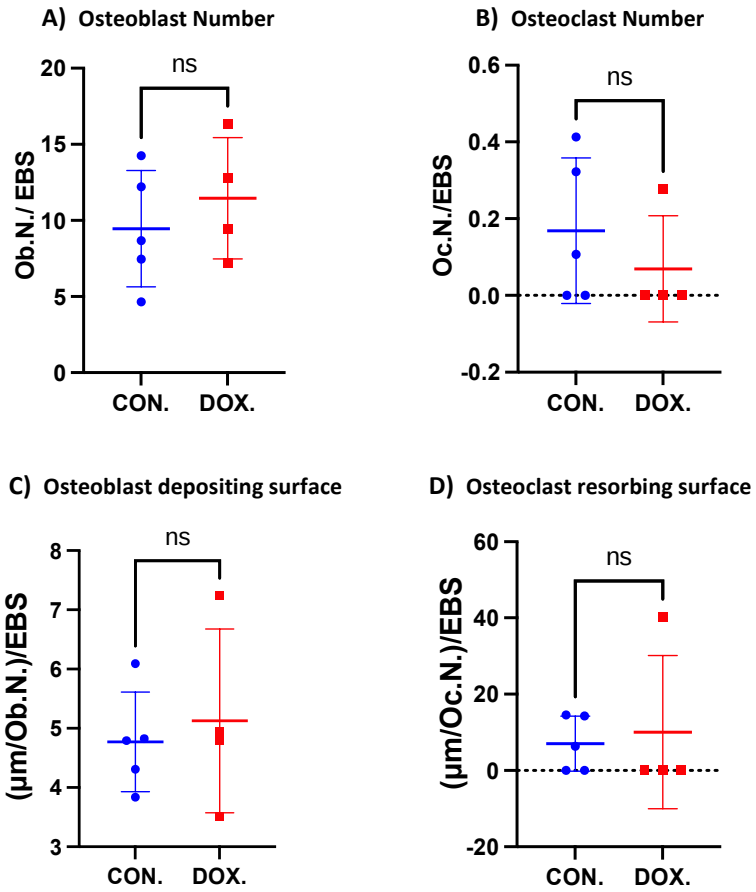

	Control	DOX	P
Osteoblast Number (Ob.N./mm EBS)	9.45±3.82	11.46±3.98	ns:0.47
Osteoclast Number (Oc.N./ mm EBS)	0.17±0.19	0.07±0.14	ns:0.41
Osteoblast depositing surface ((µm/Ob.N.)/ mm EBS)	4.77±0.84	5.13±1.55	ns:0.67
Osteoclast resorbing surface ((µm/Oc.N.)/ mm EBS)	7.04±7.22	10.07±20.13	ns:0.76

Figure 4-19: 6 mg/kg doxorubicin effect on bone remodelling cellsin endocortical bone in immunocompetent mice.

7-week-old female BALB/c mice received a single dose of doxorubicin (DOX, 6mg/kg, i.p.) or sterile PBS control once a week for four weeks. (A) Effects on osteoblast number (Ob.N.) per mm endocortical bone surface (EBS), (B) effects on osteoclast number (Oc.N.) per mm EBS, (C) overall of each osteoblast bone depositing surface per mm EBS, (D) overall of each osteoclast bone resorbing surface per mm EBS were compared between DOX and saline-treated groups, T-Test was used for statistical analysis, ns is non-significant, data show Mean±SD n=5 for CON. and n=4 for DOX.

Similar to data found for the 4mg/kg dose of DOX, no effect on bone remodelling cells in the endocortical bone region of BALB/c female mice was observed following weekly administration of 6mg/kg dose of DOX for four weeks (Figure 4-19).

Trabecular Bone

As seen in Figure 4-20, no difference was found in the bone structure in the trabecular bone of the immunocompetent mice with a 6 mg dose of DOX. Interestingly, a previous increase in the osteoclast number with 4 mg DOX was not observed with 6 mg DOX. However, there was considerable variability in the measured parameters, and some samples had zero osteoblast or osteoclast numbers, probably caused by the low sample size.

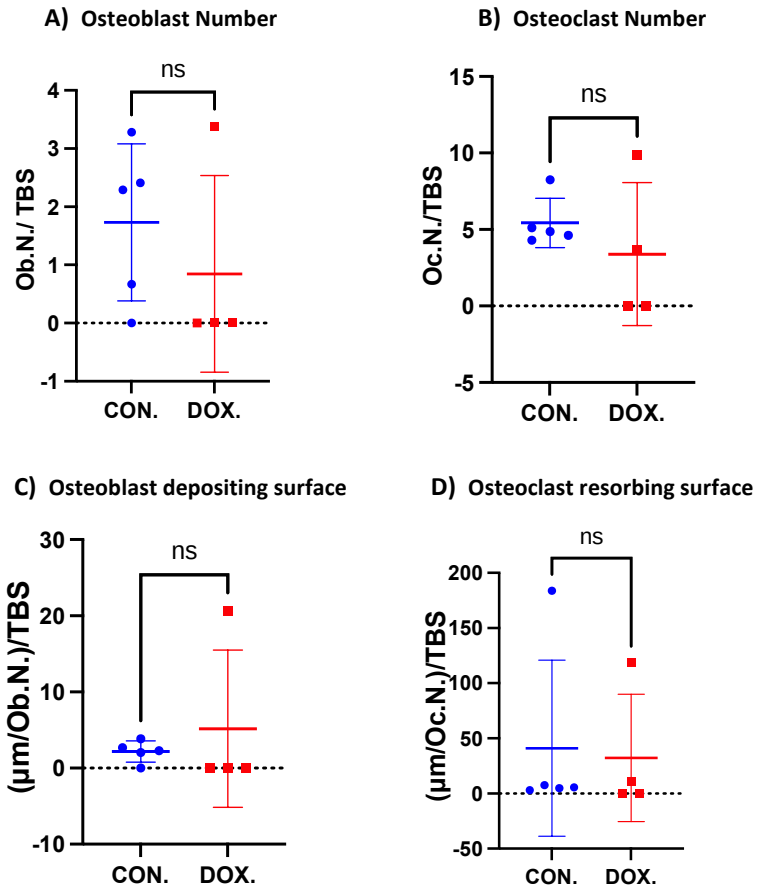

	Control	DOX	P
Osteoblast Number (Ob.N./mm TBS)	1.73±1.35	0.84±1.69	ns:0.41
Osteoclast Number (Oc.N./ mm TBS)	5.44±1.6	3.4±4.68	ns:0.39
Osteoblast depositing surface ((µm/Ob.N.)/ mm TBS)	2.17±1.40	5.16±10.33	ns:0.54
Osteoclast resorbing surface ((µm/Oc.N.)/ mm TBS)	40.99±79.93	32.25±57.69	ns:0.86

Figure 4-20: 6 mg/kg doxorubicin effect on bone remodelling cells in immunocompetent mouse trabecular bone.

7-week-old female BALB/c mice received a single dose of doxorubicin (DOX, 6mg/kg, i.p.) or sterile PBS control once a week for four weeks. (A) Effects on osteoblast number (Ob.N.) per mm trabecular bone surface (TBS), (B) effects on osteoclast number (Oc.N.) per mm TBS, (C) overall of each osteoblast bone depositing surface per mm TBS, (D) overall of per osteoclast bone resorbing surface per mm TBS were compared between DOX and saline-treated groups, T-Test was used for statistical analysis, ns is non-significant, data show Mean±SD n=5 for CON. and n=4 for DOX.

HSCs

HSCs and progenitors are suggested to play a crucial role in cancer metastasis (Shiozawa *et al*, 2011a; Allocca *et al*, 2019), and I decided to use flow cytometry to determine whether DOX altered HSCs and progenitors counts. In the mouse, LSK cells (Lineage(-), Sca-1(+), C-Kit(+)) are defined as HSCs and progenitors in general, and LK cells (Lineage(-), Sca-1(-), C-Kit(+)) are the common myeloid populations, granulocyte-macrophage progenitors, and megakaryocytes-erythrocyte progenitors.

Flow cytometry results showed that the LSK cell population was similar in the saline control and DOX treated groups (CON: 0.54±0.13, DOX:0.54±0.09, p: ns,0.93, % of the Live Cells) (Figure 4-21A). On the other hand, the proportion of LK cells was found to be significantly higher in the DOX-treated group compared to the saline control (CON: 2.97±0.62, DOX:7.35±1.48, p: ****, <0.0001, % of the Live Cells) (Figure 4-21B).

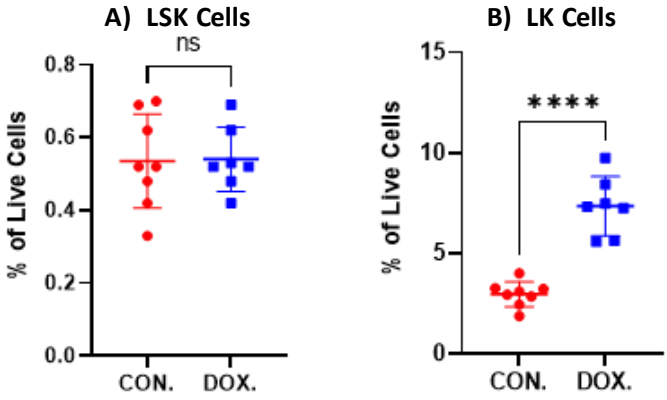

Figure 4-21: Effect of 6 mg/kg DOX on haematopoietic stem cells and progenitors in immunocompetent mice.

*Comparison of A) LSK Cells and B) LK Cells from BALB/c mice bone marrow, both saline control and DOX treated groups, shown as % of Live Cells from flow cytometry. T-Test was used for statistical analysis, and ns is non-significant, **** is ≤0.000 data show Mean±SD n=8 for CON. and n=7 for DOX.*

Since the 4mg/kg DOX effects on HSCs were assessed with the semi-solid medium colony formation assay (Figure 4-12), LSK cells were sorted with Melody FACS sorter and 250 cells/well seeded onto a 6-well-plate to observe whether DOX affects their function (colony formation ability). Due to the rarity of the HSC populations in the liquid bone marrow, 10% of the bone marrow collected from each mouse was pooled as the control and DOX treated groups as three replicates. As seen in Figure 4-21, seeding the same number of LSK cells from control and DOX-treated mice resulted in forming a similar number of colonies in a semi-solid medium (CON:30.33±1.53, DOX:35±1, p: ns, 0.19).

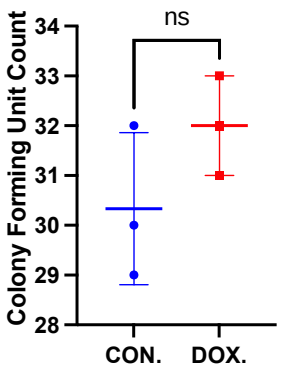

Figure 4-22: Functionality of LSK cells from saline or 6mg/kg DOX treated immunocompetent mice.

Colony count comparison of the sorted LSK cells from saline and 6 mg DOX treated animals' bone marrow. T-Test was used for statistical analysis, and ns is non-significant. Data show Mean±SD n=3 for pooled CON and DOX groups.

In summary, these data demonstrate that 6mg/kg DOX did not affect the number and function of HSCs and their progenitors in the bone marrow, whereas the LK cell populations were significantly increased in response to the treatment (Figure 4-21).

Lymphocytes

Essential components of the immune system, B/T lymphocytes, are produced in the bone marrow. B Cells mature in the bone marrow, whereas T Cells mature in the thymus, from where they can return to the bone marrow. Moreover, another crucial innate lymphocyte are NK cells, which initiate from bone marrow and mature in the tissues. The significant roles of these cells are antibody production, direct killing of virus-infected and cancer cells, and regulation of the immune system (Larosa & Orange, 2008). Chemotherapy is known to induce an inflammatory response by damaging the healthy dividing cells, yet whether there is an observable effect on the lymphocyte population in the liquid bone marrow following DOX treatment is not certain. To determine the effects of DOX on B Lymphocytes, CD8+ T Lymphocytes, CD4+ T Lymphocytes and NK Cells, flow cytometry was used to assess liquid bone marrow obtained from both saline and DOX-treated mice.

I found that weekly treatment of immunocompetent mice with 6 mg/kg DOX for four weeks significantly reduced B cell numbers (CON: 40.99±7.16, DOX:12.36±3.51, p: ****, <0.0001, % of the Live CD45(+) Cells)(Figure 4-23A). Also, CD8+ T cell numbers were significantly lowered in DOX treated group compared to saline control (CON: 0.1±0.06, DOX:0.05±0.01, p: *,0.02, % of the Live CD45(+) Cells)(Figure 4-23B). On the other hand, CD4+ T cells were significantly higher in DOX treated group compared to control (CON: 0.13±0.07, DOX:0.2±0.04, p: *,0.01, % of the Live CD45(+) Cells)(Figure

4-23C). As the antibody used to determine NK Cells in this panel (NK1.1) did not work in this experiment, no NK Cells data were obtained.

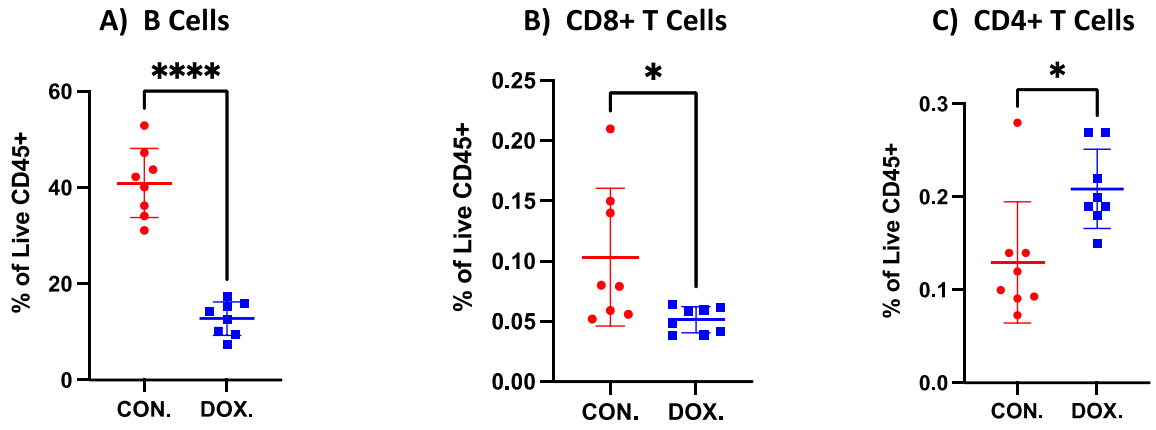

Figure 4-23: 6 mg/kg DOX effect on lymphocytes in immunocompetent strain.

*Comparison of A) B Cells, B) CD8+ T Cells, and C) CD4+ T Cells saline control and DOX treated groups of BALB/c mice as % of Live CD45 (+) Cells from flow cytometry. Data show Mean±SD n=8 for both CON. and DOX. T-Test was used for statistical analysis, and ns is non-significant, ns is non-significant, * is ≤0.05,** is ≤0.01, *** is ≤0.001, **** is ≤0.000.*

My data show that exposure to 6 mg/kg DOX for four weeks significantly impacts B and some T cell populations in the bone marrow (Figure 4-23).

Myeloid Cells

Another immune population, myeloid cells, play essential roles in protective immunity (Stegelmeier *et al*, 2019). To determine the effects of DOX on myeloid cells, flow cytometry was used with liquid bone marrow from both saline and DOX-treated populations. Table 4-1 shows that macrophages, monocytes, neutrophils, granulocytes, and dendritic cells were detected with flow cytometry using specific antibodies.

Results showed that macrophages significantly increased with 6 mg/kg DOX treatment compared to the saline control (CON: 1.45±0.14, DOX:2.53±0.41, p:<0.0001, % of the Live CD45(+) Cells) (Figure 4-24A). In contrast, monocyte numbers were significantly lower in the DOX treated group compared to control (CON: 0.91±0.18, DOX:7.15±0.98, p: <0.0001, % of the Live CD45(+) Cells) (Figure 4-24B). Further statistical tests revealed that the number of neutrophils was significantly increased in the DOX-treated group (CON: 23.21±3.1, DOX:43.53±3.71, p: <0.0001, % of the Live CD45(+) Cells) (Figure 4-24C). On average, granulocyte numbers were notably increased in DOX treated group when compared to the saline control (CON: 12.51±2.64, DOX:27.39±4.15, p: <0.0001, % of the Live CD45(+) Cells) (Figure 4-24D). The antibody to determine dendritic cell populations (MHCII) did not tag efficiently; therefore, the population could not be determined.

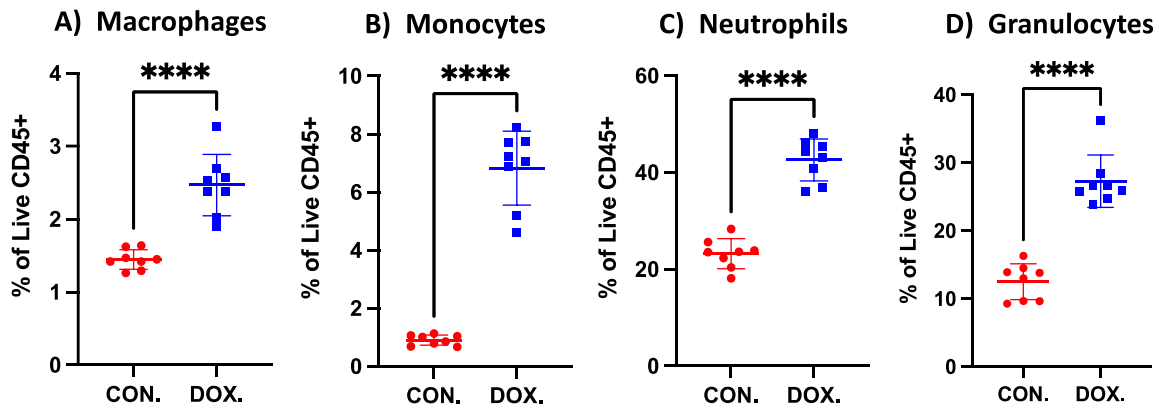

Figure 4-24: 6 mg/kg DOX effect on myeloid cells in immunocompetent strain.

*Comparison of A) Macrophages, B) Monocytes, C) Neutrophils, and D) Granulocytes saline control and DOX treated groups of BALB/c mice's bone marrow as % of Live CD45 (+) Cells from flow cytometry. T-Test was used for statistical analysis, ****, <0.0001, data show Mean±SD n=8 for both CON. and DOX.*

Flow cytometry quantification of myeloid populations showed that their numbers increased in the bone marrow following a weekly 6 mg/kg dose of DOX for four weeks (Figure 4-24). These data suggest that DOX induces an inflammatory response in the bone marrow.

Haematology Analysis

Haematology analysis provides valuable information on markers for disease in both humans and mice. Despite the differences between mice and humans, such as lower neutrophils in peripheral blood or higher bone marrow and peripheral blood percentages in mice, they still can give information about the changes in the general immune cell populations in the peripheral blood (O'Connell *et al*, 2015).

Blood cells were quantified with Sci Vet ABC plus (Figure 4-25). Results indicated an increase in white blood cell counts in DOX treated group; however, this increase was not significant (CON: 2.34±0.88, DOX: 2.97±0.9. p: ns) (Figure 4-25A). Also, lymphocyte counts were similar between control, and DOX treated groups (CON: 1.86±0.71, DOX: 1.76±0.5. p: ns) (Figure 4-25B). On the other hand, monocytes were significantly increased with DOX treatment (CON: 0.07±0.08, DOX: 0.19±0.07. p: **) (Figure 4-25C). Similarly, granulocyte cell counts were increased in the DOX group compared to the control (CON: 0.41±0.15, DOX: 1.03±0.51. p: **) (Figure 4-25D). No significant eosinophil cell counts were found between saline control, and the DOX treated group (CON: 0.06±0.05, DOX: 0.04±0.02. p: ns) (Figure 4-25E).

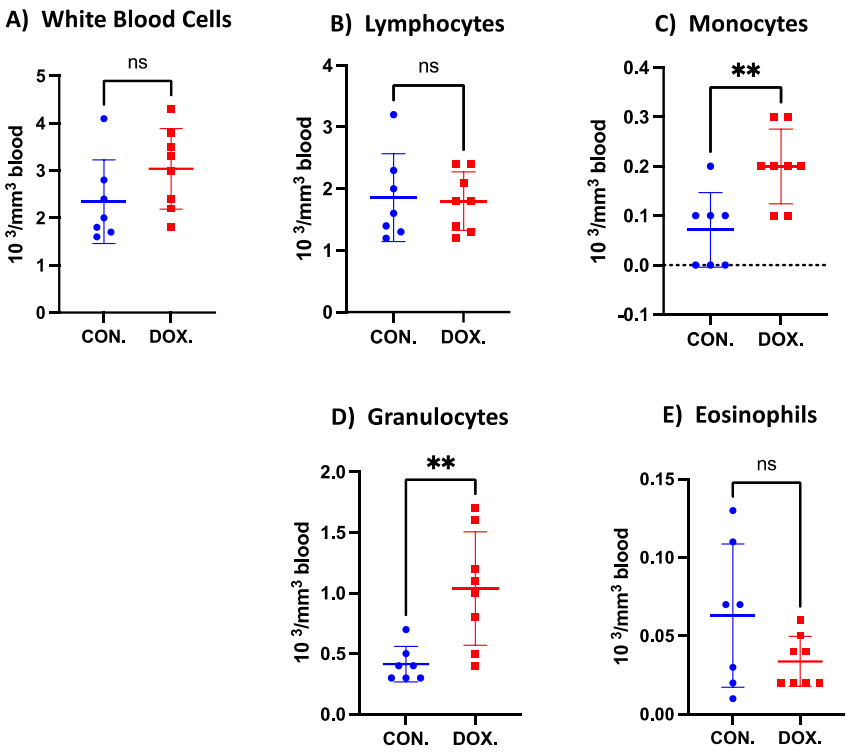

	Control	DOX	P
White Blood Cells (10^3/mm^3)	2.34±0.88	2.97±0.9	ns:0.14
Lymphocyte Cell Counts (10^3/mm^3)	1.86±0.71	1.76±0.5	ns:0.86
Monocyte Cell Counts (10^3/mm^3)	0.07±0.08	0.19±0.07	**:0.006
Granulocyte Cell Counts (10^3/mm^3)	0.41±0.15	1.03±0.51	**:0.005
Eosinophil Cell counts (10^3/mm^3)	0.06±0.05	0.04±0.02	ns:0.11

Figure 4-25: Effects of 6 mg/kg DOX treatment on blood cell counts in immunocompetent mice

*A) White Blood Cells, B) Lymphocyte Cell Counts, C) Monocyte Cell Counts, D) Granulocyte Cell Counts, and E) Eosinophils from peripheral blood of saline-treated control group and DOX treated group from BALB/c strain that was obtained with Sci Vet ABC+ was given as 10^3 cells per mm3 peripheral blood. T-Test was used for statistical analysis, and ns is non-significant, ** is ≤0.01, and data show Mean±SD n=7 for CON. And n=8 for DOX.*

Overall, granulocytes and monocytes were increased due to DOX treatment, yet the lymphocyte with the highest cell count in the total white blood cell count was not affected (Figure 4-25).

4.5.3.1. Immunocompromised mice

The study was repeated in immunocompromised mice by treating 7-week-old female BALB/c Nude mice (n=8/group) with a single dose of DOX (6 mg/kg, i.v.) or sterile PBS control given once a week for four weeks. Animals were culled 48h after the last drug injection, and bones were collected for downstream analysis.

Bone Structure and Integrity

As Figure 4-26 shows, trabecular bone density (ratio of the trabecular bone volume to tissue volume)(CON: 11.24±2.09, DOX: 6.02±0.66, p:***,0.0007)(Figure 4-26A) and trabecular number (CON: 2.65±0.4, DOX: 1.37±0.4, p:***,0.0002)(Figure 4-26B) was significantly reduced with DOX treatment compared to control. However, the trabecular bone thickness was similar in the saline control, and DOX treated groups (CON: 0.04±0.002, DOX: 0.04±0.002, p: ns) (Figure 4-26C). Trabecular bone was increased in DOX-treated mice compared to the saline-treated controls (CON: 0.24±0.018, DOX: 0.35±0.05, p: **,0.0016) (Figure 4-26D). On the other hand, there was no significant difference in cortical bone volume between the control and DOX treated groups (CON: 11.24±2.09, DOX: 6.02±0.66, p: ***,0.0007) (Figure 4-26E).

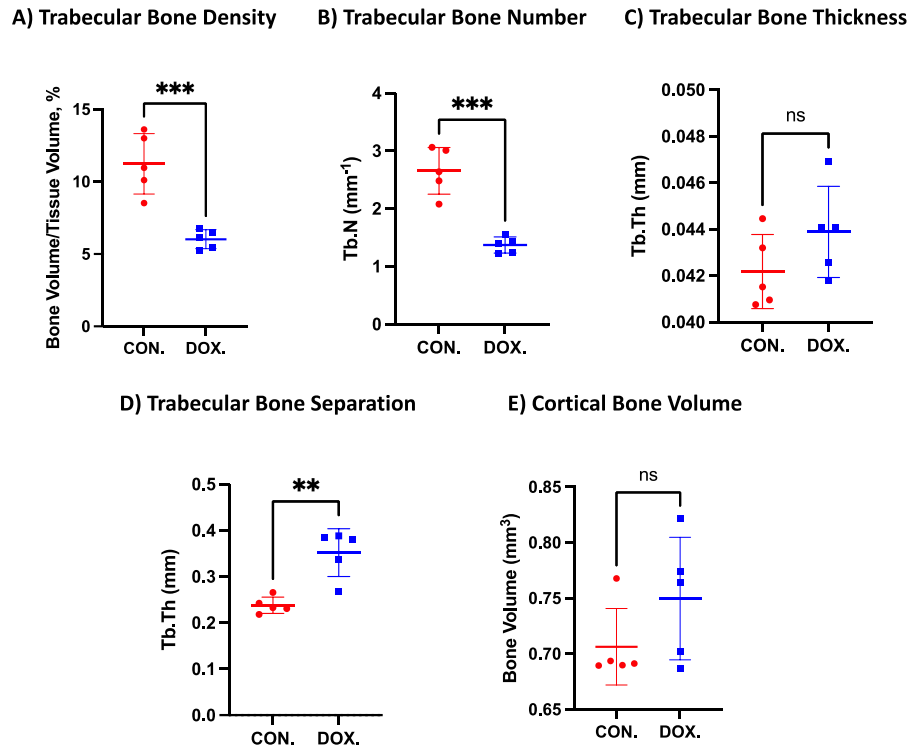

	Control	DOX	P
Trabecular Bone Density (BV/TV, %)	11.24±2.09	6.02±0.66	***:0.0007
Trabecular Number (Tb.N., mm)	2.65±0.4	1.37±0.14	***:0.0002
Trabecular Thickness (Tb.Th., mm)	0.04±0.002	0.04±0.002	ns:0.17
Trabecular Separation (Tb.Sp., mm)	0.24±0.018	0.35±0.05	**:0.0016
Cortical Bone Volume (BV, mm^3)	0.71±0.034	0.75±0.055	ns:0.17

Figure 4-26: 6 mg/kg DOX reduces trabecular bone number in immunocompromised mice.

*7-week-old female BALB/c Nude mice received a single dose of doxorubicin (DOX, 6 mg/kg, i.p.) or sterile PBS control once a week for four weeks. (A) Effects on trabecular bone density (%), (B) Trabecular Thickness (mm^{-1}), (C) Trabecular Bone Thickness (mm), (D)Trabecular Bone Separation (mm), (E) Cortical Bone Volume (mm^3), T-Test was used for statistical analysis, and ns is non-significant, ** is ≤0.01, *** is ≤0.001, **** is ≤0.0001 data show Mean±SD n=5 for CON. and DOX.*

Overall, administration of 6 mg/kg DOX (weekly for four weeks) to immunocompromised mice reduced the number of trabecular bones whilst not affecting cortical bone (Figure 4-26).

Bone Remodelling Cells

To determine the effects of 6 mg/kg DOX on osteoblasts and osteoclasts, bones from BALB/c Nude mice (n=4 for saline-treated, n=3 for DOX treated) were cut and stained for TRAP (a marker for osteoclastic activity) at the end of the experiment. Bone cells in the endocortical and trabecular bone regions were scored as previously described.

Endocortical Bone

Osteoblasts are found close to the endocortical bone surface, but this does not mean they are active. Therefore, active bone depositing osteoblasts (that are lined on the bone surface with a rectangular shape) and active bone-resorbing osteoclasts were quantified to determine whether their numbers were affected by DOX treatment.

From the data shown in Figure 4-27, osteoblast (CON: 16.47±3.96, DOX: 18.32±8.4, p: ns) (Figure 4-27A) and osteoclast numbers (CON: 0.13±0.15, DOX: 0.79±1.24, p: ns) (Figure 4-27B) were not significantly different between saline and DOX treated groups. Also, no significant difference was found in the average of osteoblast's bone depositing surface (CON: 4.61±0.5, DOX: 4.41±0.41, p: ns) (Figure 4-27C) and the average of osteoclast's bone resorbing surface (CON: 0.89±1.05, DOX: 2.11±2.02, p: ns) (Figure 4-27D) between saline control and DOX groups.

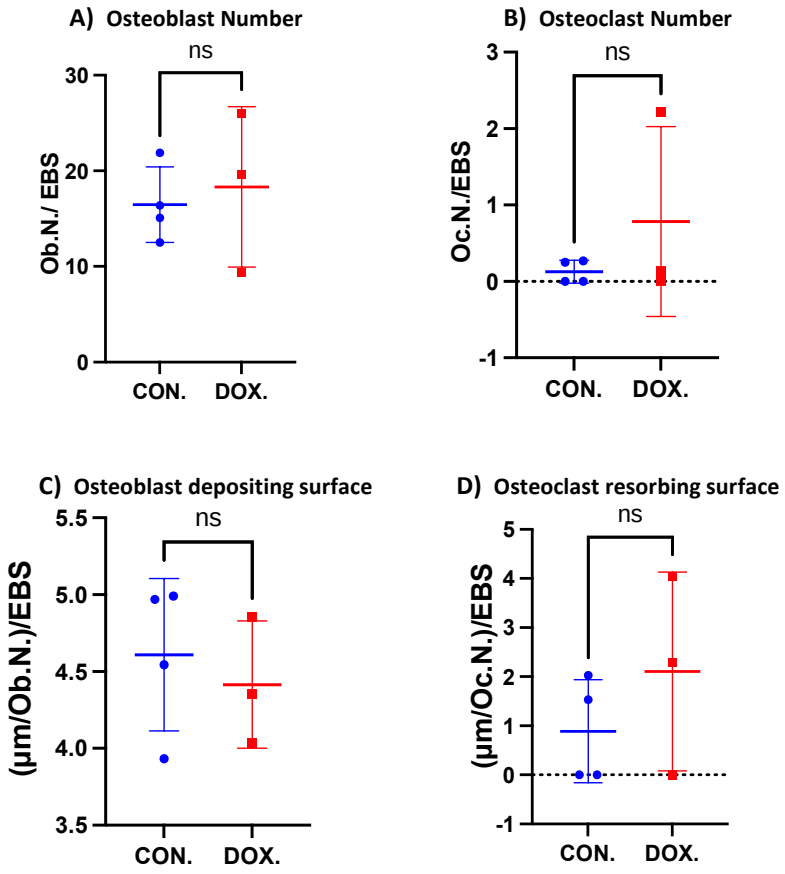

	Control	DOX	P
Osteoblast Number (Ob.N./mm EBS)	16.47±3.96	18.32±8.4	ns:0.7
Osteoclast Number (Oc.N./ mm EBS)	0.13±0.15	0.79±1.24	ns:0.33
Osteoblast depositing surface ((µm/Ob.N.)/ mm EBS)	4.61±0.5	4.41±0.41	ns:0.6
Osteoclast resorbing surface ((µm/Oc.N.)/ mm EBS)	0.89±1.05	2.11±2.02	ns:0.34

Figure 4-27: Effects of 6 mg/kg doxorubicin on endocortical bone remodelling cells of immunocompromised mice.

7-week-old female BALB/c mice received a single dose of doxorubicin (DOX, 6mg/kg, i.p.) or sterile PBS control once a week for four weeks. (A) Effects on osteoblast number (Ob.N.) per mm endocortical bone surface (EBS), (B) effects on osteoclast number (Oc.N.) per mm EBS, (C) overall of per osteoblast bone depositing surface per mm EBS, (D) overall of per osteoclast bone resorbing surface per mm EBS were compared between DOX and saline-treated groups, T-Test was used for statistical analysis, ns is non-significant, data show Mean±SD n=4 for CON. and n=3 for DOX.

Overall, no significant effect was found in immunocompromised mice's bone remodelling cells in endocortical bone after treatment with 6mg/kg DOX (Figure 4-27).

Trabecular Bone

As can be seen from Figure 4-27, no significant differences were found between control and DOX groups in their osteoblast (CON: 1.9±0.64, DOX: 5.23±3.27, p: ns)(Figure 4-28A) and osteoclast (CON: 4.39±2.22, DOX: 4.37±1.17, p: ns)(Figure 4-28B) numbers per mm trabecular bone. Student T-Test did not show any significant chance of osteoblast depositing surface (CON: 3.99±2.63, DOX:

10.01±5.43, p: ns)(Figure 4-28C) and osteoclast resorbing surface (CON: 11±4.12, DOX: 10.46±3.12, p: ns)(Figure 4-28D) per mm trabecular bone between control and DOX groups.

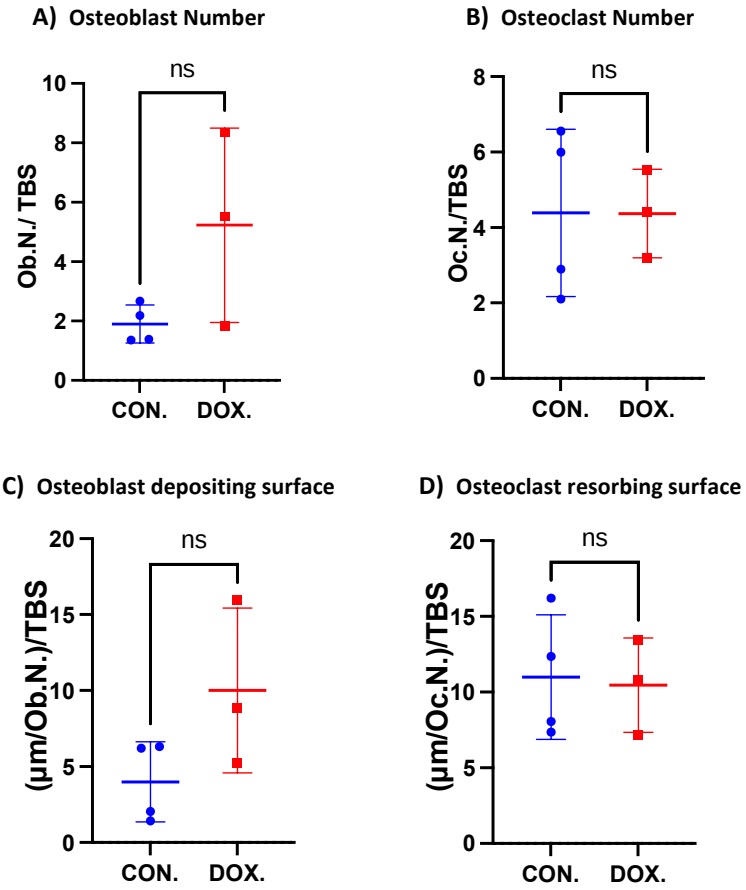

	Control	DOX	P
Osteoblast Number (Ob.N./mm TBS)	1.9±0.64	5.23±3.27	ns:0.1
Osteoclast Number (Oc.N./ mm TBS)	4.39±2.22	4.37±1.17	ns:0.99
Osteoblast depositing surface ((µm/Ob.N.)/ mm TBS)	3.99±2.63	10.01±5.43	ns:0.1
Osteoclast resorbing surface ((µm/Oc.N.)/ mm TBS)	11±4.12	10.46±3.12	ns:0.86

Figure 4-28: 6 mg/kg doxorubicin effect on bone remodelling cells in immunocompromised mouse trabecular bone.

7-week-old female BALB/c mice received a single dose of doxorubicin (DOX, 6mg/kg, i.p.) or sterile PBS control once a week for four weeks. (A) Effects on osteoblast number (Ob.N.) per mm trabecular bone surface (TBS), (B) effects on osteoclast number (Oc.N.) per mm TBS, (C) overall of per osteoblast bone depositing surface per mm TBS, (D) overall of per osteoclast bone resorbing surface per mm TBS were compared between DOX and saline-treated groups. T-test was used for statistical analysis, and ns is non-significant. Data show Mean±SD n=4 for CON. and n=3 for DOX.

To summarise, a weekly, single dose of 6 mg/kg DOX administration to immunocompromised mice had no significant effect on the bone remodelling cells in the trabecular bone region (Figure 4-28).

HSCs

I also determined the effects of DOX on LSK cells (Lineage(-), Sca-1(+), C-Kit(+)) (defined as HSCs and progenitors) and LK cells (Lineage(-), Sca-1(-), C-Kit(+)) (common myeloid populations, granulocyte-macrophage progenitors and megakaryocytes-erythrocyte progenitors) in the bone marrow by flow cytometry.

As shown in Figure 4-28, as a % of live cells, LSK cells were found to be significantly increased in the DOX treated group compared to saline control (CON: 0.19±0.05, DOX:0.34±0.09, p: ***,0.0009) (Figure 4-29A). Alongside LSK cells, LK cells were found to be significantly higher in the DOX-treated group compared to the control (CON: 1.86±0.35, DOX:2.27±0.35, p: *,0.0352) (Figure 4-29B).

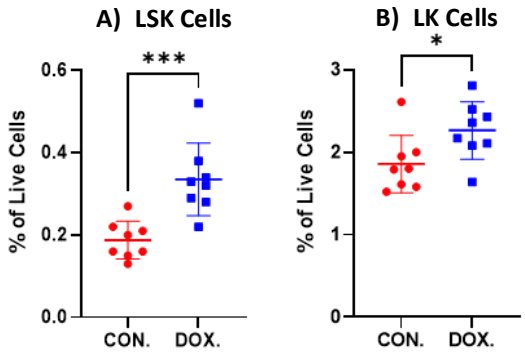

Figure 4-29: Effects of 6 mg/kg DOX on haematopoietic stem cells and progenitors in immunocompromised mice.

*Comparison of A) LSK Cells and B) LK Cells from BALB/c Nude strain's saline control and DOX treated groups as % of Live Cells from flow cytometry. T-Test was used for statistical analysis ns is non-significant, * is ≤0.05, *** is ≤0.001, data show Mean±SD n=8 for both CON. and DOX.*

Overall, HSCs, their progenitors and LK cell populations were increased in immunocompromised mice in response to weekly administration of 6 mg/kg DOX for four weeks (Figure 4-29).

Lymphocytes

As previously mentioned, the BALB/c Nude strain is immunodeficient, lacking mature T cells; however, they have mature B cells and NK cells. Therefore, flow cytometry was used to assess liquid bone marrow from both saline and DOX-treated mice to observe DOX's effects on immunodeficient mice lymphocytes.

Results showed that B cells were significantly lower in DOX treated group than in the saline control (CON: 17.42±6.58, DOX:5.86±3.98, p: ***,0.0008) (Figure 4-30A). However, there were **no significant change** in **CD8+ T Cells** (CON: 0.1±0.07, DOX:0.15±0.14, p:0.37)(Figure 4-30B), **CD4+ T Cells** (CON: 0.16±0.06, DOX:0.13±0.02, p:0.16)(Figure 4-30C) or **NK Cells** (CON: 0.33±0.34, DOX:0.65±0.3, p:0.065)(Figure 4-30D).

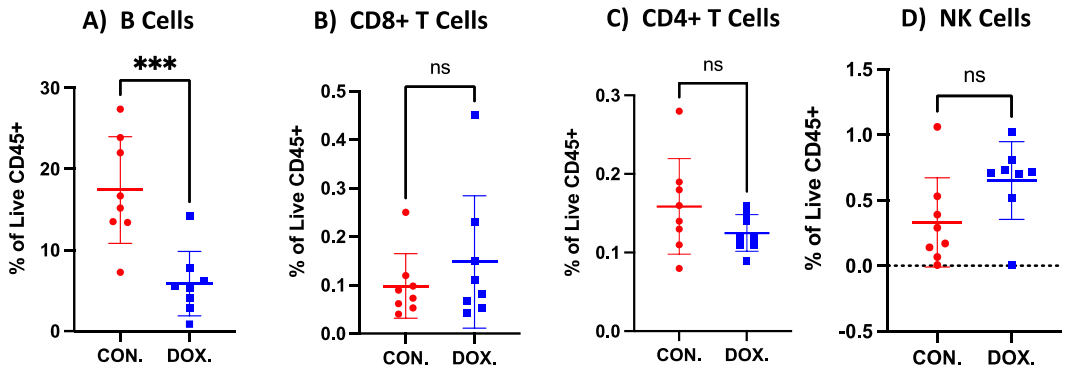

Figure 4-30: 6 mg/kg DOX effect on lymphocytes in immunocompromised strain.

*Comparison of A) B Cells, B) CD8+ T Cells, C) CD4+ T Cells and D) NK Cells of BALB/c Nude strain's both saline control and DOX treated groups as % of Live CD45 (+) Cells from flow cytometry. T-Test was used for statistical analysis ns is non-significant, *** is ≤0.001, data show Mean±SD n=8 for both CON. and DOX.*

In summary, only B cells were affected in immunocompromised mice, and their percentage decreased with DOX treatment (Figure 4-30).

Myeloid Cells

Despite lacking a functional thymus, mice of the BALB/c Nude strain have a myeloid cell population. Flow cytometry was used to analyse the liquid bone marrow isolated from both saline and DOX treated mice to determine the effects of DOX on myeloid cells in immunocompromised mice. As shown in Figure 4-31, there were no significant differences found in macrophages (CON: 1.66±1.7, DOX: 1±1.1, p: ns)(Figure 4-31A) and monocytes (CON: 0.01±0.02, DOX: 0.01±0.01, p: ns)(Figure 4-31B) between control and DOX treated groups. On the other hand, neutrophils (CON: 0.01±0.02, DOX: 0.01±0.01, p:**,0.0085)(Figure 4-31C), granulocytes (CON: 4.72±1.08, DOX: 6.58±1.82, p:*,0.014)(Figure 4-31D) and dendritic cells (CON: 0.55±0.21, DOX: 0.83±0.24, p:*,0.019)(Figure 4-31E) were all significantly increased with DOX treatment compared to saline control.

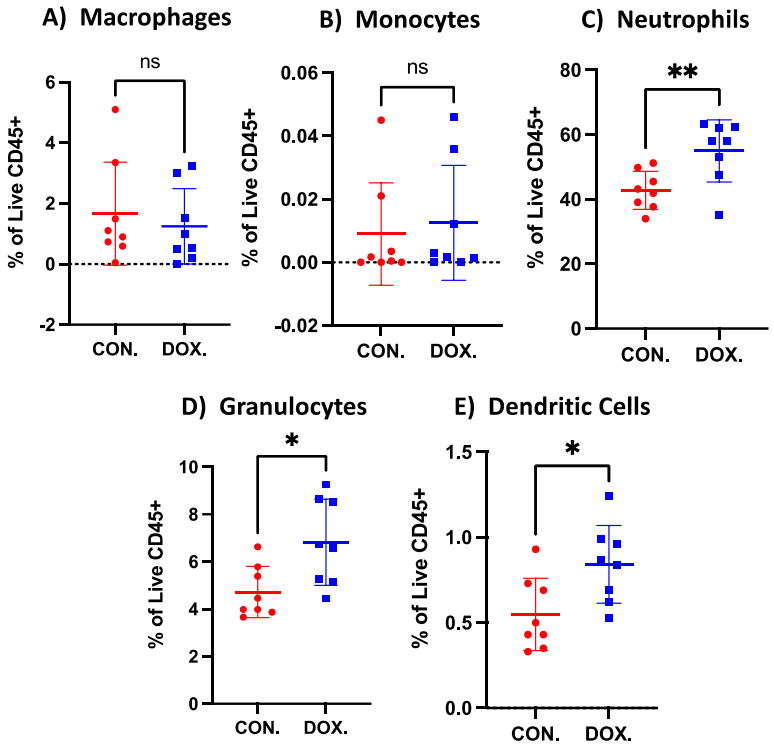

	Control	DOX	P
Macrophages (% of Live CD45+)	1.66±1.7	1.25±1.24	ns:0.58
Monocytes (% of Live CD45+)	0.01±0.02	0.01±0.02	ns:0.69
Neutrophils (% of Live CD45+)	42.8±5.92	54.98±9.58	**:0.0085
Granulocytes (% of Live CD45+)	4.72±1.08	6.83±1.82	*:0.014
Dendritic Cells (% of Live CD45+)	0.55±0.21	0.84±0.23	*:0.019

Figure 4-31: Effects of 6 mg/kg DOX on myeloid cells in immunocompromised mice.

*Comparison of A) Macrophages, B) Monocytes, C) Neutrophils, D) Granulocytes and E) Dendritic Cells of BALB/c Nude strain's both saline control and DOX treated groups as % of Live CD45 (+) Cells from flow cytometry. T-Test was used for statistical analysis; ns is non-significant, * is ≤0.05,** is ≤0.01, and data show Mean±SD n=8 for both CON. and DOX.*

Neutrophils are the predominant cells in the acute inflammatory responses to eliminate the foreign material, and then macrophages are recruited to the area to clean the residues (Medzhitov, 2008). My results support that DOX may have induced an inflammatory response in the bone marrow of the immunocompromised mice, associated with an increase in the neutrophil population (Figure 4-31).

Haematology Results

To determine whether there was a measurable effect of 6 mg/kg DOX treatment on hematopoietic cells in the circulation of immunocompromised mice, total blood count was analysed with Sci Vet ABC plus

As can be seen in

Figure 4-32, there were no significant differences between the control and the DOX treated group in any of the measured cell populations, except for increased granulocytes in the DOX treated group (CON: 0.81±0.2, DOX: 1.44±0.6, ps:*,0.015)(

Figure 4-32D).

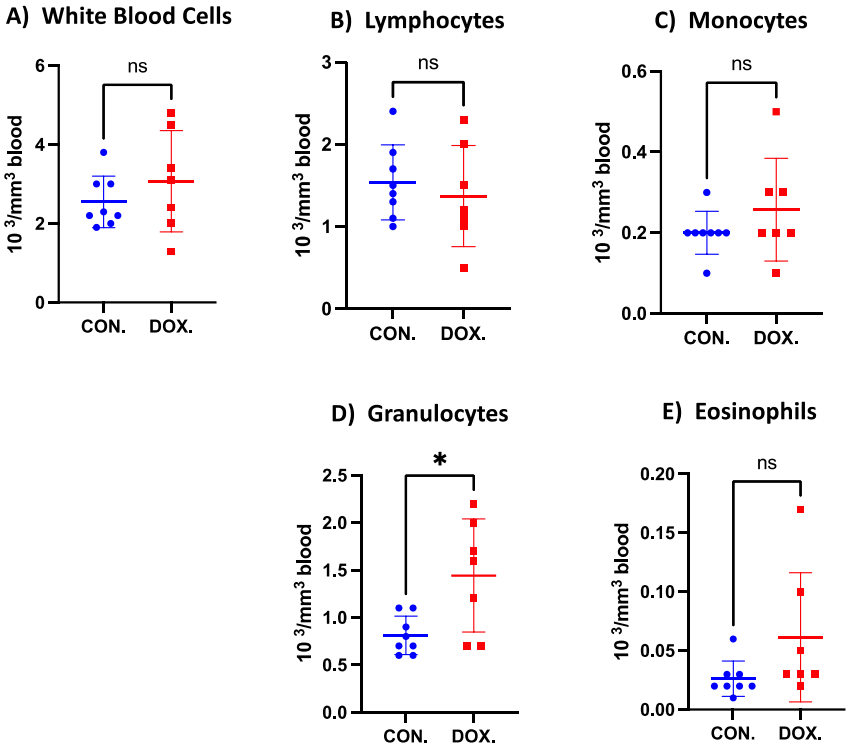

	Control	DOX	P
White Blood Cells (10^3/mm^3)	2.55±0.65	3.07±1.28	ns:0.33
Lymphocyte Cell Counts (10^3/mm^3)	1.54±0.46	1.37±0.62	ns:0.56
Monocyte Cell Counts (10^3/mm^3)	0.2±0.05	0.26±0.13	ns:0.27
Granulocyte Cell Counts (10^3/mm^3)	0.81±0.2	1.44±0.6	*:0.015
Eosinophil Cell counts (10^3/mm^3)	0.03±0.02	0.06±0.05	ns:0.1

Figure 4-32: Effects of 6 mg/kg DOX treatment on blood cell counts in immunocompromised mice

*Total White Blood Cell counts from peripheral blood of saline-treated control group, and DOX treated group from BALB/c Nude strain's peripheral blood. T-Test was used for statistical analysis; ns is non-significant, * is ≤0.05, and data show Mean±SD n=8 for CON. and n=7 for DOX.*

As shown in Table 4-2, the 4 mg dose of doxorubicin reduced trabecular bone numbers in the immunocompetent strain, which did not alter the bone structure in the immunocompromised strain, whereas the 6 mg dose reduced trabecular bones for both strains. Also, the only difference found in the bone remodelling cells in immunocompetent mice was an increase in osteoclast numbers of the im trabecular bone when treated with the 4 mg dose of doxorubicin. Lastly, all immune cell populations in the immunocompetent stain were affected by 6 mg DOX treatment; however, HSCs cells and progenitors (LSK Cells) were not affected. Interestingly, LSK Cells were affected by DOX in immunocompromised strain. Despite some similar trends observed in immunocompromised strain, the differences in myeloid cells were not as pronounced as in the immunocompetent strain.

Table 4-2: Summary of all results

Summary table of all data obtained from this chapter for both 4 mg and 6 mg dose of doxorubicin effect on both immunocompetent and immunocompromised strains.

	4 mg/kg DOXORUBICIN						6 mg/kg DOXORUBICIN					
	Immunocompetent			Immunocompromised			Immunocompetent			Immunocompromised		
	Control	DOX	P	Control	DOX	P	Control	DOX	P	Control	DOX	P
	Bone Structure and Integrity											
Trabecular Bone Density (BV/TV, %)	11.35±1.42	6.09±1.89	****≤0.0001	9±2	7.36±2.58	ns:0.18	11.37±1.51	4.39±0.48	****≤0.0001	11.24±2.09	6.02±0.66	***:0.0007
Trabecular Number (Tb.N., mm)	2.68±0.31	1.43±0.46	****≤0.0001	2.15±0.47	1.78±0.58	ns:0.19	2.54±0.24	0.99±0.16	****≤0.0001	2.65±0.4	1.37±0.14	***:0.0002
Trabecular Thickness (Tb.Th., mm)	0.04±0.002	0.04±0.002	ns:0.9	0.04±0.002	0.04±0.002	ns:0.46	0.04±0.002	0.04±0.003	ns:0.98	0.04±0.002	0.04±0.002	ns:0.17
Trabecular Separation (Tb.Sp., mm)	0.18±0.02	0.23±0.03	**:0.0048	0.26±0.03	0.28±0.04	ns:0.49	0.234±0.02	0.387±0.08	**≤0.0051	0.24±0.018	0.35±0.05	**:0.0016
Cortical Bone Volume (BV, mm^3)	0.83±0.07	0.83±0.05	ns:0.92	0.67±0.06	0.65±0.08	ns:0.6	0.8±0.025	0.79±0.046	ns:0.73	0.71±0.034	0.75±0.055	ns:0.17
	Bone Remodelling Cells											
Osteoblast Number (Ob.N./mm EBS)	9.04±5.02	8.32±4.21	ns:0.83	7.49±1.51	11.8±3.37	ns:0.07	9.45±3.82	11.46±3.98	ns:0.47	16.47±3.96	18.32±8.4	ns:0.7
Osteoclast Number (Oc.N./mm EBS)	0.84±1.02	0.12±0.15	ns:0.21	0.381±0.218	0.9±0.8	ns:0.25	0.17±0.19	0.07±0.14	ns:0.41	0.13±0.15	0.79±1.24	ns:0.33
Osteoblast depositing surface ((µm/Ob.N.)/ mm EBS)	2.17±0.24	2.47±0.45	ns:0.29	2.27±0.25	2.1±0.24	ns:0.25	4.77±0.84	5.13±1.55	ns:0.67	4.61±0.5	4.41±0.41	ns:0.6
Osteoclast resorbing surface ((µm/Oc.N.)/ mm EBS)	3.14±1.42	0.96±1.22	ns:0.06	2.45±2.02	2.28±1.98	ns:0.92	7.04±7.22	10.07±20.13	ns:0.76	0.89±1.05	2.11±2.02	ns:0.34
Osteoblast/Osteoclast Ratio (Ob.N./Oc.N.)	43.22±54.91	56.93±38.57	ns:0.68	24.63±11.62	9.71±0.86	ns:0.08	*No Data was obtained*					
Osteoblast Number (Ob.N./mm TBS)	4.57±0.92	6.66±3.54	ns:0.3	3.24±0.7	5.18±2.37	ns:0.17	1.73±1.35	0.84±1.69	ns:0.41	1.9±0.64	5.23±3.27	ns:0.1
Osteoclast Number (Oc.N./mm TBS)	4.09±0.71	6.49±1.08	**:0.0099	4.21±0.19	5.76±1.58	ns:0.1	5.44±1.6	3.4±4.68	ns:0.39	4.39±2.22	4.37±1.17	ns:0.99
Osteoblast depositing surface ((µm/Ob.N.)/ mm TBS)	3.08±1.64	5.86±2.07	ns:0.08	2.27±0.25	2.98±1.57	ns:0.76	2.17±1.40	5.16±10.33	ns:0.54	3.99±2.63	10.01±5.43	ns:0.1
Osteoclast resorbing surface ((µm/Oc.N.)/ mm TBS)	5.5±2.99	10.1±2.32	ns:0.051	6.83±2.95	5.8±2.44	ns:0.65	40.99±79.93	32.25±57.69	ns:0.86	11±4.12	10.46±3.12	ns:0.86
Osteoblast/Osteoclast Ratio (Ob.N./Oc.N.)	1.15±0.31	1.03±0.56	ns:0.71	0.77±0.19	0.91±0.41	ns:0.56	*No Data was obtained*					
	Bone Marrow Cell Populations											
LSK Cells (% of Live)	*No Flow Cytometry was done for this experiment*						0.54±0.13	0.54±0.09	ns:0.93	0.19±0.05	0.34±0.09	***:0.0009
LK Cells (% of Live)	*No Flow Cytometry was done for this experiment*						2.97±0.62	7.35±1.48	****≤0.0001	1.86±0.35	2.27±0.35	*:0.0352
B Lymphocytes (% of Live CD45+)	*No Flow Cytometry was done for this experiment*						40.99±7.16	12.36±3.51	****≤0.0001	17.42±6.58	5.86±3.98	***:0.0008
CD8+ Lymphocytes (% of Live CD45+)	*No Flow Cytometry was done for this experiment*						0.1±0.06	0.05±0.01	*:0.02	0.1±0.07	0.15±0.14	ns:0.37
CD4+ Lymphocytes (% of Live CD45+)	*No Flow Cytometry was done for this experiment*						0.13±0.07	0.2±0.04	*:0.01	0.16±0.06	0.13±0.02	ns:0.16
NK Cells (% of Live CD45+)	*No Flow Cytometry was done for this experiment*						*No Data was obtained*			0.33±0.34	0.65±0.3	ns:0.065
Macrophages (% of Live CD45+)	*No Flow Cytometry was done for this experiment*						1.45±0.14	2.53±0.41	****≤0.0001	1.66±1.7	1.25±1.24	ns:0.58
Monocytes (% of Live CD45+)	*No Flow Cytometry was done for this experiment*						0.91±0.18	7.15±0.98	****≤0.0001	0.01±0.02	0.01±0.02	ns:0.69
Neutrophils (% of Live CD45+)	*No Flow Cytometry was done for this experiment*						23.21±3.1	43.53±3.71	****≤0.0001	42.8±5.92	54.98±9.58	**:0.0085
Granulocytes (% of Live CD45+)	*No Flow Cytometry was done for this experiment*						12.51±2.64	27.39±4.15	****≤0.0001	4.72±1.08	6.83±1.82	*:0.014
Dendritic Cells (% of Live CD45+)	*No Flow Cytometry was done for this experiment*						*No Data was obtained*			0.55±0.21	0.84±0.23	*:0.019
	Haematology Analysis											
White Blood Cells ($10^3/mm^3$)	*No Haematology Analysis was done for this experiment*						2.34±0.88	2.97±0.9	ns:0.14	2.55±0.65	3.07±1.28	ns:0.33
Lymphocyte Cell Counts ($10^3/mm^3$)	*No Haematology Analysis was done for this experiment*						1.86±0.71	1.76±0.5	ns:0.86	1.54±0.46	1.37±0.62	ns:0.56
Monocyte Cell Counts ($10^3/mm^3$)	*No Haematology Analysis was done for this experiment*						0.07±0.08	0.19±0.07	**:0.006	0.2±0.05	0.26±0.13	ns:0.27
Granulocyte Cell Counts ($10^3/mm^3$)	*No Haematology Analysis was done for this experiment*						0.41±0.15	1.03±0.51	**:0.005	0.81±0.2	1.44±0.6	*:0.015
Eosinophil Cell counts ($10^3/mm^3$)	*No Haematology Analysis was done for this experiment*						0.06±0.05	0.04±0.02	ns:0.11	0.03±0.02	0.06±0.05	ns:0.1

4.6. Discussion

The experiments described in this chapter aimed to investigate how the administration of a clinically used chemotherapy agent (doxorubicin) affects vital components of the bone microenvironment *in vivo*. Bone and bone marrow are under constant regeneration, with bone remodelling cells continuously destroying and rebuilding new bone at different rates, depending on age. We know that in young mice, bone development continues, whereas, in mature mice (age 10 weeks +), bone remodelling is slower (Jilka, 2013), and this, in turn, modifies tumour growth in bone (Haley *et al*, 2018). Because of this, metastatic outgrow models are designed with young mice; since metastatic outgrowing is rare with adult mice, they are more suitable for dormancy models (Ottewell & Lawson, 2021). The impact of anti-cancer agents on the BME has not been extensively studied but may affect tumour development and progression. The bone marrow is the source of red blood and immune cells and is a highly proliferative environment. Since constant cell production and maintenance occurs, it is essential to understand the effects of chemotherapy, mainly targeting the fast-dividing cells.

In treating breast cancer, DOX is mainly used in the adjuvant setting, starting after surgical removal of the primary breast tumour (Ozer & Aydiner, 2019). At this point, there is no evidence of tumour spread to the bone; hence, the vast majority of cells exposed to adjuvant DOX will be normal healthy cells. It is known that a cumulative dose of DOX can cause cardiotoxicity, either by producing iron-related free radicals or by causing damage to the cell mitochondria (Thorn *et al*, 2011). Less is known about the potentially detrimental effects of DOX on bone; however, there are murine studies that report DOX-induced bone loss (Rana *et al*, 2013; Fan *et al*, 2017). This bone loss effect of DOX is an important factor, especially for osteolytic bone metastasis, where bone structure and integrity are also reduced by the tumour (Riffel *et al*, 2022).

Side effects of DOX like cardiotoxicity and bone marrow aplasia are common, and another side effect is myeloid suppression (Carvalho *et al*, 2009). Yang et al. studied the effects of doxorubicin on *ex vivo* rat bone marrow mesenchymal cells (MSCs) and determined that it induces cell apoptosis by detecting p38, JNK and p53 pathway apoptosis markers (Yang *et al*, 2013). Another study by Oliveira et al. showed the toxic effects of DOX using an *in vivo* rat model. In their study, 6-8 week old male rats were treated with weekly 5 mg DOX for four weeks. They showed that MSCs had reduced alkaline phosphate and *ex vivo* proliferation in response to DOX (Oliveira *et al*, 2014). Spallarossa et al. tested DOX toxicity *in vitro* on endothelial cell progenitors and similar to the report by Yang et al., found that p38 JNK and MAPK pathways were activated in the DOX treated group compared to control(Spallarossa *et al*, 2010). Fan et al. tested combination therapy of 4 cycles of 2 mg DOX/ 20 mg

cyclophosphamide in a female rat model and showed reduced trabecular bone volume and serum alkaline phosphates (Fan *et al*, 2017). Bone marrow cellularity was drastically reduced alongside increased bone marrow adiposity following DOX treatment and also found reduced trabecular bone volume. Also, the current study observed (by eye) an increased fat content in DOX-treated bone marrow in the immunocompetent strain, yet this must be confirmed with proper analyses with an increased sample size (Figure 4-33). Since Fan et al. found chemotherapy (cyclophosphamide, epirubicin and 5-fluorouracil) resulted in bone marrow adiposity in rats (Fan *et al*, 2016) a similar effect with DOX can be observed. All these studies are evidence that normal cells are affected by DOX treatment. In this chapter, I have used tumour-free mouse models to mimic the adjuvant use of DOX for four weeks.

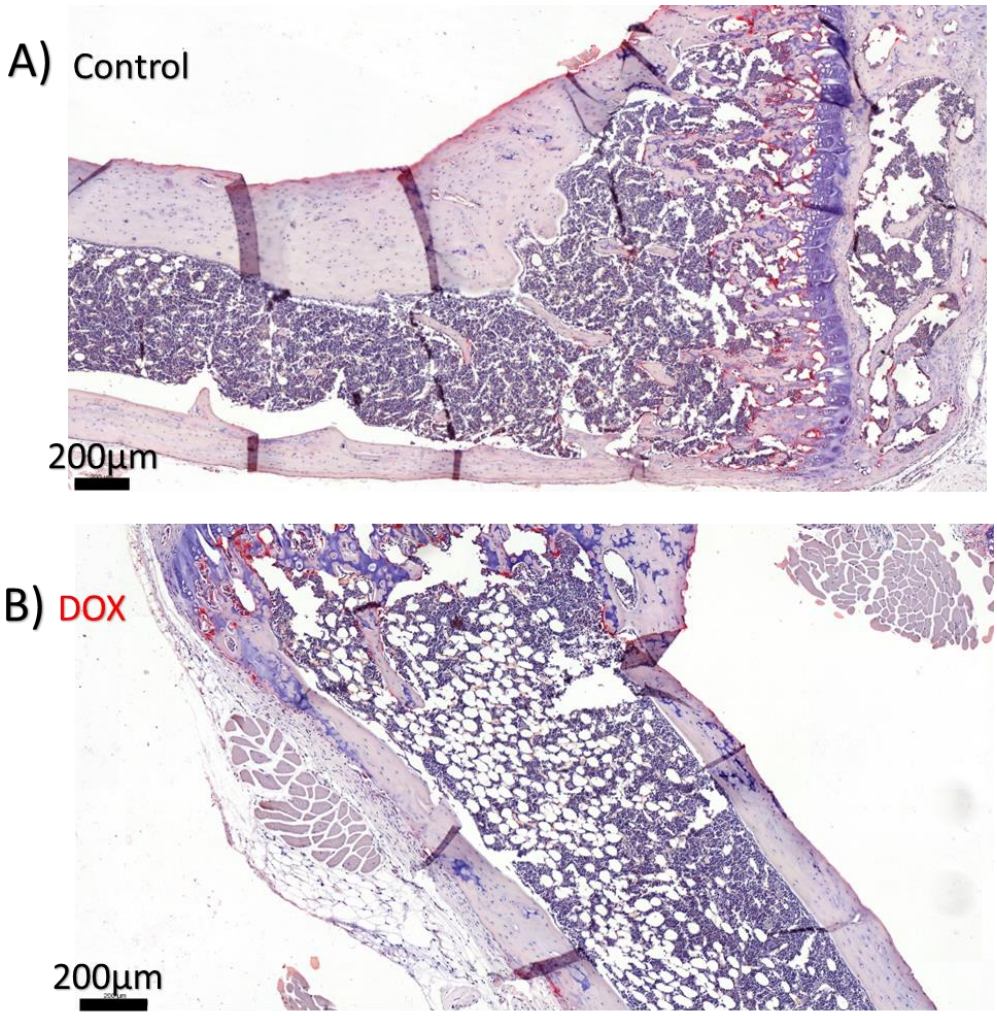

Figure 4-33: Increased fat adipocytes observed with the DOX treated samples' slides stained for TRAP.

Example images of slides stained for TRAP from A) control and B) DOX-treated groups. Space occurred in the control group caused by the fixation artefact, yet a spherical pattern was seen in DOX-treated samples.

The environment in which a tumour develops also influences the chemotherapy-mediated effects. Crenn et al. created multiple osteosarcoma models with different tumour sites and tested different chemotherapy agents, including the 4 mg DOX dose administered once when tumour size reached 100 mm^3. They showed that an intra-osseous tumour model had an increased tumour necrosis area than an intra-muscular tumour following 4 mg DOX treatment which shows the importance of the environment in the response to treatment (Crenn *et al*, 2017). This chapter presents the data from my experiments modifying the bone and bone marrow with different doses of DOX to establish any alterations in bone structure and integrity, bone remodelling cells and in the significant cell populations such as HSCs and immune cells in clinically relevant mouse models.

Inhibitory effect of DOX on triple-negative breast cancer cell line

One of the early studies to test the effects of DOX on bone was designed with rats, given a dose of DOX of 1 mg/kg for five days, which reduced the trabecular bone volume (Friedlaender *et al*, 1984). Ottewell et al. tested different doses of doxorubicin on subcutaneous triple-negative breast cancer tumours and found that both 4 and 8 mg /kg DOX doses weekly for six weeks effectively reduced the tumour size (Ottewell *et al*, 2008b). However, their study did not show effects on the bone with DOX. No toxicity was reported, showing that a dose 50% higher than the highest dose I used in my study can safely be used. A recent review summarises the general toxicity effects of DOX and shows how doses of DOX vary between animals and experiments (1-25 mg/kg, for a single dose) (Pugazhendhi *et al*, 2018). Therefore, I decided to start with the lowest effective dose (4 mg/kg DOX) from Ottewell's study (Ottewell *et al*, 2008b) and to ensure that the batch of DOX was working as expected by testing it on the MDA-MB-231 breast cancer cell line to generate an IC50. I found that a dose of 0.049 µM of DOX is required to inhibit growth of half of the cells *in vitro*. Published studies have reported different IC50 of DOX, with Lovitt et al. finding an *in vitro* IC50 dose of DOX with MDA-MB-231 of 0.087 µM (Lovitt *et al*, 2018), whereas Wen et al. reported a much higher DOX IC50 of 3.16 µM on MDA-MB-231 cells (Wen *et al*, 2018). One possible way to explain this difference in IC50 is seeding density. Sullivan and Graham investigated the effect of confluence-dependent resistance (Fang *et al*, 2007), which means that when cancer cells are grown in a dense monolayer, they develop more resistance to the anti-cancer agents, probably due to their lack of cycling or as suggested due to variation in HIF-1 activity (Fang *et al*, 2007). However, when we compare the studies described above, Wen et al. seeded 2,632 cells/cm^2 of a 12-well-plate and incubated for 16h, then treated with DOX for 48 hours, and Lovitt et al. seeded 10,714 cells/cm^2 of a 384-well CellCarrier microplate and incubated for 24 hours then applied DOX for six days. I used 10,000 cell/cm^2 per well in a 96-well-plate and seeded overnight. Cells were treated for 72 hours with different doses of DOX. Therefore, these protocols differ, and

initial seeding density and pre-incubation time might explain the difference between the IC50 values, or the MDA-MB-231 cell line may differ between laboratories. However, I could show that the batch of DOX I was going to use for my *in viv*o studies had anti-cancer activity *in vitro*, as expected. IC50 *in vitro* cytotoxicity test helps determine chemicals' relative toxicity in specific cases (toxicity on skin or specific tissue etc.). However, the LD50 (lethal dose that requires killing 50% of the animals tested) does not correlate with the IC50 due to drug pharmacokinetics and administration route, biodistribution etc (Garle *et al*, 1994).

DOX effect on bone structure and integrity

Doxorubicin is an anthracycline that targets DNA and interrupts cell division, causing cell death. As bone and bone marrow have cell populations that are constantly produced, it is possible DOX can cause harm to those cells. Since doxorubicin is used in both early and late-stage metastatic breast cancer treatment, it might add to the problem of osteolytic bone metastasis. A review describing children with leukaemia who had been treated with different doses and various lengths of time (accumulative dose of DOX between 45-550 mg/m^2) summarised the follow-up findings, showing that patients suffer from increased fracture risk and reduced height in adulthood despite the increased survival percentage after the treatment (Shusterman & Meadows, 2000). Another clinical study showed that pre-menopausal women with breast cancer (without metastatic or osteoporosis-related disease) treated with DOX/cyclophosphamide had lower bone mineral density and significant bone loss in their spine and hip compared to healthy controls (Hadji *et al*, 2009). In my studies, two different doses of DOX (4 and 6 mg/kg) were used; the 4 mg/kg DOX dose was the lowest effective dose shown to reduce tumour growth in a xenograft model (Ottewell *et al*, 2008b). . I found that the 4 mg/kg DOX dose reduced the number of trabecular bones and reduced bone density in immunocompetent mice; however, this was not seen in the immunocompromised mice. There are multiple potential reasons including differences in drug uptake, pharmacodynamics and kinetics between strains, differences in bone turnover, and no thymus in immunocompromised mice. If there is one, future studies must investigate the primary mechanism behind this difference.

The next step was to increase the dose in two strains to see if that would alter the bone structure. Again, there was a significant decrease in trabecular bone density and numbers in immunocompetent mice; however, 6 mg/kg DOX also reduced the trabecular bone density and number in the immunocompromised strain. These results support the previous evidence of DOX damaging bone marrow, but the exact molecular pathways involved must be investigated to reveal the mechanisms behind these observations. Rana et al. investigated DOX-mediated bone loss in mice

(weekly 5mg DOX for three weeks) and found that the circulation of TGFβ levels increased. They treated mice with anti-TGFβ (10 mg/kg 3 days per week) after DOX treatment and showed that the osteolytic lesions caused by DOX treatment could be reduced by using anti-TGFβ, and recommended clinical use of anti-TGFβ alongside DOX treatment (Rana *et al*, 2013). Another known effect of DOX is the production of reactive oxygen species, and it was suggested that ROS could cause bone damage and bone loss (Domazetovic *et al*, 2017). Although this mechanism might be involved, it does not explain why different effects were seen when 4mg/kg DOX was used in different mouse strains. A recent review by Zhang et al. summarises the interactions between T lymphocytes and bone remodelling. It discusses an interesting relationship between T cells and bone remodellings, such as Th17 cells supporting resorption and Treg cells suppressing the resorption, thus suggesting their potential target on bone diseases (Zhang *et al*, 2020). This might explain why I did not see any bone damage with the lower dose of DOX in immunocompromised mice and increasing the dose might increase the overall effects such as causing more cell damage, increasing ROS, and overall effects can cause reduction of bone. Beak et al. investigated the relationship between ROS and bone turnover markers in healthy postmenopausal woman (aged 60-78) and found a relationship between the levels of oxidative stress and bone turnover markers (Baek *et al*, 2010). They also observed increased TRAP activity following H_2O_2 treatment of human bone marrow cells *in vitro* (Baek *et al*, 2010). The link between ROS and bone remodelling has been reviewed in multiple papers. A straightforward explanation is that ROS causes a reduction in osteoblast activity, thus directly or indirectly resulting in RANKL production that induces HSCs to osteoclasts differentiation and osteoclastic activity (Wauquier *et al*, 2009; Domazetovic *et al*, 2017). A recent review of tumour treatment by ROS and its effect on bone marrow haematopoiesis summarises the possible mechanisms involved and points out how increased ROS levels can harm bone marrow cells by damaging the HSCs (Chen *et al*, 2020b). Reviews of chemotherapy-induced bone loss in breast cancer patients tend to focus on damage during treatment and long-term effects; with their focus on clinically relevant endocrine effects since the other cellular effects cannot be observed with human trials. However, they also underline the importance of understanding the non-endocrine effects, as some murine studies show that oestrogen is not the key factor for bone loss during the treatment and suggest a nonendocrine mechanism could be a better explanation for postmenopausal patients (Fan *et al*, 2016, 2017; Rayner-Myers *et al*, 2022).

DOX effect on the bone microenvironment

This chapter has shown that DOX caused damage to the bone structure and integrity, measured at the end of a 4-week treatment period. The effect of DOX on the significant cells in the bone microenvironment was investigated to determine whether there was a quantifiable difference

between control and DOX-treated animals of different strains. Since the initial focus was on the damage to the bone cells, osteoblasts and osteoclasts were compared in two different bone regions (endocortical and trabecular). A previous study on twelve week old female rats by Fan et al. showed bone damage with DOX and combination chemotherapy treatments (weekly 2 mg DOX and 20 mg cyclophosphamide for four weeks) but did not show any difference in osteoblast and osteoclast numbers (Fan *et al*, 2016, 2017). My findings agree with these studies, as the 4 and 6 mg DOX doses did not alter bone remodelling cells or their active surfaces. Bone cell numbers may be unaffected by DOX, whereas their activity (and therefore effect on bone volume) is changed. Cell activity is not captured by bone histomorphometry at the endpoint, so to measure bone turnover, serum bone turnover markers (like ALP and OPG) should be tracked over time (Shetty *et al*, 2016). Measurement of serum/urine bone turnover markers is commonly used in clinical studies; however, in murine studies, this process requires repeated bleeds which can cause stress-related problems in the mice. In this study, markers could have been detected at the end of the experiment, yet the results would have represented values at the endpoint of the study. Therefore, it might not truly represent DOX effects on bone remodelling over time.

Interestingly, *ex-vivo* experiments from Rana et al. indicate osteoblast-suppressing and osteoclast-inducing effects of DOX, where they observed increased osteoclasts from murine bone marrow and spleen mononuclear cells when treated with osteoclast differentiation media containing DOX compared to its control (Rana *et al*, 2013). However, these results do not correlate with *in vivo* cell numbers and result from other studies, with DOX treatment showing alterations in the bone turnover markers such as ALP (Fan *et al*, 2016, 2017). Therefore, there is an indication of a functional effect of DOX on bone remodelling cells; however, further analysis must be done to reveal the exact mechanisms.

Other important bone cell populations that may be affected by DOX are the HSCs; chapter 5 describes the importance of the HSC niche in tumour cell homing to the bone. Anthracyclines are reported to be toxic to the bone marrow; Sundman-Engberg et al. collected bone marrow from 36 different donors and treated them with different anthracycline agents (including DOX) for possible toxic doses for one hour, three hours or continuously for 10-12 days. Their colony-forming unit assay results showed that all of the anthracyclines have toxicity to the bone marrow at different doses (DOX's most significant toxicity effect was achieved after 3 hours of incubation with 0.2µM) (Sundman-Engberg *et al*, 1998). Aramvash et al. treated *ex-vivo* mouse bone marrow cells with different doses of daunomycin (similar to DOX) for four hours and showed the toxicity on HSCs even with lower doses (Aramvash *et al*, 2012). However, another study by Aramvash et al. investigated DOX's and

daunorubicin's effects on *ex vivo* mice HSCs from bone marrow. They observed the apoptosis effects of these anthracyclines by morphological changes, DNA fragmentation and PARP cleavage; thus, they showed that anthracyclines are toxic to HSCs by inducing apoptosis (Aramvash *et al*, 2017). Using the colony forming unit assay to determine the number of functional HSCs isolated from the bone marrow, I found that the 4 mg/kg dose of DOX did not alter functional HSCs in either strain.

Early research by Huybrechts et al. investigated the effects of a single dose of DOX and daunorubicin (another anthracycline) between 5-20 mg/kg for both drugs on pluripotent stem cells. 24h after the injection, mice were culled (10-14 weeks old female C57BL/6j), and bone marrow pooled for CFU assay. Their results suggested that at the earliest point (1-2 days after drug injection), damage to the bone marrow cells was observed (as reduced bone marrow cell counts); however, they suggested that bone marrow cells recovered after 4-5 days. The suggested day for the most significant damage by DOX on pluripotent stem cells was observed on day 2. In agreement with my studies, they did not see an effect of a 5 mg/kg dose, and only a 20mg/kg single dose of DOX induced the changes in the bone marrow cells (Huybrechts *et al*, 1979). In my studies using 6 mg/kg DOX, flow cytometry was used to separate the LSK and LK cell populations as this allowed sorting of the same number of cells from each population of animals in the different treatment groups to compare their ability to form colonies. In immunocompetent mice, LSK cells were unaffected, yet LK cells significantly increased with DOX treatment. In immunocompromised mice, both the LSK and LK cells were significantly increased by DOX. These surprising results suggest that DOX stimulates HSCs in the bone marrow, potentially as part of a mechanism to try and compensate for the cytotoxic effects; however, this would need further investigation. One study has found that DOX induces a DNA damage response in, *in vitro* human mesenchymal stem cells (Cruet-Hennequart *et al*, 2012). As mentioned in the review by Want et al., chemotherapy and radiotherapy leave long-term damage to bone marrow and HSCs were suggested to be another target (Wang *et al*, 2006). However, HSCs mostly stay quiescent in the bone marrow; therefore, drugs that target proliferation should not affect HSCs. A possible explanation for this can be the awakening of dormant HSCs as a response to the ROS produced by DOX, and when they have started to compensate for the damage, they might then become targets of DOX. Nevertheless, this and other explanations should be investigated since this might reveal potential pathways which could be protected to prevent long-term chemotherapy effects.

The immune cell composition is the main difference between the two strains used in the current study; thus, I wanted to elaborate the effects of DOX on different immune populations (mainly lymphocytes and myeloid cells) using flow cytometry. In immunocompetent mice, I observed a decrease in B Lymphocytes and CD8+ T Lymphocytes, while CD4+ T cells and all the myeloid cells were

increased. In immunocompromised mice, depletion of B cells was detected; however, there were no differences in the T Lymphocytes and NK cells. Despite macrophages, monocytes and the remaining myeloid cells being significantly increased by DOX treatment, the difference was not as marked as in immunocompetent mice. Also, total white blood cell counts from PB were similar between saline and treated groups for both strains. Only monocytes and granulocytes were increased following DOX treatment in the circulation of immunocompetent mice, and granulocytes were increased in immunocompromised mice. Overall, my data demonstrate that DOX treatment does affect the bone microenvironment, that this effect is dose-dependent and that there are differences in DOX response between immunocompetent and compromised mouse strains. Due to time constraints, I could not determine which of the changes I observed were most important for subsequent tumour progression in bone.

4.7. Summary

In summary, these data:

- Show that doxorubicin causes damage to the bone.
- Suggest that T Lymphocytes are a possible target to investigate bone damage induced by doxorubicin.

CHAPTER 5. EFFECTS OF HSC NICHE MODULATION ON TUMOUR DEVELOPMENT IN BONE.

5.1. Summary

Hematopoietic stem cells give rise to many different cell types in the bone marrow and are capable of self-renewal. Despite their rarity (around 0.01% of the bone marrow population), HSCs interact with numerous other bone and bone marrow cell types and may therefore be involved in processes like bone metastasis. HSCs mainly reside in a specialised supportive environment (the HSC niche), which includes elements of both the endosteal and perivascular niches. There are no distinct borders between these overlapping niches, so that HSCs can be found in all three areas. Studies using murine models have shown that when breast cancer cells are disseminated in the bone, they potentially reside in the HSC niche. Previous experiments carried out in our group showed that when HSCs were mobilised from bone niches with AMD3100 (a CXCR4 antagonist), increased numbers of disseminated cancer cells were found in the metastatic bone niche (Allocca *et al*, 2019). However, whether this results in increased tumour development in bone is still unknown.

The experiments in this chapter aimed to establish protocols to modify the HSC niche *in vivo*, assess differences between mouse strains in response to HSC mobilisation, and investigate the effects of HSC modification on tumour development. Effects of different drugs (AMD3100 and G-CSF) that mobilise HSCs in the bone marrow were compared in different mouse strains, allowing the comparison of immunocompetent and immunocompromised animals. After determination of the drug and strain match for efficient modification, breast cancer metastasis models were created, and effects on tumour development were monitored over subsequent weeks. Bones without tumours were used for µCT and stained for TRAP to compare the effects of HSC mobilising agents on bone structure, integrity, and remodelling cells, thereby indirectly affecting tumour cells through alterations of the metastatic bone niche.

AMD3100 and G-CSF caused a significant increase in HSC numbers in the circulation in BALB/c and C57BL/6j compared to the control. Treatment of BALB/c Nude mice with AMD3100 resulted in increased and earlier emergence of hind limb tumours with no detrimental effects on bone structure and/or remodelling cells. AMD3100 and G-CSF were tested in BALB/c and C57BL/6j strains to confirm efficient HSC mobilisation. G-CSF treatment caused a higher level of HSC mobilisation in C57BL/6j compared to BALB/c mice, whereas AMD3100 increased HSCs in the BALB/c strain compared to the

C57BL/6j strain. Modifying the HSC niche in BALB/c mice with G-CSF resulted in earlier tumour development in the hind limbs (at day 7, ~50% tumour positive animals in control vs ~90% in the G-CSF treated group). However, the tumour burden at the study endpoint was not increased by either agent compared to the control. My findings support the proposed role of the HSC niche in the early stages of tumour development in bone, with further studies required to establish the cellular and molecular mechanisms involved.

5.2. Introduction

The skeleton is the most common site for metastasis in advanced breast cancer, and primary cancer cells secretes factors that supports the pre-metastatic niche in the bone before dissemination(Mundy, 2002). Research using breast and prostate cancer models has shown that cancer cells reside in nutrient-rich areas where HSC and mesenchymal stem cells are commonly found. The precise location of this metastatic niche is still unclear, yet it is suggested that it covers the bone area where the HSC niche, endosteal niche and perivascular niche overlap (Haider *et al*, 2020; Méndez-Ferrer *et al*, 2020). Interactions between tumour cells and cells in the different niches play a crucial role in bone metastasis, and a common approach is to treat effects caused by disease, such as cancer-induced bone resorption, to improve patients' quality of life (Clézardin *et al*, 2000; Coleman *et al*, 2010; Coleman, 2016). To develop better treatment for patients with bone metastases, interactions between the tumour and the cells/molecules of the bone environment must be better understood, including the location and regulation of the cellular and molecular interactions in the metastatic bone niche. The lack of access to patient-derived material with tumour cells present in bone, limits our opportunity to investigate the human metastatic niche (Cawthorn *et al*, 2009); most of our understanding is from studies using murine models. *In vivo* model studies using prostate and breast cancer cells have shown that they locate within the HSC niche (Ren *et al*, 2015). Shiozawa *et al*. showed that removing the HSCs from bone marrow to the bloodstream with the mobilising agents AMD3100 and G-CSF resulted in increased prostate cancer cell seeding in the niche and Allocca *et al.* observed similar results with breast cancer cells following pretreatment of animals with AMD3100 (Shiozawa *et al*, 2011b; Allocca *et al*, 2019). However, whether this modification can alter subsequent tumour development or whether a similar mechanism would mobilise the disseminated cancer cells from the niche back into the circulation remains to be determined.

HSCs mobilisation agents such as granulocyte colony-stimulating factors (G-CSF, filgrastim) are commonly used to increase platelets and white blood cells to reduce the risk of infections in patients who receives high dose chemotherapy (Sheridan *et al*, 1992). Different agents are used to mobilise

HSCs, including AMD3100 (plerixafor) (Porfyriou *et al*, 2021). **Filgrastim** is one of the G-CSFs, which induces HSC mobilisation in multiple ways. It downregulates osteoblast production of CXCL12, induces immune cells to produce proteases to cleave adhesion molecules such as CXCR4, and induces HSCs proliferation and growth (Greenbaum & Link, 2011). **AMD3100 (plerixafor)** is a CXCR4 antagonist; it binds to CXCR4 on the HSCs blocking binding to CXCL12, thus mobilising HSCs (Rosenkilde *et al*, 2004). CXCR4/CXCL12 (aka SDF-1) binding is a known anchoring mechanism for HSCs; thus, one of the aims of mobilisation is to block this interaction. G-CSF and AM3100 reduce HSC counts in the bone marrow; thus, the primary purpose of clinical use of these drugs is to enhance HSCs in the peripheral blood (Suárez-Álvarez *et al*, 2012).

The CXCR4/CXCL12 axis is proposed to be one of the essential pathways for breast or prostate cancer cell homing to bone marrow (Müller *et al*, 2001; Taichman *et al*, 2002; Chinni *et al*, 2006). In addition, CXCL12 is a known element for HSCs to self-renewal alongside mobilisation homing, and thus it is involved in HSC maintenance and quiescence (Ara *et al*, 2003; Ceradini *et al*, 2004). These factors indicate a possible competition between HSCs and cancer cells for space in the niche; however, not all cancer cells express CXCR4; hence additional mechanisms for tumour cell homing to bone must exist. Many questions regarding this possibility remain to be answered: can you alter cancer cell seeding via the CXCR4/CXCL12 pathway? Would this modification affect dormant cancer cells? Would removing HSCs (or modification of the niche before seeding) alter tumour development? In this chapter, I have investigated how altering the HSC niche by mobilising HSCs into the circulation before cancer cell seeding affects the bone microenvironment and subsequent tumour development in bone.

5.3. Aims

The work presented in this chapter aims to understand the effects of HSC niche alteration on breast cancer bone metastasis. The main goals of the work are:

- To assess the effects of different HSC mobilising agents in immunocompromised and immunocompetent murine models
- To establish the effects of HSC mobilisation on the bone microenvironment in the different models
- To determine the effects of HSC modification on breast tumour development in bone in both immunocompromised and immunocompetent mice

5.4. Materials and Methods

Detailed information can be found in the main Material and Methods Chapter 2.

5.4.1. Breast Cancer Cell Lines

The triple negative human MDA-MB-231-IV PX462 cell line was cultured in RPMI 1640 with 10% FCS while murine 4T1 LUC BONE cells were cultured in DMEM -pyruvate medium with 10% FCS at 37°C 5%CO_2.

5.4.2. In vivo Studies

All *in vivo* studies were carried out according to local guidelines and with Home Office approval under project licence PPL 70/8964 held by Professor Nicola Brown or P99922A2E held by Dr Penelope D Ottewell, University of Sheffield, UK. Studies were carried out using female BALB/c and C57BL/6j (immunocompetent) and BALB/c Nude (immunocompromised) mice.

HSC mobilisation was achieved using AMD3100 (a CXCR4 Antagonist) (5 mg/ kg, i.p., daily for 5 days) and filgrastim (G-CSF) (123 µg/ kg, i.p., daily for 5 days).

5.4.2.1. Effect of haematopoietic stem cell mobilising agents in immunocompetent mouse strains

To compare the effects of different mobilising agents on HSCs, 8-10 weeks old female BALB/c and C57BL/6j were treated with either AMD3100 (5 mg/kg, i.p.) or Filgrastim (G-CSF; 123 µg/kg, i.p.) or saline for five days. Animals that received AMD3100 were culled 2 hours after the last injection. Saline control and G-CSF treated groups were culled 6 hours after the last injection, which is their efficient mobilisation time. Peripheral blood (PB) was collected with a cardiac puncture for colony formation assays and haematopoietic cell analyses. Bone marrow was collected for colony formation assays (Figure 5-1).

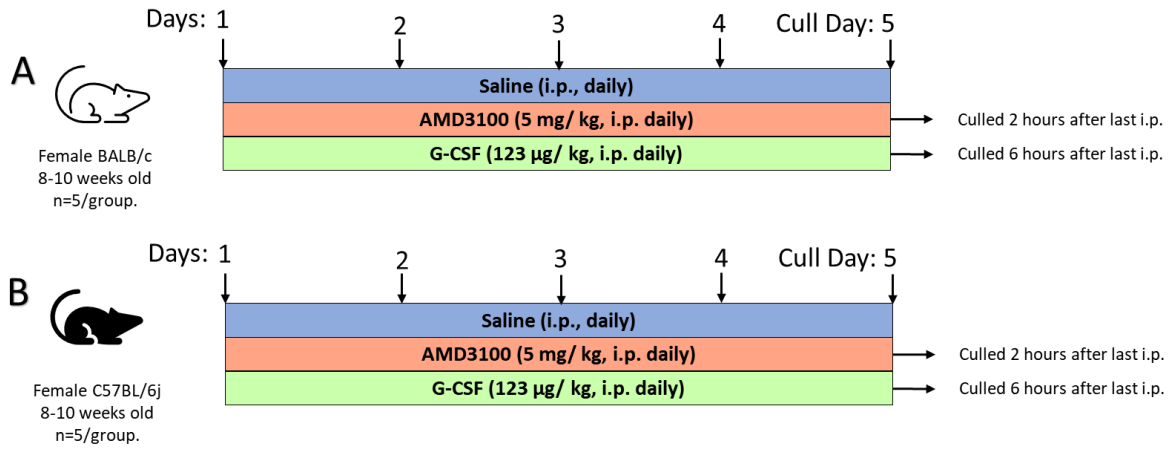

Figure 5-1: Outline of different mobilising agents using immunocompetent strains.

Experimental design A) 8-10 week old female BALB/c (n=5/per group) were injected either with saline control or 123 µg/kg G-CSF or 5 mg/kg AMD3100 for five days, i.p. 2 hours after the last AMD3100 and 6 hours after the last G-CSF injection, PB was collected with a cardiac puncture for colony formation assay and haematopoietic cell analyse. B) 8-10 week old female C57BL/6J (n=5/per group) were be injected either with saline control or 123 µg/kg G-CSF or 5 mg/kg AMD3100 for five days, i.p.

5.4.2.2. Effects of AMD3100 on tumour development in immunocompromised mice.

To determine changes in tumour growth by stimulation of HSC mobilisation with AMD3100, mature (10-week-old) female BALB/c Nude mice (n=8/group) were treated with either AMD3100 (5mg/kg, i.p.) or saline control daily for five days. 3-4 hours after the last drug injection, animals were injected with $1x10^5$ Luc2+ve MDA-MB-231 cell via intra-cardiac injection (in 100 µl saline). Tumour development was monitored 1-2 times/week by *in vivo* imaging. When 70% of the animals had detectable hind limb tumours (≈50 days), animals were culled, and hind limbs were collected for *ex vivo* analysis (Figure 5-2). The dose of AMD3100 (5mg/kg, daily for 5 days) was chosen to allow comparison to the studies published by Allocca *et al* and Shiozawa *et al* (Shiozawa *et al*, 2011a; Allocca *et al*, 2019). The Allocca study showed that this AMD3100 dosing schedule successfully mobilised HSCs into the circulation.

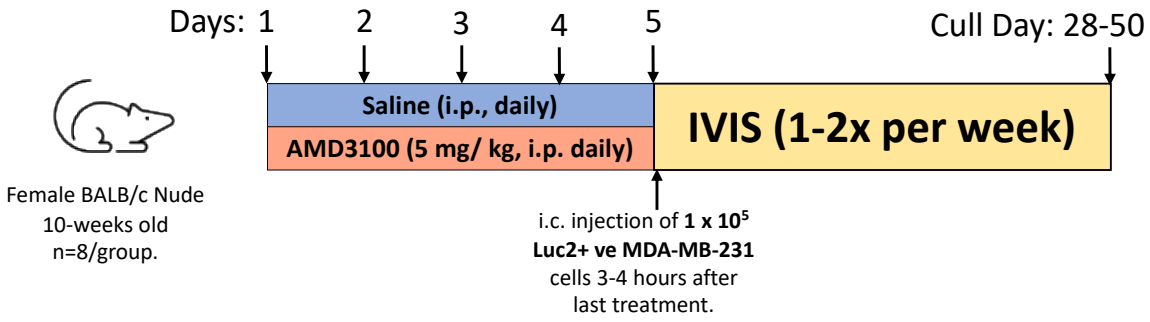

Figure 5-2: Experimental outline of AMD3100 effect on tumour development.

Experimental outline: 10-week-old female BALB/c Nude mice were injected with 5mg/Kg AMD3100 (i.p) for five days. 3-4 hours following the last AMD3100 injection, mice were injected with 1x105 Luc2+ve MDA-MB-231 cells. Tumour growth was observed once or twice a week with in vivo imaging, and the study terminated when 70% of animals had developed hind limb tumours.

5.4.2.3. Effects of G-CSF on tumour development in immunocompetent mice.

To determine changes in tumour growth by stimulation of HSC mobilisation with filgrastim (G-CSF), mature (8-week-old) female BALB/c mice (n=10/group) were treated with either filgrastim (G-CSF; 123 µg/kg, i.p.) or saline control daily for five days. 6 hours after the last drug treatment, animals were injected with $3x10^4$ 4T1 LUC BONE cell via the intra-cardiac route (in 100 µl saline). Tumour development was monitored by *in vivo* imaging under isoflurane anaesthesia (1-2x/week). Animals were culled one week after confirmed hind limb tumour development (≈30 days) or when tumour sizes would cause distress, and hind limbs were collected for *ex vivo* analysis (Figure 5-3). In the literature, there is no given dose for G-CSF that mobilises HSCs in mice; however, patients undergoing autologous peripheral blood progenitor cell collection and therapy receive 10 µg/kg/day G-CSF. It is recommended to use it four days before leukapheresis (collection of white blood cells) and continues until the last leukapheresis (Hopman & DiPersio, 2014). To achieve mobilisation in mice, the 10 µg/kg/day human dose was converted to the equivalent mouse dose which was given daily for five days. The following equation was used to calculate the mouse dose, based on body surface area (Nair & Jacob, 2016).

$$Animal\ Equivalent\ Dose\ (AED)\left(\frac{mg}{kg}\right) = \ Human\ dose\ \left(\frac{mg}{kg}\right) x K_m\ ratio$$

The reference Km ratio for humans (60 kg) is 37, and for mice (0.02 kg) is 3, which means that to calculate AED, the human dose should be multiplied by 12.3 or divided by 0.081. According to this calculation, 123 µg/kg filgrastim (G-CSF) mouse/day used.

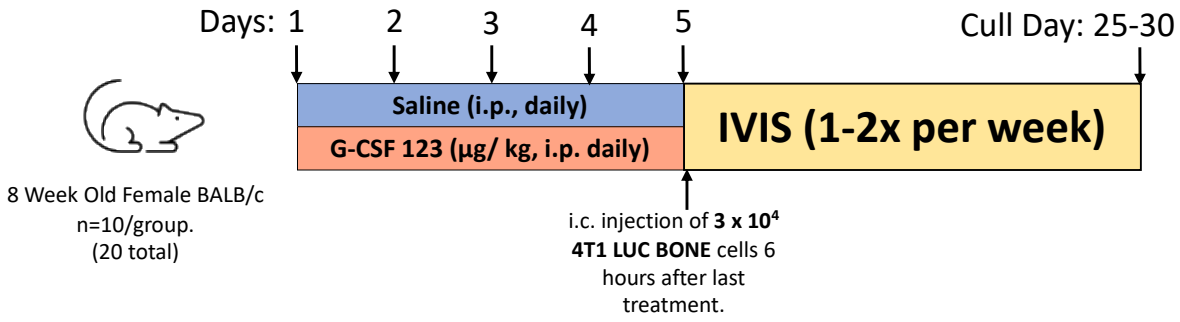

Figure 5-3: Outline of filgrastim treatment effect on tumour development.

Experimental outline: 8-Week-Old female BALB/c mice were treated with either G-CSF or saline control daily for five days (i.p.). A syngeneic model was created 6 hours after the last drug injections with 3x10^4 4T1 LUC BONE cells administered via i.c. route. Tumour growth was monitored by in vivo imaging, and animals culled one week after hind limb tumour development or had tumour size that would cause distress. Hind limb bones were collected for ex vivo analysis.

5.4.3. *In Vivo* imaging of tumour development

Mice were put under anaesthesia with 2.5% isoflurane, then injected with 100 µl 30 mg/mm Luciferin subcutaneously. After 5 minutes, animals were placed in the imaging chamber, and non-invasive *in-vivo* imaging was performed. The bioluminescent signal was visualised in animals at different time intervals to compare tumour development. First, images were normalised by setting thresholds that depend on the image that has the lowest detectable tumour (Figure 5-4,i), each circled area was counted as a separate tumour, and images in Figure 5-4,ii represent different signals from tumours in the skull (A), spine (B), hind limbs (C) and jaw (D). Depending on the model, some animals had chest signals caused by tumour cells in the sternum or the lungs. After the collection of hind limb bones, *ex vivo* images were captured to detect the numbers/location of tumours inside the bones (Figure 5-4, iii); the total count of the signal was divided by 4 to calculate the overall tumour number/per mouse hind limb bone (example calculation for the image in Figure 5-4,ii: 4 bones had signals which are 4 / 4 = 1 tumour per bone).

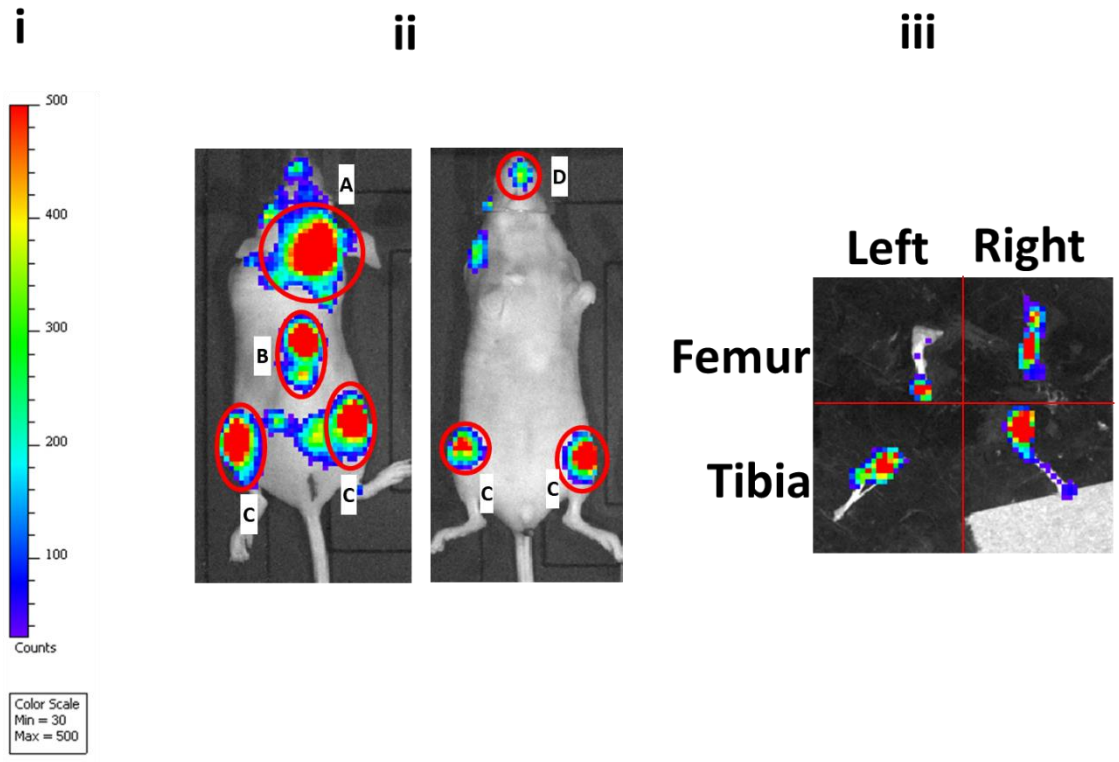

Figure 5-4: Calculating *in vivo* and *ex vivo* bone tumour numbers.

Example images to illustrate tumour number calculations. i) Example threshold to normalise the tumour signals for that specific experiment, given threshold was used in these example images. ii) In Vivo imaging of a mouse that has a signal in the skull (A), spine (B), hind limbs (C) and jaw (D), each spherical signal counts as one tumour. iii) Ex Vivo image of hind limb bones, where each signal count as a different tumour.

5.4.4. *Ex Vivo* analyses of tumour growth in bone

5.4.3.1. Collection and preparation of the bones for microcomputed tomography (µCT) and histology.

Hind limbs were removed from the carcass, all soft tissue removed, and tibias separated from the femurs. Bones were placed in 4% PFA overnight and then washed and stored in PBS at 4°C. Random tumour-free tibias (n=3-4) were selected for µCT and then decalcified, processed, embedded in wax and sectioned to 3 µm slides. Slides were either stained with TRAP or H&E for bone remodelling cell analyses.

5.4.3.2. Collection of bone marrow.

After separation of the femurs from the carcass, they were dipped in 100% EtOH for surface disinfection. Under the sterile hood, the femoral head was removed, and the bone was placed into 0.2 ml PCR tubes with a hole pierced in the bottom. Tubes were placed into 1.5 ml Eppendorf containing 200 ml PBS and bone marrow spun out with 3000 g for 5 min. After collection of bone marrow, it was washed with PBS containing 10% FCS and processed with colony formation assays or stained for flow cytometry.

5.4.3.3. Collection and preparation of peripheral blood of colony forming unit and blood count.

Peripheral blood (PB) was collected via terminal cardiac puncture. 0.5-1 ml PB was taken from each animal to the syringe, and 100 µl of PB was transferred into 1.5 ml Eppendorf containing 50 µl EDTA (anticoagulant) for blood analyses and 0.5 ml for colony-forming assays.

5.4.3.5. Colony Forming Unit analyses.

As described in detail in section 2.2.3.9, $1x10^4$ cells/well from both PB (after red blood cells were lysed) and BM were seeded at a 6-well plate with 1.1 ml MethoCult GFM3434 (StemCell Technologies, UK) + 10% IMDM (2% FCS+%1 P/S/A), samples were seeded in triplicate. Samples were checked once every two days to detect colony formation for 14 days.

5.5. Results

Homing to bone is necessary, yet it is not sufficient to develop overt breast cancer metastasis in the bone. BC cells require a fertile environment to support their growth, and many disseminated tumour cells remain dormant under the control of the surrounding microenvironment (Croucher *et al*, 2016). A previous study carried out by our group showed that BC locates in the HSC niche in an immunocompromised murine model. After mobilisation of HSCs, increased numbers of disseminated BC cells were found in the niche. (Allocca *et al*, 2019). However, whether this modification influences tumour development and modification of niche with multiple agents in multiple strains were not determined. I, therefore, investigated the impact of HSC mobilisation on tumour outgrowth and development in different murine models using two agents with different mechanisms of action.

5.5.1. Modification of HSC niche in immunocompetent mice.

I first carried out an experiment to determine the effects of HSC mobilisation agents (AMD3100 and G-CSF) in 2 different immunocompetent mouse strains, BALB/c and C57BL/6j (see the outline in Figure 5-1). PB and BM were collected, and the number of mature HSCs and their progenitors were compared between G-CSF and saline control to determine the effects of the agents. The tibias of the mice were analysed by µCT and stained with H&E and TRAP to determine the effects of agents on bone integrity and bone remodelling cells.

Both mobilising agents increased HSC counts in PB in both mouse strains.

As described in detail in the introduction section, both agents' mechanism of action results in an increased number of HSCs in PB. Therefore, PB was collected after mice were treated with mobilising agents to determine whether this effect varied between different mouse strains, similarly to the clinical applications. The recommended dosage in patients with cancer receiving myelosuppressive chemotherapy or induction and/or consolidation chemotherapy for acute myeloid leukaemia is five µg filgrastim/kg/day (FDA, 2015). The dose used in patients undergoing autologous peripheral blood progenitor cell collection and therapy is ten µg/kg/day. It is recommended to use it four days before leukapheresis (collection of white blood cells) and continues until the last leukapheresis (Hopman & DiPersio, 2014).

In order to achieve mobilisation, a 10 µg/kg/day dose will be used for five days. To calculate the animal dose, simple animal dose conversion based on body surface area is used (Nair & Jacob, 2016).

$$Animal\ Equivalent\ Dose\ (AED)\left(\frac{mg}{kg}\right) = \ Human\ dose\ \left(\frac{mg}{kg}\right) x K_m\ ratio$$

The reference K_m ratio for humans (60 kg) is 37, and for mice (0.02 kg) is 3, which means that to calculate AED, the human dose should be multiplied by 12.3 or divided by 0.081. According to this calculation, 123 µg/kg filgrastim (G-CSF) mouse/day should be used.

As used in the study by Allocca et al., a 5mg/kg dose of AMD3100 was used to treat both BALB/c and C57BL/6j mice (Allocca *et al*, 2019).

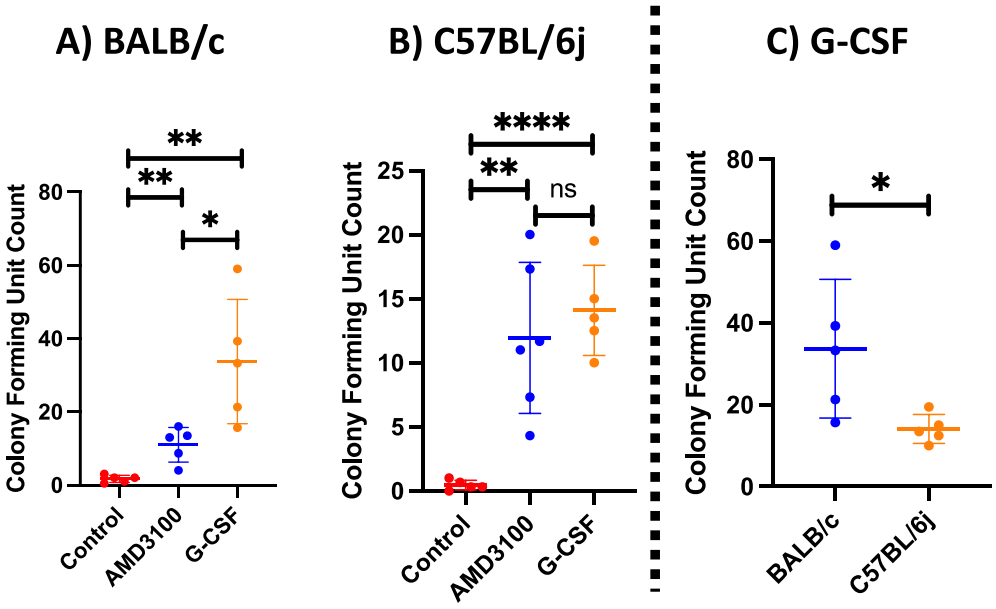

Figure 5-5: Colony forming unit counts of haematopoietic stem cells from peripheral blood in BALB/c and C57BL/6j mice

*Colony Forming Unit (CFU) counts for HSCs and their progenitors from A) BALB/c and B) C57BL/6j strains and comparison of C) G-CSF agent effects on CFU counts between BALB/c and G-CSF. Data are shown as Mean+SD; T-Test was used for statistical analysis, n = 5/group for all except n= 6 for AMD3100 group in C57BL/6j strain, ns: non-significant and * is P<0.05.*

To assess the mobilisation effect of both agents, HSC and progenitor colony forming unit (CFU) counts from PB were compared following 11 days of cultivation in semi-solid media (Methocult GF M3434) (Figure 5-5). As explained, only functional HSCs will produce countable colonies with this analysis. Both AMD3100 (11.03±4.74, $p_{amd/con}$=0.0026) and G-CSF (33.73±16.96, $p_{g\text{-}csf/con}$=0.0029) significantly increased HSCs CFU counts in samples from BALB/c mice, compared to control (1.7±0.97). Despite some variability, G-CSF caused a greater increase in HSC counts compared to AMD3100 in the BALB/c strain (AMD3100: 11.03±4.74, G-CSF: 33.73±16.96, p:0.02) (Figure 5-5, A). If we now turn to effects on C57BL/6j, again both drugs (AMD3100:11.94±5.9, $p_{amd/con}$=0.002)(G-CSF:14.1±3.52, $p_{g\text{-}csf/con}$=<0.0001) increased the CFU counts compared to control (0.47±0.38), however there was no

difference in counts in between AMD3100 and G-CSF treated animals (AMD3100: 11.94±5.9, G-CSF: 14.1±3.52, p:0.49)(Figure 5-5,B). Comparing the results, it can be seen that G-CSF mobilised more HSCs to the PB in the BALB/c strain when compared to C57BL/6j strain (p:0.035) (Figure 5-5, C).

HSC counts from bone marrow in BALB/c and C57BL/6j mice.

Next, I asked whether a mobilisation effect could be observed in the bone marrow by comparing CFU counts following five days of AMD3100 or G-CSF treatment. Like HSC CFU counts from PB, the semi-solid medium was used to culture HSCs from the liquid bone marrow. Mobilising the HSCs to PB might reduce the CFU counts from BM; however, spinning out of the bone marrow may not capture all of the HSCs, especially those closer to the growth plate or firmly embedded in their niches.

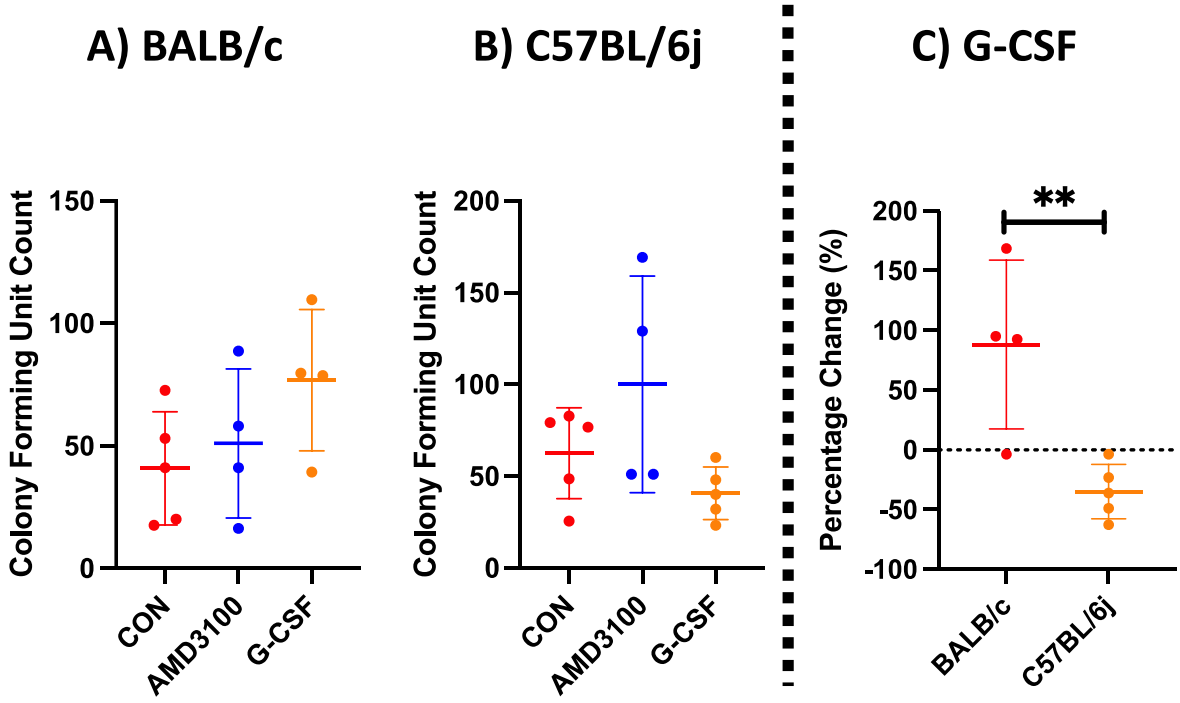

Figure 5-6: Colony forming unit counts of haematopoietic stem cells in bone marrow from BALB/c and C57BL/6j mice.

*Colony Forming Unit (CFU) counts for HSCs and their progenitors from A) BALB/c and B) C57BL/6j strains' BM C) G-CSF agent effect on CFU counts' percentage change in BALB/c and C57BL/6j. Data show Mean+SD, and T-Test was used for statistical analysis, n = 4/group for AMD3100 treatment and G-CSF on BALB/c, n= 5 for the rest, ns: non-significant and ** is P<0.01.*

As shown in Figure 5-6, neither mobilisation agent significantly altered the numbers of colonies generated from HSCs in the liquid bone marrow. Since the initial HSC counts in liquid BM were different in each strain, the percentage change was used to compare to monitor any difference between strains. As shown in Figure 5-6, C, G-CSF increased overall HSCs counts in BALB/c by 88.17±70 %, reducing overall HSCs counts in C57BL/6j by 34.85±22.84 % (p:0.0075).

Haematology analysis

A complete blood count is a commonly used clinical assay providing information about different disorders such as anaemia, infection and leukaemia. I wanted to establish whether HSC mobilising agents affected white blood cell counts since this is the effect of G-CSF in clinical use and would also be expected to alter the blood cell populations in mice. To determine whether there is a measurable effect of both mobilising agents on both strains, total blood count was analysed with Sci Vet ABC plus (Table 5-1 and Figure 5-7).

Table 5-1: Haematology data from AMD3100 and G-CSF treated BALB/c and C57BL/6j mice.

White Blood Cell Counts ($10^3/mm^3$)					
BALB/c			**C57BL/6j**		
CONTROL	**AMD3100**	**G-CSF**	**CONTROL**	**AMD3100**	**G-CSF**
2.32±1.31	4.16±1.49	5.8±4.2	0.8±0.36	9.73±4.15	4.67±1.42
p(CON/AMD)	**p(CON/GCSF)**	**p(AMD/GCSF)**	**p(CON/AMD)**	**p(CON/GCSF)**	**p(AMD/GCSF)**
0.07:ns	0.115:ns	0.43:ns	0.02:*	0.01:*	0.11:ns
Lymphocyte Cell Counts ($10^3/mm^3$)					
BALB/c			**C57BL/6j**		
CONTROL	**AMD3100**	**G-CSF**	**CONTROL**	**AMD3100**	**G-CSF**
1.98±1.05	3.3±1.04	2.76±1	0.67±0.31	5.83±1.94	2.6±0.69
p(CON/AMD)	**p(CON/GCSF)**	**p(AMD/GCSF)**	**p(CON/AMD)**	**p(CON/GCSF)**	**p(AMD/GCSF)**
0.08:ns	0.26:ns	0.42:ns	0.01:*	0.01:*	0.05:ns
Monocyte Cell Counts ($10^3/mm^3$)					
BALB/c			**C57BL/6j**		
CONTROL	**AMD3100**	**G-CSF**	**CONTROL**	**AMD3100**	**G-CSF**
0.04±0.09	0.2±0.1	0.34±0.21	0±0	0.6±0.26	0.2±0.1
p(CON/AMD)	**p(CON/GCSF)**	**p(AMD/GCSF)**	**p(CON/AMD)**	**p(CON/GCSF)**	**p(AMD/GCSF)**
0.029:*	0.018:*	0.21:ns	0.017:*	0.026:*	0.07:ns
Granulocyte Cell Counts ($10^3/mm^3$)					
BALB/c			**C57BL/6j**		
CONTROL	**AMD3100**	**G-CSF**	**CONTROL**	**AMD3100**	**G-CSF**
0.3±0.19	0.66±0.36	2.7±3.23	0.13±0.06	3.3±2.12	1.87±0.75
p(CON/AMD)	**p(CON/GCSF)**	**p(AMD/GCSF)**	**p(CON/AMD)**	**p(CON/GCSF)**	**p(AMD/GCSF)**
0.08:ns	0.13:ns	0.2:ns	0.06:ns	0.016:*	0.33:ns
Eosinophil Cell Counts ($10^3/mm^3$)					
BALB/c			**C57BL/6j**		
CONTROL	**AMD3100**	**G-CSF**	**CONTROL**	**AMD3100**	**G-CSF**
0.05±0.03	0.12±0.08	0.11±0.07	0.05±0.04	0.15±0.02	0.08±0.01
p(CON/AMD)	**p(CON/GCSF)**	**p(AMD/GCSF)**	**p(CON/AMD)**	**p(CON/GCSF)**	**p(AMD/GCSF)**
0.09:ns	0.13:ns	0.7:ns	0.02:*	0.39:ns	0.0018:**
Platelet to Lymphocyte Ratio					
BALB/c			**C57BL/6j**		
CONTROL	**AMD3100**	**G-CSF**	**CONTROL**	**AMD3100**	**G-CSF**
414.93±117.98	150.94±31.04	119.96±41.36	460.81±247.5	109.01±65.67	143.91±88.15
p(CON/AMD)	**p(CON/GCSF)**	**p(AMD/GCSF)**	**p(CON/AMD)**	**p(CON/GCSF)**	**p(AMD/GCSF)**
0.0018:**	0.0097:**	0.27:ns	0.015:*	0.046:*	0.51:ns

*Blood cell counts from Sci Vet ABC+ were 10^3 cells per mm^3 peripheral blood. Data are shown as mean±STD, n=3 for C57BL/6j and n=5 for BALB/c, T-Test was used for statistical analysis, AMD3100 and G-CSF treated groups compared to each other and to saline control, *= <0.05, **= <0.01.*

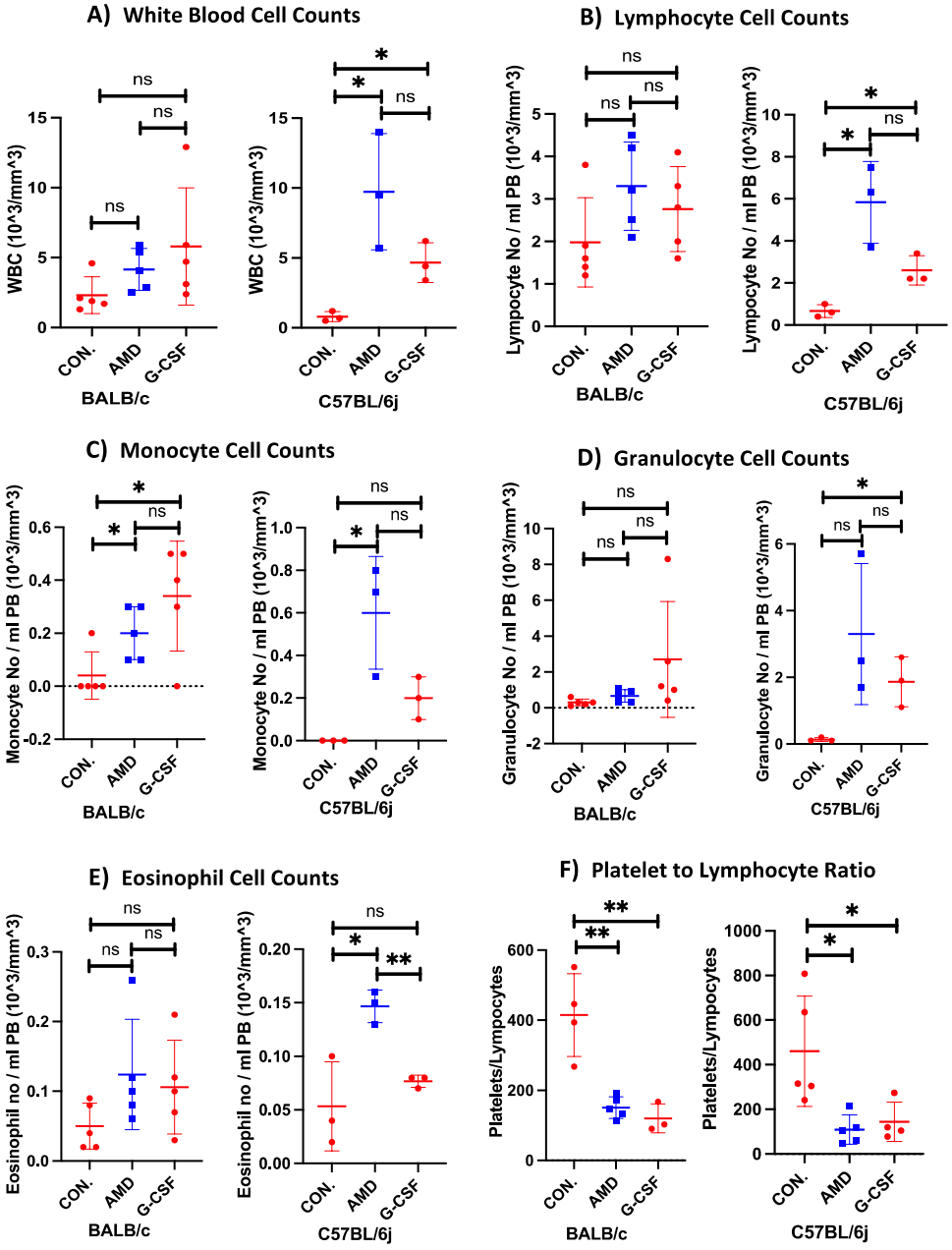

Figure 5-7: Haematology results from AMD3100 and G-CSF treated BALB/c and C57BL/6j mice.

*Blood cell counts from Sci Vet ABC+ were given as 10^3 cells per mm^3 peripheral blood collected 4 hours after the final treatment. Data are shown as mean±STD, n=3 for C57BL/6j and n=5 for BALB/c, T-Test was used for statistical analysis, AMD3100 and G-CSF treated groups compared to each other and to saline control, *= <0.05, **= <0.01.*

As seen in Table 5-1 and Figure 5-7, there was considerable variability in the measurements of the different cell populations between the animals, reflecting the small sample number used for this analysis. Cell counts from BALB/c mice indicate that the drugs do not affect total white blood cells (Figure 5-7A). However, monocyte counts significantly increased in the presence of both drugs (Figure 5-7C), whereas other cells were not altered (Figure 5-7). AMD3100 and G-CSF significantly increased

total white blood cell counts in C57BL/6j mice (Figure 5-7A), and AMD3100 increased all cell numbers more than G-CSF (Figure 5-7B-E).

5.5.2. Earlier tumour development when HSC niche modified with AMD3100 in immunocompromised mice.

As described in the previous sections, the HSC niche can be modified by mobilisation of HSC. Initial studies were designed to determine if this mobilisation influences tumour development in bone, followed by a slightly revised repeat experiment. Both individual results and, in some cases combination of data from the two experiments will be described in section 5.5.1.3. As shown in Figure 5-2, female BALB/c Nude mice were injected with a triple-negative breast cancer cell line ($1x10^5$ Luc2+ve MDA-MB-231) via the intracardiac route to create the bone metastasis model after treatment with the HSC mobiliser AMD3100.

To test the hypothesis that HSC mobilisation alters tumour progression in bone, a slow progression model was chosen, using 10-week-old (mature) female BALB/c Nude mice. The initial endpoint was to achieve hind limb signals from 80-90% of the mice in the treatment group. As shown in Figure 5-14A, the initial experiment indicated that more hind limb tumours emerged earlier in the AMD3100 treated group than in the control group. This experiment was repeated to increase the power (number of animals/tumours available for analysis), and although the tumour cells and mouse strain/age were identical, tumour development was quicker in the second experiment; thus, this was terminated at day 30.

The following sections describe the analyses of bone parameters from the tumour growth experiments, followed by the tumour growth data.

Bone integrity and structure

As described above, the metastatic bone niche overlaps with multiple niches, including the HSC and endosteal niche. Therefore, changing the cellular composition of one niche may also impact other niches. Measurement of bone integrity with structure, alongside numbers of bone remodelling cells, gives information about the changes in the endosteal niche. To determine if modification of the HSC niche had any effect on bone integrity and structure, I used µCT; please see chapter 2, sections 2.3.6 and 2.3.8 for detailed information about the methodology.

The µCT results (Table 5-2) showed that trabecular bone density (BV/TV, %) was 13.32±1.91 for saline-treated and 13.89±3.63 for the AMD3100 treated group (Figure 5-8, A). Trabecular bone

numbers (Tb.N., mm^{-1}) were 2.84±0.31 for saline control and 2.97±0.74 for the treated group (Figure 5-8, B). Trabecular thickness (Tb.Th., mm) was 0.05±0 for both groups (Figure 5-8, C). Trabecular Separation (Tb.Sp., mm) was similar for both groups (CON: 0.21±0.02, AMD: 0.19±0.05, p:0.54, ns) (Figure 5-8, D). Cortical bone volume (BV, mm^3) was 0.75±0.05 for the saline-treated group and 0.79±0.05 for the AMD3100-treated group (Figure 5-8, E). Overall, no difference was found at the end of the experiment (day 30) in these parameters, demonstrating that five days of AMD3100 does not alter bone integrity and structure that remains detectable 25 days after the end of the treatment.

Table 5-2: Summary of µCT analysis data

	Control	**AMD3100**	**p**
Trabecular Bone Density (BV/TV, %)	13.32±1.91	13.89±3.63	0.79: ns
Trabecular Number (Tb.N., mm^{-1})	2.84±0.31	2.97±0.74	0.76: ns
Trabecular Thickness (Tb.Th., mm)	0.05±0	0.05±0	0.96: ns
Trabecular Separation (Tb.Sp., mm)	0.21±0.02	0.19±0.05	0.54: ns
Cortical Bone Volume (BV, mm^3)	0.75±0.05	0.79±0.05	0.35: ns

Trabecular bone density (BV/TV, %), Trabecular Number (Tb.N., mm), Trabecular Thickness (Tb.Th., mm), Trabecular Separation (Tb.Sp., mm) and Cortical Bone Volume (BV, mm3) from the female BALB/c Nude was assessed at the end of the experiment. T-Test was used for statistical analysis, and ns is non-significant; data show Mean±STD, n=4 for Control and AMD3100 treated group.

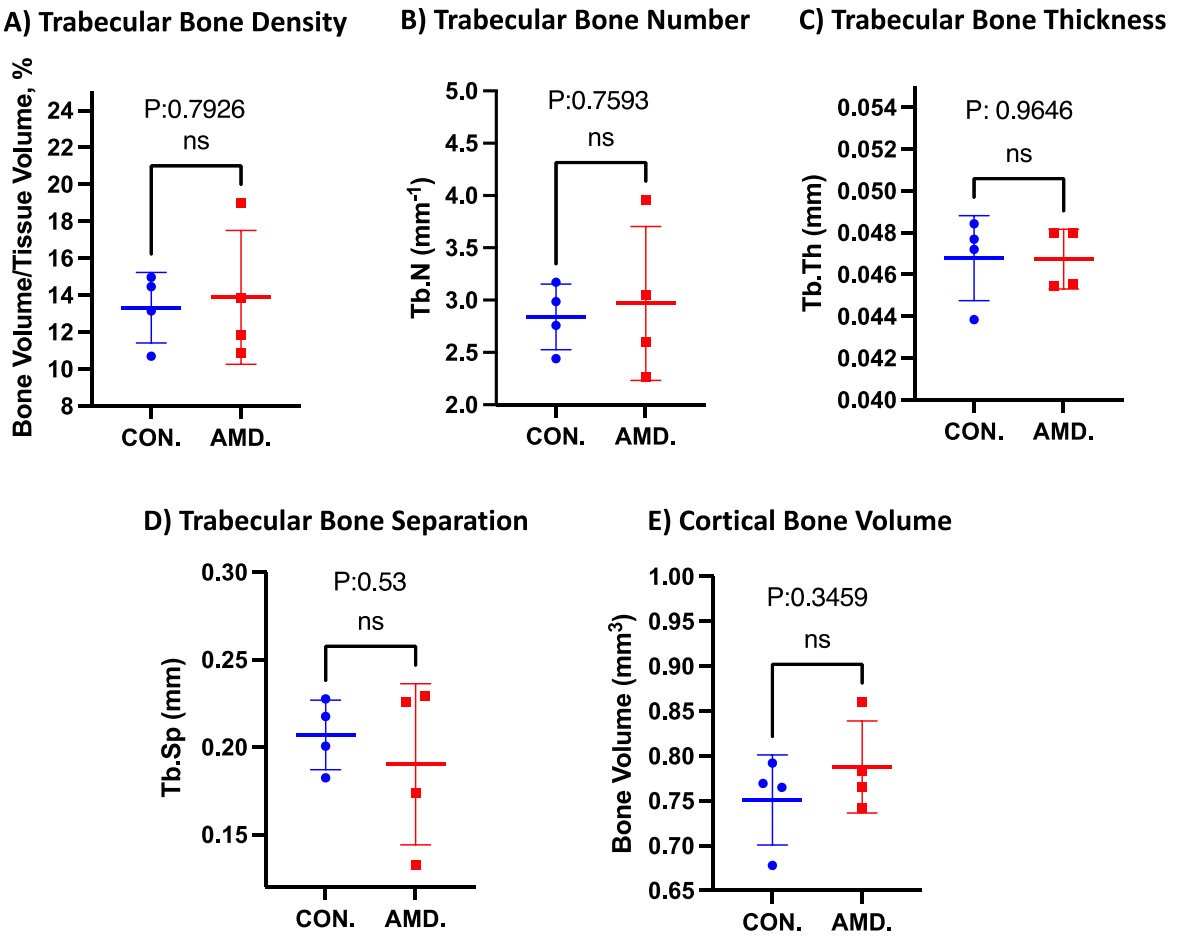

Figure 5-8: AMD3100 does not modify bone structure and integrity in immunocompromised mice.

Bones without tumours (n=4) from BALB/c Nude mice were analysed to compare differences in bone integrity between AMD3100 treated and control (saline treated) groupsat the end of the experiment. Effects on (A) trabecular bone density (BV/TV, %), (B) trabecular bone number (Tb.N., mm^{-1}), (C)trabecular thickness (Tb.Th., mm), (D) trabecular bone separation (Tb.Sp., mm) and (E) cortical bone volume (BV, mm^3) were shown as mean±STD, n=4/group for Control and AMD3100, T-Test was used for statistical analysis.

Bone remodelling cells

Differences in the physical bone structure assessed by µCT are informative for bone health; however, it does not allow assessment of how treatments impact bone remodelling cells. To evaluate if mobilisation of HSCs had any effects on osteoblasts and osteoclasts, tumour-free bones (n=3 for AMD 3100 treated group for both experiments, n=4 for control in the first experiment, n=5 for control in the second experiment) were cut and stained for TRAP (osteoclast marker). Numbers of osteoblasts, osteoclasts (per mm endocortical bone or mm trabecular bone) and perimeters of osteoblast (osteoblast bone depositing surface per mm endocortical bone or mm trabecular bone) and osteoclast (osteoclast bone resorbing surface per mm endocortical bone or trabecular bone) were scored. Since the numbers of osteoblasts and osteoclasts differ in different bone regions (more osteoblasts are

found in endocortical bone whereas more osteoclasts are found in trabecular bone), depending on the effect on different bone cells, would be significantly meaningful in different regions if identified. Please see section 2.2.3.8 for detailed information.

Endocortical Bone

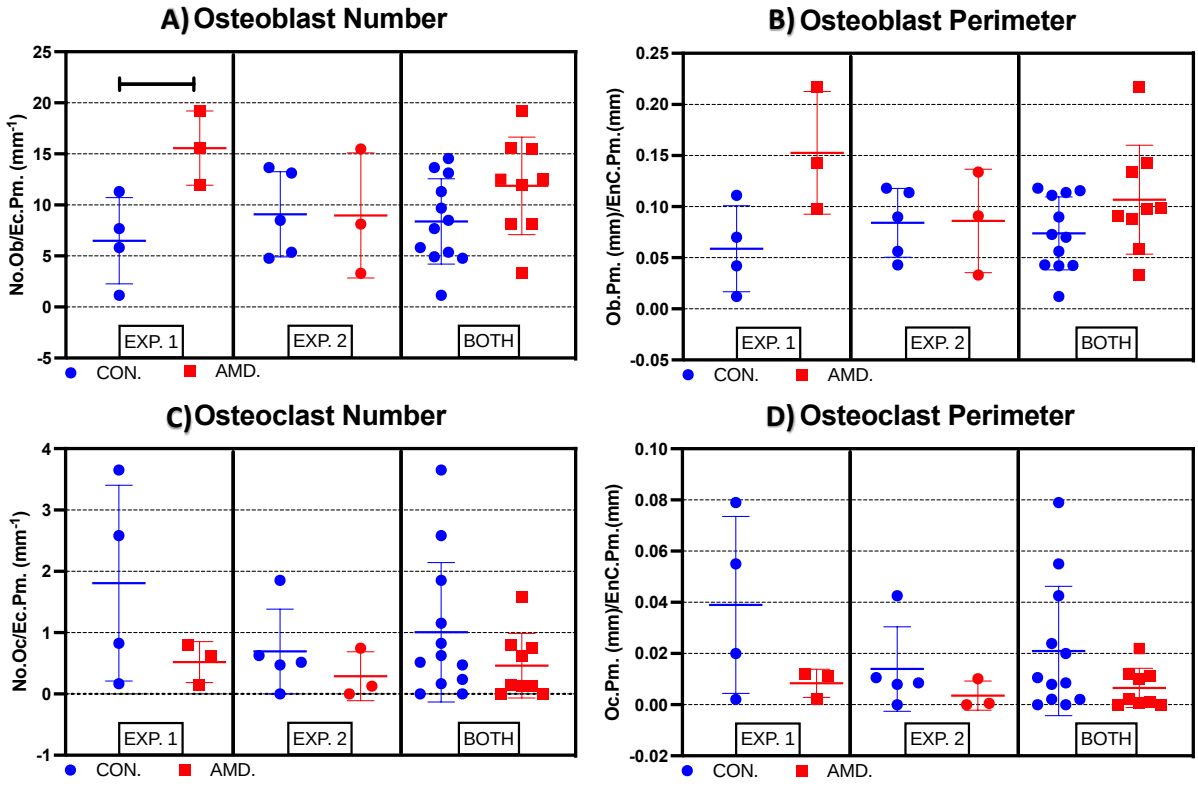

Figure 5-9: Bone remodelling cells in endocortical bone after AMD3100 treatment.

*AMD3100 treatment effect on the female BALB/c Nude mice's bone remodelling cells in endocortical bone was given as numbers and their perimeter (osteoblast: depositing surface per mm bone, osteoclast: resorption surface per mm bone). Three levels from each bone were scored, and (A) osteoblast number and (B) perimeter, (C) osteoclast number and (D) perimeter were shown on graphs for individual experiments and both data combined. Data show Mean±SD, n=3 for AMD treated group for both experiments, n=4 for control in the first experiment, and n=5 for control in the second experiment. T-Test was used for statistical analysis, *: p<0.05.*

There was considerable variability between the samples; however, I found no evidence that AMD3100 had an influence on endocortical bone cell parameters except osteoblast number (p:0.03) in samples from the first experiment; however, the sample size for AMD3100 was only three due to loosing some of the samples while cutting the bone (Figure 5-9, Table 5-3).

Table 5-3: Bone remodelling cells in endocortical bone.

Experiment 1		Experiment 2		Both Experiments	
CONTROL	**AMD3100**	**CONTROL**	**AMD3100**	**CONTROL**	**AMD3100**
Osteoblast Perimeter					
0.058±0.042	0.152±0.06	0.08±0.03	0.08±0.05	0.07±0.03	0.1±0.05
p:0.05, ns		p:0.95, ns		p:0.1, ns	
Osteoclast Perimeter					
0.039±0.03	0.008±0.005	0.014±0.01	0.0035±0.005	0.02±0.025	0.006±0.007
p:0.19, ns		p:0.34, ns		p:0.11, ns	
Osteoblast Number					
6.5±4.22	15.55±3.63	9.08±4.18	8.97±6.12	8.37±4.17	11.9±4.77
p:0.03, *		p:0.97, ns		p:0.09, ns	
Osteoclast Number					
1.8±1.6	0.51±0.33	0.69±0.69	0.29±0.39	1±1.13	0.46±0.52
p:0.23, ns		p:0.4, ns		p:0.19, ns	

*Summary data for osteoblast perimeter, osteoclast perimeter, osteoblast number and osteoclast number for both experiments and their combination result. Data show Mean±STD, and T-Test was used for statistical analysis, ns= no significance, * is ≤ 0.05, n=4 for Control and n=3 for AMD treated for experiment 1, n=5 for Control and n=3 for AMD treated for experiment 2.*

Trabecular Bone

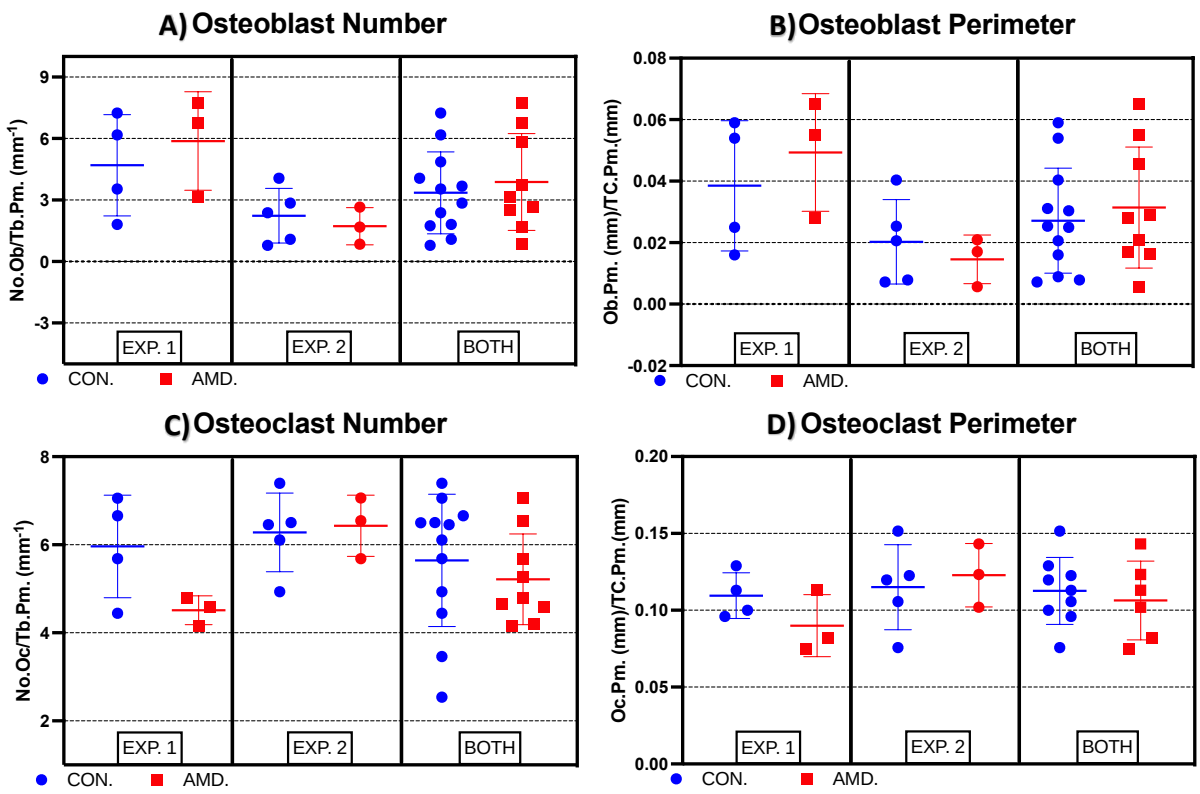

Figure 5-10: Effect of AMD3100 treatment on bone remodelling cells in trabecular bone.

AMD3100 treatment effect on the female BALB/c Nude mice's bone remodelling cells in trabecular bone were given as numbers and their perimeter (osteoblast: depositing surface per mm bone, osteoclast: resorption surface per mm bone). 3 Layers from each bone were scored, and (A) osteoblast number and (B) its perimeter, (C) osteoclast number and (D) its perimeter were shown on graphs for individual experiments and both data combined. Data show Mean±STD, n=3 for the AMD3100 treated group for both experiments, n=4 for control in the first experiment, and n=5 for control in the second experiment. T-Test was used for statistical analysis.

There were no significant differences in mean scores on the trabecular bone remodelling cells number and their perimeters between control, and AMD3100 treated animals (Figure 5-10, Table 5-4). Overall, the bone histomorphometric analyses demonstrated that the agents used to mobilise HSCs did not have a significant impact on bone remodelling cells, supporting that the main effect of 5 days of treatment with AMD3100 is to modify the HSC niche (by mobilising HCS and altering its composition), without impacting osteoblasts/osteoclasts. Any changes in tumour development would therefore be caused by modification of the HSC niche, not by altering bone, as is explored in the following section.

Table 5-4: Bone remodelling cells in trabecular bone.

Experiment 1		Experiment 2		Both Experiments	
CONTROL	**AMD3100**	**CONTROL**	**AMD3100**	**CONTROL**	**AMD3100**
Osteoblast Perimeter					
0.038±0.02	0.05±0.02	0.02±0.01	0.014±0.008	0.02±0.01	0.03±0.02
p:0.51, ns		p:0.54, ns		p:0.6, ns	
Osteoclast Perimeter					
0.1±0.015	0.09±0.02	0.11±0.02	0.12±0.02	0.09±0.04	0.1±0.025
p:0.2, ns		p:0.69, ns		p:0.62, ns	
Osteoblast Number					
4.7±2.47	5.88±2.4	2.23±1.33	1.72±0.9	3.35±2	3.88±2.36
p:0.55, ns		p:0.58, ns		p:0.58, ns	
Osteoclast Number					
5.96±1.16	4.51±0.32	6.28±0.89	6.43±0.69	5.64±1.5	5.21±1
p:0.09, ns		p:0.81, ns		p:0.47, ns	

Summary data for osteoblast perimeter, osteoclast perimeter, osteoblast number and osteoclast number for both experiments and their combination result. Data show Mean±STD, and T-Test was used for statistical analysis, n=4 for Control and n=3 for AMD treated for experiment 1, n=5 for Control and n=3 for AMD treated for experiment 2.

Effect of HSC mobilisation on tumour development and burden

To determine whether HSC mobilisation with AMD3100 affects tumour development, 10-week-old (mature) female nude mice were injected with a human triple-negative breast cancer cell line as described above. Tumour development and the burden were compared by *in vivo* imaging, and tumours were visualised with H&E; please see above and chapter 2 for detailed information.

Despite using identical designs, cell lines and animal age, the progression of tumour development was very different in the two experiments. In the first experiment, no difference was found in *ex-vivo* hind limb bone tumour counts per mouse between control (0.14±0.38), and AMD3100 treated (0.38±0.51) animals at the endpoint. In addition, the total tumour number count per mouse in any areas detected in control (2.5 ± 1.69) was not significantly different compared to the AMD3100 treated group (2.13 ± 1.25) (Figure 5-11). These data were gathered at the end of the experiment (day 55).

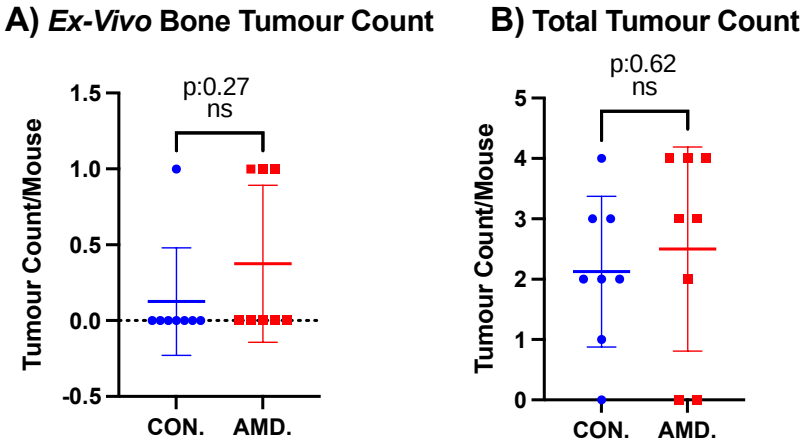

Figure 5-11: Tumour number at the end of the first experiment (day 55).

Detected tumour numbers in the female BALB/c Nude mice at the end of experiment 1, day 55 by in vivo imaging. A) Ex-vivo hind limb bone tumour count per mouse and B) In Vivo tumour counts detected in any area of the mice per mouse. T-Test was used for statistical analysis, n=8/ group. Data is represented as mean+/- SD.

In the second experiment, similar results were observed, with no significant difference found in *ex-vivo* hind limb bone tumour counts (CON:2±1.77 AMD:2.5±1.3, p:0.53) or in total tumour number per mouse (CON:5.13±2.8 AMD:4.25±2.5, p:0.51) between control and the AMD3100 treated group at the end of the experiment (Figure 5-12).

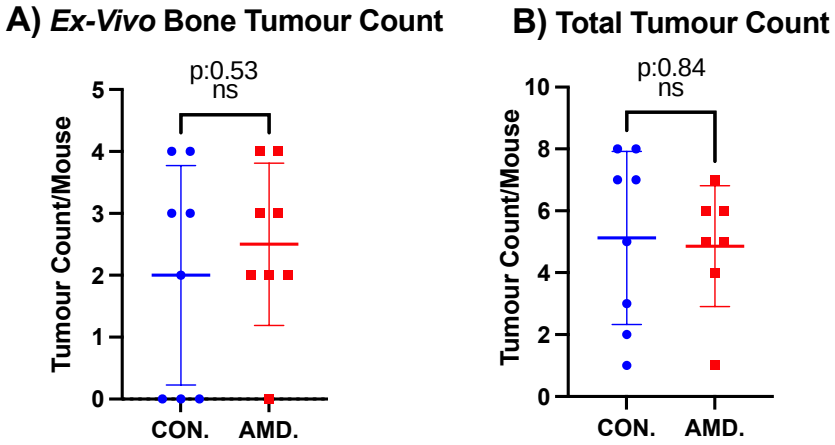

Figure 5-12: Tumour number at the end of the second experiment.

Tumour numbers in the female BALB/c Nude mice at the end of experiment 2, day 30, as detected by in vivo imaging. A) Ex-vivo hind limb bone tumour count per mouse and B) In-vivo tumour counts detected in any area of the mice per mouse. T-Test was used for statistical analysis, n=8/ group except 7 for AMD group in B. Data is represented as mean+/- SD

I next investigated tumour development in more detail to determine if there was any effect of AMD3100 treatment on the time the tumours first emerged as detected via IVIS and compared with Mantel-Cox analyses. In this analysis, animals who developed signal in any skeletal area marked on the calculation, however, all animals were culled at the end of the experiment where *ex-vivo* analyses

carried on the end tumour burden. First, any detectable tumour development in any skeletal site was compared and there was no significant difference between the AMD3100 treated and control groups (Figure 5-13A, $\chi 2 = 0.087$, df = 1, P = ns, 0.77, Figure 5-13B, $\chi 2 = 0.3346$, df = 1, P = ns, 0.56).

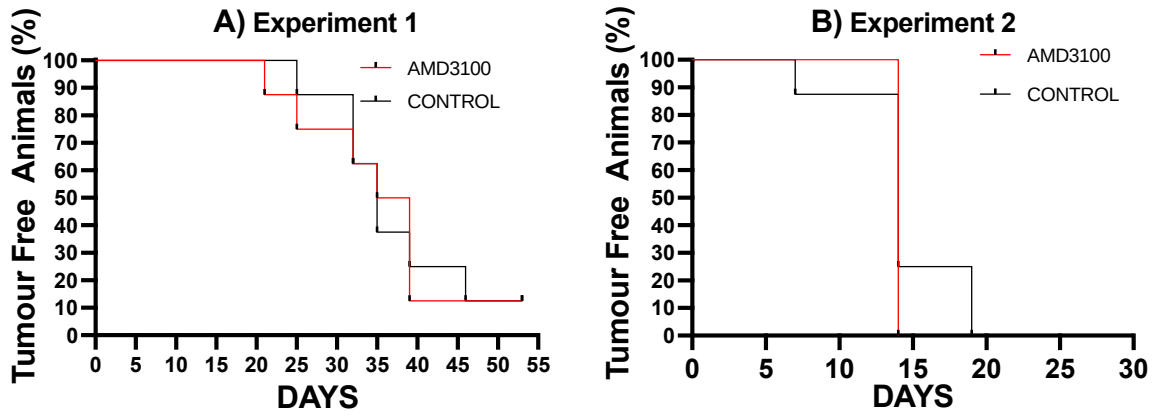

Figure 5-13: Tumour signal in any skeletal site.

Detection of tumour in any skeletal area of the female BALB/c Nude mice by day, tumour signal in any skeletal area is recorded. (A) tumour-free animal ratio per day from experiment 1, up until the end of the experiment (day 55), and (B) tumour-free animal ratio per day from experiment 2 Mantel-Cox analyses were used for statistical analysis, and data show n=8/group.

Similar Mantel-Cox analysis was also used to determine any tumour development in the hind limbs, where there is a high proportion of haematopoietic bone marrow and where the majority of tumours develop following i.c injection of tumour cells. Dates of the animals that developed hind limb signal was marked and statistical analyses carried according to the emergence of hind limb tumours. Then, all animals were culled at the end of the experiment which allowed to carry on *ex-vivo* analysis on the end tumour burden.

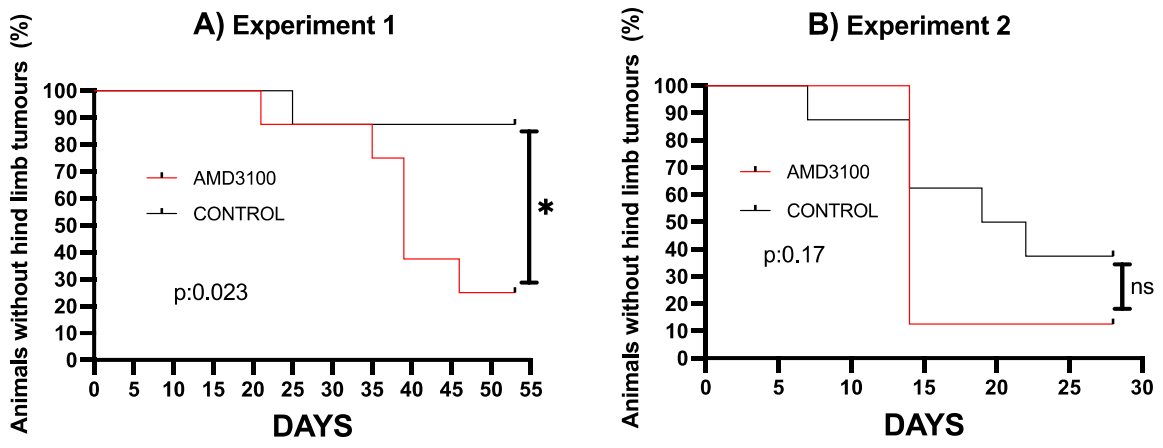

Figure 5-14: Analysis of experiments by detectable tumour signal in the hind limbs.

*Ratio (as %) of mice without any in vivo imaging hind limb signal in the female BALB/c Nude mice. Mantel-Cox analysis is carried out when the tumour signal in hind limbs is detected. All results are given as animals percentage without hind limb tumour signal. Graph (A) shows mice percentage without signal increase in the first experiment until the end of the experiment (Day 55), and graph (B) shows mice percentage without signal increase in the second experiment until the end of the experiment (Day 30). Mantel-Cox analyses were used for statistical analysis, and ns is non-significant, * is P<0.05, and data show n=8/group for A and B.*

The results from the first experiment showed earlier emergence and more hind limb tumours developing in the AMD3100 treated compared to the control group (Figure Figure 5-14A, $\chi 2 = 4.393$, df = 1, P = *, 0.036), with a similar, non-significant, trend observed in the second experiment (Figure Figure 5-14B $\chi 2 = 1.178$, df = 1, P = ns, 0.28).

Disease progression in the two experiments was different; in the first experiment, 7/8 AMD3100 treated animals had detectable tumours (any site) at day 39 (Figure 5-13A). In contrast, in experiment number 2, all of the mice in the AMD3100 treated group (8/8) had detectable tumours by day 14 (Figure 5-13B). In experiment 1, 5/8 mice in the AMD3100 treatment group developed hind limb tumours by day 39, compared to only 1/8 mice in the control group. In the second experiment, 7/8 mice in the AMD3100 treatment group had developed hind limb tumours on day 14 compared to only 3/8 mice in the control group.

The alteration of the HSC niche indicates earlier and more overt metastases, but further studies are required to support this hypothesis due to the difference in tumour progression between the two experiments I carried out.

5.5.3. The effect of HSCs niche modification on tumour development in immunocompetent mice

As I had established that G-CSF mobilises HSCs in tumour-free, immunocompetent mice, I investigated whether HSC mobilisation with G-CSF could affect tumour development and progression in BALB/c mice.

Tumour Development and Burden

As described earlier (Figure 5-3), 8-week-old female BALB/c mice (n=10/group) were treated either with saline (100 µl) or G-CSF (123 µg/kg) for five days before a bone metastasis model was created using intracardiac injection of the triple-negative mouse mammary carcinoma cell line ($3x10^4$ 4T1 LUC BONE) 6 hours after the last drug treatment. This model is aggressive, with tumours developing faster than the xenograft model using the BALB/c Nude strain (Canuas-Landero *et al*, 2021). *In vivo* imaging was used to compare both *in vivo* tumour development and to calculate average radiance for *ex vivo* tumour burden comparison.

Tumour development, burden and white blood cell counts were compared between G-CSF treated and control animals as described in previous sections. Since this is an aggressive model, insufficient numbers of tumour-free bones were available for use as bone analysis controls. In the G-CSF treated group, 8/10 animals had tumours in all four hind limb bones, compared to only 3/10 of the control mice.

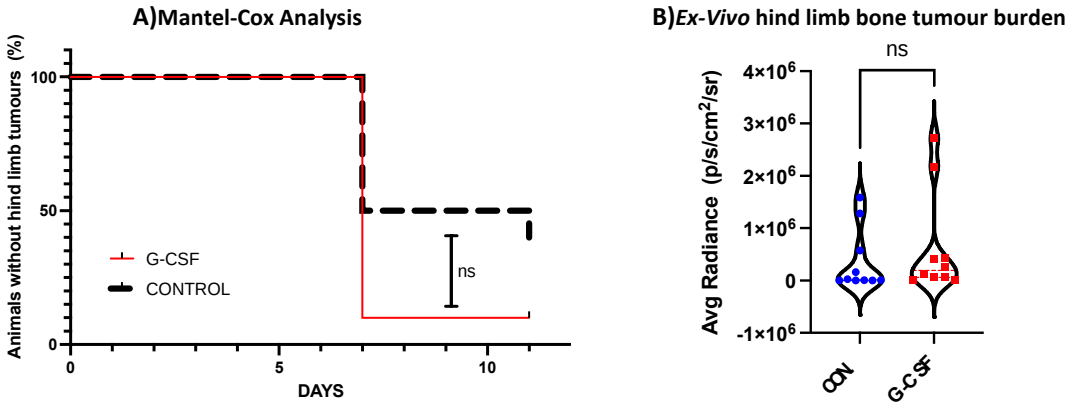

Figure 5-15: Hind limb tumour development in immunocompetent mice with/out G-CSF treatment.

In vivo imaging was used to determine tumour development in the female BALB/c mice for both in-vivo and ex-vivo comparisons. A) Mantel-Cox analysis was used to determine whether tumour development was affected by treatment. B) Violin plot of average luciferase radiance was used to compare ex vivo tumour burden in hind limbs, t-test was used for statistical analysis, n=10/ groups.

As mentioned before, hind limb tumours were first detected on day 7 in the syngeneic model (Figure 5-15A), whereas no signal was found in the faster xenograft model until day 14 (Figure 5-14B), demonstrating the faster disease progression in the BALB/c strain.

There was a non-significant, trend to more tumour emergence in the G-CSF pre-treated group compared to the control group (Figure 5-15A, $\chi 2 = 3.402$, df = 1, P = ns, 0.065). On day 7, 9/10 mice had developed hind limb tumours in the G-CSF treated group, compared to 5/10 animals in the control group. As shown in Figure 5-15B, final tumour burden, measured by average radiance values (the sum of the radiance from each pixel inside the ROI/number of pixels or super pixels: photons/sec/cm^2/sr) from *ex vivo* hind limb bone tumours was not significantly different between the groups (Control: $3.7x10^5 \pm 6x10^5$, G-CSF: $6.3x10^5 \pm 1x10^6$, p=0.47, ns) which indicates that final tumour development was not affected. Only the time point at which tumours first emerge might be affected by treatment.

White Blood Cell Counts

White blood cell counts are clinically used as an indication of infections, and some publications indicate that a chronic inflammatory response might indicate some cancer development and can be used to observe disease progression (Park *et al*, 2019; Singh *et al*, 2019).

As we can see from Table 5-1, the white blood cell count from the non-tumour bearing BALB/c was 2.32±1.31, whereas this was 20.68±8.37 for the tumour bearing BALB/c mice. There is at least ten

times increase in total white blood cell counts, and there is a general increase in all individual types of white blood cells (control groups from Figure 5-7 and Figure 5-16).

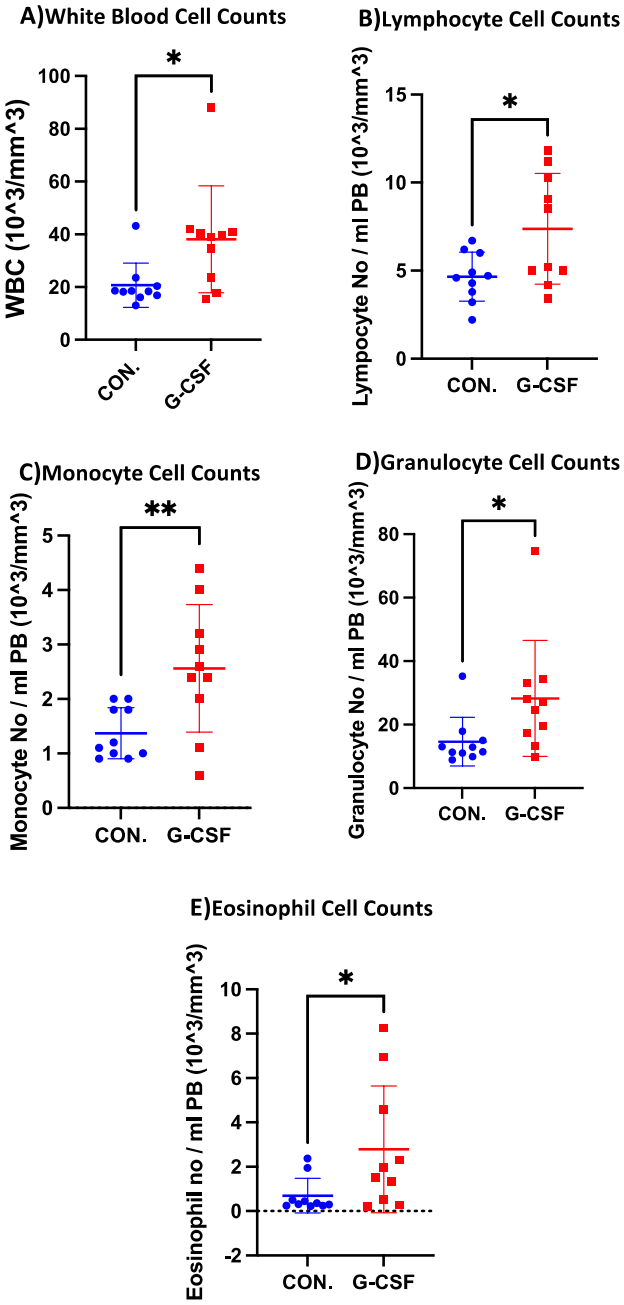

Figure 5-16: White blood cells count results from the immunocompetent mouse model

*Total cell number per ml peripheral blood from the female BALB/c mice was compared between saline control, and G-CSF treated groups. A) Total white blood cell counts, B) Lymphocyte cell counts, C) Monocyte cell counts, D) Granulocyte cell counts and E) Eosinophil cell counts were analysed with GraphPad using t-test, n=10/group, ns is not significant, * is 0≤0.05, ** is ≤.0.01, and data is shown as Mean ± SD.*

Total white blood cell counts per mm peripheral blood significantly increased in the treated group (CON: 20.68±8.37, G-CSF: 38.15±20.26, p:0.02 *<0.05) (Figure 5-16A). As expected, all of the

individual white blood cell types analysed were significantly increased in the G-CSF treated group compared to the control (Table 5-5). Also, the response to the tumour's increase in blood cell counts can be observed when comparing tumour-bearing BALB/c (Figure 5-7) with non-tumour bearing BALB/c mice (Figure 5-17), when both were treated with saline control only. Overall, the data show that the presence of tumours in bone induces changes in blood cells indicative of an inflammatory response.

Table 5-5: White blood cell count per mm peripheral blood for immunocompetent mouse model.

.	Control	G-CSF	p
White Blood Cell Count ($10^3/mm^3$)	20.68±8.37	38.15±20.26	0.02: *
Lymphocyte Cell Count ($10^3/mm^3$)	4.66±1.39	7.37±3.14	0.02: *
Monocyte Cell Count ($10^3/mm^3$)	1.37±0.47	2.56±1.17	0.008: **
Granulocyte Cell Count ($10^3/mm^3$)	14.65±7.67	28.22±18.25	0.04: *
Eosinophil Cell Count ($10^3/mm^3$)	0.69±0.78	2.78±2.86	0.04: *

*Blood cell counts from Sci Vet ABC+ were 10^3 cells per mm^3 peripheral blood. Data are shown as mean±STD, n=10 for both groups; the T-Test was used for statistical analysis. *= <0.05, **= <0.01*

5.6. Discussion

The experiment in this chapter aimed to investigate how modification of the HSC niche affects metastatic breast cancer tumour development in bone. The HSC niche consists of many different cell types, is influenced by a range of chemokines, growth factors etc. and has been proposed to be part of the bone metastatic niche due to their multiple, close interactions. In addition, some studies have shown that there might be competition for the niche between HSCs and disseminated cancer cells (Shiozawa *et al*, 2011a; Forest *et al*, 2013; Jung *et al*, 2015; Decker *et al*, 2016; Allocca *et al*, 2019) and underlined the similar pathways that might be used for homing, quiescence and survival within the niche. Whereas a few studies have investigated whether disseminated cancer cells are home to the HSC niche, there are no studies that directly investigated if HSC niche alterations affect tumour development in bone. This chapter presents the data from my experiments modifying the niche by only altering the HSCs in different mouse models, providing new information about the effects on metastatic breast cancer development in bone.

In murine models of bone metastasis from breast and prostate cancer, tumours most commonly develop in areas of the long bones that are also responsible for supporting haematopoiesis termed 'the hematopoietic stem cell niche (HSC). After Schofield proposed a specialised bone niche for HSC maintenance and multipotency (Schofield, 1978), many studies have contributed to the identification of its location and cellular components (reviewed in (Ren *et al*, 2015)). This niche consists of different cells that support HSC properties with cell-cell contacts, extracellular matrix molecules, growth factors and chemokines (Chatterjee *et al*, 2021). In the murine bone marrow, HSCs are located close to the vascular niche and have close contact with cells like MSCs, endothelial cells, bone cells and immune cells (macrophages, megakaryocytes etc.) (Broudy, 1997; Calvi *et al*, 2003; Boulais & Frenette, 2015; Haider *et al*, 2020). To maintain their HSC population, cells enter a quiescent state (Cheng *et al*, 2000). It was shown that these quiescent HSC populations are found close to the endosteum, where it interfaces with bone marrow located close to the trabecular bone area (Morrison & Scadden, 2014). Calvi et al. (2003) showed increased HSCs linked with trabecular bone growth and osteoblastic cell numbers, which supports the interaction between HSCs and bone cells in this region. As described in the introduction, HSCs cycle between dormancy and proliferation and many chemokines secreted by cells in the niche support HSCs maintenance (Li *et al*, 2012). One of the best-described interactions is the CXCL12/CXCR4 pathway (Sugiyama *et al*, 2006; Singh & Pelus, 2020) which also plays a crucial role in bone remodelling (Semerad *et al*, 2005; Xu *et al*, 2017a) and tumour development in bone (Teicher & Fricker, 2010; Wang *et al*, 2014; Nguyen *et al*, 2020). Deletion of

CXCR4 caused a reduction in HSC numbers (Sugiyama & Nagasawa, 2012), and one of the CXCL12 sources is osteoblasts (Barker, 1997). Therefore all of these findings put the HSCs niche under the spotlight for investigation; thus, the current study focused on the bone area where possible HSC interactions occur in the bone as suggested by Boulais and Frenette (2015) and Haider et al. (2020) (Figure 5-17).

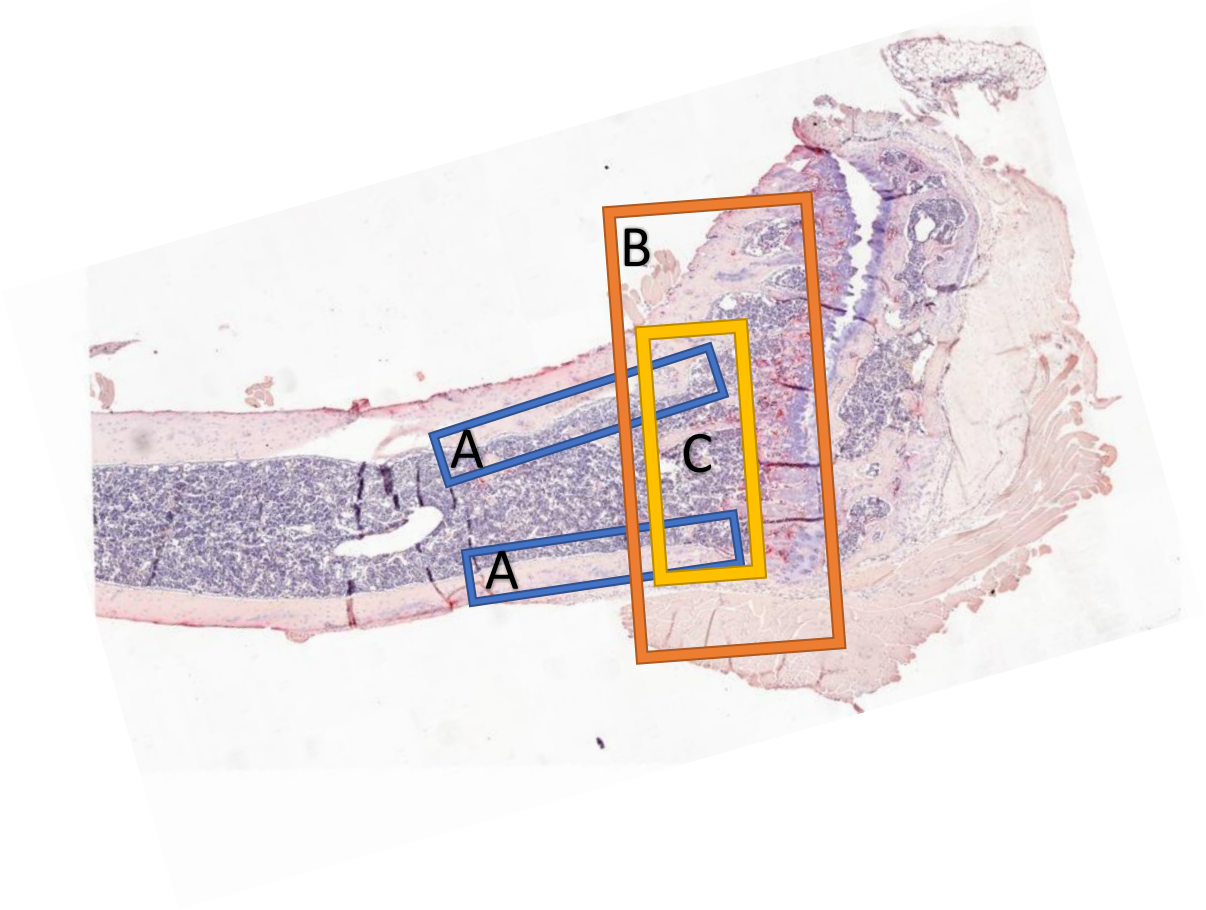

Figure 5-17: Haematopoietic Stem Cell Niche Location in Mouse Bone

Histological staining of mouse femur for TRAP where the (A) endosteal niche is shown in the blue bracket for HSC niche as reviewed in Boulais and Frenette (2015) and (B) suggested bone metastatic niche by Haider et al. (2020) showed in the orange bracket. (C) The area shown with the yellow bracket is the targeted area for HSC niche alteration where possible interactions might have occurred with bone cells and is a potential location for cancer cell dissemination.

Studies using advanced imaging to track individual tumour cells in bone have shown that they are primarily located in the sinusoidal area, thereby broadly overlapping with the location of the HSC niche (Shiozawa *et al*, 2011a; T. *et al*, 2016; Allocca *et al*, 2019). Although widely accepted as a target site for colonising DTCs, direct evidence that tumour cells 'parasitise' the HSC niche is surprisingly limited. Shiozawa et al. were the first to demonstrate that prostate cancer cells (PCCs) metastasise to

the HSC niche and compete with HSCs for the niche in a mouse model (2011a). They created primary prostate tumour models (SCID and NOD/SCID) by implanting scaffolds with PCCs either subcutaneously or orthotopically (prostate) and removed primary tumours after three weeks. PCCs were detected by real-time PCR for human-specific ALU sequences and expressed luciferase. At different time points, animals were culled, DNA extracted from different tissues, metastatic lesions were observed with bioluminescent imaging, and HSC engraftment was analysed with FACS. Their results showed that HSC engraftment is reduced in tumour-bearing mice, indicating tumour cell occupation of the HSC niche. To confirm that this reduction was caused by PCC/HSC competition, they used a competitive engraftment assay, transplanting lethally irradiated animals with BM cells, PCC or prostate epithelial cells. Histological scoring of the bone marrow showed that the group receiving PCC had a significant delay in HSC engraftment compared to the control groups, demonstrating competition between HSCs and PCCs. Detection of prelabelled HSCs and PCCs by confocal microscopy showed that they home within a few microns of each other in the bone marrow. Finally, they showed increased HSCs in PB in patients with bone metastatic prostate disease compared to their age-matched controls, further supporting the PCC-driven mobilisation of HSCs. Like prostate cancer, breast cancer commonly spreads to the skeleton, potentially by tumour cell homing to the HSC niche. This was investigated by Allocca et al. (2019), who used a BALB/c Nude mouse model to show increased breast cancer dissemination in bone when luciferase labelled MDA-MB-231 triple-negative breast cancer cells were injected following HSC mobilisation with AMD3100. They showed that independent of the age of the mice, breast cancer cells preferably homed to the trabecular region adjacent to components of the perivascular niche and close to the bone surface. These studies identified the HSC niche as a possible metastasis location, yet they did not assess whether subsequent tumour growth is influenced by pre-treatment with HSC mobilising agents.

Annexin 2 (a cell attachment factor) in the osteoblastic niche (Jung *et al*, 2007) may also play a role in anchoring the cells, and Jung et al. (2015) showed that Annexin 2 promotes prostate cancer recruitment to the niche (alongside CXL12) and protects cancer cells from chemotherapy-induced apoptosis. The HSC niche could therefore be a potential target to limit disease progression. On the other hand, disseminated tumour cells (DTCs) can enter a quiescent stage that will protect them from the elimination by the immune system (Townson & Chambers, 2006). As described in the introduction, this quiescent stage involves multiple interactions with the surrounding microenvironment, and DTCs can stay dormant for many years. As we currently know, not all DTCs go on to form tumours in patients (Aguirre-Ghiso, 2007; Farmen *et al*, 2008; Tjensvoll *et al*, 2012). Under normal conditions, HSCs in the bone marrow sometimes enter the circulation and differentiate into progenitor cells. Evidence shows

that DTCs could increase this mobilisation to PB without inducing HCS apoptosis and that HSCs are chemotactic to PCCs (similar attraction was not found from PCC towards to HSCs) (Shiozawa *et al*, 2011a). However, whether these HSCs mobilised by DTCs remain functional is still unknown.

After studies from *in vivo* models suggested the HSC niche as a homing area for DTCs this raised the possibility that similar mechanisms may regulate them as HSCs, and modification of the HSC niche was tested to determine the effect on homing of circulating tumour cells (CTCs) (Shiozawa *et al*, 2011a; Allocca *et al*, 2019). As described previously, the CXCR4/CXCL12 (SDF-1) axis plays a crucial role in both HSCs mobilisation, cancer cell homing, and tumour progression through a vicious cycle. Kollet et al. blocked CXCR4 with antibodies and found reduced skeletal metastases of PCC (Kollet *et al*, 2001). Thus, blocking this pathway could mobilise the HSCs and might have possible benefits. AMD3100 is a CXCR4 antagonist that inhibits CXCL12 binding and function with high affinity and potency (Rosenkilde *et al*, 2004). Shiozawa et al. showed increased PCCs in blood in AMD3100 treated mice compared to vehicle control (Shiozawa *et al*, 2011a), suggesting a clinical benefit by reducing tumour cell homing. G-CSF induces different mobilisation mechanisms, and it acts directly on HSCs (without needing of G-CSF receptor) (Liu *et al*, 2000), induces the production of proteases that cleave surface adhesion proteins (c-kit (Lévesque *et al*, 2003), VCAM-1 (Lévesque *et al*, 2001), and reduces the production of CXCL12 in the bone environment following a single single injection at 24 hours (Petit *et al*, 2002). Since both drugs are used clinically to mobilise stem cells, e.g., G-CSF to replenish white blood cells after chemotherapy, I aimed to determine their effects in different murine models to confirm that these agents mobilise HSCs from their niche. Although xenograft models allow us to determine effects on human cancer cells, effects on the adaptive immune system cannot be ignored. That is why, to understand whether the HSC niche alteration effects may differ, I also used a syngeneic immunocompetent model. Alteration of the BALB/c nude HSC niche by mobilising HSCs to peripheral blood was shown by Allocca et al. (2019), using the CXCR4 antagonist AMD3100. To test whether similar mobilisation can be achieved in immunocompetent strains (BALB/c and C67BL/6j), mice were treated with AMD3100 or G-CSF for five days PB and BM were collected to carry out colony forming unit assays. As expected, both drugs resulted in increased colonies from peripheral blood compared to saline control, confirming successful HSC mobilisation from BM. These results were similar to previous studies reported in the literature (Iwasaki *et al*, 2005; Broxmeyer, 2008; Dar *et al*, 2011; Lee *et al*, 2014a; Chen *et al*, 2021). My data indicate that after this treatment regime, G-CSF increased the number of colonies when compared to AMD3100 in the BALB/c strain. Lee et al. (2014a) performed similar mobilisation experiments with AMD3100 and G-CSF in both BALB/c C57BL/6j mice. In their study, they used 5mg/kg AMD3100 for six days, whereas I used the same dose for five days, and G-

CSF was used as 250g/kg, whereas I used 123 µg/kg. Despite the higher dose of G-CSF and longer AMD3100 treatment, their findings are comparable to mine; they also showed that G-CSF-mediated HSC mobilisation is more efficient than AMD3100 in the BALB/c strain.

Another question was to determine whether this HSCs mobilisation effect can also be detected in bone marrow, reducing the number of HSCs in the BM niche. To investigate this, liquid bone marrow was collected, and a similar colony-forming assay was used. I did not detect any significant change in HSC CFU counts from either strain of bone marrow with AMD3100 or G-CSF treatment compared to saline controls. However, in C57BL/6j, there was a trend toward reduced HSCs colonies after G-CSF treatment, which might reflect different bone marrow compositions between strains. Lee et al. (2014a) showed that BALB/c mice have fewer stem and progenitor cells responsive to CXCL12 and S1P in bone marrow compared to C57BL/6j mice, which they suggested could be a reason for reduced HSC mobilisation by AMD3100. This might also be why WBC counts were not affected in BALB/c mice following treatment with either mobilising agent and only increased in C57BL/6j mice with both drugs in this study. However, the method I used to quantify HSCs produced variable results and may not have captured HSCs in a reproducible manner. Alternative methods like confocal imaging can be better for quantifying and observing locations. Nombela-Arrieta et al. investigated location and hypoxia in HSCs; they used confocal and multiphoton imaging and detected HSCs' location close to the endosteal niche (Nombela-Arrieta *et al*, 2013). Allocca et al. also used two-photon microscopy to quantify the disseminated cancer cells when altering the niche (Allocca *et al*, 2019). The current protocol published by Saçma et al. shows how useful can be 3D imaging with confocal microscopy to study stem cells in tissue and organs (Saçma *et al*, 2022).

The only difference between the studies relates to the blood count effects of G-CSF on BALB/c mice. Lee et al. showed increased WBC counts, whereas, in my study, there was a trend towards an increase that did not reach statistical significance. This might be because of biological variables between strains since their control groups had 5-8 $x10^3$ WBC cells per ml PB, whereas, in my studies, this number was 0-3 x 10^3 WBC cells per ml PB. However, these data also suggest that despite biological variations, mobilisation can be achieved with both AMD3100 and G-CSF, paving the way for studies to determine whether such treatments would impact tumour development and progression in bone.

As I wanted to ensure that HSC mobilisation did not significantly impact the endosteal niche, I performed a detailed µCT analysis of the bone structure and bone histomorphometric analysis of bone remodelling cells throughout. Published studies have not included this, and it is possible that

altering the cellular content of one niche may have an impact on the overlapping ones. The results confirmed that the limited treatment period (5 days) was sufficient to modify HSCs but did not cause significant changes to the BME, with the exception of osteoblast number in endosteal bone from the first experiment. However, this trend was not observed in the repeated experiment, which might be related to the biological variation or limitations of the sample size.

It is suggested that the HSC niche might be involved in breast cancer tumour development in the skeleton, and Allocca et al. (2019), showed increased cancer cell dissemination to the HSC niche after mobilisation of HSCs from the niche. Whether this would result in increased tumour development was not investigated, with studies of DTCs being terminated five days after tumour cell injection. To determine whether HSC mobilisation would increase bone tumour growth, a bone metastasis model was created with an injection of triple-negative breast cancer cells (MDA-MB-231) via the intracardiac route after treating BALB/c Nude mice with AMD3100 and tumour development was monitored with IVIS over the next 3-4 weeks. In our model the main site of the HSC niche is in hind limb bones; thus, *in vivo* observation of hind limb tumour development was carried out to determine the effects of mobilisation. I hypothesised that mobilisation of HSCs will open space for cancer cells to disseminate and that increased cancer cell dissemination could result in earlier and/or increased development of overt metastasis compared to the control group. Therefore, IVIS analysis was carried out twice a week to detect overt metastasis and allow a comparison of the timing of metastatic development between control and AMD3100 treated animals. My results showed that more tumours emerged earlier in the treated group than in the control group, with approximately 90% of the animals in the control group not developing hind limb tumours by the end of the experiment (Day 54). In comparison, only 25% of the animals in the treated group did not develop hind limb tumours. This experiment was repeated with the second batch of animals.

Similar, to what was observed in the first experiment, more mice in the AMD3100 treated group developed hind limb tumours at earlier time points than in the control group, but disease progression was faster. The experiment was concluded on day 27 compared to day 54 in the first experiment, precluding pooling of the results in a single analysis. This is probably due to the biological variations (potential batch differences between animals) and other factors, such as disease progression speed, affecting breast cancer bone metastases. White blood cell counts can be given as an example about variability between animals, difference of the lowest and highest white blood cell counts detected by the supplier was 100,000 cells per ml PB. From the point at which most animals in the AMD3100 treated group displayed overt metastases, it took two weeks to conclude the

experiment. When these time intervals were taken together, reduced surviving rates of treated animals became more significant.

The xenograft model was an example of a human triple-negative breast cancer model in immunocompromised mice, which has relatively slow tumour progression compared to the mouse triple-negative mammary carcinoma model in immunocompetent mice. To observe the effects of immune cell populations in a similar experiment, immunocompetent mice were injected with triple-negative mouse mammary carcinoma to create a syngeneic model. BALB/c mice were treated with G-CSF to mobilise HSCs from the niche. After treatment, triple negative mouse bone metastatic mammary carcinoma cells (4T1 LUC BONE) were injected via the intracardiac route, and hind limb tumour development was observed with IVIS. Disease progression was faster than in the xenograft model, reaching a terminal stage 11 days after tumour cell injection compared to 29-54 days for the xenograft model, despite injecting fewer cells ($1x10^5$ cells for the xenograft model and $3x10^4$ cells for the syngenetic model). However, as seen in the xenograft model, more hind limb tumours were observed at the earliest time in the G-CSF treated compared to the control group. The tumour burden in hind limb bones measured *ex vivo* at the end of the experiment was similar for both treated and control groups.

As expected, the white blood cell counts were found to be significantly increased following G-CSF treatment in C57BL/6j mice. White blood cell counts are an indicator for inflammatory response known to support cancer development (Balkwill & Mantovani, 2001; Coussens & Werb, 2002; Mantovani *et al*, 2008; Mantovani & Sica, 2010). WBC counts were an essential indicator of breast cancer's response to chemotherapy (Andre *et al*, 2013). Immune indicators from PB (neutrophil/lymphocyte ratio, platelet/lymphocyte ratio and WBC/lymphocyte ratio) have been insensitively studied for response to the treatment, and the low ratio of these parameters indicates reduced inflammation and immune system activation (Asano *et al*, 2016; Chen *et al*, 2016; Xu *et al*, 2017b; Chae *et al*, 2018; Marín Hernández *et al*, 2018; Qian *et al*, 2018; Graziano *et al*, 2019). Since both AMD3100 and G-CSF reduced the platelet/lymphocyte ratio, it might support the therapy response of cancer in the clinic. In our study, we showed no significant increase in white blood cell counts after only G-CSF treatment in BALB/c mice; thus, this effect cannot be carried out after tumour development and maybe only be an indicator for treatment response.

When white blood cell counts were compared with tumour bearing and non-tumour bearing mice from BALB/c controls, it was found that all the individual values for lymphocytes, monocytes, granulocytes etc. were increased with an almost 10-fold increase in total white blood cell counts which

shows the detectable inflammatory effects of the tumour on peripheral blood. A clinical study carried out by Park et al. also showed the difference in WBC counts in patients with different breast cancer burdens (which also depends on the menopausal status, hormone receptor type and BMI) (Park *et al*, 2019). All these studies suggest an important relationship between low-grade inflammation and some cancer developments. This WBC data suggest that similar phenomena can be observed in murine models, yet further studies are needed to establish the link between WBCs and early metastatic progression in bone.

The results from both models indicate that mobilisation of HSCs, or alteration of HSCs niche cellular composition with mobilisation agents, might result in earlier development of overt bone metastases. As can be seen from the syngeneic model, when conditions favour the disease, progression can be faster since we cannot precisely measure the number of disseminated cells in each mouse. Also, tumour progression has a logarithmic growth curve, when it reaches a certain amount of cell growth there is an acceleration and when it reaches a certain size, due to reduced perfusion to the tumours' centre, reduced acceleration can be observed. My data are consistent with the hypothesis that removing HSCs from the niche increases tumour cell dissemination to the bone but might also result in earlier development of overt metastases. However, this is not the only factor required, thus the sample size must be increased in future studies to reduce variation caused by biological differences and chances of different survival rates of cancer cells in the murine bloodstream.

Overall, the work described in this chapter shows that HSC mobilising agents can modify the HSC niche in murine models; thus, this modification may increase tumour development in bone and supports that the HSC niche is part of the bone metastatic niche. Alteration of this niche might cause an increase in bone metastasis (or increase the risk of metastatic spread), especially in studies involving G-CSF treatment in breast cancer (Liu *et al*, 2020). However, any micrometastatic tumour growth, which is caused by G-CSF, should be eliminated with the following chemotherapy. Further studies must be carried out to see whether HSC mobilisation has any effects on bone metastasis in models that include bone metastasis development from a primary tumour.

5.7. Conclusion

In summary, these data;

- Show that the HSCs niche can be modified with either AMD3100 or G-CSF in both immunocompetent and immunocompromised mice without affecting bone structure or bone remodelling cells
- Indicate that this modification might increase the chance of overt metastasis where tumours occur sooner.
- Demonstrate that despite the different time intervals for tumour emergence, this does not alter the final tumour burden

Overall, my results are in agreement with those of Allocca, supporting that breast cancer cells home to the HSC niche and in addition show that mobilisation of HSCs prior to tumour cell injection affects the early stages of bone metastases.

CHAPTER 6. GENERAL DISCUSSION, CONCLUSION AND FUTURE WORK

Over the past decades, breast cancer survival has increased, especially with the development of new drugs to treat advanced disease (Jani *et al*, 2021). However, breast cancer is still the most common cancer type in females (Ferlay *et al*, 2021; Sung *et al*, 2021; Siegel *et al*, 2022). Five years survival rates for local (≈99%) and regional breast (≈86%) cancer are higher compared to distant disease (≈29%) (Siegel *et al*, 2022). The skeleton is one of the most common distant sites for metastasis with ≈70% of the advanced breast cancer patients have skeletal metastases (D'Oronzo *et al*, 2019). Bone metastases are incurable and reduce patients' quality of life through pain and fractures, especially in the late stage of the disease (Hiraga, 2019). Bone has nutrient-rich niches suitable for tumour cell dissemination, and it has been suggested that those niches support cancer cells escaping from primary tumours (Mundy, 2002). For example, Luo *et al*. showed that in a murine study, increased IL-6 from senescent osteoblasts increases bone resorption by osteoclast, supporting increased tumour cell seeding (Luo *et al*, 2016). Another known mechanism, involves the CXCR4/CXCL12 pathway which is expressed in bone marrow cells such as osteoblasts, osteoclasts and HSCs, has been shown to contribute to different metastasis stages (Müller *et al*, 2001; Hirbe *et al*, 2007; Katoh, 2016; Nguyen *et al*, 2020). As previously described, many studies have supported the importance of BME interactions on metastatic breast cancer development (Chinni *et al*, 2006; Bussard *et al*, 2008; Meads *et al*, 2008; Liu *et al*, 2014; Ren *et al*, 2015; Decker *et al*, 2016; Roato & Ferracini, 2018). Therefore, it is essential to better understand the bone marrow microenvironment to establish the mechanisms underpinning disease progression. This project hypothesises that the presence of a tumour modifies the BME, including multiple cell types such as immune cells. Doxorubicin (DOX), a standard chemotherapy agent used to treat breast cancer bone metastasis, also affects the cell populations of the bone and marrow. Bone marrow niches play a crucial role in cancer progression; thus, altering the haematopoietic stem cell niche (a suggested niche for breast cancer metastasis (Forest *et al*, 2013; Allocca *et al*, 2019)) modifies the progression of bone metastasis. Bone metastasis cannot be studied in humans; therefore, the first aim is to establish the differences between widely used mouse strains in different models of bone metastasis and determine the detectable differences between tumour-bearing bone/bone marrow to that of tumour-free controls. Then, the effects of DOX on bone and marrow were investigated in immunocompromised and competent mice strains. Finally, the HSC niche was altered with known mobilisers (AMD3100 and G-CSF) to determine if this would

impact subsequent tumour development in bone. Overall, the studies in this thesis investigated the bone and bone marrow populations in models of breast cancer bone metastasis, with particular emphasis on how modification of the bone microenvironment impacted the bone metastatic niche.

6.1. The bone microenvironment differs between mouse strains.

In my initial studies I investigated DOX effects on the bone and marrow, demonstrating differential drug effects in the immunocompetent vs immunocompromised animals. As described before, most late-stage breast cancer patients have skeletal metastasis; however, in patients with early breast cancer disseminated tumour cells may stay dormant and not develop into overt metastasis for several years (Salvador *et al*, 2019). Complex interactions occur in bone metastatic breast cancer, and different models (xenograft and syngeneic models) have been developed for exploring specific hypotheses (Ottewell & Lawson, 2021). Xenograft models, which involve human cancer cells injected/implanted in immunocompromised mice are widely used. They provide faster tumour development with close genetic and epigenetic features, that allow studying induvial molecular pathways (Richmond & Yingjun, 2008). Different methods of tumour cell injection are developed for xenograft models (reviewed in (Ottewell & Lawson, 2021)); one is injecting human cancer cells directly into bone (intra-tibial model), minimising the effects outside the bone marrow (Ottewell *et al*, 2009; Wright *et al*, 2016). Injecting tumour cells via the intracardiac or intravenous route can be used to mimic metastatic dissemination through the circulation (Ottewell *et al*, 2008a; Wright *et al*, 2016; Tulotta *et al*, 2019a). Also, mouse models have been developed to study human bone metastasis via patient-derived bone engraftment (Kuperwasser *et al*, 2005; Tulotta *et al*, 2019a). Different cell lines are used with different genetic and epigenetic properties, e.g. MDA-MB-231 for triple-negative and MCF-7 for ER+ breast cancer (Holen *et al*, 2016; Ottewell & Lawson, 2021). However, the xenograft models lack essential immune components; therefore, transgenic or syngenetic models have been developed to study immune effects on different disease stages, including bone metastasis (Ottewell & Lawson, 2021). Random mutations and bone metastasis occur rarely in transgenic models (Ottewell *et al*, 2006); thus, syngenetic models are more predictable, as the host has a complementary background to the cell line (Lee *et al*, 2014b; Canuas-Landero *et al*, 2021; Ottewell & Lawson, 2021). Tumour progression and the resulting cancer-induced bone disease is often monitored with *in vivo* fluorescence imaging, *in vivo* and *ex vivo* µCT and histological staining (Ottewell & Lawson, 2021). Effects on specific pathways or cells and niches can be investigated with confocal microscopy, immunohistochemical staining or flow cytometry and biochemical analysis such

as ELISA (Brown *et al*, 2012; Allocca *et al*, 2019; Canuas-Landero *et al*, 2021; Tulotta *et al*, 2021). Choosing the right model to address a specific research question is essential, as no perfect bone metastasis model exists. Specifically, tumour interactions with the BME do not only involve one specific pathway or cell type; complex interactions between multiple cell types and soluble factors may be supporting bone metastasis. Disease progression differs between xenograft and syngenetic models; syngeneic cell lines such as E0771, 4T1 are spontaneously metastases to lung and lung metastases are fast developing and spread to additional skeletal areas (e.g. jaw and skull) with considerable heterogeneity in sites and rate between animals (Ottewell & Lawson, 2021). Therefore, mapping the cellular composition of the BMEs in different mouse strains might reveal potential therapeutic targets and also help to develop models that better represent human metastatic breast cancer.

The presence of the adaptive immune system is the main difference between BALB/c and BALB/c Nude animals. Nude animals lack thymus; they do not have mature T cells yet have other immune cells (Flanagan, 1966; Belizario, 2009). Monterio *et al*. carried a spontaneous bone metastasis model using 6-8 weeks female BALB/c mice with bone metastatic 4T1 and non-metastatic 67NR mouse mammary cancer cells. This study provides key information about the bone metastatic niche; firstly, they detected increased pro-osteoclastogenic cytokines in the metastatic bone model, which supports the hypothesis that the primary tumour prepares the future metastatic niche. Secondly, they showed increased numbers of osteoclasts in the bone of the 4T1 model, associated with early and rapid bone loss (Monteiro *et al*, 2013). Thus, they concluded that bone loss starts before detectable metastases appear. As mentioned in the introduction, T cells also play a role in bone remodelling through production of RANKL; thus, Monteiro also investigated the bone effects of T cell-specific knock-down of RANKL and IL-17F in BALB/c Nude mice. They found that RANKL from T cells is required for pre-metastatic osteolytic disease, with no or small numbers of bone metastases when T cells where RANKL had been knocked out were injected in BALB/c Nude animals (Monteiro *et al*, 2013). Bone loss and its effect on inducing metastasis will be discussed later in this chapter, yet these results underline the importance of multiple components supporting the vicious cycle in osteolytic bone metastasis, including immune cells. Feurer *et al*. found higher number of T cells in the bone marrow of cancer patients compared to in healthy donors and higher CD4+ T cells in the bone marrow samples with detectable disseminated cancer cells (Feuerer *et al*, 2001). Due to the lack of comparisons between the bone microenvironment in immunocompetent and immunocompromised strains in the literature, I decided to explore this in my studies. As discussed in chapter 3, no significant difference was observed in T cell counts from the bone marrow between the two strains, yet it is known that T cells

do not function in the immunocompromised strain, as they cannot mature due to the lack of a thymus (Belizario, 2009). However, my study only focused on the bone marrow; having information from the spleen would have allowed me to compare the T cell counts between strains. Lower numbers of B cells, granulocytes and monocyte counts were found in the bone marrow in BALB/c Nude compared to BALB/c mice. These cells originate from HSCs; since fewer HSC cells were found in BALB/c Nude mice compared to BALB/c, it makes sense to observe lower cell B cell counts due to lowered maintenance and production. However, B and T cells do not have a significant role in bone remodelling unless activated. When activated, B cells contribute to bone remodelling by expressing RANKL that stimulates osteoclast differentiation (Horowitz *et al*, 2010). The HSC niche has been suggested as a metastatic niche, and details of this are covered in chapter 5. Increased numbers of disseminated cancer cells were found following mobilisation of HSCs from the niche (Allocca *et al*, 2019). My studies showed that animals of the BALB/c Nude strain had fewer HSCs and HSC progenitors than those of the BALB/c strain; however, whether this cause any difference in bone metastases in BALB/c Nude than BALB/c is unknown. Collectively, my data support that the potential impact of these differences between immunocompetent and immunocompromised strains should be considered in preclinical studies of mechanisms of bone metastases and therapeutic effects.

6.2. Chemotherapy modifies the BME – implications for bone health and potential tumour development/progression

Doxorubicin (DOX) causes DNA breakage and is a commonly used chemotherapy agent to treat breast cancer. However, it is also toxic to normal tissues, including the bone marrow (Bachur, 2002), and can have several acute effects like nausea, vomiting, and gastrointestinal and neurologic disturbances (Carvalho *et al*, 2009). DOX is also used in treating early breast cancer without metastasis (Holmes *et al*, 1996; Biganzoli *et al*, 2002; Alba *et al*, 2004). In this setting, there is no evidence of tumour spread to the bone, however bone and marrow cells are exposed to repeated cycles of DOX. Besides the common cardiotoxicity of DOX, murine studies have showed DOX-mediated bone loss (Rana *et al*, 2013; Fan *et al*, 2017), loss of proliferation of bone marrow mesenchymal cells (Oliveira *et al*, 2014) and reduced bone marrow cell numbers (Huybrechts *et al*, 1979). Clinical studies have primarily focused on the bone destructive effects and cardiac toxicity effects of DOX (Shusterman & Meadows, 2000; Hadji *et al*, 2009). Overall, the anti-cancer benefits gained from DOX treatment are well-established, yet the effects of DOX on bone health and integrity should also be investigated.

My study determined the effects of DOX on bone that were detectable in samples obtained after repeated cycles of treatment. I administered four cycles of weekly DOX at different doses (4 and 6 mg/kg), measured the bone integrity with micro-computed tomography and used the same bones for histology so I could be able to quantify the osteoblasts and osteoclasts. Using flow cytometry, I could compare the general immune and HSC populations. The 4 mg DOX dose did damage bone integrity in BALB/c mice, whereas no significant effect was observed with this schedule in the BALB/c Nude mice. There may be several reasons for this difference in DOX sensitivity between the strains, including drug uptake, pharmacodynamics, and biological differences. However, my hypothesis about this difference is based on the findings described in chapter 3, showing that fewer HSCs are found in BALB/c Nude mice. Geerman *et al*. found that DOX is mainly harmful to cells that constantly divide when HSC maintenance is lower, which means HSCs stay more dormant (Geerman *et al*, 2018). As mentioned before, DOX targets dividing cells; thus, 4 mg/kg DOX dose might not affect LK and LSK cells in the BALB/c Nude. However, I did not carry flow cytometry analysis for 4 mg/kg DOX treatment, thus I cannot compare LK and LSK cells with the date from the 6 mg/kg DOX treatment. The colony forming unit assay showed similar numbers of functional HSCs/progenitor cells in control group of 4 mg/kg DOX experiment. In the 6 mg/kg DOX experiment, LK cells (HSCs progenitors) were increased in the DOX treated group compared to control. This increase might be caused by treatment-induced stress, causing HSCs to proliferate to recover. I hypothesise that this increase might cause bone loss, because Kuzmac *et al*. showed that creating acute stress on HSCs by bleeding C57BL/6j mice has resulted in more HSCs and increased osteoclast maturation (Kuzmac *et al*, 2014). These findings might be why no bone damage was observed with 4mg/kg treatment in the BALB/c Nude mice, because the dose was insufficient to induce HSC stress. Kuzmac *et al* also found that inducing stress on the HSCs resulted in B cell reduction, which is similar to my results (Kuzmac *et al*, 2014). Overall, maybe one of the mechanisms involved in DOX mediated bone loss is HSCs stress mechanisms, although further studies are required to test this hypothesis.

When the DOX dose was increased to 6 mg/kg, detrimental effects on the bone structure were observed in both strains, however there was no difference in the number of bone remodelling cells. Interestingly, HSC and their progenitor cells increased in the BALB/c Nude animals following DOX treatment, whereas no difference was observed in BALB/c mice. However, LK cells (i.e. common myeloid populations, granulocyte-macrophage progenitors and megakaryocytes-erythrocyte progenitors) increased in both strains following DOX treatment. All of the immune cells in the bone marrow of BALB/c except B cells were increased, and B cells were also decreased in the BALB/c Nude. However, B cells were suggested as a RANKL source and reduced RANKL from B cells reduced bone

resorption. Therefore, increased bone resorption must be caused by other mechanisms (Ponzetti & Rucci, 2019). Both strains had higher neutrophils following DOX treatment, and Bastian *et al*. suggest that increased neutrophils decrease the mineralised extracellular matrix (Bastian *et al*, 2018). Dendritic cells also increased in the bone marrow; however, only monocyte and granulocyte counts increased, and total white blood cell counts were not altered in either strain. Since dendritic cells were also found to play a role in innate immunity-induced bone loss (Liu & Teng, 2009), I hypothesise that increased general toxicity could trigger inflammation that can stimulate bone resorption, however this remains to be established, for example through measurement of inflammatory cytokines and histological assessment of immune cell infiltration in bone.

6.3. Quantifiable effects on bone marrow in the presence of tumour and effects of bone marrow alteration on bone metastasis.

As described in the introduction, the BME interacts with the tumour at all stages of development. Therefore, alteration of bone niches could affect tumour progression, as shown by Brown *et al*. They studied osteoblastic niche modification with parathyroid hormone (PTH) and observed increased osteoblasts and skeletal tumours following five days of PTH administered prior to breast tumour cell injection (Brown *et al*, 2018). HSCs are essential to maintain haematopoiesis but could also be involved in bone metastases due to the proposed shared niche with disseminated cancer cells (Allocca *et al*, 2019). However, it is not known if the mobilisation of HSCs impacts disseminated cancer cells. The HSC niche is where most HSCs reside, but as they are a rare population in the bone marrow (0.01% of the nucleated cells (Rossi *et al*, 2011)); their identification, isolation and analysis is challenging and mostly gathered with progenitors or require further purification (Hines *et al*, 2008; Challen *et al*, 2009). It has been suggested that cancer cells disseminate to the HSC niche (Shiozawa *et al*, 2011a; Allocca *et al*, 2019); these studies underlined the importance of DTC location during the dissemination but did not investigate whether mobilisation of HSCs influenced tumour development in bone. In my study, I have altered the HSCs niche with known HSC mobilisers (AMD3100 and G-CSF) and created bone metastatic breast cancer models in both immunocompetent and immunocompromised strains. After mobilising the HSCs from the bone marrow, my results showed earlier and more emergence of tumours. As discussed in chapter 5, there could be several explanations for this; however, my central hypothesis is that increased cancer cell dissemination due to the removal of HSCSs does increase survival of disseminated cancer cells in bone and hence the chances of overt

metastasis would be increased. However, there was considerable variation between the experiments I carried out to explore the effects of HSC mobilisation on bone metastasis; additional repeats of these studies are needed to allow firm conclusions to be drawn. The complex mechanisms underlying the impact of HSC mobilisation on DTCs should also be further investigated, as AMD3100 and G-CSF are used in clinical practice to support hematopoietic recovery in cancer patients undergoing chemotherapy. G-CSF are used to treat neutropenia after chemotherapy and AMD3100 is an effective HSC mobiliser. AMD3100 and G-CSF are used together to priming chemotherapy; thus replenish the patients HSCs (reviewed in (Liu *et al*, 2016)). This study creates a new question to discuss, does the use of AMD3100 or G-CSF in cancer treatment increase the chance of skeletal metastasis? To my knowledge, there are no reports suggesting this, despite stem cell support being part of routine treatment. It is likely that any stimulation of DTCs to grow would be counteracted by subsequent chemotherapy which was not covered by my study.

Another area where information is lacking in the literature is the effects on the BME caused by the presence of a tumour. Many studies have investigated the bone-destructive effects of osteolytic breast cancer, mainly focussing on tumour-induced changes to bone remodelling cells and how these may be prevented (Ottewell *et al*, 2008a, 2009; Hirbe *et al*, 2009; Lee *et al*, 2012). However, the bone environment is complex, and alterations in one bone niche can affect other, partially overlapping niches and their resident cell populations. Therefore, I have analysed the effects of the breast tumour on different bone and bone marrow populations, and white blood cell counts. An interesting finding was that there was no statistical bone volume reduction detected with CTAn software on the 21st day after tumour cell injection (end of the procedure), despite tumour-induced bone destruction being clearly visible in 3D reconstructions of tumour-bearing bones. As described in Ottewell *et al*., osteolytic lesions can be observed within 2-3 weeks with this model (BALB/c Nude animals injected with MDA-MB-231 cells via the intracardiac route) (Ottewell *et al*, 2008a). Peyruchaud *et al*. reported osteolytic lesions around 1mm^2 on the 20th day, and lesions increased seven-fold on the 30th day (Peyruchaud *et al*, 2001); therefore, a weakness of my study was ending the experiment too early for a significant tumour burden to be present, although I could detect bone metastasis in 9 out of 10 mice by IVIS. One limitation with the IVIS is that estimation of tumour size. Since IVIS detects the intensity of the signal from tumour, small tumours can be very bright depending on the labelling of the cells and the position of the tumour. I believe quantitative effects on bone integrity would be more evident if the disease progression advanced. No differences were found between the tumour-bearing and tumour-free bone marrow populations, probably due to the small size of the tumours. However, my experiment showed that if the protocol could be optimised, solid tumours could be detected and maybe quantified by flow

cytometry. Finally, I compared the white blood cell counts to determine if the tumour presence of tumours in bone resulted in any inflammatory effects of in the circulation. It is known that haematological malignancies such as leukaemia directly affects the white blood cells (Shipley & Butera, 2009). In contrast, neutropenia is mostly related with solid tumour chemotherapy side effects and studies focused on white blood cells (Asano *et al*, 2016). However, studies do not investigate if there is a detectable difference in the blood cell counts caused by a solid breast tumour in bone. In my study, there were no detectable differences in total white blood cells found between tumour bearing and tumour free animals. Overall, if the tumours are small, the bone marrow can maintain function and compensate for any tumour effects. As tumour burden increases, this ability is overcome, and the bone marrow will struggle to maintain its function. In future studies, I would repeat the experiment and study the impact of increasing tumour burden beyond three weeks if the animals are healthy under the ethical regulations.

6.4. Conclusion

This thesis describes a series of studies investigating the composition of the BMEs in different mouse models, and how they are affected by alterations using chemotherapy, stem cell mobilisers or bone metastatic breast cancer.

I found that that the numbers of HSCs, B cells and myeloid cells differed between immunocompetent and immunocompromised mice. There was also a difference in bone phenotypes (BALB/c Nude strain had less cortical bone volume and larger trabecular separation than BALB/c) between the strains, but I did not establish if the difference between these depends on the difference between cell populations; however, bone remodelling is a crucial process associated with development of bone metastases. My results indicate that the presence of an adaptive immune system might not be the only difference between immunocompromised/competent mouse models that should be considered when modelling bone metastases or interpreting the results.

Supporting that chemotherapy has detrimental effects on the skeleton, DOX-mediated bone loss was shown using both the murine models in this study, however I did observe differences in drug sensitivity between the strains. Results using the 4 mg/kg DOX dose showed that bone destructive effect was not observed in the immunocompetent strain, indicating that differences between the strains (active T lymphocytes, B lymphocytes, HSCs) could be a reason why BALB/c mice were less sensitive to DOX than BALB/c nude mice. Also, there could be differences in DOX pharmacokinetics and pharmacodynamics between the strains that contribute to these differences. Data from my study

support that effective drug doses cannot automatically be translated between different models and that dose-response experiments may need to be carried out to optimise dosing of therapeutic agents before future studies.

My results provide further support that the HSC niche may play a role in bone metastatic breast cancer, yet the precise mechanisms remain to be established. I found that removing HSCs (without altering the bone structure and remodelling cells) results in earlier overt metastasis; thus, increased cancer cell dissemination to the bone results in earlier metastatic development, although these findings should be supported by further experiments due to large variation in tumour progression. However, no visible difference was observed between the tumours when enough time was given for their development, demonstrating that any effect of HSC niche modification is at the early stages of bone metastasis (dissemination/colonisation/survival), and not on subsequent tumour progression.

My findings showed that the presence of DTCs from solid tumours in the bone marrow, as well as other cell types from the tumour-bearing bone marrow, could be detected with flow cytometry and could be quantified if the methods were further optimised, thus, allowing us to understand the effects of the tumour on the bone environment.

Overall, findings from this project support the importance of the BME on the course of breast cancer development and progression in bone that is negatively affected by chemotherapy agents and indicate that the haematopoietic niche should be further investigated to establish its role in tumour progression.

6.5. Summary of future work

Due to time limitations, I was unable to carry out further repeats and in-depth studies required to draw firmer conclusions in some areas. A summary of proposed future works is listed below:

- Further studies and optimisation of assays are needed to accurately quantify the number of different bone marrow cell populations and how they are impacted by therapy and the presence of tumour cells, as well as the differences between immunocompromised and competent mouse strains.
- One limitation of my studies is that all measurements are taken at endpoint, whereas bone remodelling and tumour progression are highly dynamic processes. To address this, larger scale experiment for DOX treatment must be performed where cohorts of mice are culled at regular intervals to allow measurement of bone integrity, bone marrow and bone turnover markers (CTX, NTX, ALP and osteocalcin) with increasing tumour burden.
- Another limitation was the size of the tumour when investigating cancer-induced bone effects. This study should be repeated to capture increased tumour burden in bone and ultimately advanced disease. This would allow us to determine the end effects of the tumour on the bone marrow cells.
- My findings indicated that commonly used drugs (AMD3100 and G-CSF) to replenish HSCs in the patients under chemotherapy caused increased tumour progression. In clinical use, patients continue to receive chemotherapy following stem cell support, and this would suppress the growth of any mobilised disseminated cancer cells. Therefore, a study using a combination study of HSCs mobilisers and chemotherapy is needed to test this hypothesis.
- Future studies are also needed to determine whether LSK, LK and B cells affect tumour progression with increased sample size, as this was one of the main limitations was on HSC mobilisation experiments in my thesis.
- If possible, the operator should be blinded to which treatment is given to which mouse to avoid bias in future studies.

REFERENCES

Aguirre-Ghiso JA (2007) Models, mechanisms and clinical evidence for cancer dormancy. *Nat Rev Cancer* **7**: 834–846, doi:10.1038/nrc2256.

Al-Mahmood S, Sapiezynski J, Garbuzenko OB, Minko T (2018) Metastatic and triple-negative breast cancer: challenges and treatment options. *Drug Deliv Transl Res* **8**: 1483–1507, doi:10.1007/s13346-018-0551-3.

Alba E, Martín M, Ramos M, Adrover E, Balil A, Jara C, Barnadas A, Fernández-Aramburo A, Sánchez-Rovira P, Amenedo M, Casado A (2004) Multicenter randomized trial comparing sequential with concomitant administration of doxorubicin and docetaxel as first-line treatment of metastatic breast cancer: A Spanish Breast Cancer Research Group (GEICAM-9903) phase III study. *J Clin Oncol* **22**: 2587–2593, doi:10.1200/JCO.2004.08.125.

Allocca G, Hughes R, Wang N, Brown HK, Ottewell PD, Brown NJ, Holen I (2019) The bone metastasis niche in breast cancer-potential overlap with the haematopoietic stem cell niche in vivo. *J Bone Oncol* **17**: doi:10.1016/j.jbo.2019.100244.

Alsamraae M, Cook LM (2021) Emerging roles for myeloid immune cells in bone metastasis. *Cancer Metastasis Rev* **40**: 413–425, doi:10.1007/s10555-021-09965-3.

Ammirante M, Luo J-L, Grivennikov S, Nedospasov S, Karin M (2010) B-cell-derived lymphotoxin promotes castration-resistant prostate cancer. *Nature* **464**: 302–305, doi:10.1038/nature08782.

Andre F, Dieci M V, Dubsky P, Sotiriou C, Curigliano G, Denkert C, Loi S (2013) Molecular Pathways: Involvement of Immune Pathways in the Therapeutic Response and Outcome in Breast Cancer. *Clin Cancer Res* **19**: 28–33, doi:10.1158/1078-0432.CCR-11-2701.

Antonio N, Bønnelykke-Behrndtz ML, Ward LC, Collin J, Christensen IJ, Steiniche T, Schmidt H, Feng Y, Martin P (2015) The wound inflammatory response exacerbates growth of pre-neoplastic cells and progression to cancer. *EMBO J* **34**: 2219–2236, doi:https://doi.org/10.15252/embj.201490147.

Ara T, Tokoyoda K, Sugiyama T, Egawa T, Kawabata K, Nagasawa T (2003) Long-term hematopoietic stem cells require stromal cell-derived factor-1 for colonizing bone marrow during ontogeny. *Immunity* **19**: 257–267, doi:10.1016/s1074-7613(03)00201-2.

Aramvash A, Chadegani AR, Lotfi S (2017) Evaluation of apoptosis in multipotent hematopoietic cells

of bone marrow by anthracycline antibiotics. *Iran J Pharm Res* **16**: 1206–1215.

Aramvash A, Rabbani-Chadegani A, Shahraki MK (2012) Evidence for the genotoxic effect of daunomycin in multipotent hematopoietic cells of mouse bone marrow: Chromatin proteins analysis. *J Pharm Biomed Anal* **66**: 204–210, doi:10.1016/j.jpba.2012.02.019.

Arron JR, Choi Y (2000) Bone versus immune system. *Nature* **408**: 535–536, doi:10.1038/35046196.

Asada N, Katayama Y, Sato M, Minagawa K, Wakahashi K, Kawano H, Kawano Y, Sada A, Ikeda K, Matsui T, Tanimoto M (2013) Matrix-Embedded Osteocytes Regulate Mobilization of Hematopoietic Stem/Progenitor Cells. *Cell Stem Cell* **12**: 737–747, doi:https://doi.org/10.1016/j.stem.2013.05.001.

Asano Y, Kashiwagi S, Onoda N, Noda S, Kawajiri H, Takashima T, Ohsawa M, Kitagawa S, Hirakawa K (2016) Platelet–Lymphocyte Ratio as a Useful Predictor of the Therapeutic Effect of Neoadjuvant Chemotherapy in Breast Cancer. *PLoS One* **11**: e0153459.

Atkinson EG, Delgado-Calle J (2019) The Emerging Role of Osteocytes in Cancer in Bone. *JBMR plus* **3**: e10186–e10186, doi:10.1002/jbm4.10186.

Aydiner A, Igci A, Cabioglu N, Ozer L, Sen F, Keskin S, Muslumanoglu M, Karanlik H, Arslan Ibis K, Kucucuk S, Dincer M, Yavuz E, Tuzlali S, Soran A (2019) Decision Pathways in Breast Cancer Management. In Breast Cancer : A Guide to Clinical Practice, A. Aydiner, A. Igci, and A. Soran, eds. (Cham: Springer International Publishing), pp. 3–97.

Bachur NR (2002) Anthracyclines. In Encyclopedia of Cancer, (Elsevier), pp. 57–61.

Baek KH, Oh KW, Lee WY, Lee SS, Kim MK, Kwon HS, Rhee EJ, Han JH, Song KH, Cha BY, Lee KW, Kang M Il (2010) Association of Oxidative Stress with Postmenopausal Osteoporosis and the Effects of Hydrogen Peroxide on Osteoclast Formation in Human Bone Marrow Cell Cultures. *Calcif Tissue Int* **87**: 226–235, doi:10.1007/s00223-010-9393-9.

BALB/c Nude Mouse | Charles River https://www.criver.com/products-services/find-model/balbc-nude-mouse?region=3616 (accessed: 04/07/2022).

Balkwill F, Mantovani A (2001) Inflammation and cancer: back to Virchow? *Lancet (London, England)* **357**: 539–545, doi:10.1016/S0140-6736(00)04046-0.

Barker JE (1997) Early transplantation to a normal microenvironment prevents the development of Steel hematopoietic stem cell defects. *Exp Hematol* **25**: 542–547.

Bastian OW, Croes M, Alblas J, Koenderman L, Leenen LPH, Blokhuis TJ (2018) Neutrophils inhibit synthesis of mineralized extracellular matrix by human bone marrow-derived stromal cells in vitro. *Front Immunol* **9**: doi:10.3389/fimmu.2018.00945.

Bayraktar S, Aydiner A (2019) Adjuvant Therapy for HER2-Positive Early-Stage Breast Cancer. In Breast Cancer : A Guide to Clinical Practice, A. Aydiner, A. Igci, and A. Soran, eds. (Cham: Springer International Publishing), pp. 383–411.

Bednarz-Knoll N, Alix-Panabières C, Pantel K (2011) Clinical relevance and biology of circulating tumor cells. *Breast Cancer Res* **13**: 228, doi:10.1186/bcr2940.

Belizario JE (2009) Immunodeficient Mouse Models: An Overview. *Open Immunol J* **2**: 79–85, doi:10.2174/1874226200902010079.

Bellido T (2014) Osteocyte-Driven Bone Remodeling. *Calcif Tissue Int* **94**: 25–34, doi:10.1007/s00223-013-9774-y.

Bellido T, Pajevic PD, Bonewald L (2018) Chapter 14 - Osteocyte Biology. R. V Thakker, M.P. Whyte, J.A. Eisman, and T.B.T.-G. of B.B. and S.D. (Second E. Igarashi, eds. (Academic Press), pp. 227–240.

Benner R, Meima F, van der Meulen GM, van Muiswinkel WB (1974) Antibody formation in mouse bone marrow. I. Evidence for the development of plaque-forming cells in situ. *Immunology* **26**: 247–255.

Berenson JR (2005) Recommendations for zoledronic acid treatment of patients with bone metastases. *Oncologist* **10**: 52–62, doi:10.1634/theoncologist.10-1-52.

Bernard M, Di Mauro P, Reynaud C, Diaz-Latoud C, Clézardin P (2019) Bone Metastases; Basic Aspects. *Encycl Endocr Dis* **4**: 304–309, doi:10.1016/b978-0-12-801238-3.65819-1.

Biganzoli L, Cufer T, Bruning P, Coleman R, Duchateau L, Calvert AH, Gamucci T, Twelves C, Fargeot P, Epelbaum R, Lohrisch C, Piccart MJ (2002) Doxorubicin and paclitaxel versus doxorubicin and cyclophosphamide as first-line chemotherapy in metastatic breast cancer: The European Organization for Research and Treatment of Cancer 10961 Multicenter Phase III Trial. *J Clin Oncol* **20**: 3114–3121, doi:10.1200/JCO.2002.11.005.

Blair HC, Teitelbaum SL, Ghiselli R, Gluck S (1989) Osteoclastic bone resorption by a polarized vacuolar proton pump. *Science (80-)* **245**: 855 LP – 857, doi:10.1126/science.2528207.

Bodogai M, Moritoh K, Lee-Chang C, Hollander CM, Sherman-Baust CA, Wersto RP, Araki Y, Miyoshi I, Yang L, Trinchieri G, Biragyn A (2015) Immunosuppressive and Prometastatic Functions of Myeloid-Derived Suppressive Cells Rely upon Education from Tumor-Associated B Cells. *Cancer Res* **75**: 3456–3465, doi:10.1158/0008-5472.CAN-14-3077.

Body J-J, Lipton A, Gralow J, Steger GG, Gao G, Yeh H, Fizazi K (2010) Effects of denosumab in patients with bone metastases with and without previous bisphosphonate exposure. *J Bone Miner Res* **25**: 440–446, doi:https://doi.org/10.1359/jbmr.090810.

Body JJ, Diel IJ, Lichinitzer M, Lazarev A, Pecherstorfer M, Bell R, Tripathy D, Bergstrom B (2004) Oral ibandronate reduces the risk of skeletal complications in breast cancer patients with metastatic bone disease: results from two randomised, placebo-controlled phase III studies. *Br J Cancer* **90**: 1133–1137, doi:10.1038/sj.bjc.6601663.

Boissier S, Ferreras M, Peyruchaud O, Magnetto S, Ebetino FH, Colombel M, Delmas P, Delaissé JM, Clézardin P (2000) Bisphosphonates inhibit breast and prostate carcinoma cell invasion, an early event in the formation of bone metastases. *Cancer Res* **60**: 2949–2954.

Bonewald LF (2010) Chapter 313 - Cell–Cell and Cell–Matrix Interactions in Bone. R.A. Bradshaw, and E.A.B.T.-H. of C.S. (Second E. Dennis, eds. (San Diego: Academic Press), pp. 2647–2662.

Bonewald LF (2011) The amazing osteocyte. *J Bone Miner Res* **26**: 229–238, doi:10.1002/jbmr.320.

Bonewald LF (2013) Chapter 10 - Osteocyte Biology. R. Marcus, D. Feldman, D.W. Dempster, M. Luckey, and J.A.B.T.-O. (Fourth E. Cauley, eds. (San Diego: Academic Press), pp. 209–234.

Boulais PE, Frenette PS (2015) Making sense of hematopoietic stem cell niches. *Blood* **125**: 2621–2629, doi:10.1182/blood-2014-09-570192.

Bray F, Ferlay J, Soerjomataram I, Siegel RL, Torre LA, Jemal A (2018) Global cancer statistics 2018: GLOBOCAN estimates of incidence and mortality worldwide for 36 cancers in 185 countries. *CA Cancer J Clin* **68**: 394–424, doi:10.3322/caac.21492.

Breastcancer.org Genetics: Breast Cancer Risk Factors https://www.breastcancer.org/risk/factors/genetics (accessed: 13/10/2020).

Broudy VC (1997) Stem Cell Factor and Hematopoiesis. *Blood* **90**: 1345–1364, doi:10.1182/blood.V90.4.1345.

Brown HK, Allocca G, Ottewell PD, Wang N, Brown NJ, Croucher PI, Eaton CL, Holen I (2018) Parathyroid hormone (PTH) increases skeletal tumour growth and alters tumour distribution in an in vivo model of breast cancer. *Int J Mol Sci* **19**: doi:10.3390/ijms19102920.

Brown HK, Ottewell PD, Evans CA, Holen I (2012) Location matters: Osteoblast and osteoclast distribution is modified by the presence and proximity to breast cancer cells in vivo. *Clin Exp Metastasis* **29**: 927–938, doi:10.1007/s10585-012-9481-5.

Broxmeyer HE (2008) Chemokines in hematopoiesis. *Curr Opin Hematol* **15**: 49–58, doi:10.1097/MOH.0b013e3282f29012.

Buenrostro D, Park SI, Sterling JA (2014) Dissecting the Role of Bone Marrow Stromal Cells on Bone Metastases. *Biomed Res Int* **2014**: 875305, doi:10.1155/2014/875305.

Bussard KM, Gay C V, Mastro AM (2008) The bone microenvironment in metastasis; what is special about bone? *Cancer Metastasis Rev* **27**: 41–55, doi:10.1007/s10555-007-9109-4.

Bussard KM, Venzon DJ, Mastro AM (2010) Osteoblasts are a major source of inflammatory cytokines in the tumor microenvironment of bone metastatic breast cancer. *J Cell Biochem* **111**: 1138–1148, doi:10.1002/jcb.22799.

Cabioglu N, Yavuz E, Aydiner A (2019) Breast Cancer Staging. In Breast Cancer : A Guide to Clinical Practice, A. Aydiner, A. Igci, and A. Soran, eds. (Cham: Springer International Publishing), pp. 99–122.

Caetano-Lopes J, Canhão H, Fonseca JE (2007) Osteoblasts and bone formation. *Acta Reumatol Port* **32**: 103–110.

Calì B, Molon B, Viola A (2017) Tuning cancer fate: the unremitting role of host immunity. *Open Biol* **7**: doi:10.1098/rsob.170006.

Calvi LM, Adams GB, Weibrecht KW, Weber JM, Olson DP, Knight MC, Martin RP, Schipani E, Divieti P, Bringhurst FR, Milner LA, Kronenberg HM, Scadden DT (2003) Osteoblastic cells regulate the haematopoietic stem cell niche. *Nature* **425**: 841–846, doi:10.1038/nature02040.

Campos SM (2004) Aromatase inhibitors for breast cancer in postmenopausal women. *Oncologist* **9**: 126–136, doi:10.1634/theoncologist.9-2-126.

Cancer Research UK (2016) Breast cancer diagnosis and treatment statistics | Cancer Research UK https://www.cancerresearchuk.org/health-professional/cancer-statistics/statistics-by-cancer-

type/breast-cancer/diagnosis-and-treatment#heading-Zero (accessed: 26/09/2020).

CancerResearch (2018) Cancer statistics for the UK http://www.cancerresearchuk.org/health-professional/cancer-statistics (accessed: 26/03/2019).

Canuas-Landero VG, George CN, Lefley D V, Corness H, Muthana M, Wilson C, Ottewell PD (2021) Oestradiol Contributes to Differential Antitumour Effects of Adjuvant Zoledronic Acid Observed Between Pre- and Post-Menopausal Women . *Front Endocrinol* **12**:.

Capietto A-H, Faccio R (2014) Immune regulation of bone metastasis. *Bonekey Rep* **3**: doi:10.1038/bonekey.2014.95.

Carlson RW (2005) The history and mechanism of action of fulvestrant. *Clin Breast Cancer* **6 Suppl 1**: S5-8, doi:10.3816/cbc.2005.s.008.

Carvalho C, Santos RX, Cardoso S, Correia S, Oliveira PJ, Santos MS, Moreira PI (2009) Doxorubicin: the good, the bad and the ugly effect. *Curr Med Chem* **16**: 3267–3285, doi:10.2174/092986709788803312.

Cawthorn TR, Amir E, Broom R, Freedman O, Gianfelice D, Barth D, Wang D, Holen I, Done SJ, Clemons M (2009) Mechanisms and pathways of bone metastasis: challenges and pitfalls of performing molecular research on patient samples. *Clin Exp Metastasis* **26**: 935–943, doi:10.1007/s10585-009-9284-5.

Ceradini DJ, Kulkarni AR, Callaghan MJ, Tepper OM, Bastidas N, Kleinman ME, Capla JM, Galiano RD, Levine JP, Gurtner GC (2004) Progenitor cell trafficking is regulated by hypoxic gradients through HIF-1 induction of SDF-1. *Nat Med* **10**: 858–864, doi:10.1038/nm1075.

Chae S, Kang KM, Kim HJ, Kang E, Park SY, Kim JH, Kim SH, Kim SW, Kim EK (2018) Neutrophil–Lymphocyte Ratio Predicts Response to Chemotherapy in Triple-Negative Breast Cancer. *Curr Oncol* **25**: doi:10.3747/co.25.3888.

Challen GA, Boles N, Lin KKY, Goodell MA (2009) Mouse hematopoietic stem cell identification and analysis. *Cytom Part A* **75**: 14–24, doi:10.1002/cyto.a.20674.

Chang AE, Wu Q V., Jenkins IC, Specht JM, Gadi VK, Gralow JR, Salazar LG, Kurland BF, Linden HM (2018) Phase I/II Trial of Combined Pegylated Liposomal Doxorubicin and Cyclophosphamide in Metastatic Breast Cancer. *Clin Breast Cancer* **18**: e143–e149, doi:10.1016/j.clbc.2017.10.005.

Charles A, Janeway J, Travers P, Walport M, Shlomchik MJ (2001) B-cell activation by armed helper T cells.

Charles KA, Kulbe H, Soper R, Escorcio-Correia M, Lawrence T, Schultheis A, Chakravarty P, Thompson RG, Kollias G, Smyth JF, Balkwill FR, Hagemann T (2009) The tumor-promoting actions of TNF-alpha involve TNFR1 and IL-17 in ovarian cancer in mice and humans. *J Clin Invest* **119**: 3011–3023, doi:10.1172/JCI39065.

Chatterjee C, Schertl P, Frommer M, Ludwig-Husemann A, Mohra A, Dilger N, Naolou T, Meermeyer S, Bergmann TC, Alonso Calleja A, Lee-Thedieck C (2021) Rebuilding the hematopoietic stem cell niche: Recent developments and future prospects. *Acta Biomater* **132**: 129–148, doi:https://doi.org/10.1016/j.actbio.2021.03.061.

Cheang MCU, Chia SK, Voduc D, Gao D, Leung S, Snider J, Watson M, Davies S, Bernard PS, Parker JS, Perou CM, Ellis MJ, Nielsen TO (2009) Ki67 index, HER2 status, and prognosis of patients with luminal B breast cancer. *J Natl Cancer Inst* **101**: 736–750, doi:10.1093/jnci/djp082.

Chen H, Senda T, Kubo K (2015) The osteocyte plays multiple roles in bone remodeling and mineral homeostasis. *Med Mol Morphol* **48**: 61–68, doi:10.1007/s00795-015-0099-y.

Chen W, Boras B, Sung T, Hu W, Spilker ME, D'Argenio DZ (2020a) Predicting Chemotherapy-Induced Neutropenia and Granulocyte Colony–Stimulating Factor Response Using Model-Based In Vitro to Clinical Translation. *AAPS J* **22**: 143, doi:10.1208/s12248-020-00529-x.

Chen Y, Chen K, Xiao X, Nie Y, Qu S, Gong C, Su F, Song E (2016) Pretreatment neutrophil-to-lymphocyte ratio is correlated with response to neoadjuvant chemotherapy as an independent prognostic indicator in breast cancer patients: a retrospective study. *BMC Cancer* **16**: 320, doi:10.1186/s12885-016-2352-8.

Chen Y, Luo X, Zou Z, Liang Y (2020b) The Role of Reactive Oxygen Species in Tumor Treatment and its Impact on Bone Marrow Hematopoiesis. *Curr Drug Targets* **21**: 477–498, doi:10.2174/1389450120666191021110208.

Chen YC, Sosnoski DM, Mastro AM (2010) Breast cancer metastasis to the bone: Mechanisms of bone loss. *Breast Cancer Res* **12**: doi:10.1186/bcr2781.

Chen Z, Ren X, Ren R, Wang Y, Shang J (2021) The combination of G-CSF and AMD3100 mobilizes bone marrow-derived stem cells to protect against cisplatin-induced acute kidney injury in mice.

Stem Cell Res Ther **12**: 209, doi:10.1186/s13287-021-02268-y.

Cheng T, Rodrigues N, Shen H, Yang Y, Dombkowski D, Sykes M, Scadden DT (2000) Hematopoietic Stem Cell Quiescence Maintained by p21cip1/waf1. *Science (80-)* **287**: 1804 LP – 1808, doi:10.1126/science.287.5459.1804.

Chinni SR, Sivalogan S, Dong Z, Filho JCT, Deng X, Bonfil RD, Cher ML (2006) CXCL12/CXCR4 signaling activates Akt-1 and MMP-9 expression in prostate cancer cells: the role of bone microenvironment-associated CXCL12. *Prostate* **66**: 32–48, doi:10.1002/pros.20318.

Chu E, DeVita VT (2018) Physicians' Cancer Chemotherapy Drug Manual 2019 (Jones & Bartlett Learning).

Clements ME, Johnson RW (2019) Breast Cancer Dormancy in Bone. *Curr Osteoporos Rep* **17**: 353–361, doi:10.1007/s11914-019-00532-y.

Clézardin P, Coleman R, Puppo M, Ottewell P, Bonnelye E, Paycha F, Confavreux CB, Holen I (2020) Bone metastasis: mechanisms, therapies, and biomarkers. *Physiol Rev* **101**: 797–855, doi:10.1152/physrev.00012.2019.

Clézardin P, Gligorov J, Delmas P (2000) Mechanisms of action of bisphosphonates on tumor cells and prospects for use in the treatment of malignant osteolysis. *Jt bone spine* **67**: 22–29.

Coffelt SB, Wellenstein MD, de Visser KE (2016) Neutrophils in cancer: neutral no more. *Nat Rev Cancer* **16**: 431–446, doi:10.1038/nrc.2016.52.

Coleman R (2016) Bone targeted treatments in cancer – The story so far. *J Bone Oncol* **5**: 90–92, doi:10.1016/j.jbo.2016.03.002.

Coleman R (2019) Clinical benefits of bone targeted agents in early breast cancer. *The Breast* **48**: S92–S96, doi:https://doi.org/10.1016/S0960-9776(19)31133-6.

Coleman R, de Boer R, Eidtmann H, Llombart A, Davidson N, Neven P, von Minckwitz G, Sleeboom HP, Forbes J, Barrios C, Frassoldati A, Campbell I, Paija O, Martin N, Modi A, Bundred N (2013) Zoledronic acid (zoledronate) for postmenopausal women with early breast cancer receiving adjuvant letrozole (ZO-FAST study): final 60-month results. *Ann Oncol Off J Eur Soc Med Oncol* **24**: 398–405, doi:10.1093/annonc/mds277.

Coleman R, Cameron D, Dodwell D, Bell R, Wilson C, Rathbone E, Keane M, Gil M, Burkinshaw R,

Grieve R, Barrett-Lee P, Ritchie D, Liversedge V, Hinsley S, Marshall H (2014) Adjuvant zoledronic acid in patients with early breast cancer: final efficacy analysis of the AZURE (BIG 01/04) randomised open-label phase 3 trial. *Lancet Oncol* **15**: 997–1006, doi:10.1016/S1470-2045(14)70302-X.

Coleman R, Finkelstein DM, Barrios C, Martin M, Iwata H, Hegg R, Glaspy J, Periañez AM, Tonkin K, Deleu I, Sohn J, Crown J, Delaloge S, Dai T, Zhou Y, Jandial D, Chan A (2020a) Adjuvant denosumab in early breast cancer (D-CARE): an international, multicentre, randomised, controlled, phase 3 trial. *Lancet Oncol* **21**: 60–72, doi:https://doi.org/10.1016/S1470-2045(19)30687-4.

Coleman R, Gnant M, Morgan G, Clezardin P (2012) Effects of bone-targeted agents on cancer progression and mortality. *J Natl Cancer Inst* **104**: 1059–1067, doi:10.1093/jnci/djs263.

Coleman R, Gray R, Powles T, Paterson A, Gnant M, Bergh J, Pritchard KI, Bliss J, Cameron D, Bradley R, Pan H, Peto R, Powles T, Burrett J, Clarke M, Davies C, Duane F, Evans V, Gettins L, Godwin J, Liu H, McGale P, Mackinnon E, McHugh T, James S, Morris P, Read S, Taylor C, Wang Y, Wang Z, Anderson S, Diel I, Gralow J, von Minckwitz G, Moebus V, Bartsch R, Dubsky P, Fesl C, Fohler H, Greil R, Jakesz R, Lang A, Luschin-Ebengreuth G, Marth C, Mlineritsch B, Samonigg H, Singer CF, Steger GG, Stoger H, Olivotto I, Ragaz J, Christiansen P, Ejlertsen B, Ewertz M, Jensen MB, Moller S, Mouridsen HT, Eiermann W, Hilfrich J, Jonat W, Kaufmann M, Kreienberg R, Schumacher M, Blohmer JU, Costa SD, Eidtmann H, Gerber B, Jackisch C, Loibl S, Dafni U, Markopoulos C, Blomqvist C, Saarto T, Ahn JH, Jung KH, Perrone F, Bass G, Brown A, Bryant J, Costantino J, Dignam J, Fisher B, Geyer C, Mamounas EP, Paik S, Redmond C, Swain S, Wickerham L, Wolmark N, Hadji P, Hern R, Dowsett M, Makris A, Parton M, Pennert K, Smith IE, Yarnold JR, Clack G, Van Poznak C, Safra T, Bell R, Dodwell D, Hinsley S, Marshall HC, Solomayer E, Fehm T, Lester J, Winter MC, Horsman JM, Aft R, Brufsky AM, Llombart HA, Perez E, Ingle JN, Suman VJ, Pritchard K, Albain K, Arriagada R, Barlow W, Bergsten-Nordstrom E, Boccardo F, Buyse M, Coates A, Correa C, Cuzick J, Davidson N, Di Leo A, Forbes J, Gelber R, Gianni L, Goldhirsch A, Hayes D, Hill C, Ingle J, Janni W, Martin M, Norton L, Ohashi Y, Piccart M, Pierce L, Raina V, Ravdin P, Robertson J, Rutgers E, Sparano J, Viale G, Wang X, Whelan T, Wilcken N, Winer E, Wood W (2015) Adjuvant bisphosphonate treatment in early breast cancer: Meta-analyses of individual patient data from randomised trials. *Lancet* **386**: 1353–1361, doi:10.1016/S0140-6736(15)60908-4.

Coleman RE, Collinson M, Gregory W, Marshall H, Bell R, Dodwell D, Keane M, Gil M, Barrett-Lee P, Ritchie D, Bowman A, Liversedge V, De Boer RH, Passos-Coelho JL, O'Reilly S, Bertelli G, Joffe J, Brown JE, Wilson C, Tercero JC, Jean-Mairet J, Gomis R, Cameron D (2018) Benefits and risks of adjuvant treatment with zoledronic acid in stage II/III breast cancer. 10 years follow-up of the AZURE

randomized clinical trial (BIG 01/04). *J bone Oncol* **13**: 123–135, doi:10.1016/j.jbo.2018.09.008.

Coleman RE, Croucher PI, Padhani AR, Clézardin P, Chow E, Fallon M, Guise T, Colangeli S, Capanna R, Costa L (2020b) Bone metastases. *Nat Rev Dis Prim* **6**: 83, doi:10.1038/s41572-020-00216-3.

Coleman RE, Lipton A, Roodman GD, Guise TA, Boyce BF, Brufsky AM, Clézardin P, Croucher PI, Gralow JR, Hadji P, Holen I, Mundy GR, Smith MR, Suva LJ (2010) Metastasis and bone loss: Advancing treatment and prevention. *Cancer Treat Rev* **36**: 615–620, doi:10.1016/j.ctrv.2010.04.003.

Coleman RE, Marshall H, Cameron D, Dodwell D, Burkinshaw R, Keane M, Gil M, Houston SJ, Grieve RJ, Barrett-Lee PJ, Ritchie D, Pugh J, Gaunt C, Rea U, Peterson J, Davies C, Hiley V, Gregory W, Bell R (2011) Breast-Cancer Adjuvant Therapy with Zoledronic Acid. *N Engl J Med* **365**: 1396–1405, doi:10.1056/NEJMoa1105195.

Coles CE, Choudhury A, Hoskin PJ, Jones CM, O'Leary B, Roques TW, Tharmalingam H, Yuille FAP (2020) COVID-19: A Catalyst for Change for UK Clinical Oncology. *Int J Radiat Oncol* **108**: 462–465, doi:https://doi.org/10.1016/j.ijrobp.2020.06.041.

Copson ER, Maishman TC, Tapper WJ, Cutress RI, Greville-Heygate S, Altman DG, Eccles B, Gerty S, Durcan LT, Jones L, Evans DG, Thompson AM, Pharoah P, Easton DF, Dunning AM, Hanby A, Lakhani S, Eeles R, Gilbert FJ, Hamed H, Hodgson S, Simmonds P, Stanton L, Eccles DM (2018) Germline BRCA mutation and outcome in young-onset breast cancer (POSH): a prospective cohort study. *Lancet Oncol* **19**: 169–180, doi:10.1016/S1470-2045(17)30891-4.

Costanzo-Garvey DL, Keeley T, Case AJ, Watson GF, Alsamraae M, Yu Y, Su K, Heim CE, Kielian T, Morrissey C, Frieling JS, Cook LM (2020) Neutrophils are mediators of metastatic prostate cancer progression in bone. *Cancer Immunol Immunother* **69**: 1113–1130, doi:10.1007/s00262-020-02527-6.

Coussens LM, Werb Z (2002) Inflammation and cancer. *Nature* **420**: 860–867, doi:10.1038/nature01322.

Cox TR, Rumney RMH, Schoof EM, Perryman L, Høye AM, Agrawal A, Bird D, Latif NA, Forrest H, Evans HR, Huggins ID, Lang G, Linding R, Gartland A, Erler JT (2015) The hypoxic cancer secretome induces pre-metastatic bone lesions through lysyl oxidase. *Nature* **522**: 106–110, doi:10.1038/nature14492.

Crane GM, Jeffery E, Morrison SJ (2017) Adult haematopoietic stem cell niches. *Nat Rev Immunol* **17**:

573–590, doi:10.1038/nri.2017.53.

Crenn V, Biteau K, Amiaud J, Dumars C, Guiho R, Vidal L, Nail L-R Le, Heymann D, Moreau A, Gouin F, Redini F (2017) Bone microenvironment has an influence on the histological response of osteosarcoma to chemotherapy: retrospective analysis and preclinical modeling. *Am J Cancer Res* **7**: 2333–2349.

Croucher PI, McDonald MM, Martin TJ (2016) Bone metastasis: the importance of the neighbourhood. *Nat Rev Cancer* **16**: 373–386, doi:10.1038/nrc.2016.44.

Cruet-Hennequart S, Prendergast ÁM, Shaw G, Barry FP, Carty MP (2012) Doxorubicin induces the DNA damage response in cultured human mesenchymal stem cells. *Int J Hematol* **96**: 649–656, doi:10.1007/s12185-012-1196-5.

Cui Y-XX, Evans BAJJ, Jiang WG (2016) New roles of osteocytes in proliferation, migration and invasion of breast and prostate cancer cells. *Anticancer Res* **36**: 1193–1202.

D'Oronzo S, Coleman R, Brown J, Silvestris F, Oronzo SD, Coleman R, Brown J, Silvestris F, D'Oronzo S, Coleman R, Brown J, Silvestris F (2019) Metastatic bone disease: Pathogenesis and therapeutic options: Up-date on bone metastasis management. *J Bone Oncol* **15**: 100205, doi:10.1016/j.jbo.2018.10.004.

Dai R, Wu Z, Chu HY, Lu J, Lyu A, Liu J, Zhang G (2020) Cathepsin K: The Action in and Beyond Bone . *Front Cell Dev Biol* **8**: 433.

Dallas SL, Bonewald LF (2010) Dynamics of the transition from osteoblast to osteocyte. *Ann N Y Acad Sci* **1192**: 437–443, doi:10.1111/j.1749-6632.2009.05246.x.

Dar A, Schajnovitz A, Lapid K, Kalinkovich A, Itkin T, Ludin A, Kao W-M, Battista M, Tesio M, Kollet O, Cohen NN, Margalit R, Buss EC, Baleux F, Oishi S, Fujii N, Larochelle A, Dunbar CE, Broxmeyer HE, Frenette PS, Lapidot T (2011) Rapid mobilization of hematopoietic progenitors by AMD3100 and catecholamines is mediated by CXCR4-dependent SDF-1 release from bone marrow stromal cells. *Leukemia* **25**: 1286–1296, doi:10.1038/leu.2011.62.

Daubiné F, Le Gall C, Gasser J, Green J, Clézardin P (2007) Antitumor Effects of Clinical Dosing Regimens of Bisphosphonates in Experimental Breast Cancer Bone Metastasis. *JNCI J Natl Cancer Inst* **99**: 322–330, doi:10.1093/jnci/djk054.

Davies C, Pan H, Godwin J, Gray R, Arriagada R, Raina V, Abraham M, Medeiros Alencar VH, Badran

A, Bonfill X, Bradbury J, Clarke M, Collins R, Davis SR, Delmestri A, Forbes JF, Haddad P, Hou M-F, Inbar M, Khaled H, Kielanowska J, Kwan W-H, Mathew BS, Mittra I, Muller B, Nicolucci A, Peralta O, Pernas F, Petruzelka L, Pienkowski T, Radhika R, Rajan B, Rubach MT, Tort S, Urrutia G, Valentini M, Wang Y, Peto R (2013) Long-term effects of continuing adjuvant tamoxifen to 10 years versus stopping at 5 years after diagnosis of oestrogen receptor-positive breast cancer: ATLAS, a randomised trial. *Lancet (London, England)* **381**: 805–816, doi:10.1016/S0140-6736(12)61963-1.

Decker AM, Jung Y, Cackowski F, Taichman RS (2016) The role of hematopoietic stem cell niche in prostate cancer bone metastasis. *J Bone Oncol* **5**: 117–120, doi:10.1016/j.jbo.2016.02.005.

Decker M, Leslie J, Liu Q, Ding L (2018) Hepatic thrombopoietin is required for bone marrow hematopoietic stem cell maintenance. *Science (80-)* **360**: 106 LP – 110, doi:10.1126/science.aap8861.

DeLeo FR, Nauseef WM (2015) 8 - Granulocytic Phagocytes. J.E. Bennett, R. Dolin, and M.J.B.T.-M. Blaser Douglas, and Bennett's Principles and Practice of Infectious Diseases (Eighth Edition), eds. (Philadelphia: W.B. Saunders), pp. 78-92.e6.

Delves P, Martin S, Burton D, Roitt I (2017) Roitt's essential immunology.

Deryugina EI, Zajac E, Juncker-Jensen A, Kupriyanova TA, Welter L, Quigley JP (2014) Tissue-infiltrating neutrophils constitute the major in vivo source of angiogenesis-inducing MMP-9 in the tumor microenvironment. *Neoplasia* **16**: 771–788, doi:10.1016/j.neo.2014.08.013.

Dieudonne F-X, Sévère N, Biosse-Duplan M, Weng J-J, Su Y, Marie PJ (2013) Promotion of osteoblast differentiation in mesenchymal cells through Cbl-mediated control of STAT5 activity. *Stem Cells* **31**: 1340–1349, doi:10.1002/stem.1380.

Ding L, Saunders TL, Enikolopov G, Morrison SJ (2012) Endothelial and perivascular cells maintain haematopoietic stem cells. *Nature* **481**: 457–462, doi:10.1038/nature10783.

Domazetovic V, Marcucci G, Iantomasi T, Brandi ML, Vincenzini MT (2017) Oxidative stress in bone remodeling: role of antioxidants. *Clin Cases Miner Bone Metab* **14**: 209–216, doi:10.11138/ccmbm/2017.14.1.209.

van de Donk NWCJ, Pawlyn C, Yong KL (2021) Multiple myeloma. *Lancet* **397**: 410–427, doi:https://doi.org/10.1016/S0140-6736(21)00135-5.

Drake MT, Clarke BL, Khosla S (2008) Bisphosphonates: mechanism of action and role in clinical

practice. *Mayo Clin Proc* **83**: 1032–1045, doi:10.4065/83.9.1032.

Dranoff G (2004) Cytokines in cancer pathogenesis and cancer therapy. *Nat Rev Cancer* **4**: 11–22, doi:10.1038/nrc1252.

Dunn LK, Mohammad KS, Fournier PGJ, McKenna CR, Davis HW, Niewolna M, Peng XH, Chirgwin JM, Guise TA (2009) Hypoxia and TGF-beta drive breast cancer bone metastases through parallel signaling pathways in tumor cells and the bone microenvironment. *PLoS One* **4**: e6896–e6896, doi:10.1371/journal.pone.0006896.

Early Breast Cancer Trialists' Collaborative Group (EBCTCG) (2015) Adjuvant bisphosphonate treatment in early breast cancer: meta-analyses of individual patient data from randomised trials. *Lancet* **386**: 1353–1361, doi:https://doi.org/10.1016/S0140-6736(15)60908-4.

Eash KJ, Greenbaum AM, Gopalan PK, Link DC (2010) CXCR2 and CXCR4 antagonistically regulate neutrophil trafficking from murine bone marrow. *J Clin Invest* **120**: 2423–2431, doi:10.1172/JCI41649.

Edwards CM, Zhuang J, Mundy GR (2008) The pathogenesis of the bone disease of multiple myeloma. *Bone* **42**: 1007–1013, doi:10.1016/j.bone.2008.01.027.

Emadi A, Jones RJ, Brodsky RA (2009) Cyclophosphamide and cancer: Golden anniversary. *Nat Rev Clin Oncol* **6**: 638–647, doi:10.1038/nrclinonc.2009.146.

Erler JT, Bennewith KL, Cox TR, Lang G, Bird D, Koong A, Le Q-TT, Giaccia AJ (2009) Hypoxia-Induced Lysyl Oxidase Is a Critical Mediator of Bone Marrow Cell Recruitment to Form the Premetastatic Niche. *Cancer Cell* **15**: 35–44, doi:10.1016/j.ccr.2008.11.012.

Ettl J, Quek RGW, Lee K-H, Rugo HS, Hurvitz S, Gonçalves A, Fehrenbacher L, Yerushalmi R, Mina LA, Martin M, Roché H, Im Y-H, Markova D, Bhattacharyya H, Hannah AL, Eiermann W, Blum JL, Litton JK (2018) Quality of life with talazoparib versus physician's choice of chemotherapy in patients with advanced breast cancer and germline BRCA1/2 mutation: patient-reported outcomes from the EMBRACA phase III trial. *Ann Oncol Off J Eur Soc Med Oncol* **29**: 1939–1947, doi:10.1093/annonc/mdy257.

Fabian CJ (2007) The what, why and how of aromatase inhibitors: hormonal agents for treatment and prevention of breast cancer. *Int J Clin Pract* **61**: 2051–2063, doi:10.1111/j.1742-1241.2007.01587.x.

Fan C, Georgiou KR, McKinnon RA, Keefe DMK, Howe PRC, Xian CJ (2016) Combination chemotherapy with cyclophosphamide, epirubicin and 5-fluorouracil causes trabecular bone loss, bone marrow cell depletion and marrow adiposity in female rats. *J Bone Miner Metab* **34**: 277–290, doi:10.1007/s00774-015-0679-x.

Fan C, Georgiou KR, Morris HA, McKinnon RA, Keefe DMKK, Howe PR, Xian CJ (2017) Combination breast cancer chemotherapy with doxorubicin and cyclophosphamide damages bone and bone marrow in a female rat model. *Breast Cancer Res Treat* **165**: 41–51, doi:10.1007/s10549-017-4308-3.

Fang Y, Sullivan R, Graham CH (2007) Confluence-dependent resistance to doxorubicin in human MDA-MB-231 breast carcinoma cells requires hypoxia-inducible factor-1 activity. *Exp Cell Res* **313**: 867–877, doi:https://doi.org/10.1016/j.yexcr.2006.12.004.

Farmen RK, Nordgård O, Gilje B, Shammas F V, Kvaløy JT, Oltedal S, Heikkilä R (2008) Bone marrow cytokeratin 19 mRNA level is an independent predictor of relapse-free survival in operable breast cancer patients. *Breast Cancer Res Treat* **108**: 251–258, doi:10.1007/s10549-007-9592-x.

FDA (2015) Zarxio Package Insert http://www.accessdata.fda.gov/drugsatfda_docs/label/2015/125553lbl.pdf (accessed: 20/06/2022).

Ferlay J, Colombet M, Soerjomataram I, Parkin DM, Piñeros M, Znaor A, Bray F (2021) Cancer statistics for the year 2020: An overview. *Int J Cancer* **149**: 778–789, doi:10.1002/ijc.33588.

Feuerer M, Rocha M, Bai L, Umansky V, Solomayer EF, Bastert G, Diel IJ, Schirrmacher V (2001) Enrichment of memory T cells and other profound immunological changes in the bone marrow from untreated breast cancer patients. *Int J Cancer* **92**: 96–105, doi:10.1002/1097-0215(200102)9999:9999<::AID-IJC1152>3.0.CO;2-Q.

Fidler IJ (2003) The pathogenesis of cancer metastasis: the 'seed and soil' hypothesis revisited. *Nat Rev Cancer* **3**: 453–458, doi:10.1038/nrc1098.

Finn RS, Crown JP, Lang I, Boer K, Bondarenko IM, Kulyk SO, Ettl J, Patel R, Pinter T, Schmidt M, Shparyk Y, Thummala AR, Voytko NL, Fowst C, Huang X, Kim ST, Randolph S, Slamon DJ (2015) The cyclin-dependent kinase 4/6 inhibitor palbociclib in combination with letrozole versus letrozole alone as first-line treatment of oestrogen receptor-positive, HER2-negative, advanced breast cancer (PALOMA-1/TRIO-18): a randomised phase 2 study. *Lancet Oncol* **16**: 25–35, doi:10.1016/S1470-2045(14)71159-3.

Finn RS, Martin M, Rugo HS, Jones S, Im S-A, Gelmon K, Harbeck N, Lipatov ON, Walshe JM, Moulder S, Gauthier E, Lu DR, Randolph S, Diéras V, Slamon DJ (2016) Palbociclib and Letrozole in Advanced Breast Cancer. *N Engl J Med* **375**: 1925–1936, doi:10.1056/NEJMoa1607303.

Fizazi K, Lipton A, Mariette X, Body J-J, Rahim Y, Gralow JR, Gao G, Wu L, Sohn W, Jun S (2009) Randomized phase II trial of denosumab in patients with bone metastases from prostate cancer, breast cancer, or other neoplasms after intravenous bisphosphonates. *J Clin Oncol Off J Am Soc Clin Oncol* **27**: 1564–1571, doi:10.1200/JCO.2008.19.2146.

Flanagan SP (1966) 'Nude', a new hairless gene with pleiotropic effects in the mouse. *Genet Res* **8**: 295–309, doi:10.1017/s0016672300010168.

Fluegen G, Avivar-Valderas A, Wang Y, Padgen MR, Williams JK, Nobre AR, Calvo V, Cheung JF, Bravo-Cordero JJ, Entenberg D, Castracane J, Verkhusha V, Keely PJ, Condeelis J, Aguirre-Ghiso JA (2017) Phenotypic heterogeneity of disseminated tumour cells is preset by primary tumour hypoxic microenvironments. *Nat Cell Biol* **19**: 120–132, doi:10.1038/ncb3465.

Fong MY, Zhou W, Liu L, Alontaga AY, Chandra M, Ashby J, Chow A, O'Connor STF, Li S, Chin AR, Somlo G, Palomares M, Li Z, Tremblay JR, Tsuyada A, Sun G, Reid MA, Wu X, Swiderski P, Ren X, Shi Y, Kong M, Zhong W, Chen Y, Wang SE (2015) Breast-cancer-secreted miR-122 reprograms glucose metabolism in premetastatic niche to promote metastasis. *Nat Cell Biol* **17**: 183–194, doi:10.1038/ncb3094.

Fong PC, Boss DS, Yap TA, Tutt A, Wu P, Mergui-Roelvink M, Mortimer P, Swaisland H, Lau A, O'Connor MJ, Ashworth A, Carmichael J, Kaye SB, Schellens JHM, de Bono JS (2009) Inhibition of poly(ADP-ribose) polymerase in tumors from BRCA mutation carriers. *N Engl J Med* **361**: 123–134, doi:10.1056/NEJMoa0900212.

Fonseca H, Carvalho A, Esteves J, Esteves VI, Moreira-Gonçalves D, Duarte JA (2016) Effects of doxorubicin administration on bone strength and quality in sedentary and physically active Wistar rats. *Osteoporos Int* **27**: 3465–3475, doi:10.1007/s00198-016-3672-x.

Fontanges E, Fontana A, Delmas P (2004) Osteoporosis and breast cancer. *Jt Bone Spine* **71**: 102–110, doi:10.1016/j.jbspin.2003.02.001.

Forest AE, Shiozawa Y, Pienta KJ, Taichman RS (2013) The Hematopoietic Stem Cell Niche and Bone Metastasis https://www.ncbi.nlm.nih.gov/books/NBK169225/ (accessed: 04/10/2020).

Foulkes WD, Smith IE, Reis-filho JS, Ph D (2010) Triple-negative breast cancer. *N Engl J Med* **363**: 1938–1948, doi:10.1056/NEJMra1001389.

Fournier PG, Stresing V, Ebetino FH, Clézardin P (2010) How do bisphosphonates inhibit bone metastasis in vivo? *Neoplasia* **12**: 571–578, doi:10.1593/neo.10282.

Fremder E, Munster M, Aharon A, Miller V, Gingis-Velitski S, Voloshin T, Alishekevitz D, Bril R, Scherer SJ, Loven D, Brenner B, Shaked Y (2014) Tumor-derived microparticles induce bone marrow-derived cell mobilization and tumor homing: a process regulated by osteopontin. *Int J cancer* **135**: 270–281, doi:10.1002/ijc.28678.

Friedlaender GE, Tross RB, Doganis AC, Kirkwood JM, Baron R (1984) Effects of chemotherapeutic agents on bone. I. Short-term methotrexate and doxorubicin (adriamycin) treatment in a rat model. *J Bone Jt Surg* **66**: 602–607, doi:10.2106/00004623-198466040-00016.

Fujiwara Y, Ando Y, Mukohara T, Kiyota N, Chayahara N, Mitsuma A, Inada-Inoue M, Sawaki M, Ilaria R, Kellie Turner P, Funai J, Maeda K, Minami H (2013) A phase i study of tasisulam sodium using an albumin-tailored dose in Japanese patients with advanced solid tumors. *Cancer Chemother Pharmacol* **71**: 991–998, doi:10.1007/s00280-013-2092-2.

Gajria D, Chandarlapaty S (2011) HER2-amplified breast cancer: mechanisms of trastuzumab resistance and novel targeted therapies. *Expert Rev Anticancer Ther* **11**: 263–275, doi:10.1586/era.10.226.

Galán-Díez M, Kousteni S (2018) A bone marrow niche-derived molecular switch between osteogenesis and hematopoiesis. *Genes Dev* **32**: 324–326, doi:10.1101/gad.314013.118.

Ganatra S, Nohria A, Shah S, Groarke JD, Sharma A, Venesy D, Patten R, Gunturu K, Zarwan C, Neilan TG, Barac A, Hayek SS, Dani S, Solanki S, Mahmood SS, Lipshultz SE (2019) Upfront dexrazoxane for the reduction of anthracycline-induced cardiotoxicity in adults with preexisting cardiomyopathy and cancer: a consecutive case series. *Cardio-Oncology* **5**: 1, doi:10.1186/s40959-019-0036-7.

Gao JJ, Swain SM (2018) Luminal A Breast Cancer and Molecular Assays: A Review. *Oncologist* **23**: 556–565, doi:10.1634/theoncologist.2017-0535.

García-Aranda M, Redondo M (2019) Immunotherapy: A Challenge of Breast Cancer Treatment. *Cancers (Basel)* **11**: doi:10.3390/cancers11121822.

Garcia JA, Hutson TE, Shepard D, Elson P, Dreicer R (2011) Gemcitabine and docetaxel in metastatic,

castrate-resistant prostate cancer. *Cancer* **117**: 752–757, doi:10.1002/cncr.25457.

Garle MJ, Fentem JH, Fry JR (1994) In vitro cytotoxicity tests for the prediction of acute toxicity in vivo. *Toxicol Vitr* **8**: 1303–1312, doi:https://doi.org/10.1016/0887-2333(94)90123-6.

Gawrzak S, Rinaldi L, Gregorio S, Arenas EJ, Salvador F, Urosevic J, Figueras-Puig C, Rojo F, del Barco Barrantes I, Cejalvo JM, Palafox M, Guiu M, Berenguer-Llergo A, Symeonidi A, Bellmunt A, Kalafatovic D, Arnal-Estapé A, Fernández E, Müllauer B, Groeneveld R, Slobodnyuk K, Stephan-Otto Attolini C, Saura C, Arribas J, Cortes J, Rovira A, Muñoz M, Lluch A, Serra V, Albanell J, Prat A, Nebreda AR, Benitah SA, Gomis RR (2018) MSK1 regulates luminal cell differentiation and metastatic dormancy in ER+ breast cancer. *Nat Cell Biol* **20**: 211–221, doi:10.1038/s41556-017-0021-z.

Geerman S, Brasser G, Bhusha S, Salerno F, Kragten NA, Hoogenboezem M, de Haan G, Wolkers M, Pascutti M, Nolte M (2018) Memory CD8+ T cells support the maintenance of hematopoietic stem cells in the bone marrow. *Haematologica* **103**: e230–e233, doi:10.3324/haematol.2017.169516.

Gerratana L, Fanotto V, Bonotto M, Bolzonello S, Minisini AM, Fasola G, Puglisi F (2015) Pattern of metastasis and outcome in patients with breast cancer. *Clin Exp Metastasis* **32**: 125–133, doi:10.1007/s10585-015-9697-2.

Ghajar CM, Peinado H, Mori H, Matei IR, Evason KJ, Brazier H, Almeida D, Koller A, Hajjar KA, Stainier DYR, Chen EI, Lyden D, Bissell MJ (2013) The perivascular niche regulates breast tumour dormancy. *Nat Cell Biol* **15**: 807–817, doi:10.1038/ncb2767.

Gillespie MT (2007) Impact of cytokines and T lymphocytes upon osteoclast differentiation and function. *Arthritis Res Ther* **9**: 103, doi:10.1186/ar2141.

Gnant M, Eidtmann H (2010) The anti-tumor effect of bisphosphonates ABCSG-12, ZO-FAST and more .. *Crit Rev Oncol Hematol* **74 Suppl 1**: S2-6, doi:10.1016/S1040-8428(10)70003-2.

Gomis RR, Gawrzak S (2017) Tumor cell dormancy. *Mol Oncol* **11**: 62–78, doi:10.1016/j.molonc.2016.09.009.

Graziano V, Grassadonia A, Iezzi L, Vici P, Pizzuti L, Barba M, Quinzii A, Camplese A, Di Marino P, Peri M, Veschi S, Alberti S, Gamucci T, Di Gioacchino M, De Tursi M, Natoli C, Tinari N (2019) Combination of peripheral neutrophil-to-lymphocyte ratio and platelet-to-lymphocyte ratio is predictive of pathological complete response after neoadjuvant chemotherapy in breast cancer patients. *The Breast* **44**: 33–38, doi:https://doi.org/10.1016/j.breast.2018.12.014.

Greenbaum A, Hsu Y-MS, Day RB, Schuettpelz LG, Christopher MJ, Borgerding JN, Nagasawa T, Link DC (2013) CXCL12 in early mesenchymal progenitors is required for haematopoietic stem-cell maintenance. *Nature* **495**: 227–230, doi:10.1038/nature11926.

Greenbaum AM, Link DC (2011) Mechanisms of G-CSF-mediated hematopoietic stem and progenitor mobilization. *Leukemia* **25**: 211–217, doi:10.1038/leu.2010.248.

Gusmão CVB de, Belangero WD (2015) HOW DO BONE CELLS SENSE MECHANICAL LOADING? *Rev Bras Ortop* **44**: 299–305, doi:10.1016/S2255-4971(15)30157-9.

Hadji P, Ziller M, Maskow C, Albert U, Kalder M (2009) The influence of chemotherapy on bone mineral density, quantitative ultrasonometry and bone turnover in pre-menopausal women with breast cancer. *Eur J Cancer* **45**: 3205–3212, doi:10.1016/j.ejca.2009.09.026.

Hadjidakis DJ, Androulakis II (2006) Bone Remodeling. *Ann N Y Acad Sci* **1092**: 385–396, doi:10.1196/annals.1365.035.

Haider M-T, Holen I, Dear TN, Hunter K, Brown HK (2014) Modifying the osteoblastic niche with zoledronic acid in vivo—Potential implications for breast cancer bone metastasis. *Bone* **66**: 240–250, doi:https://doi.org/10.1016/j.bone.2014.06.023.

Haider MT, Hunter KD, Robinson SP, Graham TJ, Corey E, Dear TN, Hughes R, Brown NJ, Holen I (2015) Rapid modification of the bone microenvironment following short-term treatment with Cabozantinib in vivo. *Bone* **81**: 581–592, doi:10.1016/j.bone.2015.08.003.

Haider MT, Smit DJ, Taipaleenmäki H (2020) The Endosteal Niche in Breast Cancer Bone Metastasis. *Front Oncol* **10**: 1–11, doi:10.3389/fonc.2020.00335.

Haley HR, Shen N, Qyli T, Buschhaus JM, Pirone M, Luker KE, Luker GD (2018) Enhanced Bone Metastases in Skeletally Immature Mice. *Tomogr (Ann Arbor, Mich)* **4**: 84–93, doi:10.18383/j.tom.2018.00010.

Hanley DA, Adachi JD, Bell A, Brown V (2012) Denosumab: mechanism of action and clinical outcomes. *Int J Clin Pract* **66**: 1139–1146, doi:10.1111/ijcp.12022.

Harbeck N, Penault-Llorca F, Cortes J, Gnant M, Houssami N, Poortmans P, Ruddy K, Tsang J, Cardoso F (2019) Breast cancer.

Hauge EM, Qvesel D, Eriksen EF, Mosekilde L, Melsen F (2001) Cancellous Bone Remodeling Occurs

in Specialized Compartments Lined by Cells Expressing Osteoblastic Markers. *J Bone Miner Res* **16**: 1575–1582, doi:10.1359/jbmr.2001.16.9.1575.

He N, Zhang L, Cui J, Li Z (2014) Bone Marrow Vascular Niche: Home for Hematopoietic Stem Cells. *Bone Marrow Res* **2014**: 128436, doi:10.1155/2014/128436.

He R, Geha RS (2010) Thymic stromal lymphopoietin. *Ann N Y Acad Sci* **1183**: 13–24, doi:10.1111/j.1749-6632.2009.05128.x.

Hill BS, Pelagalli A, Passaro N, Zannetti A (2017) Tumor-educated mesenchymal stem cells promote pro-metastatic phenotype. *Oncotarget* **8**: 73296–73311, doi:10.18632/oncotarget.20265.

Hines M, Nielsen L, Cooper-White J (2008) The hematopoietic stem cell niche: What are we trying to replicate? *J Chem Technol Biotechnol* **83**: 421–443, doi:10.1002/jctb.1856.

Hiraga T (2019) Bone metastasis: Interaction between cancer cells and bone microenvironment. *J Oral Biosci* **61**: 95–98, doi:10.1016/j.job.2019.02.002.

Hiraga T, Kizaka-Kondoh S, Hirota K, Hiraoka M, Yoneda T (2007) Hypoxia and hypoxia-inducible factor-1 expression enhance osteolytic bone metastases of breast cancer. *Cancer Res* **67**: 4157–4163, doi:10.1158/0008-5472.CAN-06-2355.

Hiraoka K, Zenmyo M, Watari K, Iguchi H, Fotovati A, Kimura YN, Hosoi F, Shoda T, Nagata K, Osada H, Ono M, Kuwano M (2008) Inhibition of bone and muscle metastases of lung cancer cells by a decrease in the number of monocytes/macrophages. *Cancer Sci* **99**: 1595–1602, doi:10.1111/j.1349-7006.2008.00880.x.

Hiratsuka S, Watanabe A, Aburatani H, Maru Y (2006) Tumour-mediated upregulation of chemoattractants and recruitment of myeloid cells predetermines lung metastasis. *Nat Cell Biol* **8**: 1369–1375, doi:10.1038/ncb1507.

Hirbe AC, Roelofs AJ, Floyd DH, Deng H, Becker SN, Lanigan LG, Apicelli AJ, Xu Z, Prior JL, Eagleton MC, Piwnica-Worms D, Rogers MJ, Weilbaecher K (2009) The bisphosphonate zoledronic acid decreases tumor growth in bone in mice with defective osteoclasts. *Bone* **44**: 908–916, doi:https://doi.org/10.1016/j.bone.2009.01.010.

Hirbe AC, Uluçkan Ö, Morgan EA, Eagleton MC, Prior JL, Piwnica-Worms D, Trinkaus K, Apicelli A, Weilbaecher K (2007) Granulocyte colony-stimulating factor enhances bone tumor growth in mice in an osteoclast-dependent manner. *Blood* **109**: 3424–3431, doi:10.1182/blood-2006-09-048686.

Hoffman-La Roche (2000) Product Monograph: PrXELODA®.

Holen I, Walker M, Nutter F, Fowles A, Evans CA, Eaton CL, Ottewell PD (2016) Oestrogen receptor positive breast cancer metastasis to bone: inhibition by targeting the bone microenvironment in vivo. *Clin Exp Metastasis* **33**: 211–224, doi:10.1007/s10585-015-9770-x.

Holmes FA, Madden T, Newman RA, Valero V, Theriault RL, Fraschini G, Walters RS, Booser DJ, Buzdar AU, Willey J, Hortobagyi GN (1996) Sequence-dependent alteration of doxorubicin pharmacokinetics by paclitaxel in a phase I study of paclitaxel and doxorubicin in patients with metastatic breast cancer. *J Clin Oncol* **14**: 2713–2721, doi:10.1200/JCO.1996.14.10.2713.

Hopman RK, DiPersio JF (2014) Advances in stem cell mobilization. *Blood Rev* **28**: 31–40, doi:10.1016/j.blre.2014.01.001.

Horowitz MC, Fretz JA, Lorenzo JA (2010) How B cells influence bone biology in health and disease. *Bone* **47**: 472–479, doi:10.1016/j.bone.2010.06.011.

Houghton AM, Rzymkiewicz DM, Ji H, Gregory AD, Egea EE, Metz HE, Stolz DB, Land SR, Marconcini LA, Kliment CR, Jenkins KM, Beaulieu KA, Mouded M, Frank SJ, Wong KK, Shapiro SD (2010) Neutrophil elastase-mediated degradation of IRS-1 accelerates lung tumor growth. *Nat Med* **16**: 219–223, doi:10.1038/nm.2084.

Huen MSY, Sy SMH, Chen J (2010) BRCA1 and its toolbox for the maintenance of genome integrity. *Nat Rev Mol Cell Biol* **11**: 138–148, doi:10.1038/nrm2831.

Hughes DE, Wright KR, Uy HL, Sasaki A, Yoneda T, Roodman GD, Mundy GR, Boyce BF (1995) Bisphosphonates promote apoptosis in murine osteoclasts in vitro and in vivo. *J bone Miner Res Off J Am Soc Bone Miner Res* **10**: 1478–1487, doi:10.1002/jbmr.5650101008.

Hughes R, Chen X, Cowley N, Ottewell PD, Hawkins RJ, Hunter KD, Hobbs JK, Brown NJ, Holen I (2021) Osteoblast-Derived Paracrine and Juxtacrine Signals Protect Disseminated Breast Cancer Cells from Stress. *Cancers (Basel)* **13**: doi:10.3390/cancers13061366.

Huybrechts M, Symann M, Trouet A (1979) Effects of Daunorubicin and Doxorubicin, Free and Associated with DNA, on Hemopoietic Stem Cells1. *Cancer Res* **39**: 3738–3743.

Infante JR, Cassier PA, Gerecitano JF, Witteveen PO, Chugh R, Ribrag V, Chakraborty A, Matano A, Dobson JR, Crystal AS, Parasuraman S, Shapiro GI (2016) A Phase I Study of the Cyclin-Dependent Kinase 4/6 Inhibitor Ribociclib (LEE011) in Patients with Advanced Solid Tumors and Lymphomas.

Clin cancer Res an Off J Am Assoc Cancer Res **22**: 5696–5705, doi:10.1158/1078-0432.CCR-16-1248.

Iqbal N, Iqbal N (2014) Human Epidermal Growth Factor Receptor 2 (HER2) in Cancers: Overexpression and Therapeutic Implications. *Mol Biol Int* **2014**: 852748, doi:10.1155/2014/852748.

Iwasaki M, Adachi Y, Minamino K, Suzuki Y, Zhang Y, Okigaki M, Nakano K, Koike Y, Wang J, Mukaide H, Taketani S, Mori Y, Takahashi H, Iwasaka T, Ikehara S (2005) Mobilization of Bone Marrow Cells by G-CSF Rescues Mice from Cisplatin-Induced Renal Failure, and M-CSF Enhances the Effects of G-CSF. *J Am Soc Nephrol* **16**: 658 LP – 666, doi:10.1681/ASN.2004010067.

Janeway CA, Travers JP, Walport M, Shlomchick MJ (2001) Immunobiology: The Immune System in Health and Disease. 5th edition. (New York: Garland Science).

Jani C, Salciccioli I, Rupal A, Al Omari O, Goodall R, Salciccioli JD, Marshall DC, Hanbury G, Singh H, Weissmann L, Shalhoub J (2021) Trends in Breast Cancer Mortality Between 2001 and 2017: An Observational Study in the European Union and the United Kingdom. *JCO Glob Oncol* 1682–1693, doi:10.1200/go.21.00288.

Janssen LME, Ramsay EE, Logsdon CD, Overwijk WW (2017) The immune system in cancer metastasis: Friend or foe? *J Immunother Cancer* **5**: 1–14, doi:10.1186/s40425-017-0283-9.

Jiang P, Gao W, Ma T, Wang R, Piao Y, Dong X, Wang P, Zhang X, Liu Y, Su W, Xiang R, Zhang J, Li N (2019) CD137 promotes bone metastasis of breast cancer by enhancing the migration and osteoclast differentiation of monocytes/macrophages. *Theranostics* **9**: 2950–2966, doi:10.7150/thno.29617.

Jiang Z, Yang Y, Li L, Yue Z, Lan L, Pan Z (2018) Capecitabine monotherapy in advanced breast cancer resistant to anthracycline and taxane: A meta-analysis. *J Cancer Res Ther* **14**: 957–963, doi:10.4103/0973-1482.187384.

Jilka RL (2013) The relevance of mouse models for investigating age-related bone loss in humans. *Journals Gerontol - Ser A Biol Sci Med Sci* **68**: 1209–1217, doi:10.1093/gerona/glt046.

Johnston S, Cheung K (2010) Fulvestrant - A Novel Endocrine Therapy for Breast Cancer. *Curr Med Chem* **17**: 902–914, doi:10.2174/092986710790820633.

Jones DH, Nakashima T, Sanchez OH, Kozieradzki I, Komarova S V, Sarosi I, Morony S, Rubin E, Sarao R, Hojilla C V, Komnenovic V, Kong Y-Y, Schreiber M, Dixon SJ, Sims SM, Khokha R, Wada T, Penninger JM (2006) Regulation of cancer cell migration and bone metastasis by RANKL. *Nature* **440**: 692–696, doi:10.1038/nature04524.

Joo YN, Jin H, Eun SY, Park SW, Chang KC, Kim HJ (2014) P2Y2R activation by nucleotides released from the highly metastatic breast cancer cell MDA-MB-231 contributes to pre-metastatic niche formation by mediating lysyl oxidase secretion, collagen crosslinking, and monocyte recruitment. *Oncotarget* **5**: 9322–9334, doi:10.18632/oncotarget.2427.

Jordan VC, Gapstur S, Morrow M (2001) Selective Estrogen Receptor Modulation and Reduction in Risk of Breast Cancer, Osteoporosis, and Coronary Heart Disease. *JNCI J Natl Cancer Inst* **93**: 1449–1457, doi:10.1093/jnci/93.19.1449.

Jung T, Castellana D, Klingbeil P, Cuesta Hernández I, Vitacolonna M, Orlicky DJ, Roffler SR, Brodt P, Zöller M (2009) CD44v6 dependence of premetastatic niche preparation by exosomes. *Neoplasia* **11**: 1093–1105, doi:10.1593/neo.09822.

Jung Y, Wang J, Lee E, McGee S, Berry JE, Yumoto K, Dai J, Keller ET, Shiozawa Y, Taichman RS (2015) Annexin 2-CXCL12 interactions regulate metastatic cell targeting and growth in the bone marrow. *Mol Cancer Res* **13**: 197–207, doi:10.1158/1541-7786.MCR-14-0118.

Jung Y, Wang J, Song J, Shiozawa Y, Wang J, Havens A, Wang Z, Sun Y-X, Emerson SG, Krebsbach PH, Taichman RS (2007) Annexin II expressed by osteoblasts and endothelial cells regulates stem cell adhesion, homing, and engraftment following transplantation. *Blood* **110**: 82–90, doi:10.1182/blood-2006-05-021352.

Kaplan RN, Riba RD, Zacharoulis S, Bramley AH, Vincent L, Costa C, MacDonald DD, Jin DK, Shido K, Kerns SA, Zhu Z, Hicklin D, Wu Y, Port JL, Altorki N, Port ER, Ruggero D, Shmelkov S V, Jensen KK, Rafii S, Lyden D (2005) VEGFR1-positive haematopoietic bone marrow progenitors initiate the pre-metastatic niche. *Nature* **438**: 820–827, doi:10.1038/nature04186.

Karnoub AE, Dash AB, Vo AP, Sullivan A, Brooks MW, Bell GW, Richardson AL, Polyak K, Tubo R, Weinberg RA (2007) Mesenchymal stem cells within tumour stroma promote breast cancer metastasis. *Nature* **449**: 557–563, doi:10.1038/nature06188.

Katoh M (2016) FGFR inhibitors: Effects on cancer cells, tumor microenvironment and whole-body homeostasis (Review). *Int J Mol Med* **38**: 3–15, doi:10.3892/ijmm.2016.2620.

Kawamoto H, Minato N (2004) Myeloid cells. *Int J Biochem Cell Biol* **36**: 1374–1379, doi:10.1016/j.biocel.2004.01.020.

Kenkre JS, Bassett JHD (2018) The bone remodelling cycle. *Ann Clin Biochem* **55**: 308–327,

doi:10.1177/0004563218759371.

Khosla S, Oursler MJ, Monroe DG (2012) Estrogen and the skeleton. *Trends Endocrinol Metab* **23**: 576–581, doi:10.1016/j.tem.2012.03.008.

Kimura S, Roberts AW, Metcalf D, Alexander WS (1998) Hematopoietic stem cell deficiencies in mice lacking c-Mpl, the receptor for thrombopoietin. *Proc Natl Acad Sci U S A* **95**: 1195–1200, doi:10.1073/pnas.95.3.1195.

Kloc M, Kubiak JZ, Li XC, Ghobrial RM (2015) Pericytes, microvasular dysfunction, and chronic rejection. *Transplantation* **99**: 658–667, doi:10.1097/TP.0000000000000648.

Kobayashi H, Butler JM, O'Donnell R, Kobayashi M, Ding B-S, Bonner B, Chiu VK, Nolan DJ, Shido K, Benjamin L, Rafii S (2010) Angiocrine factors from Akt-activated endothelial cells balance self-renewal and differentiation of haematopoietic stem cells. *Nat Cell Biol* **12**: 1046–1056, doi:10.1038/ncb2108.

Koboldt DC, Fulton RS, McLellan MD, Schmidt H, Kalicki-Veizer J, McMichael JF, Fulton LL, Dooling DJ, Ding L, Mardis ER, Wilson RK, Ally A, Balasundaram M, Butterfield YSN, Carlsen R, Carter C, Chu A, Chuah E, Chun HJE, Coope RJN, Dhalla N, Guin R, Hirst C, Hirst M, Holt RA, Lee D, Li HI, Mayo M, Moore RA, Mungall AJ, Pleasance E, Robertson AG, Schein JE, Shafiei A, Sipahimalani P, Slobodan JR, Stoll D, Tam A, Thiessen N, Varhol RJ, Wye N, Zeng T, Zhao Y, Birol I, Jones SJM, Marra MA, Cherniack AD, Saksena G, Onofrio RC, Pho NH, Carter SL, Schumacher SE, Tabak B, Hernandez B, Gentry J, Nguyen H, Crenshaw A, Ardlie K, Beroukhim R, Winckler W, Getz G, Gabriel SB, Meyerson M, Chin L, Kucherlapati R, Hoadley KA, Auman JT, Fan C, Turman YJ, Shi Y, Li L, Topal MD, He X, Chao HH, Prat A, Silva GO, Iglesia MD, Zhao W, Usary J, Berg JS, Adams M, Booker J, Wu J, Gulabani A, Bodenheimer T, Hoyle AP, Simons J V., Soloway MG, Mose LE, Jefferys SR, Balu S, Parker JS, Hayes DN, Perou CM, Malik S, Mahurkar S, Shen H, Weisenberger DJ, Triche T, Lai PH, Bootwalla MS, Maglinte DT, Berman BP, Van Den Berg DJ, Baylin SB, Laird PW, Creighton CJ, Donehower LA, Noble M, Voet D, Gehlenborg N, Di Cara D, Zhang J, Zhang H, Wu CJ, Yingchun Liu S, Lawrence MS, Zou L, Sivachenko A, Lin P, Stojanov P, Jing R, Cho J, Sinha R, Park RW, Nazaire MD, Robinson J, Thorvaldsdottir H, Mesirov J, Park PJ, Reynolds S, Kreisberg RB, Bernard B, Bressler R, Erkkila T, Lin J, Thorsson V, Zhang W, Shmulevich I, Ciriello G, Weinhold N, Schultz N, Gao J, Cerami E, Gross B, Jacobsen A, Sinha R, Aksoy BA, Antipin Y, Reva B, Shen R, Taylor BS, Ladanyi M, Sander C, Anur P, Spellman PT, Lu Y, Liu W, Verhaak RRG, Mills GB, Akbani R, Zhang N, Broom BM, Casasent TD, Wakefield C, Unruh AK, Baggerly K, Coombes K, Weinstein JN, Haussler D, Benz CC, Stuart JM, Benz SC, Zhu J, Szeto CC, Scott GK, Yau

C, Paull EO, Carlin D, Wong C, Sokolov A, Thusberg J, Mooney S, Ng S, Goldstein TC, Ellrott K, Grifford M, Wilks C, Ma S, Craft B, Yan C, Hu Y, Meerzaman D, Gastier-Foster JM, Bowen J, Ramirez NC, Black AD, Pyatt RE, White P, Zmuda EJ, Frick J, Lichtenberg TM, Brookens R, George MM, Gerken MA, Harper HA, Leraas KM, Wise LJ, Tabler TR, McAllister C, Barr T, Hart-Kothari M, Tarvin K, Saller C, Sandusky G, Mitchell C, Iacocca M V., Brown J, Rabeno B, Czerwinski C, Petrelli N, Dolzhansky O, Abramov M, Voronina O, Potapova O, Marks JR, Suchorska WM, Murawa D, Kycler W, Ibbs M, Korski K, Spychała A, Murawa P, Brzeziński JJ, Perz H, Łaźniak R, Teresiak M, Tatka H, Leporowska E, Bogusz-Czerniewicz M, Malicki J, Mackiewicz A, Wiznerowicz M, Van Le X, Kohl B, Viet Tien N, Thorp R, Van Bang N, Sussman H, Phu BD, Hajek R, Hung NP, Phuong TVT, Thang HQ, Khan KZ, Penny R, Mallery D, Curley E, Shelton C, Yena P, Ingle JN, Couch FJ, Lingle WL, King TA, Gonzalez-Angulo AM, Dyer MD, Liu S, Meng X, Patangan M, Waldman F, Stöppler H, Rathmell WK, Thorne L, Huang M, Boice L, Hill A, Morrison C, Gaudioso C, Bshara W, Daily K, Egea SC, Pegram MD, Gomez-Fernandez C, Dhir R, Bhargava R, Brufsky A, Shriver CD, Hooke JA, Campbell JL, Mural RJ, Hu H, Somiari S, Larson C, Deyarmin B, Kvecher L, Kovatich AJ, Ellis MJ, Stricker T, White K, Olopade O, Luo C, Chen Y, Bose R, Chang LW, Beck AH, Pihl T, Jensen M, Sfeir R, Kahn A, Chu A, Kothiyal P, Wang Z, Snyder E, Pontius J, Ayala B, Backus M, Walton J, Baboud J, Berton D, Nicholls M, Srinivasan D, Raman R, Girshik S, Kigonya P, Alonso S, Sanbhadti R, Barletta S, Pot D, Sheth M, Demchok JA, Shaw KRM, Yang L, Eley G, Ferguson ML, Tarnuzzer RW, Zhang J, Dillon LAL, Buetow K, Fielding P, Ozenberger BA, Guyer MS, Sofia HJ, Palchik JD (2012) Comprehensive molecular portraits of human breast tumours. *Nature* **490**: 61–70, doi:10.1038/nature11412.

Kollet O, Spiegel A, Peled A, Petit I, Byk T, Hershkoviz R, Guetta E, Barkai G, Nagler A, Lapidot T (2001) Rapid and efficient homing of human CD34(+)CD38(-/low)CXCR4(+) stem and progenitor cells to the bone marrow and spleen of NOD/SCID and NOD/SCID/B2m(null) mice. *Blood* **97**: 3283–3291, doi:10.1182/blood.v97.10.3283.

Kong C-Y, Guo Z, Song P, Zhang X, Yuan Y-P, Teng T, Yan L, Tang Q-Z (2022) Underlying the Mechanisms of Doxorubicin-Induced Acute Cardiotoxicity: Oxidative Stress and Cell Death. *Int J Biol Sci* **18**: 760–770, doi:10.7150/ijbs.65258.

Kristensen B, Ejlertsen B, Groenvold M, Hein S, Loft H, Mouridsen HT (1999) Oral clodronate in breast cancer patients with bone metastases: a randomized study. *J Intern Med* **246**: 67–74, doi:10.1046/j.1365-2796.1999.00507.x.

Kuchenbaecker KB, Hopper JL, Barnes DR, Phillips K-A, Mooij TM, Roos-Blom M-J, Jervis S, van Leeuwen FE, Milne RL, Andrieu N, Goldgar DE, Terry MB, Rookus MA, Easton DF, Antoniou AC,

Consortium and the B and BC (2017) Risks of Breast, Ovarian, and Contralateral Breast Cancer for BRCA1 and BRCA2 Mutation Carriers. *JAMA* **317**: 2402–2416, doi:10.1001/jama.2017.7112.

Kunisaki Y, Frenette PS (2014) Influences of vascular niches on hematopoietic stem cell fate. *Int J Hematol* **99**: 699–705, doi:10.1007/s12185-014-1580-4.

Kuperwasser C, Dessain S, Bierbaum BE, Garnet D, Sperandio K, Gauvin GP, Naber SP, Weinberg RA, Rosenblatt M (2005) A mouse model of human breast cancer metastasis to human bone. *Cancer Res* **65**: 6130–6138, doi:10.1158/0008-5472.CAN-04-1408.

Kusumbe AP (2016) Vascular niches for disseminated tumour cells in bone. *J Bone Oncol* **5**: 112–116, doi:10.1016/j.jbo.2016.04.003.

Kusumbe AP, Ramasamy SK, Adams RH (2014) Coupling of angiogenesis and osteogenesis by a specific vessel subtype in bone. *Nature* **507**: 323–328, doi:10.1038/nature13145.

Kuzmac S, Grcevic D, Sucur A, Ivcevic S, Katavic V (2014) Acute hematopoietic stress in mice is followed by enhanced osteoclast maturation in the bone marrow microenvironment. *Exp Hematol* **42**: 966–975, doi:10.1016/j.exphem.2014.07.262.

Lal JC, Townsend MG, Mehta AK, Oliwa M, Miller E, Sotayo A, Cheney E, Mittendorf EA, Letai A, Guerriero JL (2021) Comparing syngeneic and autochthonous models of breast cancer to identify tumor immune components that correlate with response to immunotherapy in breast cancer. *Breast Cancer Res* **23**: 83, doi:10.1186/s13058-021-01448-1.

Larosa DF, Orange JS (2008) 1. Lymphocytes. *J Allergy Clin Immunol* **121**: S364-9; quiz S412, doi:10.1016/j.jaci.2007.06.016.

Lee H-W, Choi H-J, Ha S-J, Lee K-T, Kwon Y-G (2013) Recruitment of monocytes/macrophages in different tumor microenvironments. *Biochim Biophys Acta - Rev Cancer* **1835**: 170–179, doi:https://doi.org/10.1016/j.bbcan.2012.12.007.

Lee H, Che J-H, Oh JE, Chung SS, Jung HS, Park KS (2014a) Bone marrow stem/progenitor cell mobilization in C57BL/6J and BALB/c mice. *Lab Anim Res* **30**: 14–20, doi:10.5625/lar.2014.30.1.14.

Lee J-HH, Kim H-HH-NHHHN, Kim K-OO, Jin WJ, Lee S, Kim H-HH-NHHHN, Ha H, Lee ZH (2012) CXCL10 Promotes Osteolytic Bone Metastasis by Enhancing Cancer Outgrowth and Osteoclastogenesis. *Cancer Res* **72**: 3175 LP – 3186, doi:10.1158/0008-5472.CAN-12-0481.

Lee JH, Kim B, Jin WJ, Kim JW, Kim HH, Ha H, Lee ZH (2014b) Trolox inhibits osteolytic bone metastasis of breast cancer through both PGE2-dependent and independent mechanisms. *Biochem Pharmacol* **91**: 51–60, doi:10.1016/j.bcp.2014.06.005.

Lee S-K, Kadono Y, Okada F, Jacquin C, Koczon-Jaremko B, Gronowicz G, Adams DJ, Aguila HL, Choi Y, Lorenzo JA (2006) T Lymphocyte–Deficient Mice Lose Trabecular Bone Mass With Ovariectomy. *J Bone Miner Res* **21**: 1704–1712, doi:https://doi.org/10.1359/jbmr.060726.

Lefley D, Howard F, Arshad F, Bradbury S, Brown H, Tulotta C, Eyre R, Alférez D, Wilkinson JM, Holen I, Clarke RB, Ottewell P (2019) Development of clinically relevant in vivo metastasis models using human bone discs and breast cancer patient-derived xenografts. *Breast Cancer Res* **21**: 130, doi:10.1186/s13058-019-1220-2.

Lévesque J-P, Hendy J, Winkler IG, Takamatsu Y, Simmons PJ (2003) Granulocyte colony-stimulating factor induces the release in the bone marrow of proteases that cleave c-KIT receptor (CD117) from the surface of hematopoietic progenitor cells. *Exp Hematol* **31**: 109–117, doi:https://doi.org/10.1016/S0301-472X(02)01028-7.

Lévesque J-P, Takamatsu Y, Nilsson SK, Haylock DN, Simmons PJ (2001) Vascular cell adhesion molecule-1 (CD106) is cleaved by neutrophil proteases in the bone marrow following hematopoietic progenitor cell mobilization by granulocyte colony-stimulating factor. *Blood* **98**: 1289–1297, doi:10.1182/blood.V98.5.1289.

Li J-Y, Tawfeek H, Bedi B, Yang X, Adams J, Gao KY, Zayzafoon M, Weitzmann MN, Pacifici R (2011) Ovariectomy disregulates osteoblast and osteoclast formation through the T-cell receptor CD40 ligand. *Proc Natl Acad Sci* **108**: 768–773, doi:10.1073/pnas.1013492108.

Li P, Lu M, Shi J, Hua L, Gong Z, Li Q, Shultz LD, Ren G (2020) Dual roles of neutrophils in metastatic colonization are governed by the host NK cell status. *Nat Commun* **11**: 4387, doi:10.1038/s41467-020-18125-0.

Li Z, Lan Y, He W, Chen D, Wang J, Zhou F, Wang Y, Sun H, Chen X, Xu C, Li S, Pang Y, Zhang G, Yang L, Zhu L, Fan M, Shang A, Ju Z, Luo L, Ding Y, Guo W, Yuan W, Yang X, Liu B (2012) Mouse Embryonic Head as a Site for Hematopoietic Stem Cell Development. *Cell Stem Cell* **11**: 663–675, doi:https://doi.org/10.1016/j.stem.2012.07.004.

Liang Y, Zhang H, Song X, Yang Q (2020) Metastatic heterogeneity of breast cancer: Molecular mechanism and potential therapeutic targets. *Semin Cancer Biol* **60**: 14–27,

doi:https://doi.org/10.1016/j.semcancer.2019.08.012.

Lipton A, Fizazi K, Stopeck AT, Henry DH, Brown JE, Yardley DA, Richardson GE, Siena S, Maroto P, Clemens M, Bilynskyy B, Charu V, Beuzeboc P, Rader M, Viniegra M, Saad F, Ke C, Braun A, Jun S (2012) Superiority of denosumab to zoledronic acid for prevention of skeletal-related events: A combined analysis of 3 pivotal, randomised, phase 3 trials. *Eur J Cancer* **48**: 3082–3092, doi:https://doi.org/10.1016/j.ejca.2012.08.002.

Liu F, Poursine-Laurent J, Link DC (2000) Expression of the G-CSF receptor on hematopoietic progenitor cells is not required for their mobilization by G-CSF. *Blood* **95**: 3025–3031, doi:10.1182/blood.V95.10.3025.

Liu L, Liu Y, Yan X, Zhou C, Xiong X (2020) The role of granulocyte colony-stimulating factor in breast cancer development: A review. *Mol Med Rep* **21**: 2019–2029, doi:10.3892/mmr.2020.11017.

Liu S, Jiang M, Zhao Q, Li S, Peng Y, Zhang P, Han M (2014) Vascular endothelial growth factor plays a critical role in the formation of the pre-metastatic niche via prostaglandin E2. *Oncol Rep* **32**: 2477–2484, doi:10.3892/or.2014.3516.

Liu T, Li X, You S, Bhuyan SS, Dong L (2016) Effectiveness of AMD3100 in treatment of leukemia and solid tumors: From original discovery to use in current clinical practice. *Exp Hematol Oncol* **5**: 19, doi:10.1186/s40164-016-0050-5.

Liu W-X, Li Z-J, Niu X-L, Yao Z, Deng W-M (2015) The Role of T Helper 17 Cells and Other IL-17-Producing Cells in Bone Resorption and Remodeling. *Int Rev Immunol* **34**: 332–347, doi:10.3109/08830185.2014.952414.

Liu Y, Zeng G (2012) Cancer and innate immune system interactions: translational potentials for cancer immunotherapy. *J Immunother* **35**: 299–308, doi:10.1097/CJI.0b013e3182518e83.

Liu YCG, Teng YTA (2009) Dendritic Cell-Associated Osteoclastogenesis and Bone Loss. *Clin Rev Bone Miner Metab* **7**: 269–284, doi:10.1007/s12018-009-9059-1.

Longley DB, Harkin DP, Johnston PG (2003) 5-Fluorouracil: Mechanisms of action and clinical strategies. *Nat Rev Cancer* **3**: 330–338, doi:10.1038/nrc1074.

Lorenzo J, Horowitz M, Choi Y (2008) Osteoimmunology: Interactions of the Bone and Immune System. *Endocr Rev* **29**: 403–440, doi:10.1210/er.2007-0038.

Lovitt CJ, Shelper TB, Avery VM (2018) Doxorubicin resistance in breast cancer cells is mediated by extracellular matrix proteins. *BMC Cancer* **18**: 41, doi:10.1186/s12885-017-3953-6.

Lowe JS, Anderson PG (2015a) Chapter 13 - Musculoskeletal System. J.S. Lowe, and P.G.B.T.-S.& L.H.H. (Fourth E. (Fourth E. Anderson, eds. (Philadelphia: Mosby), pp. 239–262.

Lowe JS, Anderson PG (2015b) Chapter 7 - Blood Cells. J.S. Lowe, and P.G.B.T.-S.& L.H.H. (Fourth E. (Fourth E. Anderson, eds. (Philadelphia: Mosby), pp. 105–122.

Lowe JS, Anderson PG (2015c) Chapter 8 - Immune System. J.S. Lowe, and P.G.B.T.-S.& L.H.H. (Fourth E. (Fourth E. Anderson, eds. (Philadelphia: Mosby), pp. 123–142.

Lubberts E, van den Bersselaar L, Oppers-Walgreen B, Schwarzenberger P, Coenen-de Roo CJJ, Kolls JK, Joosten LAB, van den Berg WB (2003) IL-17 Promotes Bone Erosion in Murine Collagen-Induced Arthritis Through Loss of the Receptor Activator of NF-κB Ligand/Osteoprotegerin Balance. *J Immunol* **170**: 2655–2662, doi:10.4049/jimmunol.170.5.2655.

Luga V, Zhang L, Viloria-Petit AM, Ogunjimi AA, Inanlou MR, Chiu E, Buchanan M, Hosein AN, Basik M, Wrana JL (2012) Exosomes Mediate Stromal Mobilization of Autocrine Wnt-PCP Signaling in Breast Cancer Cell Migration. *Cell* **151**: 1542–1556, doi:https://doi.org/10.1016/j.cell.2012.11.024.

Lugini L, Cecchetti S, Huber V, Luciani F, Macchia G, Spadaro F, Paris L, Abalsamo L, Colone M, Molinari A, Podo F, Rivoltini L, Ramoni C, Fais S (2012) Immune Surveillance Properties of Human NK Cell-Derived Exosomes. *J Immunol* **189**: 2833 LP – 2842, doi:10.4049/jimmunol.1101988.

Luo X, Fu Y, Loza AJ, Murali B, Leahy KM, Ruhland MK, Gang M, Su X, Zamani A, Shi Y, Lavine KJ, Ornitz DM, Weilbaecher KN, Long F, Novack D V., Faccio R, Longmore GD, Stewart SA (2016) Stromal-Initiated Changes in the Bone Promote Metastatic Niche Development. *Cell Rep* **14**: 82–92, doi:10.1016/j.celrep.2015.12.016.

Lv X, Dobrolecki LE, Ding Y, Rosen JM, Lewis MT, Chen X (2020) Orthotopic Transplantation of Breast Tumors as Preclinical Models for Breast Cancer. *J Vis Exp* doi:10.3791/61173.

Mackie EJ (2003) Osteoblasts: novel roles in orchestration of skeletal architecture. *Int J Biochem Cell Biol* **35**: 1301–1305, doi:https://doi.org/10.1016/S1357-2725(03)00107-9.

Maluf FC, de Oliveira FAM, Liedke PER, Brust L, Inocêncio CG, Monteiro FSM, Smaletz O, Cubero DI (2021) Neutropenia Prevention in the Treatment of Post-docetaxel Metastatic, Castration-resistant Prostate Cancer With Cabazitaxel and Prednisone: A Multicenter, Open-label, Single-arm Phase IV

Study. *Clin Genitourin Cancer* **19**: e171–e177, doi:10.1016/j.clgc.2020.12.008.

Mangialardi G, Cordaro A, Madeddu P (2016) The bone marrow pericyte: An orchestrator of vascular niche. *Regen Med* **11**: 883–895, doi:10.2217/rme-2016-0121.

Mantovani A, Allavena P, Sica A, Balkwill F (2008) Cancer-related inflammation. *Nature* **454**: 436–444, doi:10.1038/nature07205.

Mantovani A, Sica A (2010) Macrophages, innate immunity and cancer: balance, tolerance, and diversity. *Curr Opin Immunol* **22**: 231–237, doi:10.1016/j.coi.2010.01.009.

Marín Hernández C, Piñero Madrona A, Gil Vázquez PJ, Galindo Fernández PJ, Ruiz Merino G, Alonso Romero JL, Parrilla Paricio P (2018) Usefulness of lymphocyte-to-monocyte, neutrophil-to-monocyte and neutrophil-to-lymphocyte ratios as prognostic markers in breast cancer patients treated with neoadjuvant chemotherapy. *Clin Transl Oncol* **20**: 476–483, doi:10.1007/s12094-017-1732-0.

Maroni P (2019) Megakaryocytes in Bone Metastasis: Protection or Progression? *Cells* **8**: 134, doi:10.3390/cells8020134.

Massagué J, Obenauf AC (2016) Metastatic colonization by circulating tumour cells. *Nature* **529**: 298–306, doi:10.1038/nature17038.

Mayhew V, Omokehinde T, Johnson RW (2020) Tumor dormancy in bone. *Cancer Rep* **3**: e1156, doi:10.1002/cnr2.1156.

Mayol K, Biajoux V, Marvel J, Balabanian K, Walzer T (2011) Sequential desensitization of CXCR4 and S1P5 controls natural killer cell trafficking. *Blood* **118**: 4863–4871, doi:10.1182/blood-2011-06-362574.

McCann KE, Hurvitz SA (2018) Advances in the use of PARP inhibitor therapy for breast cancer. *Drugs Context* **7**: 212540, doi:10.7573/dic.212540.

Meads MB, Hazlehurst LA, Dalton WS (2008) The Bone Marrow Microenvironment as a Tumor Sanctuary and Contributor to Drug Resistance. *Clin Cancer Res* **14**: 2519–2526, doi:10.1158/1078-0432.CCR-07-2223.

Medzhitov R (2008) Origin and physiological roles of inflammation. *Nature* **454**: 428–435, doi:10.1038/nature07201.

Mehta RS, Barlow WE, Albain KS, Vandenberg TA, Dakhil SR, Tirumali NR, Lew DL, Hayes DF, Gralow

JR, Livingston RB, Hortobagyi GN (2012) Combination anastrozole and fulvestrant in metastatic breast cancer. *N Engl J Med* **367**: 435–444, doi:10.1056/NEJMoa1201622.

Méndez-Ferrer S, Bonnet D, Steensma DP, Hasserjian RP, Ghobrial IM, Gribben JG, Andreeff M, Krause DS (2020) Bone marrow niches in haematological malignancies. *Nat Rev Cancer* doi:10.1038/s41568-020-0245-2.

Méndez-Ferrer S, Michurina T V, Ferraro F, Mazloom AR, MacArthur BD, Lira SA, Scadden DT, Ma'ayan A, Enikolopov GN, Frenette PS (2010) Mesenchymal and haematopoietic stem cells form a unique bone marrow niche. *Nature* **466**: 829–834, doi:10.1038/nature09262.

Miki Y, Swensen J, Shattuck-Eidens D, Futreal PA, Harshman K, Tavtigian S, Liu Q, Cochran C, Bennett LM, Ding W (1994) A strong candidate for the breast and ovarian cancer susceptibility gene BRCA1. *Science* **266**: 66–71, doi:10.1126/science.7545954.

Di Mitri D, Toso A, Chen JJ, Sarti M, Pinton S, Jost TR, D'Antuono R, Montani E, Garcia-Escudero R, Guccini I, Da Silva-Alvarez S, Collado M, Eisenberger M, Zhang Z, Catapano C, Grassi F, Alimonti A (2014) Tumour-infiltrating Gr-1+ myeloid cells antagonize senescence in cancer. *Nature* **515**: 134–137, doi:10.1038/nature13638.

Mizushima N (2007) Autophagy: process and function. *Genes Dev* **21**: 2861–2873, doi:10.1101/gad.1599207.

Mohanty SS, Sahoo CR, Padhy RN (2022) Role of hormone receptors and HER2 as prospective molecular markers for breast cancer: An update. *Genes Dis* **9**: 648–658, doi:https://doi.org/10.1016/j.gendis.2020.12.005.

Mönkkönen H, Auriola S, Lehenkari P, Kellinsalmi M, Hassinen IE, Vepsäläinen J, Mönkkönen J (2006) A new endogenous ATP analog (AppppI) inhibits the mitochondrial adenine nucleotide translocase (ANT) and is responsible for the apoptosis induced by nitrogen-containing bisphosphonates. *Br J Pharmacol* **147**: 437–445, doi:10.1038/sj.bjp.0706628.

Monteiro AC, Leal AC, Gonçalves-Silva T, Mercadante ACT, Kestelman F, Chaves SB, Azevedo RB, Monteiro JP, Bonomo A (2013) T cells induce pre-metastatic osteolytic disease and help bone metastases establishment in a mouse model of metastatic breast cancer. *PLoS One* **8**: e68171, doi:10.1371/journal.pone.0068171.

Morris E V., Edwards CM (2016) The role of bone marrow adipocytes in bone metastasis. *J Bone*

Oncol **5**: 121–123, doi:10.1016/j.jbo.2016.03.006.

Morrison SJ, Scadden DT (2014) The bone marrow niche for haematopoietic stem cells. *Nature* **505**: 327–334, doi:10.1038/nature12984.

Müller A, Homey B, Soto H, Ge N, Catron D, Buchanan ME, McClanahan T, Murphy E, Yuan W, Wagner SN, Barrera JL, Mohar A, Verástegui E, Zlotnik A (2001) Involvement of chemokine receptors in breast cancer metastasis. *Nature* **410**: 50–56, doi:10.1038/35065016.

Mundy GR (2002) Metastasis to bone: Causes, consequences and therapeutic opportunities. *Nat Rev Cancer* **2**: 584–593, doi:10.1038/nrc867.

Munster PN, Thurn KT, Thomas S, Raha P, Lacevic M, Miller A, Melisko M, Ismail-Khan R, Rugo H, Moasser M, Minton SE (2011) A phase II study of the histone deacetylase inhibitor vorinostat combined with tamoxifen for the treatment of patients with hormone therapy-resistant breast cancer. *Br J Cancer* **104**: 1828–1835, doi:10.1038/bjc.2011.156.

Murray Brunt A, Haviland JS, Wheatley DA, Sydenham MA, Alhasso A, Bloomfield DJ, Chan C, Churn M, Cleator S, Coles CE, Goodman A, Harnett A, Hopwood P, Kirby AM, Kirwan CC, Morris C, Nabi Z, Sawyer E, Somaiah N, Stones L, Syndikus I, Bliss JM, Yarnold JR, Alhasso A, Armstrong A, Bliss J, Bloomfield D, Bowen J, Brunt M, Chan C, Chantler H, Churn M, Cleator S, Coles C, Donovan E, Goodman A, Griffin S, Haviland J, Hopwood P, Kirby A, Kirk J, Kirwan C, MacLennan M, Morris C, Nabi Z, Sawyer E, Sculphur M, Sinclair J, Somaiah N, Stones L, Sydenham M, Syndikus I, Tremlett J, Venables K, Wheatley D, Yarnold J (2020) Hypofractionated breast radiotherapy for 1 week versus 3 weeks (FAST-Forward): 5-year efficacy and late normal tissue effects results from a multicentre, non-inferiority, randomised, phase 3 trial. *Lancet* **395**: 1613–1626, doi:https://doi.org/10.1016/S0140-6736(20)30932-6.

Murthy RK, Loi S, Okines A, Paplomata E, Hamilton E, Hurvitz SA, Lin NU, Borges V, Abramson V, Anders C, Bedard PL, Oliveira M, Jakobsen E, Bachelot T, Shachar SS, Müller V, Braga S, Duhoux FP, Greil R, Cameron D, Carey LA, Curigliano G, Gelmon K, Hortobagyi G, Krop I, Loibl S, Pegram M, Slamon D, Palanca-Wessels MC, Walker L, Feng W, Winer EP (2019) Tucatinib, Trastuzumab, and Capecitabine for HER2-Positive Metastatic Breast Cancer. *N Engl J Med* **382**: 597–609, doi:10.1056/NEJMoa1914609.

Nagahisa H, Nagata Y, Ohnuki T, Osada M, Nagasawa T, Abe T, Todokoro K (1996) Bone marrow stromal cells produce thrombopoietin and stimulate megakaryocyte growth and maturation but

suppress proplatelet formation. *Blood* **87**: 1309–1316.

Nair AB, Jacob S (2016) A simple practice guide for dose conversion between animals and human. *J basic Clin Pharm* **7**: 27–31, doi:10.4103/0976-0105.177703.

Nakashima T, Hayashi M, Fukunaga T, Kurata K, Oh-Hora M, Feng JQ, Bonewald LF, Kodama T, Wutz A, Wagner EF, Penninger JM, Takayanagi H (2011) Evidence for osteocyte regulation of bone homeostasis through RANKL expression. *Nat Med* **17**: 1231–1234, doi:10.1038/nm.2452.

Nakashima T, Kobayashi Y, Yamasaki S, Kawakami A, Eguchi K, Sasaki H, Sakai H (2000) Protein expression and functional difference of membrane-bound and soluble receptor activator of NF-kappaB ligand: modulation of the expression by osteotropic factors and cytokines. *Biochem Biophys Res Commun* **275**: 768–775, doi:10.1006/bbrc.2000.3379.

National Statics (2020) Breast Screening Programme, England 2018-19 [NS] https://digital.nhs.uk/data-and-information/publications/statistical/breast-screening-programme/england---2018-19 (accessed: 25/05/2020).

Nehls M, Pfeifer D, Schorpp M, Hedrich H, Boehm T (1994) New member of the winged-helix protein family disrupted in mouse and rat nude mutations. *Nature* **372**: 103–107, doi:10.1038/372103a0.

Nesbitt S, Nesbit A, Helfrich M, Horton M (1993) Biochemical characterization of human osteoclast integrins. Osteoclasts express alpha v beta 3, alpha 2 beta 1, and alpha v beta 1 integrins. *J Biol Chem* **268**: 16737–16745.

Neudert M, Fischer C, Krempien B, Bauss F, Seibel MJ (2003) Site-specific human breast cancer (MDA-MB-231) metastases in nude rats: model characterisation and in vivo effects of ibandronate on tumour growth. *Int J cancer* **107**: 468–477, doi:10.1002/ijc.11397.

Neville-Webbe HL, Rostami-Hodjegan A, Evans CA, Coleman RE, Holen I (2005) Sequence- and schedule-dependent enhancement of zoledronic acid induced apoptosis by doxorubicin in breast and prostate cancer cells. *Int J Cancer* **113**: 364–371, doi:https://doi.org/10.1002/ijc.20602.

Nguyen KTP, Druhan LJ, Avalos BR, Zhai L, Rauova L, Nesmelova I V., Dréau D (2020) CXCL12-CXCL4 heterodimerization prevents CXCL12-driven breast cancer cell migration. *Cell Signal* **66**: 109488, doi:10.1016/j.cellsig.2019.109488.

NICE (2020) Managing advanced breast cancer - NICE Pathways https://pathways.nice.org.uk/pathways/advanced-breast-

cancer#path=view%3A/pathways/advanced-breast-cancer/managing-advanced-breast-cancer.xml&content=view-node%3Anodes-triple-negative-disease (accessed: 27/09/2020).

Nik-Zainal S, Davies H, Staaf J, Ramakrishna M, Glodzik D, Zou X, Martincorena I, Alexandrov LB, Martin S, Wedge DC, Van Loo P, Ju YS, Smid M, Brinkman AB, Morganella S, Aure MR, Lingjaerde OC, Langerod A, Ringner M, Ahn S-M, Boyault S, Brock JE, Broeks A, Butler A, Desmedt C, Dirix L, Dronov S, Fatima A, Foekens JA, Gerstung M, Hooijer GKJ, Jang SJ, Jones DR, Kim H-Y, King TA, Krishnamurthy S, Lee HJ, Lee J-Y, Li Y, McLaren S, Menzies A, Mustonen V, O'Meara S, Pauporte I, Pivot X, Purdie CA, Raine K, Ramakrishnan K, Rodriguez-Gonzalez FG, Romieu G, Sieuwerts AM, Simpson PT, Shepherd R, Stebbings L, Stefansson OA, Teague J, Tommasi S, Treilleux I, Van den Eynden GG, Vermeulen P, Vincent-Salomon A, Yates L, Caldas C, van't Veer L, Tutt A, Knappskog S, Tan BKT, Jonkers J, Borg A, Ueno NT, Sotiriou C, Viari A, Futreal PA, Campbell PJ, Span PN, Van Laere S, Lakhani SR, Eyfjord JE, Thompson AM, Birney E, Stunnenberg HG, van de Vijver MJ, Martens JWM, Borresen-Dale A-L, Richardson AL, Kong G, Thomas G, Stratton MR (2016) Landscape of somatic mutations in 560 breast cancer whole-genome sequences. *Nature* **534**: 47–54, doi:10.1038/nature17676.

Nombela-Arrieta C, Pivarnik G, Winkel B, Canty KJ, Harley B, Mahoney JE, Park S-Y, Lu J, Protopopov A, Silberstein LE (2013) Quantitative imaging of haematopoietic stem and progenitor cell localization and hypoxic status in the bone marrow microenvironment. *Nat Cell Biol* **15**: 533–543, doi:10.1038/ncb2730.

Norum JH, Andersen K, Sørlie T (2014) Lessons learned from the intrinsic subtypes of breast cancer in the quest for precision therapy. *Br J Surg* **101**: 925–938, doi:10.1002/bjs.9562.

Nutter F, Holen I, Brown HK, Cross SS, Alyson Evans C, Walker M, Coleman RE, Westbrook JA, Selby PJ, Brown JE, Ottewell PD (2014) Different molecular profiles are associated with breast cancer cell homing compared with colonisation of bone: Evidence using a novel bone-seeking cell line. *Endocr Relat Cancer* **21**: 327–341, doi:10.1530/ERC-13-0158.

O'Connell KE, Mikkola AM, Stepanek AM, Vernet A, Hall CD, Sun CC, Yildirim E, Staropoli JF, Lee JT, Brown DE (2015) Practical murine hematopathology: a comparative review and implications for research. *Comp Med* **65**: 96–113.

Oh D-Y, Bang Y-J (2020) HER2-targeted therapies — a role beyond breast cancer. *Nat Rev Clin Oncol* **17**: 33–48, doi:10.1038/s41571-019-0268-3.

Oliveira MS, Carvalho JL, Campos ACDA, Gomes DA, de Goes AM, Melo MM (2014) Doxorubicin has

in vivo toxicological effects on ex vivo cultured mesenchymal stem cells. *Toxicol Lett* **224**: 380–386, doi:10.1016/j.toxlet.2013.11.023.

Ono M, Kosaka N, Tominaga N, Yoshioka Y, Takeshita F, Takahashi R, Yoshida M, Tsuda H, Tamura K, Ochiya T (2014) Exosomes from bone marrow mesenchymal stem cells contain a microRNA that promotes dormancy in metastatic breast cancer cells. *Sci Signal* **7**: ra63, doi:10.1126/scisignal.2005231.

Ono T, Hayashi M, Sasaki F, Nakashima T (2020) RANKL biology: bone metabolism, the immune system, and beyond. *Inflamm Regen* **40**: 2, doi:10.1186/s41232-019-0111-3.

Ono T, Nakashima T (2018) Recent advances in osteoclast biology. *Histochem Cell Biol* **149**: 325–341, doi:10.1007/s00418-018-1636-2.

Ottewell PD (2016) The role of osteoblasts in bone metastasis. *J Bone Oncol* **5**: 124–127, doi:10.1016/j.jbo.2016.03.007.

Ottewell PD, Coleman RE, Holen I (2006) From genetic abnormality to metastases: Murine models of breast cancer and their use in the development of anticancer therapies. *Breast Cancer Res Treat* **96**: 101–113, doi:10.1007/s10549-005-9067-x.

Ottewell PD, Deux B, Mönkkönen H, Cross S, Coleman RE, Clezardin P, Holen I (2008a) Differential effect of doxorubicin and zoledronic acid on intraosseous versus extraosseous breast tumor growth in vivo. *Clin Cancer Res* **14**: 4658–4666, doi:10.1158/1078-0432.CCR-07-1545.

Ottewell PD, Lawson MA (2021) Advances in murine models of breast cancer bone disease. *J Cancer Metastasis Treat* **7**: 11, doi:10.20517/2394-4722.2021.14.

Ottewell PD, Monkkonen H, Jones M, Lefley D V., Coleman RE, Holen I (2008b) Antitumor Effects of Doxorubicin Followed by Zoledronic Acid in a Mouse Model of Breast Cancer. *JNCI J Natl Cancer Inst* **100**: 1167–1178, doi:10.1093/jnci/djn240.

Ottewell PD, Wang N, Brown HK, Reeves KJ, Fowles CA, Croucher PI, Eaton CL, Holen I (2014) Zoledronic Acid Has Differential Antitumor Activity in the Pre- and Postmenopausal Bone Microenvironment In Vivo. *Clin Cancer Res* **20**: 2922–2932, doi:10.1158/1078-0432.CCR-13-1246.

Ottewell PD, Woodward JK, Lefley D V., Evans CA, Coleman RE, Holen I (2009) Anticancer mechanisms of doxorubicin and zoledronic acid in breast cancer tumor growth in bone. *Mol Cancer Ther* **8**: 2821–2832, doi:10.1158/1535-7163.MCT-09-0462.

Ozer L, Aydiner A (2019) Adjuvant Chemotherapy for HER2-Negative Early-Stage Breast Cancer. In Breast Cancer : A Guide to Clinical Practice, A. Aydiner, A. Igci, and A. Soran, eds. (Cham: Springer International Publishing), pp. 357–381.

Palmieri C, Fullarton JR, Brown J (2013) Comparative efficacy of bisphosphonates in metastatic breast and prostate cancer and multiple myeloma: a mixed-treatment meta-analysis. *Clin cancer Res an Off J Am Assoc Cancer Res* **19**: 6863–6872, doi:10.1158/1078-0432.CCR-13-2275.

Pandya PH, Murray ME, Pollok KE, Renbarger JL (2016) The Immune System in Cancer Pathogenesis: Potential Therapeutic Approaches. *J Immunol Res* **2016**: 4273943, doi:10.1155/2016/4273943.

Paplomata E, O'Regan R (2014) The PI3K/AKT/mTOR pathway in breast cancer: targets, trials and biomarkers. *Ther Adv Med Oncol* **6**: 154–166, doi:10.1177/1758834014530023.

Park B, Lee HS, Lee JW, Park S (2019) Association of white blood cell count with breast cancer burden varies according to menopausal status, body mass index, and hormone receptor status: a case-control study. *Sci Rep* **9**: 5762, doi:10.1038/s41598-019-42234-6.

Park S-Y, Nam J-S (2020) The force awakens: metastatic dormant cancer cells. *Exp Mol Med* **52**: 569–581, doi:10.1038/s12276-020-0423-z.

Parvizi J, Kim GK (2010) Chapter 160 - Osteoblasts. J. Parvizi, and G.K.B.T.-H.Y.O. Kim, eds. (Philadelphia: W.B. Saunders), pp. 331–332.

Pasquini E, Gianni L, Aitini E, Nicolini M, Fattori PP, Cavazzini G, Desiderio F, Monti F, Forghieri ME, Ravaioli A (1995) Acute disseminated intravascular coagulation syndrome in cancer patients. *Oncol* **52**: 505–508, doi:10.1159/000227520.

Patel SA, Meyer JR, Greco SJ, Corcoran KE, Bryan M, Rameshwar P (2010) Mesenchymal stem cells protect breast cancer cells through regulatory T cells: role of mesenchymal stem cell-derived TGF-beta. *J Immunol* **184**: 5885–5894, doi:10.4049/jimmunol.0903143.

Peinado H, Zhang H, Matei IR, Costa-Silva B, Hoshino A, Rodrigues G, Psaila B, Kaplan RN, Bromberg JF, Kang Y, Bissell MJ, Cox TR, Giaccia AJ, Erler JT, Hiratsuka S, Ghajar CM, Lyden D (2017) Pre-metastatic niches: Organ-specific homes for metastases. *Nat Rev Cancer* **17**: 302–317, doi:10.1038/nrc.2017.6.

Pereira JP, An J, Xu Y, Huang Y, Cyster JG (2009) Cannabinoid receptor 2 mediates the retention of immature B cells in bone marrow sinusoids. *Nat Immunol* **10**: 403–411, doi:10.1038/ni.1710.

Perou CM, Sørlie T, Eisen MB, van de Rijn M, Jeffrey SS, Rees CA, Pollack JR, Ross DT, Johnsen H, Akslen LA, Fluge Ø, Pergamenschikov A, Williams C, Zhu SX, Lønning PE, Børresen-Dale A-L, Brown PO, Botstein D (2000) Molecular portraits of human breast tumours. *Nature* **406**: 747–752, doi:10.1038/35021093.

Petit I, Szyper-Kravitz M, Nagler A, Lahav M, Peled A, Habler L, Ponomaryov T, Taichman RS, Arenzana-Seisdedos F, Fujii N, Sandbank J, Zipori D, Lapidot T (2002) G-CSF induces stem cell mobilization by decreasing bone marrow SDF-1 and up-regulating CXCR4. *Nat Immunol* **3**: 687–694, doi:10.1038/ni813.

Peyruchaud O, Winding B, Pécheur I, Serre CM, Delmas P, Clézardin P (2001) Early detection of bone metastases in a murine model using fluorescent human breast cancer cells: Application to the use of the bisphosphonate zoledronic acid in the treatment of osteolytic lesions. *J Bone Miner Res* **16**: 2027–2034, doi:10.1359/jbmr.2001.16.11.2027.

Phan TG, Croucher PI (2020) The dormant cancer cell life cycle. *Nat Rev Cancer* **20**: 398–411, doi:10.1038/s41568-020-0263-0.

Piccart M, Parker LM, Pritchard KI (2003) Oestrogen receptor downregulation: an opportunity for extending the window of endocrine therapy in advanced breast cancer. *Ann Oncol* **14**: 1017–1025, doi:https://doi.org/10.1093/annonc/mdg290.

Planes-Laine G, Rochigneux P, Bertucci F, Chrétien A-S, Viens P, Sabatier R, Gonçalves A (2019) PD-1/PD-L1 Targeting in Breast Cancer: The First Clinical Evidences Are Emerging. A Literature Review. *Cancers (Basel)* **11**: 1033, doi:10.3390/cancers11071033.

Plumb JA (2004) Cell Sensitivity Assays: The MTT Assay BT - Cancer Cell Culture: Methods and Protocols. S.P. Langdon, ed. (Totowa, NJ: Humana Press), pp. 165–169.

Pohlmann PR, Mayer IA, Mernaugh R (2009) Resistance to Trastuzumab in Breast Cancer. *Clin Cancer Res* **15**: 7479–7491, doi:10.1158/1078-0432.CCR-09-0636.

Ponzetti M, Rucci N (2019) Updates on osteoimmunology: What's new on the cross-talk between bone and immune system. *Front Endocrinol (Lausanne)* **10**: doi:10.3389/fendo.2019.00236.

Porfyriou E, Letsa S, Kosmas C (2021) Hematopoietic stem cell mobilization strategies to support high-dose chemotherapy: A focus on relapsed/refractory germ cell tumors. *World J Clin Oncol* **12**: 746–766, doi:10.5306/wjco.v12.i9.746.

Pradhan S, Sperduto JL, Farino CJ, Slater JH (2018) Engineered In Vitro Models of Tumor Dormancy and Reactivation. *J Biol Eng* **12**: 37, doi:10.1186/s13036-018-0120-9.

Pritchard H, Micklem HS (1973) Haemopoietic stem cells and progenitors of functional T-lymphocytes in the bone marrow of 'nude' mice. *Clin Exp Immunol* **14**: 597–607.

Pugazhendhi A, Edison TNJI, Velmurugan BK, Jacob JA, Karuppusamy I (2018) Toxicity of Doxorubicin (Dox) to different experimental organ systems. *Life Sci* **200**: 26–30, doi:https://doi.org/10.1016/j.lfs.2018.03.023.

Qian Y, Tao J, Li X, Chen H, Lu Q, Yang J, Pan H, Wang C, Zhou W, Liu X (2018) Peripheral inflammation/immune indicators of chemosensitivity and prognosis in breast cancer patients treated with neoadjuvant chemotherapy. *Onco Targets Ther* **11**: 1423–1432, doi:10.2147/OTT.S148496.

Quail DF, Joyce JA (2013) Microenvironmental regulation of tumor progression and metastasis. *Nat Med* **19**: 1423–1437, doi:10.1038/nm.3394.

Quayle L, Ottewell P, Holen I (2015) Bone Metastasis: Molecular Mechanisms Implicated in Tumour Cell Dormancy in Breast and Prostate Cancer. *Curr Cancer Drug Targets* **15**: 469–480, doi:10.2174/1568009615666150506092443.

Ragonnaud E, Moritoh K, Bodogai M, Gusev F, Garaud S, Chen C, Wang X, Baljinnyam T, Becker KG, Maul RW, Willard-Gallo K, Rogaev E, Biragyn A (2019) Tumor-Derived Thymic Stromal Lymphopoietin Expands Bone Marrow B-cell Precursors in Circulation to Support Metastasis. *Cancer Res* **79**: 5826–5838, doi:10.1158/0008-5472.CAN-19-1058.

Rakha EA, Reis-Filho JS, Ellis IO (2008) Basal-like breast cancer: A critical review. *J Clin Oncol* **26**: 2568–2581, doi:10.1200/JCO.2007.13.1748.

Ramani K V, Ramani H, Alurkar S, Ajaikumar BS, Trivedi RG (2017) Breast Cancer: Medical Treatment, Side Effects, and Complementary Therapies (Momentum Press).

Ramasamy SK (2017) Structure and Functions of Blood Vessels and Vascular Niches in Bone. *Stem Cells Int* **2017**: 5046953, doi:10.1155/2017/5046953.

Ramasamy SK, Kusumbe AP, Adams RH (2015) Regulation of tissue morphogenesis by endothelial cell-derived signals. *Trends Cell Biol* **25**: 148–157, doi:https://doi.org/10.1016/j.tcb.2014.11.007.

Rana T, Chakrabarti A, Freeman M, Biswas S (2013) Doxorubicin-Mediated Bone Loss in Breast Cancer Bone Metastases Is Driven by an Interplay between Oxidative Stress and Induction of TGFβ. *PLoS One* **8**: e78043, doi:10.1371/journal.pone.0078043.

Rayner-Myers SD, Hunter K, Pituskin E (2022) Direct and Indirect Mechanisms of Chemotherapy-Induced Bone Loss in Adjuvant Breast Cancer: An Integrative Review. *Semin Oncol Nurs* **38**: 151280, doi:https://doi.org/10.1016/j.soncn.2022.151280.

Redig AJ, McAllister SS (2013) Breast cancer as a systemic disease: a view of metastasis. *J Intern Med* **274**: 113–126, doi:10.1111/joim.12084.

Ren G, Esposito M, Kang Y (2015) Bone metastasis and the metastatic niche. *J Mol Med (Berl)* **93**: 1203–1212, doi:10.1007/s00109-015-1329-4.

Ricciardelli C, Sakko AJ, Ween MP, Russell DL, Horsfall DJ (2009) The biological role and regulation of versican levels in cancer. *Cancer Metastasis Rev* **28**: 233–245, doi:10.1007/s10555-009-9182-y.

Richmond A, Yingjun S (2008) Mouse xenograft models vs GEM models for human cancer therapeutics. *DMM Dis Model Mech* **1**: 78–82, doi:10.1242/dmm.000976.

Rifas L, Arackal S, Weitzmann MN (2003) Inflammatory T cells rapidly induce differentiation of human bone marrow stromal cells into mature osteoblasts. *J Cell Biochem* **88**: 650–659, doi:10.1002/jcb.10436.

Riffel RM, Göbel A, Rachner TD (2022) Bone Metastases: From Mechanisms to Treatment. *Semin Oncol Nurs* **38**: 151277, doi:https://doi.org/10.1016/j.soncn.2022.151277.

Roato I, Ferracini R (2018) Cancer Stem Cells, Bone and Tumor Microenvironment: Key Players in Bone Metastases. *Cancers (Basel)* **10**: 56, doi:10.3390/cancers10020056.

Rodan GA, Fleisch HA (1996) Bisphosphonates: mechanisms of action. *J Clin Invest* **97**: 2692–2696, doi:10.1172/JCI118722.

Roder D, Houssami N, Farshid G, Gill G, Luke C, Downey P, Beckmann K, Iosifidis P, Grieve L, Williamson L (2008) Population screening and intensity of screening are associated with reduced breast cancer mortality: Evidence of efficacy of mammography screening in Australia. *Breast Cancer Res Treat* **108**: 409–416, doi:10.1007/s10549-007-9609-5.

Rogers MJ (2003) New insights into the molecular mechanisms of action of bisphosphonates. *Curr*

Pharm Des **9**: 2643–2658, doi:10.2174/1381612033453640.

Romagnolo DF, Daniels KD, Grunwald JT, Ramos SA, Propper CR, Selmin OI (2016) Epigenetics of breast cancer: Modifying role of environmental and bioactive food compounds. *Mol Nutr Food Res* **60**: 1310–1329, doi:10.1002/mnfr.201501063.

Rose AAN, Pepin F, Russo C, Abou Khalil JE, Hallett M, Siegel PM (2007) Osteoactivin Promotes Breast Cancer Metastasis to Bone. *Mol Cancer Res* **5**: 1001–1014, doi:10.1158/1541-7786.MCR-07-0119.

Rose AAN, Siegel PM (2006) Breast cancer-derived factors facilitate osteolytic bone metastasis. *Bull Cancer* **93**: 931–943.

Rosenkilde MM, Gerlach L-OO, Jakobsen JS, Skerlj RT, Bridger GJ, Schwartz TW (2004) Molecular Mechanism of AMD3100 Antagonism in the CXCR4 Receptor: TRANSFER OF BINDING SITE TO THE CXCR3 RECEPTOR*. *J Biol Chem* **279**: 3033–3041, doi:https://doi.org/10.1074/jbc.M309546200.

Rossi L, Challen GA, Sirin O, Lin KKY, Goodell MA (2011) Hematopoietic stem cell characterization and isolation. In Methods in Molecular Biology (Clifton, N.J.), pp. 47–59.

Russell RGG (2006) Bisphosphonates: from bench to bedside. *Ann N Y Acad Sci* **1068**: 367–401, doi:10.1196/annals.1346.041.

Saçma M, Matteini F, Mulaw MA, Hageb A, Bogeska R, Sakk V, Vollmer A, Marka G, Soller K, Milsom MD, Florian MC, Geiger H (2022) Fast and high-fidelity in situ 3D imaging protocol for stem cells and niche components for mouse organs and tissues. *STAR Protoc* **3**: 101483, doi:https://doi.org/10.1016/j.xpro.2022.101483.

Salhotra A, Shah HN, Levi B, Longaker MT (2020) Mechanisms of bone development and repair. *Nat Rev Mol Cell Biol* **21**: 696–711, doi:10.1038/s41580-020-00279-w.

Salvador F, Llorente A, Gomis RR (2019) From latency to overt bone metastasis in breast cancer: potential for treatment and prevention. *J Pathol* **249**: 6–18, doi:10.1002/path.5292.

Sapoznikov A, Pewzner-Jung Y, Kalchenko V, Krauthgamer R, Shachar I, Jung S (2008) Perivascular clusters of dendritic cells provide critical survival signals to B cells in bone marrow niches. *Nat Immunol* **9**: 388–395, doi:10.1038/ni1571.

Scherz-Shouval R, Santagata S, Mendillo ML, Sholl LM, Ben-Aharon I, Beck AH, Dias-Santagata D,

Koeva M, Stemmer SM, Whitesell L, Lindquist S (2014) The reprogramming of tumor stroma by HSF1 is a potent enabler of malignancy. *Cell* **158**: 564–578, doi:10.1016/j.cell.2014.05.045.

Schofield R (1978) The relationship between the spleen colony-forming cell and the haemopoietic stem cell. *Blood Cells* **4**: 7–25.

Schuettpelz LG, Link DC (2011) Niche competition and cancer metastasis to bone. *J Clin Invest* **121**: 1253–1255, doi:10.1172/JCI57229.

Scully OJ, Bay B-H, Yip G, Yu Y (2012) Breast Cancer Metastasis. *Cancer Genomics - Proteomics* **9**: 311–320.

Semerad CL, Christopher MJ, Liu F, Short B, Simmons PJ, Winkler I, Levesque J-P, Chappel J, Ross FP, Link DC (2005) G-CSF potently inhibits osteoblast activity and CXCL12 mRNA expression in the bone marrow. *Blood* **106**: 3020–3027, doi:10.1182/blood-2004-01-0272.

Seubert B, Grünwald B, Kobuch J, Cui H, Schelter F, Schaten S, Siveke JT, Lim NH, Nagase H, Simonavicius N, Heikenwalder M, Reinheckel T, Sleeman JP, Janssen K-P, Knolle PA, Krüger A (2015) Tissue inhibitor of metalloproteinases (TIMP)-1 creates a premetastatic niche in the liver through SDF-1/CXCR4-dependent neutrophil recruitment in mice. *Hepatology* **61**: 238–248, doi:10.1002/hep.27378.

Shah M, Nunes MR, Stearns V (2018) CDK4/6 Inhibitors: Game Changers in the Management of Hormone Receptor–Positive Advanced Breast Cancer? *Oncology (Williston Park)* **32**: 216–222.

Shapiro G, Rosen LS, Tolcher AW, Goldman JW, Gandhi L, Papadopoulos KP, Tolaney SM, Beeram M, Rasco DW, Kulanthaivel P, Li Q, Hu T, Cronier D, Chan EM, Flaherty K, Wen PY, Patnaik A (2013) A first-in-human phase I study of the CDK4/6 inhibitor, LY2835219, for patients with advanced cancer. *J Clin Oncol* **31**: 2500, doi:10.1200/jco.2013.31.15_suppl.2500.

Sheridan WP, Fox RM, Begley CG, Maher D, McGrath KM, Begley CG, Juttner CA, To LB, Szer J, Mostyn G (1992) Effect of peripheral-blood progenitor cells mobilised by filgrastim (G-CSF) on platelet recovery after high-dose chemotherapy. *Lancet* **339**: 640–644, doi:https://doi.org/10.1016/0140-6736(92)90795-5.

Shetty S, Kapoor N, Bondu J, Thomas N, Paul T (2016) Bone turnover markers: Emerging tool in the management of osteoporosis. *Indian J Endocrinol Metab* **20**: 846–852, doi:10.4103/2230-8210.192914.

Shiovitz S, Korde LA (2015) Genetics of breast cancer: A topic in evolution. *Ann Oncol* **26**: 1291–1299, doi:10.1093/annonc/mdv022.

Shiozawa Y, Pedersen EA, Havens AM, Jung Y, Mishra A, Joseph J, Kim JK, Patel LR, Ying C, Ziegler AM, Pienta MJ, Song J, Wang J, Loberg RD, Krebsbach PH, Pienta KJ, Taichman RS (2011a) Human prostate cancer metastases target the hematopoietic stem cell niche to establish footholds in mouse bone marrow. *J Clin Invest* **121**: 1298–1312, doi:10.1172/JCI43414.

Shiozawa Y, Pedersen EA, Patel LR, Ziegler AM, Havens AM, Jung Y, Wang J, Zalucha S, Loberg RD, Pienta KJ, Taichman RS (2010) GAS6/AXL Axis Regulates Prostate Cancer Invasion, Proliferation, and Survival in the Bone Marrow Niche. *Neoplasia* **12**: 116-IN4, doi:https://doi.org/10.1593/neo.91384.

Shiozawa Y, Pienta KJ, Taichman RS (2011b) Hematopoietic stem cell niche is a potential therapeutic target for bone metastatic tumors. *Clin Cancer Res* **17**: 5553–5558, doi:10.1158/1078-0432.CCR-10-2505.

Shipley JL, Butera JN (2009) Acute myelogenous leukemia. *Exp Hematol* **37**: 649–658, doi:10.1016/j.exphem.2009.04.002.

Shojaei F, Wu X, Zhong C, Yu L, Liang X-H, Yao J, Blanchard D, Bais C, Peale F V, van Bruggen N, Ho C, Ross J, Tan M, Carano RAD, Meng YG, Ferrara N (2007) Bv8 regulates myeloid-cell-dependent tumour angiogenesis. *Nature* **450**: 825–831, doi:10.1038/nature06348.

Shortman K, Liu Y-J (2002) Mouse and human dendritic cell subtypes. *Nat Rev Immunol* **2**: 151–161, doi:10.1038/nri746.

Shusterman S, Meadows AT (2000) Long term survivors of childhood leukemia. *Curr Opin Hematol* **7**: 217–222, doi:10.1097/00062752-200007000-00004.

Siegel RL, Miller KD, Fuchs HE, Jemal A (2022) Cancer statistics, 2022. *CA Cancer J Clin* **72**: 7–33, doi:10.3322/caac.21708.

Singh N, Baby D, Rajguru JP, Patil PB, Thakkannavar SS, Pujari VB (2019) Inflammation and cancer. *Ann Afr Med* **18**: 121–126, doi:10.4103/aam.aam_56_18.

Singh P, Pelus LM (2020) CXCR4 expression in the bone marrow microenvironment is required for hematopoietic stem and progenitor cell maintenance and early hematopoietic regeneration after myeloablation. 1–11, doi:10.1002/stem.3174.

Slamon DJ, Crown J, Lang I, Kulyk SO, Schmidt M, Patel R, Thummala A, Voytko NL, Randolph S, Kim S, Huang X, Bartlett CH, Schnell P, Finn RS (2015) Long-term safety profile of palbociclib (P) in combination with letrozole (L) as first-line treatment for postmenopausal patients with ER+ and HER2- advanced breast cancer (ABC) (PALOMA-1/TRIO-18). *J Clin Oncol* **33**: 570, doi:10.1200/jco.2015.33.15_suppl.570.

Slamon DJ, Neven P, Chia S, Fasching PA, De Laurentiis M, Im S-A, Petrakova K, Bianchi GV, Esteva FJ, Martín M, Nusch A, Sonke GS, De la Cruz-Merino L, Beck JT, Pivot X, Vidam G, Wang Y, Rodriguez Lorenc K, Miller M, Taran T, Jerusalem G (2018) Phase III Randomized Study of Ribociclib and Fulvestrant in Hormone Receptor-Positive, Human Epidermal Growth Factor Receptor 2-Negative Advanced Breast Cancer: MONALEESA-3. *J Clin Oncol Off J Am Soc Clin Oncol* **36**: 2465–2472, doi:10.1200/JCO.2018.78.9909.

Söderström K, Stein E, Colmenero P, Purath U, Müller-Ladner U, Teixeira de Matos C, Tarner IH, Robinson WH, Engleman EG (2010) Natural killer cells trigger osteoclastogenesis and bone destruction in arthritis. *Proc Natl Acad Sci* **107**: 13028 LP – 13033, doi:10.1073/pnas.1000546107.

Sosa MS, Bragado P, Aguirre-Ghiso JA (2014) Mechanisms of disseminated cancer cell dormancy: an awakening field. *Nat Rev Cancer* **14**: 611–622, doi:10.1038/nrc3793.

Sosa MS, Bragado P, Debnath J, Aguirre-Ghiso JA (2013) Regulation of Tumor Cell Dormancy by Tissue Microenvironments and Autophagy BT - Systems Biology of Tumor Dormancy. H. Enderling, N. Almog, and L. Hlatky, eds. (New York, NY: Springer New York), pp. 73–89.

de Sousa GF, Wlodarczyk SR, Monteiro G (2014) Carboplatin: Molecular mechanisms of action associated with chemoresistance. *Brazilian J Pharm Sci* **50**: 693–702, doi:10.1590/S1984-82502014000400004.

Sousa S, Clézardin P (2018) Bone-Targeted Therapies in Cancer-Induced Bone Disease. *Calcif Tissue Int* **102**: 227–250, doi:10.1007/s00223-017-0353-5.

Spallarossa P, Altieri P, Barisione C, Passalacqua M, Aloi C, Fugazza G, Frassoni F, Podestà M, Canepa M, Ghigliotti G, Brunelli C (2010) p38 MAPK and JNK Antagonistically Control Senescence and Cytoplasmic p16INK4A Expression in Doxorubicin-Treated Endothelial Progenitor Cells. *PLoS One* **5**: e15583.

Srivastava K, Hu J, Korn C, Savant S, Teichert M, Kapel SS, Jugold M, Besemfelder E, Thomas M, Pasparakis M, Augustin HG (2014) Postsurgical adjuvant tumor therapy by combining anti-

angiopoietin-2 and metronomic chemotherapy limits metastatic growth. *Cancer Cell* **26**: 880–895, doi:10.1016/j.ccell.2014.11.005.

Stegelmeier AA, van Vloten JP, Mould RC, Klafuric EM, Minott JA, Wootton SK, Bridle BW, Karimi K (2019) Myeloid Cells during Viral Infections and Inflammation. *Viruses* **11**: doi:10.3390/v11020168.

Stopeck AT, Lipton A, Body J-J, Steger GG, Tonkin K, de Boer RH, Lichinitser M, Fujiwara Y, Yardley DA, Viniegra M, Fan M, Jiang Q, Dansey R, Jun S, Braun A (2010) Denosumab compared with zoledronic acid for the treatment of bone metastases in patients with advanced breast cancer: a randomized, double-blind study. *J Clin Oncol Off J Am Soc Clin Oncol* **28**: 5132–5139, doi:10.1200/JCO.2010.29.7101.

Straume O, Shimamura T, Lampa MJG, Carretero J, Øyan AM, Jia D, Borgman CL, Soucheray M, Downing SR, Short SM, Kang S-Y, Wang S, Chen L, Collett K, Bachmann I, Wong K-K, Shapiro GI, Kalland KH, Folkman J, Watnick RS, Akslen LA, Naumov GN (2012) Suppression of heat shock protein 27 induces long-term dormancy in human breast cancer. *Proc Natl Acad Sci U S A* **109**: 8699–8704, doi:10.1073/pnas.1017909109.

Suárez-Álvarez B, López-Vázquez A, López-Larrea C (2012) Mobilization and Homing of Hematopoietic Stem Cells BT - Stem Cell Transplantation. C. López-Larrea, A. López-Vázquez, and B. Suárez-Álvarez, eds. (New York, NY: Springer US), pp. 152–170.

Sugiyama T, Kohara H, Noda M, Nagasawa T (2006) Maintenance of the hematopoietic stem cell pool by CXCL12-CXCR4 chemokine signaling in bone marrow stromal cell niches. *Immunity* **25**: 977–988, doi:10.1016/j.immuni.2006.10.016.

Sugiyama T, Nagasawa T (2012) Bone marrow niches for hematopoietic stem cells and immune cells. *Inflamm Allergy Drug Targets* **11**: 201–206, doi:10.2174/187152812800392689.

Sundman-Engberg B, Tidefelt U, Paul C (1998) Toxicity of cytostatic drugs to normal bone marrow cells in vitro. *Cancer Chemother Pharmacol* **42**: 17–23, doi:10.1007/s002800050779.

Sung H, Ferlay J, Siegel RL, Laversanne M, Soerjomataram I, Jemal A, Bray F (2021) Global Cancer Statistics 2020: GLOBOCAN Estimates of Incidence and Mortality Worldwide for 36 Cancers in 185 Countries. *CA Cancer J Clin* **71**: 209–249, doi:10.3322/caac.21660.

Suzuki Y, Tokuda Y (2001) Docetaxel. *Gan To Kagaku Ryoho* **28**: 1363–1367, doi:10.2165/11209660-000000000-00000.

T. PT, L. BM, Ayelet S, J. WM, Renee C, H. LC, Lindsey O, Karrie C, John M, H. KL, Qing C, M. MC, A. SD (2016) Dormant breast cancer micrometastases reside in specific bone marrow niches that regulate their transit to and from bone. *Sci Transl Med* **8**: 340ra73-340ra73, doi:10.1126/scitranslmed.aad4059.

Taichman RS, Cooper C, Keller ET, Pienta KJ, Taichman NS, McCauley LK (2002) Use of the stromal cell-derived factor-1/CXCR4 pathway in prostate cancer metastasis to bone. *Cancer Res* **62**: 1832–1837.

Takano-Yamamoto T (2014) Osteocyte function under compressive mechanical force. *Jpn Dent Sci Rev* **50**: 29–39, doi:https://doi.org/10.1016/j.jdsr.2013.10.004.

Tamma R, Ribatti D (2017) Bone Niches, Hematopoietic Stem Cells, and Vessel Formation. *Int J Mol Sci* **18**: 151, doi:10.3390/ijms18010151.

Tang Z-N, Zhang F, Tang P, Qi X-W, Jiang J (2011) RANKL-induced migration of MDA-MB-231 human breast cancer cells via Src and MAPK activation. *Oncol Rep* **26**: 1243–1250, doi:10.3892/or.2011.1368.

Teicher BA, Fricker SP (2010) CXCL12 (SDF-1)/CXCR4 pathway in cancer. *Clin Cancer Res* **16**: 2927–2931, doi:10.1158/1078-0432.CCR-09-2329.

Teitelbaum SL (2000) Bone Resorption by Osteoclasts. *Science (80-)* **289**: 1504 LP – 1508, doi:10.1126/science.289.5484.1504.

Terashima A, Okamoto K, Nakashima T, Akira S, Ikuta K, Takayanagi H (2016) Sepsis-Induced Osteoblast Ablation Causes Immunodeficiency. *Immunity* **44**: 1434–1443, doi:10.1016/j.immuni.2016.05.012.

Terashima A, Takayanagi H (2018) Overview of Osteoimmunology. *Calcif Tissue Int* **102**: 503–511, doi:10.1007/s00223-018-0417-1.

Thorn CF, Oshiro C, Marsh S, Hernandez-Boussard T, McLeod H, Klein TE, Altman RB (2011) Doxorubicin pathways: pharmacodynamics and adverse effects. *Pharmacogenet Genomics* **21**: 440–446, doi:10.1097/FPC.0b013e32833ffb56.

Tjensvoll K, Oltedal S, Heikkilä R, Kvaløy JT, Gilje B, Reuben JM, Smaaland R, Nordgård O (2012) Persistent tumor cells in bone marrow of non-metastatic breast cancer patients after primary surgery are associated with inferior outcome. *BMC Cancer* **12**: 190, doi:10.1186/1471-2407-12-190.

Tolar J, Teitelbaum SL, Orchard PJ (2004) Osteopetrosis. *N Engl J Med* **351**: 2839–2849, doi:10.1056/NEJMra040952.

Toraya-Brown S, Fiering S (2014) Local tumour hyperthermia as immunotherapy for metastatic cancer. *Int J Hyperth* **30**: 531–539, doi:10.3109/02656736.2014.968640.

Townson JL, Chambers AF (2006) Dormancy of solitary metastatic cells. *Cell Cycle* **5**: 1744–1750, doi:10.4161/cc.5.16.2864.

Tsé C, Gauchez A-S, Jacot W, Lamy P-J (2012) HER2 shedding and serum HER2 extracellular domain: Biology and clinical utility in breast cancer. *Cancer Treat Rev* **38**: 133–142, doi:https://doi.org/10.1016/j.ctrv.2011.03.008.

Tseng H-C, Kanayama K, Kaur K, Park S-H, Park S, Kozlowska A, Sun S, McKenna CE, Nishimura I, Jewett A (2015) Bisphosphonate-induced differential modulation of immune cell function in gingiva and bone marrow in vivo: role in osteoclast-mediated NK cell activation. *Oncotarget* **6**: 20002.

Tsuda B, Miyamoto A, Yokoyama K, Ogiya R, Oshitanai R, Terao M, Morioka T, Niikura N, Okamura T, Miyako H, Saito Y, Suzuki Y, Kametani Y, Tokuda Y (2018) B-cell populations are expanded in breast cancer patients compared with healthy controls. *Breast Cancer* **25**: 284–291, doi:10.1007/s12282-017-0824-6.

Tsukasaki M, Takayanagi H (2019) Osteoimmunology: evolving concepts in bone–immune interactions in health and disease. *Nat Rev Immunol* **19**: 626–642, doi:10.1038/s41577-019-0178-8.

Tulotta C, Groenewoud A, Snaar-Jagalska BE, Ottewell P (2019a) Animal models of breast cancer bone metastasis. *Methods Mol Biol* **1914**: 309–330, doi:10.1007/978-1-4939-8997-3_17.

Tulotta C, Lefley D V, Freeman K, Gregory WM, Hanby AM, Heath PR, Nutter-Howard F, Wilkinson JM, Spicer-Hadlington AR, Liu X, Bradbury S, Hambley L, Cookson V, Allocca G, Kruithof-de-Julio M, Coleman RE, Brown JE, Holen I, Ottewell PD (2019b) Endogenous production of IL-1B by breast cancer cells drives metastasis and colonisation of the bone microenvironment. *Clin Cancer Res* clincanres.2202.2018, doi:10.1158/1078-0432.CCR-18-2202.

Tulotta C, Lefley D V, Moore CK, Amariutei AE, Spicer-Hadlington AR, Quayle LA, Hughes RO, Ahmed K, Cookson V, Evans CA, Vadakekolathu J, Heath P, Francis S, Pinteaux E, Pockley AG, Ottewell PD (2021) IL-1B drives opposing responses in primary tumours and bone metastases; harnessing combination therapies to improve outcome in breast cancer. *npj Breast Cancer* **7**: 95,

doi:10.1038/s41523-021-00305-w.

Turner NC, Slamon DJ, Ro J, Bondarenko I, Im S-A, Masuda N, Colleoni M, DeMichele A, Loi S, Verma S, Iwata H, Harbeck N, Loibl S, André F, Puyana Theall K, Huang X, Giorgetti C, Huang Bartlett C, Cristofanilli M (2018) Overall Survival with Palbociclib and Fulvestrant in Advanced Breast Cancer. *N Engl J Med* **379**: 1926–1936, doi:10.1056/NEJMoa1810527.

Ubellacker JM, Haider M-T, DeCristo MJ, Allocca G, Brown NJ, Silver DP, Holen I, McAllister SS (2017) Zoledronic acid alters hematopoiesis and generates breast tumor-suppressive bone marrow cells. *Breast Cancer Res* **19**: 23, doi:10.1186/s13058-017-0815-8.

Ugarte F, Forsberg EC (2013) Haematopoietic stem cell niches: new insights inspire new questions. *EMBO J* **32**: 2535–2547, doi:10.1038/emboj.2013.201.

Unsinger J, McGlynn M, Kasten KR, Hoekzema AS, Watanabe E, Muenzer JT, McDonough JS, Tschoep J, Ferguson TA, McDunn JE, Morre M, Hildeman DA, Caldwell CC, Hotchkiss RS (2010) IL-7 Promotes T Cell Viability, Trafficking, and Functionality and Improves Survival in Sepsis. *J Immunol* **184**: 3768 LP – 3779, doi:10.4049/jimmunol.0903151.

Vaananen HK, Zhao H, Mulari M, Halleen JM (2000) The cell biology of osteoclast function. *J Cell Sci* **113**: 377 LP – 381.

Valabrega G, Montemurro F, Aglietta M (2007) Trastuzumab: mechanism of action, resistance and future perspectives in HER2-overexpressing breast cancer. *Ann Oncol* **18**: 977–984, doi:https://doi.org/10.1093/annonc/mdl475.

Venet F, Foray A-P, Villars-Méchin A, Malcus C, Poitevin-Later F, Lepape A, Monneret G (2012) IL-7 Restores Lymphocyte Functions in Septic Patients. *J Immunol* **189**: 5073 LP – 5081, doi:10.4049/jimmunol.1202062.

Vera-Ramirez L, Vodnala SK, Nini R, Hunter KW, Green JE (2018) Autophagy promotes the survival of dormant breast cancer cells and metastatic tumour recurrence. *Nat Commun* **9**: 1944, doi:10.1038/s41467-018-04070-6.

Vinayak S, Ford JM (2010) PARP Inhibitors for the Treatment and Prevention of Breast Cancer. *Curr Breast Cancer Rep* **2**: 190–197, doi:10.1007/s12609-010-0026-0.

Vu T, Claret FX (2012) Trastuzumab: updated mechanisms of action and resistance in breast cancer. *Front Oncol* **2**: 62, doi:10.3389/fonc.2012.00062.

Waks AG, Winer EP (2019) Breast Cancer Treatment: A Review. *JAMA - J Am Med Assoc* **321**: 288–300, doi:10.1001/jama.2018.19323.

Walker ND, Patel J, Munoz JL, Hu M, Guiro K, Sinha G, Rameshwar P (2016) The bone marrow niche in support of breast cancer dormancy. *Cancer Lett* **380**: 263–271, doi:https://doi.org/10.1016/j.canlet.2015.10.033.

Wang H, Yu C, Gao X, Welte T, Muscarella AM, Tian L, Zhao H, Zhao Z, Du S, Tao J, Lee B, Westbrook TF, Wong STCC, Jin X, Rosen JM, Osborne CK, Zhang XHFH-F (2015a) The Osteogenic Niche Promotes Early-Stage Bone Colonization of Disseminated Breast Cancer Cells. *Cancer Cell* **27**: 193–210, doi:10.1016/j.ccell.2014.11.017.

Wang N, Docherty FE, Brown HK, Reeves KJ, Fowles ACM, Ottewell PD, Dear TN, Holen I, Croucher PI, Eaton CL (2014) Prostate Cancer Cells Preferentially Home to Osteoblast-rich Areas in the Early Stages of Bone Metastasis: Evidence From In Vivo Models. *J Bone Miner Res* **29**: 2688–2696, doi:https://doi.org/10.1002/jbmr.2300.

Wang N, Reeves KJ, Brown HK, Fowles ACM, Docherty FE, Ottewell PD, Croucher PI, Holen I, Eaton CL (2015b) The frequency of osteolytic bone metastasis is determined by conditions of the soil, not the number of seeds; evidence from in vivo models of breast and prostate cancer. *J Exp Clin Cancer Res* **34**: 124, doi:10.1186/s13046-015-0240-8.

Wang Y, Probin V, Zhou D (2006) Cancer therapy-induced residual bone marrow injury-Mechanisms of induction and implication for therapy. *Curr Cancer Ther Rev* **2**: 271–279, doi:10.2174/157339406777934717.

Wauquier F, Leotoing L, Coxam V, Guicheux J, Wittrant Y (2009) Oxidative stress in bone remodelling and disease. *Trends Mol Med* **15**: 468–477, doi:10.1016/j.molmed.2009.08.004.

Weilbaecher KN, Guise TA, McCauley LK (2011) Cancer to bone: A fatal attraction. *Nat Rev Cancer* **11**: 411–425, doi:10.1038/nrc3055.

Weinstat-Saslow DL, Zabrenetzky VS, VanHoutte K, Frazier WA, Roberts DD, Steeg PS (1994) Transfection of thrombospondin 1 complementary DNA into a human breast carcinoma cell line reduces primary tumor growth, metastatic potential, and angiogenesis. *Cancer Res* **54**: 6504–6511.

Weiss HM, Pfaar U, Schweitzer A, Wiegand H, Skerjanec A, Schran H (2008) Biodistribution and plasma protein binding of zoledronic acid. *Drug Metab Dispos* **36**: 2043–2049,

doi:10.1124/dmd.108.021071.

Wen S-H, Su S-C, Liou B-H, Lin C-H, Lee K-R (2018) Sulbactam-enhanced cytotoxicity of doxorubicin in breast cancer cells. *Cancer Cell Int* **18**: 128, doi:10.1186/s12935-018-0625-9.

White DE, Kurpios NA, Zuo D, Hassell JA, Blaess S, Mueller U, Muller WJ (2004) Targeted disruption of β1-integrin in a transgenic mouse model of human breast cancer reveals an essential role in mammary tumor induction. *Cancer Cell* **6**: 159–170, doi:https://doi.org/10.1016/j.ccr.2004.06.025.

Widler L, Jaeggi KA, Glatt M, Müller K, Bachmann R, Bisping M, Born A-R, Cortesi R, Guiglia G, Jeker H, Klein R, Ramseier U, Schmid J, Schreiber G, Seltenmeyer Y, Green JR (2002) Highly potent geminal bisphosphonates. From pamidronate disodium (Aredia) to zoledronic acid (Zometa). *J Med Chem* **45**: 3721–3738, doi:10.1021/jm020819i.

Willett WC, Tamimi R, Hankinson SE, Hazra A, Heather Eliassen A, Colditz GA (2014) Nongenetic factors in the causation of breast cancer.

Williams C, Lin C-Y (2013) Oestrogen receptors in breast cancer: basic mechanisms and clinical implications. *Ecancermedicalscience* **7**: 370, doi:10.3332/ecancer.2013.370.

Williams K, Motiani K, Giridhar PV, Kasper S (2013) CD44 integrates signaling in normal stem cell, cancer stem cell and (pre)metastatic niches. *Exp Biol Med* **238**: 324–338, doi:10.1177/1535370213480714.

Wilson A, Trumpp A (2006) Bone-marrow haematopoietic-stem-cell niches. *Nat Rev Immunol* **6**: 93–106, doi:10.1038/nri1779.

Winkler IG, Barbier V, Nowlan B, Jacobsen RN, Forristal CE, Patton JT, Magnani JL, Lévesque JP (2012) Vascular niche E-selectin regulates hematopoietic stem cell dormancy, self renewal and chemoresistance. *Nat Med* **18**: 1651–1657, doi:10.1038/nm.2969.

Wong ALA, Lee S-C (2012) Mechanisms of Resistance to Trastuzumab and Novel Therapeutic Strategies in HER2-Positive Breast Cancer. *Int J Breast Cancer* **2012**: 415170, doi:10.1155/2012/415170.

Wooster R, Bignell G, Lancaster J, Swift S, Seal S, Mangion J, Collins N, Gregory S, Gumbs C, Micklem G (1995) Identification of the breast cancer susceptibility gene BRCA2. *Nature* **378**: 789–792, doi:10.1038/378789a0.

Wright LE, Ottewell PD, Rucci N, Peyruchaud O, Pagnotti GM, Chiechi A, Buijs JT, Sterling JA (2016) Murine models of breast cancer bone metastasis. *Bonekey Rep* **5**: 804, doi:10.1038/bonekey.2016.31.

Wu J, Lanier LL (2003) Natural Killer Cells and Cancer. *Adv Cancer Res* **90**: 127–156, doi:10.1016/S0065-230X(03)90004-2.

Wu M-YY, Li C-JJ, Yiang G-TT, Cheng Y-LL, Tsai AP-YY, Hou Y-TT, Ho Y-CC, Hou M-FF, Chu P-YY (2018) Molecular Regulation of Bone Metastasis Pathogenesis. *Cell Physiol Biochem Int J Exp Cell Physiol Biochem Pharmacol* **46**: 1423–1438, doi:10.1159/000489184.

Xiang L, Gilkes DM (2019) The contribution of the immune system in bone metastasis pathogenesis. *Int J Mol Sci* **20**: doi:10.3390/ijms20040999.

Xiong J, O'Brien CA (2012) Osteocyte RANKL: new insights into the control of bone remodeling. *J Bone Miner Res* **27**: 499–505, doi:10.1002/jbmr.1547.

Xiong J, Onal M, Jilka RL, Weinstein RS, Manolagas SC, O'Brien CA (2011) Matrix-embedded cells control osteoclast formation. *Nat Med* **17**: 1235–1241, doi:10.1038/nm.2448.

Xu J, Chen Y, Liu Y, Zhang J, Kang Q, Ho K, Chai Y, Li G (2017a) Effect of SDF-1/Cxcr4 Signaling Antagonist AMD3100 on Bone Mineralization in Distraction Osteogenesis. *Calcif Tissue Int* **100**: 641–652, doi:10.1007/s00223-017-0249-4.

Xu J, Ni C, Ma C, Zhang L, Jing X, Li C, Liu Y, Qu X (2017b) Association of neutrophil/lymphocyte ratio and platelet/lymphocyte ratio with ER and PR in breast cancer patients and their changes after neoadjuvant chemotherapy. *Clin Transl Oncol* **19**: 989–996, doi:10.1007/s12094-017-1630-5.

Yabluchanskiy A, Ma Y, Iyer RP, Hall ME, Lindsey ML (2013) Matrix metalloproteinase-9: Many shades of function in cardiovascular disease. *Physiology (Bethesda)* **28**: 391–403, doi:10.1152/physiol.00029.2013.

Yang F, Chen H, Liu Y, Yin K, Wang Y, Li X, Wang G, Wang S, Tan X, Xu C, Lu Y, Cai B (2013) Doxorubicin caused apoptosis of mesenchymal stem cells via p38, JNK and p53 Pathway. *Cell Physiol Biochem* **32**: 1072–1082, doi:10.1159/000354507.

Yu VWC, Saez B, Cook C, Lotinun S, Pardo-Saganta A, Wang Y-H, Lymperi S, Ferraro F, Raaijmakers MHGP, Wu JY, Zhou L, Rajagopal J, Kronenberg HM, Baron R, Scadden DT (2015) Specific bone cells produce DLL4 to generate thymus-seeding progenitors from bone marrow. *J Exp Med* **212**: 759–774,

doi:10.1084/jem.20141843.

Yuan F-L, Li X, Lu W-G, Xu R-S, Zhao Y-Q, Li C-W, Li J-P, Chen F-H (2010) Regulatory T cells as a potent target for controlling bone loss. *Biochem Biophys Res Commun* **402**: 173–176, doi:https://doi.org/10.1016/j.bbrc.2010.09.120.

Zaiss MM, Axmann R, Zwerina J, Polzer K, Gückel E, Skapenko A, Schulze-Koops H, Horwood N, Cope A, Schett G (2007) Treg cells suppress osteoclast formation: A new link between the immune system and bone. *Arthritis Rheum* **56**: 4104–4112, doi:10.1002/art.23138.

Zekri J, Mansour M, Karim SM (2014) The anti-tumour effects of zoledronic acid. *J bone Oncol* **3**: 25–35, doi:10.1016/j.jbo.2013.12.001.

Zhang H, Gao L, Zhang B, Zhang L, wang C (2016) Prognostic value of platelet to lymphocyte ratio in non-small cell lung cancer: a systematic review and meta-analysis. *Sci Rep* **6**: 22618, doi:10.1038/srep22618.

Zhang L, Zhang S, Yao J, Lowery FJ, Zhang Q, Huang W-C, Li P, Li M, Wang X, Zhang C, Wang H, Ellis K, Cheerathodi M, McCarty JH, Palmieri D, Saunus J, Lakhani S, Huang S, Sahin AA, Aldape KD, Steeg PS, Yu D (2015) Microenvironment-induced PTEN loss by exosomal microRNA primes brain metastasis outgrowth. *Nature* **527**: 100–104, doi:10.1038/nature15376.

Zhang W, Bado I, Wang H, Lo HC, Zhang XHF (2019) Bone Metastasis: Find Your Niche and Fit in. *Trends in Cancer* **5**: 95–110, doi:10.1016/j.trecan.2018.12.004.

Zhang W, Dang K, Huai Y, Qian A (2020) Osteoimmunology: The Regulatory Roles of T Lymphocytes in Osteoporosis. *Front Endocrinol (Lausanne)* **11**: 465, doi:10.3389/fendo.2020.00465.

Zheng Y, Zhou H, Brennan K, Blair JM, Modzelewski JRK, Seibel MJ, Dunstan CR (2007) Inhibition of bone resorption, rather than direct cytotoxicity, mediates the anti-tumour actions of ibandronate and osteoprotegerin in a murine model of breast cancer bone metastasis. *Bone* **40**: 471–478, doi:10.1016/j.bone.2006.09.016.

Zhu M, Liu X, Qu Y, Hu S, Zhang Y, Li W, Zhou X, Yang H, Zhou L, Wang Q, Hou Y, Chen Y, Wang Y, Wang Y, Lu Z, Luo Z, Hu X (2019) Bone metastasis pattern of cancer patients with bone metastasis but no visceral metastasis. *J Bone Oncol* **15**: doi:10.1016/j.jbo.2019.100219.